



This is to certify that the

dissertation entitled

The Parlamonic of Multiple Pendulum Vibrotion Absorber's Applied to Rotating Systems

presented by

CHANGPO CHAO

has been accepted towards fulfillment of the requirements for

Ph.D. degree in Mechanical Engineering

Major professor

Date Aug 13, 1997

PLACE IN RETURN BOX to remove this checkout from your record. TO AVOID FINES return on or before date due.

DATE DUE	DATE DUE	DATE DUE
JAN 27,2005		

MSU is An Affirmative Action/Equal Opportunity Institution expired attack pm3-p.1

# THE PERFORMANCE OF MULTIPLE PENDULUM VIBRATION ABSORBERS APPLIED TO ROTATING SYSTEMS

By

Chang-Po Chao

#### A DISSERTATION

Submitted to
Michigan State University
in partial fulfillment of the requirements
for the degree of

DOCTOR OF PHILOSOPHY

Department of Mechanical Engineering

#### **ABSTRACT**

# THE PERFORMANCE OF MULTIPLE PENDULUM VIBRATION ABSORBERS APPLIED TO ROTATING SYSTEMS

By

#### Chang-Po Chao

A centrifugal pendulum vibration absorber (CPVA) is a device used for reducing torsional vibrations in rotating machinery. It consists of a movable mass, the center of gravity of which is restricted to follow a prescribed path. When this path is properly designed, the motion of the CPVA is tuned so as to generate a torque that reduces torsional vibrations. CPVA's are currently widely employed to suppress torsional vibrations in light aircraft engines, and are receiving attention in experimental automotive studies.

Existing CPVA designs are based on several assumptions, including the following two: First, for a multiple-absorber system, the set of identical absorbers moves in unison, and, second, the absorber paths are manufactured exactly as designed. The present study aims to re-assess absorber performance in terms of relaxing these two assumptions. This necessitates consideration of the nonlinear dynamics of mulitple-CPVA systems.

This study starts with an overview of the operation of CPVA's and a description of some existing CPVA designs. A mathematical model is then derived that captures the nonlinear dynamics of a multi-absorber/rotor system response. Using a generic methodology which combines asymptotic techniques (averaging) and bifurcation theory, the mathematical model is analyzed for two representative absorber systems: tautochronic and subharmonic. Analysis is first conducted for the tautochronic systems.

tem, which enables one to: (1) predict the instability/bifurcation point of the unison motion, (2) investigate the dependence of the post-critical dynamics on various system parameters, and (3) assess the absorber performance in terms of two quantitative measures: the rotor acceleration and the feasible range of the applied torque. A similar analysis is carried out for system comprised of multiple pairs of subharmonic absorbers. In addition, uncertainties and intentional mistuning are incorporated into the absorber path configurations, which permits one to consider design robustness issues. It is found that the system dynamics and absorber performance measures are accurately predicted by the analyses, as verified by extensive numerical simulations for both absorber systems. Based on these predictions, design guidelines are distilled for various system parameters, including absorber damping, the number of absorbers, and intentional mistuning of the path.

 To my wife and family

#### ACKNOWLEDGMENTS

It has been six years since I first arrived in the States. During this important period of my life, I have obtained a great deal of valuable academic and non-academic assistance from a lot of generous people, especially, my advisor, Professor Steven W. Shaw. Thanks to the opportunity to work under his guidance in the past two and half years, I have experienced a wonderful research life in East Lansing. Not only have I freedom on the direction of my research, but also ground-breaking insights into problems and solid financial support throughout my Ph.D. studies. I truly believe this experience will have great impact at some points of the rest of my life. I also owe great debt to my former advisor, Dr. Philip M. FitzSimons, who introduced me to the fascinating world of control. Working under his guidance on a real mechanical model for my master's thesis and developing a novel theoretical methodology for the ensuing project give me a complete knowledge of control theory, which, I believe, will have tremendous contribution on my potential for an extended academic career. In addition, I would like to express my grateful thanks to the members of my committee, Professors Clark J. Radcliffe, Sheldon Newhouse Alan G. Haddow and Brian B. Feeny, for providing helpful comments on this study.

Michigan State University has been a joyful place for me, especially, this is the place where I met my wife, a intelligent young woman, Hsing-Yuh Chen, who has been supporting me as a family member, friend and moral booster for a long period of time. My family, of course, provided me crucial financial support in the early stages at MSU and continues to encourage me to pursue my dream. I would like to

dedicate this work to my wife and family.

Special thanks go to the members of Dynamics and Vibration Group for providing persistent encouragement and fostering an intellectual, stimulating atmosphere in the laboratory. They are Professors Shyh-Leh Chen and Jin-Wei Liang, Dr. Cheng-Tang Lee, Dr. Ramana Kappagantu, Mr. Chris Hause, Mr. Wei Li, Ms. Yihong Zhang, Mr. Choong-Ming Jung, ...... Working in such a supportive environment will always be a pleasant memory for me.

# TABLE OF CONTENTS

LIST	OF FIGURES xii
LIST	OF TABLES
LIST	OF APPENDICES
СНА	PTER
1.	INTRODUCTION 1
	1.1 Operation of CPVA's
	1.2 History and Literature Review
	1.3 Motivation
	1.4 Organization of this Dissertation
2.	PRELIMINARIES
	2.1 Assumptions
	2.2 Equations of Motion
	2.3 The Absorber System
	2.4 Limitations on Absorber Motions
	2.5 Absorber Dampings
	2.6 Symmetry Identification
	2.7 Measures of Absorber Performance

3.	STABILITY OF THE UNISON RESPONSE FOR A ROTATING	
	SYSTEM WITH MULTIPLE TAUTOCHRONIC ABSORBERS	21
	3.0 Equations of Motion	
	3.1 Scaling and Reduction of the Equations of Motion	
	3.2 The Averaged Equations	
	3.3 Stability Criterion	
	3.4 Concluding Remarks	
4.	NON-UNISON DYNAMICS OF A ROTATING SYSTEM WITH	
	MULTIPLE TAUTOCHRONIC ABSORBERS	<b>3</b> 8
	4.1 Preparation of Equations of Motion	
	4.2 The Averaged Equations	
	4.3 Steady-State Responses	
	4.4 The Post-Bifurcation Dynamics	
	4.5 Absorber Performance	
	4.6 Numerical and Simulation Results	
	4.7 Concluding Remarks	
5.	THE EFFECTS OF IMPERFECTIONS AND MISTUNING ON THE	
	PERFORMANCE OF THE PAIRED, SUBHARMONIC CPVA SYS-	
	TEM	66
	5.1 The Subharmonic Absorber System	
	5.2 Measures of Performance	
	5.3 Scaling and Reduction of the Equations of Motion	
	5.4 The Averaged Equations	

	5.7 Concluding Remarks
6.	NONLINEAR DYNAMICS OF A MULTIPLE SUBHARMONIC CPVA  SYSTEM
	6.1 The Multiple Subharmonic Absorber System
	6.2 Reduction of the Equations of Motion
	6.3 The Averaged Equations
	6.4 Case Studies
	6.5 Remarks and Design Guidelines
7.	CONCLUSIONS AND FUTURE WORK
APP	ENDIX
A.	THE EXPRESSIONS FOR $\frac{\partial H_1}{\partial \varphi_i}\Big _{s.s.}$ , $\frac{\partial H_2}{\partial \tau_i}\Big _{s.s.}$ , $\frac{\partial H_1}{\partial \varphi_j}\Big _{s.s.}$ and $\frac{\partial H_2}{\partial \tau_j}\Big _{s.s.}$ 137
В.	ON THE EIGENVALUES OF $C$
C.	ON THE EIGENVALUES OF $[A + (N-1)B]$
D.	PROOF OF EQUATION (3.17)
E.	JUSTIFICATION OF $\tilde{\bar{\psi}}_i \simeq \tilde{\bar{\psi}}_j$ , $\forall \ 2 \leq i, j \leq N \ldots 143$
F.	PROOF OF $Trace[A + (N-2)B] < 0$ AND $Det[A + (N-2)B] > 0$ AS
$\hat{ar{ ho}}  o 0$	+
G.	THE LOW-ORDER APPROXIMATION OF $yy'(\theta)$

5.5 Approximate Steady-State Solutions

5.6 Absorber Performance and Design Guidelines

BIBLIOGRAPHY	53
152	
K. THE NUMERICAL ALGORITHM FOR COUPLED-MODE SOLUTIONS	
J. STABILITY OF SOLUTIONS ON SM2 <sup>+</sup>	51
I. STABILITY OF SOLUTIONS ON SM1 <sup>+</sup>	50
H. AVERAGED EQUATIONS IN CARTESIAN COORDINATES 14	18

### LIST OF FIGURES

Figure	
1.1 The CPVA carrier assembly from the cross-section view	3
1.2 The Schematic diagram for the CPVA's and the rotor from the cross-section view	4
2.1 Cross-sectional schematic diagram of the rotor and absorbers	12
<b>3.1</b> The critical torque level, $\hat{\Gamma}_{\theta}^{*}$ , versus the number of absorbers, $N$ with $\frac{c_{\alpha}}{m_{0}\Omega} \simeq 0.0013$ . " $\bullet$ " represents the bifurcation point derived from " $Det[A-B] = 0$ ". " $\star$ " represents the bifurcation point derived from the simplified criterion (3.23). " $\star$ " represents an non-unison motion from numerical simulations. " $\circ$ " represents a unison motion from numerical simulations.	32
3.2 The critical torque level, $\hat{\Gamma}_{\theta}^*$ , versus various absorber damping $\hat{\mu}_a$ . The solid line represents bifurcation points derived from " $Det[A-B]=0$ ". The dashed line represents bifurcation points derived from the simplified criterion (3.23). "×" represents an non-unison motion from numerical simulations. "o" represents a unison motion from numerical simulations.	34
<b>3.3</b> Absorber motions before and after the bifurcation point for $N = 7$	36
<b>4.1</b> Post-bifurcation steady-state responses of the absorbers for $N=4$ (four absorbers), $\hat{\mu}_a=0.0026$ and $\hat{\Gamma}_\theta=0.048$ . Solid lines: Simulation; Dotted lines: Truncated; Dashed lines: Non-truncated; Coarsely dotted lines: Imposed unison response	56
4.2 Post-bifurcation steady-state responses of the rotor acceleration for $N=4$ (four absorbers), $\hat{\mu}_a=0.0026$ and $\hat{\Gamma}_\theta=0.048$ . Solid lines: Simulation; Dotted lines: The 2nd-order approximation; Triangles: The 3rd-order approximation; Dashed lines: Non-truncated; Coarsely dotted lines: Imposed unison response.	58
4.3 The $  s  _{ss}$ 's derived by different approximations versus the applied torque level. The system parameters used are $N=4$ (four absorbers) and $\hat{\mu}_a=0.0026$ . Solid lines: Simulation; Dotted lines: Truncated; Dashed lines: Non-truncated; Coarsely dotted lines: Imposed unison response	50

<b>4.4</b> The percent reduction in torque range, relative to the unison motion, versus the number of absorbers for $\hat{\mu}_a = 0.0026$ . "+": Simulation; " $\bullet$ ": Truncated; " $\square$ ": Non-truncated	61
<b>4.5</b> The $  yy'  _{ss}$ 's derived by different approximations versus the applied torque level, for system parameters $N=4$ (four absorbers) and $\hat{\mu}_a=0.0026$ . Solid lines: Simulation; Dotted lines: The 2nd-order approximation; Triangles: The 3rd-order approximation; Dashed lines: Non-truncated; Coarsely dotted lines: Imposed unison response	62
<b>4.6</b> The ratio of $  yy'  _{ss}$ to that for the unison response versus the number of absorbers for $\hat{\Gamma}_{\theta} = 0.0555$ and $\hat{\mu}_{a} = 0.0026$ . "+": Simulation; " $\bullet$ ": The 2nd-order approximation; " $\triangle$ ": The 3rd-order approximation; " $\square$ ": Non-truncated; " $\circ$ ": Imposed unison response.	63
<b>5.1</b> The bifurcation diagram for $n=2$ , $\tilde{\mu}_a=0.05$ , $\tilde{\delta}_{\xi 2}=0.06$ , $\tilde{\delta}_{\xi 4}=0$ , $\tilde{\delta}_{\eta 2}=0$ , $\tilde{\delta}_{\eta 4}=0$ . The solid lines represent stable solutions and the dashed lines represent unstable solutions	81
<b>5.2</b> The bifurcation set of the zero solution for $\tilde{\delta}_{\eta 2} = \tilde{\delta}_{\eta 4} = 0$ and $\tilde{\mu}_a = 0.05$ .	83
<b>5.3</b> The curves represent the relationship between $\bar{r}_{\eta}$ and $\bar{r}_{\xi}$ in coupled-mode solutions for $n=2$ , $\tilde{\delta}_{\xi 2}=0.05$ and $\tilde{\delta}_{\xi 4}=0$ . The feasible absorber motions lie inside of triangle <b>OAB</b>	90
<b>5.4</b> The response bifurcation diagram for <b>SM2</b> with $n=2$ , $\hat{\delta}_{\xi 4}=0$ , $\tilde{\delta}_{\eta 2}=0$ , $\tilde{\delta}_{\eta 4}=0$ , $\hat{\mu}_a=0.0083$ and various $\hat{\delta}_{\xi 2}$ : (A) 0.03 (B) 0.02 (C) 0.01 (D) 0.00 (E) -0.01 (F) -0.02 (G) -0.03	96
<b>5.5</b> The response bifurcation diagram for <b>SM2</b> with $n = 2$ , $\hat{\delta}_{\xi 2} = 0.02$ , $\tilde{\delta}_{\eta 2} = 0$ , $\tilde{\delta}_{\eta 4} = 0$ , $\hat{\mu}_a = 0.0083$ and various $\hat{\delta}_{\xi 4}$ : (A) -0.03 (B) -0.02 (C) -0.01 (D) 0.00 (E) 0.01 (F) 0.02 (G) 0.03	98
<b>5.6</b> The response bifurcation diagram for $n=2$ , $\tilde{\mu}_a=0.05$ , $\hat{\delta}_{\xi 2}=0.01$ , $\hat{\delta}_{\eta 2}=0.01$ , $\hat{\delta}_{\xi 4}=0$ and $\hat{\delta}_{\eta 4}=0$ . The solid lines represent stable solutions and the dashed lines represent unstable solutions	99
<b>5.7</b> The response bifurcation diagram of <b>SM2</b> for $n = 2$ , $\hat{\mu}_a = 0.0083$ , $\hat{\delta}_{\xi 2} = 0.02$ and $\hat{\delta}_{\xi 4} = 0.01$ , $\hat{\delta}_{\eta 4} = 0$ and various $\hat{\delta}_{\eta 2}$ : (A) 0.0 (B) 0.01 (C) 0.02	101
<b>5.8</b> The simulated and analytical responses on <b>SM2</b> for $n = 2$ , $\hat{\mu}_a = 0.0083$ , $\hat{\delta}_{\xi 2} = 0.02$ , $\hat{\delta}_{\xi 4} = 0.01$ , $\hat{\delta}_{\eta 2} = 0.005$ and $\hat{\delta}_{\eta 4} = 0.005$	103
<b>5.9</b> The absorber responses and rotor accelerations for $\hat{\Gamma}_{\theta} = 0.038, 0.055, 0.085,$ corresponding to points (A), (B), (C) and (D) in Figure 5.8, respectively	

6.1	The graphical interpretation of the distorted ellipsoids
6.2	The mode shapes of the steady-state solutions with various isotropy groups 122
<b>6.3</b> subgr	The stability and feasibility boundaries of the solutions with isotropy coup $S_2 \times S_2$ for $\hat{\Gamma}_{\theta} = 0.035$ , $\hat{\mu}_a = 0.005$ , $n = 2$ and $\nu = 0.1662$ 124
<b>6.4</b> subgr	The stability and feasibility boundaries of the solutions with isotropy coup $\mathbf{S_1} \times \mathbf{S_3}$ for $\hat{\Gamma}_{\theta} = 0.035$ , $\hat{\mu}_a = 0.005$ , $n = 2$ and $\nu = 0.1662$ 125
	The stability and feasibility boundaries of the solutions with isotropy coup $\mathbf{S_1} \times \mathbf{S_1} \times \mathbf{S_2}$ for $\hat{\Gamma}_{\theta} = 0.035$ , $\hat{\mu}_a = 0.005$ , $n = 2$ and $\nu = 0.1662$ 126
	The contours of the rotor accelerations for $\hat{\Gamma}_{\theta} = 0.035$ , $\hat{\mu}_{a} = 0.005$ , $n = 2$ $\nu = 0.1662$
	The feasible disturbing torque range of the $S_2 \times S_2$ solution branch for 0.005, $n=2$ and $\nu=0.1662128$
	The feasible disturbing torque range of the $S_1 \times S_3$ solution branch for 0.005, $n = 2$ and $\nu = 0.1662129$

## LIST OF TABLES

7	ľa	b	l	e

6.1	The solution	s branches	classified	by their	isotropy	subgroups	and their
mode:	shapes				. <b></b> .		12

# LIST OF APPENDICES

# **Appendix**

A.	THE EXPRESSIONS FOR $\frac{\partial H_1}{\partial \varphi_i}\Big _{s.s.}$ , $\frac{\partial H_2}{\partial \tau_i}\Big _{s.s.}$ , $\frac{\partial H_1}{\partial \varphi_j}\Big _{s.s.}$ and $\frac{\partial H_2}{\partial \tau_j}\Big _{s.s.}$	137
В.	ON THE EIGENVALUES OF $C$	138
C.	ON THE EIGENVALUES OF $[A + (N-1)B]$	140
D.	PROOF OF EQUATION (3.17)	142
E.	JUSTIFICATION OF $\tilde{\bar{\psi}}_i \simeq \tilde{\bar{\psi}}_j$ , $\forall \ 2 \leq i, j \leq N$	143
	PROOF OF $Trace[A + (N-2)B] < 0 \text{ AND } Det[A + (N-2)B] > 0 \text{ AS}$ $0^{+} \dots \dots$	
G.	THE LOW-ORDER APPROXIMATION OF $yy'(\theta)$	146
Н.	AVERAGED EQUATIONS IN CARTESIAN COORDINATES	148
I.	STABILITY OF SOLUTIONS ON SM1 <sup>+</sup>	150
J.	STABILITY OF SOLUTIONS ON SM2 <sup>+</sup>	151
Κ.	THE NUMERICAL ALGORITHM FOR COUPLED-MODE SOLUTIONS	152

#### CHAPTER 1

#### INTRODUCTION

Torsional vibrations in rotating systems are induced primarily by torques transmitted to a rotor from forces applied to attached components. For example, in internal combustion (IC) engines, cylinder gas pressure, friction and slider-crank inertia cause these torques, while in helicopter rotors aerodynamic loads on blades are the primary source. These torsional vibrations can propagate through the system and often cause fatigue and NVH (Noise, Vibrations and Harshness) difficulties. A centrifugal pendulum vibration absorber (CPVA) is a device used for reducing these torsional vibrations. It consists essentially of a mass that is restricted to move along a prescribed path relative to the base rotating system. The absorber is driven by the centrifugal field generated by rotation, and its motion provides a restoring torque which is designed to reduce torsional vibrations of the rotating system.

CPVA's were invented for the use in internal combustion engines as early as 1929 [5] and have been successfully employed to suppress torsional vibrations in light aircraft engines [27]. A number of previous works have concentrated on sizing the absorber inertia and designing the absorber path by analyzing the linear or nonlinear dynamics of the absorber system under a given order of excitation. All these designs are based on the following two assumptions: FIRST, each absorber system consists of only a single dynamic mass; SECOND, the absorber paths are exactly tuned and manufactured exactly as desired. The present study aims to re-assess the absorber performance along the lines of relaxing these two assumptions.

This chapter starts with an elaboration of the operation of CPVA's in section 1.1. In section 1.2, previous designs of the CPVA's are described in order to motivate the objectives of the present study, which are described in section 1.3. Finally, the organization of the rest of this dissertation is outlined in section 1.4.

#### 1.1 Operation of CPVA's

In a reciprocating internal combustion engine, combustion in the cylinders and inertial loads of the connecting rods and pistons generate oscillatory torques and forces that act on the crankshaft. These result in torsional oscillations of the crankshaft, which lead to several undesirable consequences, including vibration excitation of auxiliary components and fatigue failure. Several options are available to remedy this problem, including the addition of flywheels [60], torsional friction dampers [42, 27], or tuned vibration absorbers [44, 27]. These devices offer effective means of vibration reduction for rotating machines, and have the benefit of operating in an open loop manner, thus achieving a cost-favorable solution when compared to systems which employ sensors and actuators. However, each also has some shortcomings. The addition of a flywheel increases the total mass and rotational inertia of the system, thereby reducing system responsiveness. Torsional friction dampers consume energy and generate heat. Conventional tuned vibration absorbers that use elastic elements can be tuned only to a single frequency, and therefore are not useful except at one rotation rate, and may lead to detrimental effects at other rotation rates. Centrifugal pendulum vibration absorbers have many desirable features when compared to these solutions. Their main drawback is system complexity in terms of the number of moving components required.

In the following the basic operation of CPVA's is described through a particular implementation. The favorable features of the CPVA are then compared to the aforementioned devices.

Figure 1.1 shows one type of physical realization of CPVA's using a carrier assembly which, in application, is bolted onto a crankshaft at some location. This general

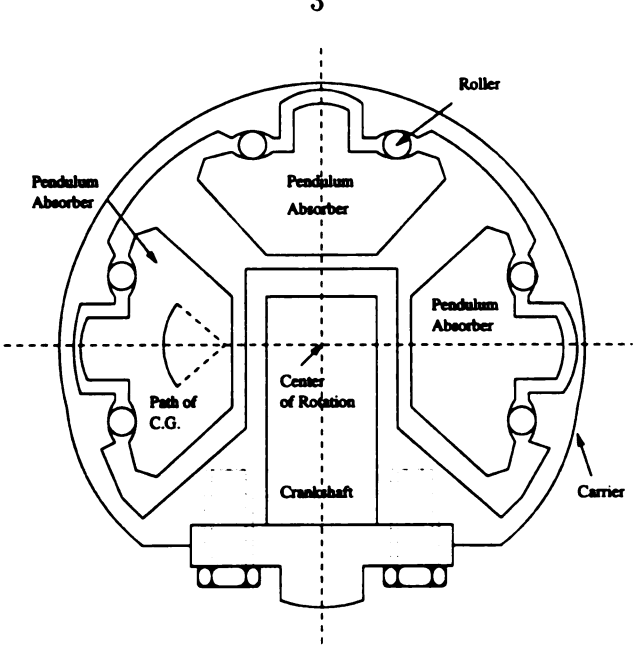


Figure 1.1: The CPVA carrier assembly from the cross-section view

configuration was employed by Borowski et al [3] for an experimental study on an automotive engine. This carrier contains three bifilar pendulums [27] which move relative to the carrier along a prescribed path as the crankshaft rotates. By using identical contact curves cut on the carrier and the absorber masses and using the circular rollers between them, the CPVA masses undergo pure translation relative to the carrier. Their centers of gravity (C.G.) will follow the path shown in Figure 1.1, which can be specified by the shape of the contact curves on the CPVA's and the carrier. Note that due to the pure translation of the CPVA's, the dynamic effect of the CPVA's on the crankshaft is equivalent to that of point masses moving along the the C.G. paths as shown in Figure 1.2, while their moments of inertia about their own C.G.'s simply add to the overall moment of inertia of the rotating system. As the CPVA's are driven by the rotation of the carrier, their motions provide restoring torques on the carrier which, when the absorber C.G. paths are properly designed, reduce the level of torsional oscillations of the crankshaft.

In the absorber configuration in Figure 1.1, the absorbers are used to replace

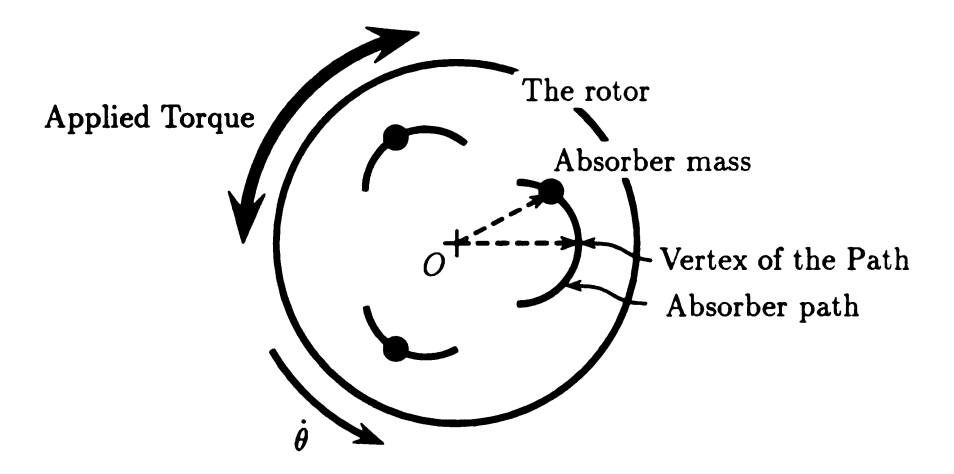


Figure 1.2: The Schematic diagram for the CPVA's and the rotor from the cross-section view.

the usual counterweights, and can thus be implemented without increasing the net mass or moment of inertia of the crankshaft. Hence, the absorber is considered to be favorable over a heavy flywheel for reducing torsional oscillations. In addition, since an insignificant amount of energy dissipated from the dynamic contact between the absorbers, rollers and the carriers, the absorber system generates much less heat than a friction damper during operation. Most importantly, the oscillating frequency of the CPVA can be tuned, by proper design of the paths, to be the same as that of the applied torque over a continuous range of rotation speeds, such that it renders much more efficient reduction on torsional vibrations than elastic, tuned vibration absorbers. The mechanism behind this favorable property of the CPVA is further elaborated in the following paragraph.

In most applications, the input torque for a rotating system can be considered as a nominal constant torque, which keeps the system running at a nominally constant speed,  $\Omega$ , plus a periodic fluctuating part whose base frequency is n times that of rotating system rotation; i.e.,  $n\Omega$ . Such a torque is referred to as a torque of order n, and this torque is typically approximated by its low-order harmonic components. As

shown in the derivation of the equations of motion for the CPVA system, one has the freedom to tune the linear oscillating frequency of the CPVA (the frequency of small amplitude motion) to  $n\Omega$  by designing the radius of curvature in the neighborhood of the path vertices. This unique feature of the CPVA is critical since, as the speed of the system varies, the torque generated by the motion of the CPVA always contains the frequency  $n\Omega$ , which is used to counteract that of the fluctuating component of the applied torque at all speeds.

#### 1.2 History and Literature Review

For a thorough history of the CPVA up to 1960, one can refer to [27]. A brief history including designs of interests for the present study is provided herein for a better understanding of the content of this dissertation.

In the earliest stage of CPVA development, implementation of the CPVA into the assembly of rotating systems drew the most attention. The first conceptual design of these absorbers can be dated back to 1911 when Kutzbach (as referred to Wilson in [27]) proposed a special mechanical arrangement which consists of moving fluid in U-shaped channels mounted in some component of the rotating system. Carter [5] in 1929 introduced a assembly consisting of absorber masses in roller-forms in a British Patent. In 1930, Meissner first demonstrated the effectiveness of the CPVA via experiments in a conference paper [33]. This study started an intensive development of CPVA arrangements over the next ten years in Europe. This included various inventions of the bifilar-and-roller suspensions of CPVA's by Sarazin [50, 51] and Salomon [49]. The Chilton and Reed Propeller Company [9] was also granted a patent in 1935 for a particular bifilar suspension system applied to radial aeroengines, which is believed to be the first implementation of the bifilar CPVA in industry. In the United States Taylor [61] introduced the CPVA in order to eliminate torsional vibrations of geared radial aircraft-engine-propeller systems. Moore [38]

in 1942 realized a design of the CPVA by incorporating it into the assembly of a crankshaft for various applications. Only the use of CPVA's allowed for the practical implementation of the light, but powerful aircraft engines used in many aircraft during World War II [66]. Without these CPVA's many of the most popular engines of that era could never have been put into service.

In the second stage, with the existing maturity of the hardware designs, tuning of the pendulum absorbers (riding on circular paths) and various applications became intensive research issues. Stieglitz [58] in 1938 identified the basis for pendulum tuning. Zdanowich and Wilson [69] refined the tuning basis of Stieglitz [58] in 1940. Meyer and Saldin [34] in 1942 presented an experimental study of absorbers applied to turbine blades. Harker [23] in 1944 lists charts and design guidelines for the absorber tuning. In 1949, Reed [48] pointed out the use of CPVA's for reduction of translational vibrations. Pluntkett [46] gives a short review on the usage of the CPVA up to 1953.

Most of the above studies were aimed at developing the tuning methods for absorbers riding on *circular* paths and were based on small amplitude, *linear theory*. Circular paths were widely used simply because they could be easily manufactured and the tuning methods are valid in the range of small oscillations. However, such designs often fail for moderate amplitude motions [41, 54] due to the fact that the pendulum frequency generally changes as a function of its amplitude (for example, it decreases as amplitude increases for the common circular path).

In the third stage, the research was extended to account for effects of nonlinear dynamics of the absorbers. *Large-amplitude motions* and the detrimental effects for circular paths were first discussed by Den Hartog [14] in 1938 and Porter [47] in 1945. Crossley in 1952 and 1953 gives more complete investigations of the associated undamped systems for free [12] and forced [13] responses, respectively. Newland [41] in 1964 identified possible catastrophic failure of circular paths due to the mistun-

ing of the CPVA. To solve this problem, both Den Hartog [14] and Newland [41] suggested that one can intentionally over-tune the linear oscillating frequency of the absorber so that it comes into a more favorable tuning for larger amplitudes. Most recently, the effects of damping, moderate amplitude motion and motion-limiting stops (snubbers) were studied by Sharif-Bakhtiar and Shaw [53, 52, 54]. Also, Shaw and Wiggins [57] found in 1988 that without motion-limiting stops, chaotic motions can exist for certain ranges of parameter values in a pendulum configuration which allows the absorber to undergo complete rotations.

Along another line of research in the third stage, efforts were dedicated to the reduction of torsional vibrations and shake forces in *helicopter rotors*. Kelley [26] in 1962 described the potential use of absorbers for reducing torsional vibrations of helicopter rotors. Paul [43] in 1969 recorded experimental data indicating significant success of the rotor absorbers for reducing vibrations of the helicopter mainframe. Wachs [64] in 1973 investigated the effects of the absorbers on helicopter reliability and maintainability by tracking repair costs over a period of time in helicopters with and without CPVA's. He found that CPVA's retrofitted to rotors saved an average of \$367,311 per aircraft per 10 years. Miao and Mouzakis [36] (1980) presented an experimental study of the nonlinear dynamics of the absorbers mounted on a rotor. Murthy and Hammond [40] (1981), Hamouda and Pierce [21] (1984) explored the use of absorbers for reducing vibrations of helicopter rotor blades. Recently, Wang et al. [65] investigated transverse vibration of rotating beams fitted with CPVA's. Also, shake reduction using multiple CPVA's has been studied by Miao and Mouzakis [35], Lim [31] and Cronin [11].

The bifilar suspension makes non-circular paths realizable. In the most recent stage, a number of works were devoted to the design and analyses of CPVA's riding on non-circular paths in order to improve performance of the absorbers at large amplitudes. As early as 1938, Bulter [4] recognized the potential value of noncircular

paths for absorber C.G.'s via bifilar suspensions. Madden [32] in 1980 first proposed cycloidal paths, which have favorable tuning behaviors at large amplitudes. Presumably Madden used the cycloidal path since it is known to be the solution of the tautochrone problem, that is, it offers the path for which a point mass, moving under a gravitational field, exhibits oscillations that are independent of the amplitude of motion. (Note that the solution of the tautochrone problem is identical to that of the more well-known brachristichrone problem [15].) This motivated an experimental study by Borowski and co-workers [3] that used absorbers riding on cycloidal paths, which was carried out by the Ford Motor Company. In this study, second-order absorbers were found to be effective in reducing the second-order torsional oscillations in an in-line, four-cylinder, four-stroke, 2.5L engine. However, the fourth-order oscillations were significantly magnified. The remedy offered for this problem was to use a combination of second and fourth order absorbers [3]. The cycloid does improve performance, but is not optimal in avoiding the mistuning problem [16, 56]. This follows since, in the centrifugal field, the force on a mass is not constant, as in a gravitational field, but is rather proportional to the radial distance from the center of rotation. The solution for the tautochronic path for this case is known to be a certain epicycloid [15, 68]. This tautochronic path enables the absorber to possess a constant oscillatory frequency, regardless of its amplitude of oscillation. Tuned to have the same frequency as the disturbing torque of order n, the motion of the absorber, said to be of order n, provides a periodic torque which counteracts most of the order n harmonic of the disturbing torque, thereby reducing torsional oscillations at that order. This promising property of the tautochronic paths launched theoretical studies [16, 11] which explored the effectiveness of epicycloid path, tautochronic, absorbers.

It should be noted at this point that all of the above absorber designs are capable of only partially counteracting the torsional vibrations that arise from a harmonic torque, even in an ideal setting [28, 29, 7, 6, 55]. There always exist residual vibrations, especially at higher order harmonics, that arise from nonlinear effects. However, Lee and Shaw [30] recently proposed a novel absorber design which consists of a pair of identical absorbers riding on special paths tuned to one — half the order of the disturbing torque. Such a configuration is referred to as the subharmonic absorber system. It was shown in [30] that the restoring torque generated by an ideal, perfectly tuned, undamped pair of subharmonic absorbers is exactly a pure harmonic over a wide range of amplitudes. This has significant potential advantages over conventional designs, since it generates no higher-harmonic torques, even when accounting for nonlinear effects. However, this type of absorber system has yet to be experimentally tested.

#### 1.3 Motivation

All designs stated in the last section for CPVA's are based on two assumptions: first, the absorber system used for addressing a given harmonic consists of only a single dynamic mass; second, the absorber paths are perfectly manufactured as desired.

In practice, it is necessary to choose the total absorber inertia to be sufficiently large such that the absorbers do not hit motion-limiting stops, or snubbers, under severe operating conditions. This is typically accomplished by stationing several absorber masses along and around the axis of rotation, which also is beneficial for balancing considerations. In addition, ideal path shapes can never be realized in practice. There always exist manufacturing tolerances, thermal and direct stress deformations, and distortions due to wear. The goal of the present study is to introduce a generic methodology that can be used to re-evaluate the performance of an absorber system by exploring the dynamics of a rotating system with multiple absorbers which follow paths that include imperfections and mistuning. The use

of this method is demonstrated herein through two cases of particular interest: (1) a system composed of a rigid rotor and N tautochronic absorbers, as proposed by Denman [16], and (2) multiple pairs of subharmonic absorbers as proposed by Lee et al [30].

#### 1.4 Organization of this Dissertation

Tha remainder of this dissertation is organized as follows. Chapter 2 covers the following topics that are common throughout the thesis: the mathematical forms of the path configurations are given; the assumptions on the system are listed; the equations of motion for general absorber paths are derived for a multiple absorber system; the symmetry characteristics of the system, which are critical in the analysis, are identified; two performance measures for an absorber system are defined; and characteristics of the absorber damping are described. In chapter 3, a stability criterion of the unison motion for a system of N multiple tautochronic absorbers of order n is derived. This is accomplished by using some scaling assumptions and transformations that massage the equations of motion into a form amenable to asymptotic analysis. In chapter 4, the performance of the tautochronic absorber system is re-assessed in the post-stable parameter range by carrying out a post-bifurcation analyses of the response. In chapter 5, the effects of imperfection and mistuning, and the nonlinear dynamics of a single pair of subharmonic absorbers proposed by Lee et al [30] are investigated in order to re-evaluate the absorber system performance. In chapter 6, the analysis in chapter 5 is extended to the case of multiple pairs of absorbers. In section 7 some conclusions and directions for future work are given.

#### CHAPTER 2

#### **PRELIMINARIES**

This chapter aims to establish a mathematical model based on some physical assumptions, which is followed by a description of limitations imposed on absorber motions, the characteristics of absorber dampings, and an identification of symmetry properties of the system. These results will be used in subsequent chapters.

#### 2.1 Assumptions

The equations of motion are derived for an idealized model that consists of a rigid rotor spinning about a fixed axis, subjected to an applied torque, and fitted with N general-path point-mass absorbers. The system is shown schematically by the cross sectional view of the rotor in Figure 2.1. This dynamical system consists of a rotor of moment of inertia  $I_d$  with respect to the center of rotation, O, and N absorbers moving freely on prescribed paths relative to the rotor. Each individual absorber, denoted by subscript i for the ith absorber, is considered to be a point mass with mass  $m_i$ . (In the common bifilar configuration, one can account for the moments of inertia of the absorbers about their respective C.G.'s by simply including them in  $I_d$ , since they rotate identically with the rotor.) The path for each absorber mass is specified by a function  $R_i = R_i(S_i)$ , where  $R_i$  is the distance from the C.G. of the absorber to point O and  $S_i$  is an arc-length variable measured along the path defined relative to a frame of reference that rotates with the rotor. The origin of each  $S_i$  is taken to be at the path vertex, that is, the point where  $R_i$  reaches its maximum value,  $R_{i0} = R_i(0)$ . The nominal moment of inertia for each absorber with respect

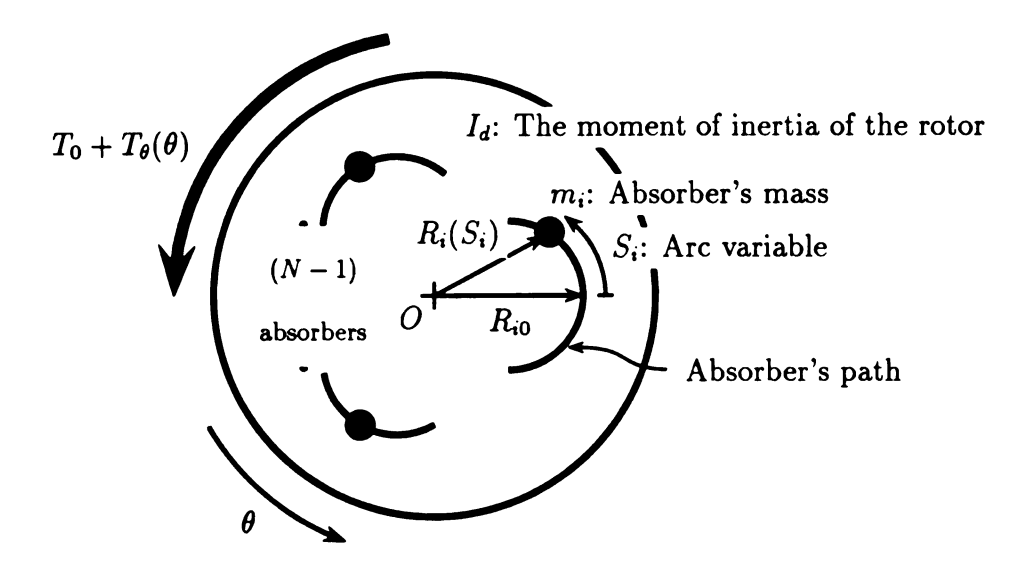


Figure 2.1: Cross-sectional schematic diagram of the rotor and absorbers.

to O is defined by  $I_i = m_i R_{i0}^2$ . The absorber path is designed to be symmetric with respect to  $S_i = 0$ ; i.e.,  $R_i(S_i) = R_i(-S_i)$ . The damping between the *i*th absorber and the rotor is assumed to be an equivalent viscous damping with coefficient  $c_{ai}$ . Resistance between the rotor and ground is also modeled as equivalent linear viscous damping, with coefficient  $c_0$ .

Let  $\theta$  denote the angular displacement of the rotor. The net applied torque (including load torques) is assumed to be a nominal constant,  $T_0$ , plus a disturbing torque  $T_{\theta}(\theta)$  which is periodic in  $\theta$ . These torques arise from a variety of sources, including attached linkages, etc., and are generally periodic with several harmonics. They may also depend on  $\dot{\theta}$  and  $\ddot{\theta}$ . Here a simple, single harmonic model for the applied torque is considered, as there is typically one dominant harmonic and the absorber system will be designed to address it. Thus, the disturbing torque is assumed to be of order n, as follows,  $T_{\theta}(\theta) = \hat{T}_{\theta}\sin(n\theta)$ , where  $\hat{T}_{\theta} > 0$ . (This leaves open the potentionally large issue of nonlinear resonances that may arise from other

harmonics in the excitation. This is left for future work, but see [29] for some results along these lines.)

#### 2.2 Equations of Motion

With these assumptions, the overall system kinetic energy can be formulated, which is given by

$$K.E. = \frac{1}{2} \left\{ I_d \dot{\theta}^2 + \sum_{i=1}^N m_i [X_i(S_i) \dot{\theta}^2 + \dot{S}_i^2 + 2G_i(S_i) \dot{\theta} \dot{S}_i] \right\}$$
(2.1)

where  $(\cdot)$  denotes  $\frac{d(\cdot)}{dt}$ , t is time and

$$X_i(S_i) = R_i^2(S_i)$$
 and  $G_i(S_i) = \sqrt{X_i(S_i) - \frac{1}{4}(\frac{dX_i}{dS_i}(S_i))^2}$ . (2.2)

In the expression for the kinetic energy (2.1),  $\frac{1}{2}I_d\dot{\theta}^2$  is the rotational energy of the rotor,  $\frac{1}{2}m_i[X_i(S_i)\dot{\theta}^2 + \dot{S}_i^2]$  is sum of the rotational energy relative the fixed frame and the translational energy relative to the rotating frame for the *i*th absorber, and the term  $2G_i(S_i)\dot{\theta}\dot{S}_i$  arises from Coriolis effects.

By considering the ratio  $g/(R_i\Omega^2)$ , it can be shown that gravitational effects are small compared to rotational effects for any reasonable rotating mechanical system. Then, by assuming that the corresponding potential energy is negligible, the governing equations of motion are determined by applying Lagrange's method to the kinetic energy and to the generalized forces associated with the dampings and the applied torque. The results are:

$$m_{i}[\ddot{S} + G_{i}(S_{i})\ddot{\theta} - \frac{1}{2}\frac{dX_{i}}{dS_{i}}(S_{i})\dot{\theta}^{2}] = -c_{ai}\dot{S}_{i}, \quad 1 \leq i \leq N$$

$$I_{d}\ddot{\theta} + \sum_{i=1}^{N} m_{i}[\frac{dX_{i}}{dS_{i}}(S_{i})\dot{S}_{i}\dot{\theta} + X_{i}(S_{i})\ddot{\theta} + G_{i}(S_{i})\ddot{S}_{i} + \frac{dG_{i}}{dS_{i}}(S_{i})\dot{S}_{i}^{2}]$$

$$= \sum_{i=1}^{N} c_{ai}G_{i}(S_{i})\dot{S}_{i} - c_{0}\dot{\theta} + T_{0} + \hat{T}_{\theta}\sin(n\theta), \qquad (2.3b)$$

where  $c_0$  and  $c_{ai}$  are damping coefficients for the rotor and the *i*th absorber respectively. Note that equation (2.3a) describes the dynamics of the *i*th absorber, which

are coupled to the dynamics of the rotor through the terms  $\ddot{\theta}$  and  $\dot{\theta}^2$ . Equation (2.3b) results from the dynamic balance among the applied torque  $T_0 + \hat{T}_{\theta}\sin(n\theta)$ , the rotor damping  $c_0\dot{\theta}$ , the damping and resistive torques caused by the motions of all absorbers — as described in the two summation terms, respectively — and the inertial resistance of the rotor  $I_d\ddot{\theta}$ .

A nondimensionalization and a change of independent variable are performed on the equations of motion for simplification. To facilitate this process, the nominal steady-state rotational speed of the rotor,  $\Omega$ , is taken to be the speed at which the constant torque  $T_0$  balances the mean component of the torque which arises from rotational damping friction; thus,

$$\Omega = \frac{T_0}{c_0}. (2.4)$$

Also, a new dimensionless dependent variable y, representing the rotor speed, is defined as

$$y \equiv \frac{\dot{\theta}}{\Omega}.\tag{2.5}$$

Then, assuming that  $\theta$  is a smooth and invertible function of t, applying the chain rule and using (2.5), one can obtain the following relationships between derivatives with respect to t and  $\theta$ ,

$$\ddot{\theta} = \Omega^2 y y', \quad (\dot{\cdot}) = \Omega y(\cdot)' \quad \text{and} \quad (\ddot{\cdot}) = \Omega^2 y y'(\cdot)' + \Omega^2 y^2(\cdot)'', \quad (2.6)$$

where  $(\cdot)'$  denotes  $\frac{d(\cdot)}{d\theta}$ . With the relationships (2.5) and (2.6), the resulting equations of motion (2.3) can be transformed into a set of periodically forced, non-autonomous equations with the independent variable  $\theta$  replacing t. This step transforms the nonlinearity,  $\hat{T}_{\theta}\sin(n\theta)$ , into a periodic forcing term.

The following steps are then performed: the equations of motion are transformed to the form that has  $\theta$  as the independent variable; they are divided through by the inertia terms,  $m_i$  and  $I_d$ , respectively, and by  $\Omega^2$ ; and the absorber displacement  $S_i$ 

rescaled in terms of  $R_{io}$ . The resulting dynamical system that describes the dynamics of the N absorbers and the rotor are then given as follows,

$$ys_{i}'' + [s_{i}' + g_{i}(s_{i})]y' - \frac{1}{2}\frac{dx_{i}}{ds_{i}}(s_{i})y = -\hat{\mu}_{ai}s_{i}', \quad 1 \leq i \leq N,$$

$$\sum_{i=1}^{N} b_{i} \left[\frac{dx_{i}}{ds_{i}}s_{i}'y^{2} + x_{i}(s_{i})yy' + g_{i}(s_{i})s_{i}'yy' + g_{i}(s_{i})s_{i}''y^{2} + \frac{dg_{i}(s_{i})}{ds_{i}}s_{i}'^{2}y^{2}\right]$$

$$+yy' = \sum_{i=1}^{N} b_{i}\hat{\mu}_{ai}g_{i}(s_{i})s_{i}'y - \hat{\mu}_{0}y + \Gamma_{0} + \hat{\Gamma}_{\theta}\sin(n\theta)$$

$$(2.7b)$$

where  $(\cdot)'$  denotes  $\frac{d(\cdot)}{d\theta}$ ,  $s_i = \frac{S_i}{R_{i0}}$ ,  $b_i = \frac{I_i}{I_d}$ ,  $\hat{\mu}_{\alpha i} = \frac{c_{\alpha i}}{m_i \Omega}$ ,  $\hat{\mu}_0 = \frac{c_0}{I_d \Omega}$ ,  $\Gamma_0 = \frac{T_0}{I_d \Omega^2}$ ,  $\hat{\Gamma}_\theta = \frac{\hat{T}_\theta}{I_d \Omega^2}$ , and

$$x_i(s_i) = \frac{R_i^2(R_{i0} \ s_i)}{R_{i0}^2}$$
 and  $g_i(s_i) = \sqrt{x_i(s_i) - \frac{1}{4} \left(\frac{dx_i}{ds_i}(s_i)\right)^2}$ , (2.8)

are functions set by the path of the absorber C.G. Note that in terms of these dimensionless quantities, the steady rotation condition (2.4) becomes

$$\Gamma_0 = \hat{\mu}_0. \tag{2.9}$$

#### 2.3 The Absorber System

It is assumed that the system is composed of N absorbers with identical individual masses  $m_i = \frac{m_0}{N}$  and identical damping coefficients  $\hat{\mu}_{ai} = \hat{\mu}_a$  for each i. Two different absorber systems will be considered in the subsequent investigations. The first system consists of N tautochronic absorbers riding on standard epicyloids tuned to order n (the same as the order of the applied torque), which can be specified in the ideal case by

$$x_i(s_i) = 1 - n^2 s_i^2$$
, with  $R_{i0} = R_0$  for each i. (2.10)

The second is composed of N tautochronic absorbers riding on subharmonic epicyloids tuned to order  $\frac{n}{2}$  (one-half the order of the applied torque), which can be
specified in the ideal case by

$$x_i(s_i) = 1 - \left(\frac{n}{2}\right)^2 s_i^2 \text{ with } R_{i0} = R_0 \text{ for each } i.$$
 (2.11)

Note that the path functions (2.10) and (2.11) presented herein assume that the paths are perfectly manufactured as desired. The formulation of imperfections will be introduced in section 5.1.2, particularly for the subharmonic absorber system.

The equations of motion for a system with N identical absorbers is then given by

$$ys_{i}'' + [s_{i}' + g_{i}(s_{i})]y' - \frac{1}{2}\frac{dx_{i}}{ds_{i}}(s_{i})y = -\hat{\mu}_{a}s_{i}', \quad 1 \leq i \leq N, \quad (2.12a)$$

$$\frac{\nu}{N} \sum_{i=1}^{N} \left[\frac{dx_{i}}{ds_{i}}s_{i}'y^{2} + x_{i}(s_{i})yy' + g_{i}(s_{i})s_{i}'yy' + g_{i}(s_{i})s_{i}''y^{2} + \frac{dg_{i}(s_{i})}{ds_{i}}s_{i}'^{2}y^{2}\right]$$

$$+ yy' = \frac{\nu}{N} \sum_{i=1}^{N} \hat{\mu}_{a}g_{i}(s_{i})s_{i}'y - \hat{\mu}_{0}y + \Gamma_{0} + \hat{\Gamma}_{\theta}\sin(n\theta) \quad (2.12b)$$

where  $I_0 = m_0 R_0^2$ , and  $\nu = \frac{I_0}{I_d}$ .

It will be shown in section 3.1 that the standard epicycloidal paths tune the oscillating frequency of each absorber to be equal to that of the disturbing torque, even when the absorbers undergo large motions. This favorable property motivates the investigation on this type of path. Also, the subharmonic epicycloidal paths tune the oscillating frequency of each absorber to be one-half that of the disturbing torque, again over a large amplitude range. The merits of this path design will be further elaborated in section 5.1.

Also, it should be noted that in practice, the inertia of the entire absorber system is much smaller than that of the overall rotary system, typically on the order of 1%-10%. This implies that  $\nu$  is generally a small parameter in these systems.

#### 2.4 Limitations on Absorber Motions

The value of the function  $g_i(s_i)$  must be kept real during absorber motions, and this leads to a restriction on the amplitudes of the absorber motions, given by

$$x_i(s_i) - \frac{1}{4} \left( \frac{dx_i}{ds_i}(s_i) \right)^2 > 0, \quad \forall \theta \text{ and } i.$$
 (2.13)

This restriction keeps the absorber from passing any cusp point that may exist on the path. For example, the epicycloid and cycloid paths have cusps at fairly large amplitudes. The explicit form for the right-hand-side of equation (2.13) depends on the type of the absorber path used, which will be derived for each particular absorber path considered in the ensuing analyses. Note that since the absorber amplitude grows as the torque level is increased, the restriction in inequality (2.13) imposes a finite operating range on the disturbing torque level, which is an important measure of the absorber system performance.

#### 2.5 Absorber Dampings

A discussion of the damping models employed in the equations of motion is pertinent at this point. The damping on the main rotor system and the mean torque simply set the nominal speed and play no other vital role in the the system dynamics. However, the damping in the absorbers plays a central role in the performance of the system, and this is a notoriously difficult effect to qualitatively determine or quantitatively measure. First, the source of the damping is complicated and depends on the specifics of how the absorbers are implemented. Some sources of damping include: rolling resistance, resistance due to movement through oil-saturated air, slippage, and pumping of fluid. Second, even if one knows the basic damping mechanisms, the physical constants are difficult to measure and they will vary with operating conditions (such as temperature). We have assumed a form of equivalent viscous damping in our equations, and will consider two different types of damping, viscous and hysteretic. Note that if the damping is viscous, the associated coefficient  $c_a$  (herein we assume that  $c_{ai} = c_i$  for each i) in equation (2.3a) is assumed to be independent of the mass of the absorber, as in the linear case, then

$$\hat{\mu}_a = \frac{Nc_a}{m_0\Omega} \tag{2.14}$$

which shows that the nondimensional "effective" damping coefficient  $\hat{\mu}_a$  is proportional to the number of absorbers. However, an experimental result given by (Cronin [11], 1992) indicates that there exists a hysteretic damping factor that is independent of the absorber mass, implying that  $c_a$  is proportional to mass of the absorber. Therefore,  $\frac{c_a}{m_i}$  is a constant in this case. According to this result, introducing the quantity  $c_{a0}$  as the coefficient for a single absorber, we can express  $\hat{\mu}_a$  as

$$\hat{\mu}_a = \frac{c_{a0}}{m_0 \Omega},\tag{2.15}$$

which renders the damping ratio to be independent of the number of absorbers.

#### 2.6 Symmetry Identification

Intuitively, due to the identical nature of each absorber, it is expected that the system described by equations (2.12a) and (2.12b) will enjoy some special properties. These properties can be mathematically characterized by transformations among the state variables that yield new sets of system equations which are both structurally and mathematically invariant from the original system equations. Such transformations are symmetries of the system. Identifying the symmetry of the system allows one to search for and characterize many solutions in an efficient way. To mathematically characterize the symmetries of the system, conventional notation from group theory is employed. (See [20] for details.) Let

$$\dot{x} = h(x, \lambda) \tag{2.16}$$

be a system of first-order differential equations, where x is a generalized state vector,  $\lambda$  is a system parameter, and  $h: \mathbf{R}^k \times \mathbf{R} \to \mathbf{R}^k$ , is a smooth transformation. Let  $\gamma$  be an invertible  $k \times k$  matrix representing a transformation among the state variables. It is said that  $\gamma$  is a symmetry of the system (2.16) if

$$h(\gamma x, \lambda) = \gamma h(x, \lambda) \quad \forall x \in \mathbf{R}^{\mathbf{k}}.$$
 (2.17)

It can be shown that system (2.16) is invariant subject to  $\gamma$  if equation (2.17) is satisfied.

If there exists a group G such that the equation (2.17) is satisfied for each  $\gamma \in G$ , then G is called a symmetry group of the system, or, equivalently, that the function h is called G-equivariant. To identify the symmetry group of the present model, first consider equation (2.12b), which describes the dynamics of the rotor. It is seen that the speed of the rotor,  $y(\theta)$ , is invariant subject to any permutation among the absorbers. Furthermore, from equation (2.12a), it can be confirmed that each absorber is coupled with all other absorbers only through y. Therefore, any permutation of absorbers should result in a system that is indistinguishable from the original. One can easily transform equations (2.12a) into 2N first-order differential equations and use condition (2.17) to show that the symmetry group of the system is  $S_N$ , known as the "symmetric group", which is a group containing all permutations on N symbols [18].

Based on group theory [20], there exist invariant subspaces in the absorber system due to the embedding symmetry  $S_N$ . A partition of particular utility in the present work is offered by splitting the phase space into components that capture the unison, or synchronous, response of the system, and its complement. In mathematical terms, we define

$$\mathbf{V} = \{ \mathbf{s} \in \mathbf{R}^{\mathbf{N}} \mid \mathbf{s} = [v, v, ..., v]^T \} \quad \text{and} \quad \mathbf{W} = \mathbf{R}^{\mathbf{N}} - \mathbf{V}$$
 (2.18)

where V is the subspace spanned by the unison mode and W is its complement. For any given initial conditions  $s(0) \in V$  or  $s(0) \in W$ , the system dynamics will stay in V or W, respectively, for all time.

It should be pointed out that bifurcations in systems with this level of symmetry can be extremely rich. In fact, due to the fact that many eigenvalues associated with **W** are identical, and thus may become simultaneously unstable (which is always true for perfect abosorber system), the corresponding bifurcation problem is highly

degenerate and there may exist numerous branches of solutions emanating from a single bifurcation point. It is not always possible to determine all these branches, let alone their stability types. In the present study, measures of absorber performance are used in conjunction with symmetric bifurcation theory in order to get a handle on the most important branches, and in particular, the dynamically stable ones that define and limit the post-bifurcation steady-state system behavior.

#### 2.7 Measures of Absorber Performance

Two measures will be used to quantify the effectiveness of an absorber system. The first is the amplitude of torsional oscillations of the rotor, here represented by its peak angular acceleration. The nondimensionalized angular acceleration of the rotor is given by  $\ddot{\theta}(t)/\Omega^2$ , and is represented in terms of the variable  $y(\theta)$  by  $yy'(\theta)$ . The corresponding measure of absorber performance is given by the peak value (that is, the infinity norm) of  $yy'(\theta)$  during a steady-state response. This quantity is denoted by  $||yy'||_{SS}$ .

The second performance measure used is the range of the applied torque amplitude over which the absorber can operate, denoted by  $\tilde{\Gamma}_{\theta}$ . This is imposed by the limiting cusps on the absorber paths, as stated in condition (2.13) above. (It should be noted that in practice, the geometry of the bifilar configuration commonly used when implementing these absorbers will impose even stricter limits than those given by the cusp.)

The general aim of an absorber system is to minimize  $||yy'||_{ss}$  over the largest possible range,  $0 < \hat{\Gamma}_{\theta} < \bar{\hat{\Gamma}}_{\theta}$ . It will be seen that these goals oppose one another, and the information obtained from the present study can be used to make informed judgments for the selection of the number of absorbers and the path parameters.

## **CHAPTER 3**

# STABILITY OF THE UNISON RESPONSE FOR A ROTATING SYSTEM WITH MULTIPLE TAUTOCHRONIC ABSORBERS

Due to spatial and balancing considerations, the implementation of CPVA's invariably requires that the total absorber mass be divided into several absorber masses that are stationed about the center of rotation and along the rotating shaft. In order to achieve the designed-for performance, a system of like-tuned, identical CPVA's is assumed to move in an exact unison response. However, due to nonlinear dynamic effects, the absorbers may undergo non-unison steady-state motions, even under a moderate level of applied torque. The study in this chapter and the next is an investigation of the dynamic stability and bifurcation of the unison response of a system of identical CPVA's operating on a rotating system.

This chapter is organized as follows. Section 3.1 gives a preparation for asymptotic analysis by re-arranging the equations of motion into a form of N weakly-coupled and weakly-nonlinear oscillators. This special formulation will also be utilized in chapter 4 for further investigation of post-bifurcation responses. Section 3.2 presents a derivation of a stability criterion for the unison motion. It indicates that for small levels of absorber damping (a condition required for satisfactory performance), the critical torque level is proportional to the square root of the absorber damping level.

#### 3.0 Equations of Motion

Results in this and the next chapter are obtained under the assumptions that the absorber paths for the N identical absorbers are tuned epicycloids of order n (Denman [16], 1992). These paths are specified by

$$x_i(s_i) = 1 - n^2 s_i^2, \ 1 \le i \le N. \tag{3.1}$$

Applying the path configuration (3.1) into equations (2.12) yields the equations of motion which describe the dynamics of the rotor and N absorbers riding on epicycloids of order n, as follows,

$$ys_{i}'' + [s_{i}' + g(s_{i})]y' + n^{2}s_{i}y = -\hat{\mu}_{a}s_{i}', \quad 1 \leq i \leq N, \quad (3.2a)$$

$$\frac{\nu}{N} \sum_{i=1}^{N} [-2n^{2}s_{i}s_{i}'y^{2} + (1-n^{2}s_{i}^{2})yy' + g(s_{i})s_{i}'yy' + g(s_{i})s_{i}''y^{2} + \frac{dg(s_{i})}{ds_{i}}s_{i}'^{2}y^{2}]$$

$$+ yy' = \frac{\nu}{N} \sum_{i=1}^{N} \hat{\mu}_{a}g(s_{i})s_{i}'y - \hat{\mu}_{0}y + \Gamma_{0} + \hat{\Gamma}_{\theta}\sin(n\theta) \quad (3.2b)$$

where

$$g(s_i) = \sqrt{1 - (n^2 + n^4)s_i^2}, \ \frac{dg(s_i)}{ds_i} = \frac{-(n^2 + n^4)s_i}{\sqrt{1 - (n^2 + n^4)s_i^2}}.$$
 (3.3)

Note that the value of the function  $g(s_i)$  must be kept real during absorber motions, and this leads to a restriction on the amplitudes of the absorber motions, given by

$$s_i(\theta) \le s_{\text{max}} = \frac{1}{n\sqrt{n^2 + 1}}, \quad \forall \ \theta \text{ and} \forall i.$$
 (3.4)

#### 3.1 Scaling and Reduction of the Equations of Motion

Approximate steady-state solutions of the system are sought by making some scaling assumptions and employing asymptotic analysis techniques. A series approximation for the equations of motion is derived below, and this leads to a form that is amenable to asymptotic analysis.

#### 3.1.1 Scaling Assumptions

In applications the total nominal moment of inertia of all absorbers about point O is much smaller than that of the entire rotating system. This motivates the definition of the small parameter,

$$\epsilon \equiv \nu,$$
 (3.5)

the ratio of absorber inertia to rotor inertia, which is used for the asymptotic analysis. With this definition, many of the system parameters can be scaled such that the desired system behavior can be captured by asymptotic analysis.

It is assumed that the nondimensional damping and excitation parameters,  $\hat{\mu}_a$ ,  $\hat{\mu}_0$ ,  $\hat{\Gamma}_0$  and  $\hat{\Gamma}_{\theta}$ , are also small such that they can be scaled as follows:

$$\hat{\mu}_a = \epsilon \tilde{\mu}_a, \qquad \hat{\mu}_0 = \epsilon \tilde{\mu}_0, \qquad \Gamma_0 = \epsilon \tilde{\Gamma}_0, \quad \text{and} \quad \hat{\Gamma}_\theta = \epsilon \tilde{\Gamma}_\theta.$$
 (3.6)

The unperturbed system dynamics for this scaling are determined by considering equation (3.2b) with  $\epsilon = 0$ , that is,  $\nu = 0$ , which yields y = 1. Using this in equation (3.2a) with  $\hat{\mu}_a = 0$  yields a linear oscillator with frequency n for the absorber motion. Thus, the steady-state solution of the unperturbed system is simply a constant rotor speed, y = 1, and the absorber motion is harmonic with frequency n and arbitrary amplitude. This limiting case can be imagined as that with a very large flywheel attached to the rotor, in which the absorbers move in a harmonic manner but have no effect on the rotor.

Since the rotor speed will change smoothly as the absorber mass, the applied torque and the absorber damping are increased from zero, y will be smooth in  $\epsilon$  and can be expanded as follows,

$$y(\theta) = 1 + \epsilon y_1(\theta) + \mathcal{O}(\epsilon^2), \tag{3.7}$$

where  $y_1$  captures the speed fluctuations induced by the net interaction of the applied torque, damping effects, and the torques induced by the motions of the absorbers.

Note that condition (2.9) is assumed to maintain as  $\epsilon$  is increased from zero, thereby keeping the mean rotational rate near y = 1.

#### 3.1.2 The Rotor Angular Acceleration

It is convenient to have an explicit expression for the rotor acceleration, since it is a measure of the torsional vibration amplitude of the rotor. This can be derived by first noting that since  $\epsilon \ll 1$  and  $y_1$  is bounded,  $y(\theta)$  oscillates about unity and is never zero. Therefore, equation (3.2a) can be divided through by y in order to obtain an expression for  $s_i''$  in terms of  $s_i$ ,  $s_i'$  and y. Substitution of this expression into equation (3.2b) and utilization of equation (2.8) gives an exact expression for  $yy'(\theta)$ , as follows,

$$yy'(\theta) = \left[1 + \frac{\nu}{N} \sum_{i=1}^{N} n^4 s_i^2\right]^{-1} \left[ -\hat{\mu}_0 y + \Gamma_0 + \hat{\Gamma}_{\theta} \sin(n\theta) + \frac{\nu}{N} \sum_{i=1}^{N} \left( 2n^2 s_i' s_i y^2 - \frac{dg(s_i)}{ds_i} s_i'^2 y^2 + n^2 s_i g(s_i) y^2 + 2\hat{\mu}_a s_i' g(s_i) y \right) \right] (3.8)$$

Utilizing the definition  $\epsilon \equiv \nu$ , the scalings in equation (3.6), the expansion in (3.7), and condition (2.9), a series approximation for yy' in terms of  $\epsilon$  can be obtained as follows,

$$yy'(\theta) = -\epsilon \left\{ \frac{1}{N} \sum_{j=1}^{N} (-2n^{2}s_{j}s'_{j} - n^{2}g(s_{j})s_{j} + \frac{dg(s_{j})}{ds_{j}}s'^{2}_{j}) - \tilde{\Gamma}_{\theta}\sin(n\theta) \right\} + \mathcal{O}(\epsilon^{2}).$$
(3.9)

The above equation shows that the nondimensionalized angular acceleration is of order  $\epsilon$ , a result consistent with the known limiting case as  $\epsilon \to 0$ .

#### 3.1.3 The Absorber Dynamics

The method of averaging is used in the next section to determine the dynamic response for  $0 < \epsilon \ll 1$ . To obtain equations in the correct form for the application

of averaging, some modifications of the equations of motion are carried out. First, based on the expansions in equations (3.7) and (3.9), one can show that  $\frac{y'}{y}$  is the same as yy' to leading order in  $\epsilon$ . Then by dividing equation (3.2a) through by y, a modified equation describing the absorber dynamics is obtained, into which the  $\epsilon$ -series approximation of  $\frac{y'}{y}$  is substituted. Expanding the result in terms of  $\epsilon$  yields a set of weakly coupled, weakly nonlinear oscillators for the absorber dynamics. These oscillators, in which the dynamics of the rotor has been eliminated to first order, are as follows,

$$s_{i}'' + n^{2}s_{i} = \epsilon f_{i}(s_{1}, ..., s_{N}, s_{1}', ..., s_{N}', \theta) + \mathcal{O}(\epsilon^{2}), \qquad 1 \leq i \leq N \quad (3.10)$$

where

$$f_{i}(s_{1},...,s_{N},s_{1}^{'},...,s_{N}^{'},\theta) = -\tilde{\mu}_{a}s_{i}^{'} + [s_{i}^{'}+g(s_{i})][\frac{1}{N}\sum_{j=1}^{N}(-2n^{2}s_{j}s_{j}^{'}-n^{2}g(s_{j})s_{j}+\frac{dg(s_{j})}{ds_{j}}s_{j}^{'2}) -\tilde{\Gamma}_{\theta}\sin(n\theta)].$$

#### Remarks:

- These equations are weakly coupled. The weak coupling arises due to the fact that the absorbers are not directly coupled in a physical sense, but only indirectly so through the rotor, and each absorber has only a small effect on the rotor due to its small relative inertia.
- The equations of motion are weakly nonlinear, even though the amplitude of motion of the absorbers is not assumed to be small. The weak nonlinearity is due to the epicycloidal path used for the absorbers, which renders a linear equation of motion valid for all feasible absorber amplitudes when the rotor speed is constant. Again, due to the relative smallness of the absorbers' inertias, the rotor speed is nearly constant (cf. equations (3.7)), rendering nearly linear equations of motion.

• The symmetry  $S_N$  is evident in equations (3.10), as the absorbers appear in a completely interchangeable manner.

#### 3.2 The Averaged Equations

The method of averaging is employed to analyze these equations. To this end, the following transformation to amplitude and phase variables is introduced,

$$s_i = a_i \cos(\phi_i - n\theta), \quad s_i' = n a_i \sin(\phi_i - n\theta), \quad 1 \le i \le N,$$

where  $a_i$  and  $\phi_i$  are slowly-varying due to the form of equation (3.10). Substituting the above transformations into equation (3.10), a set of ODE's are derived which govern the dynamics of  $a_i$  and  $\phi_i$ , of the form,

$$\frac{da_{i}}{d\theta} = \frac{\epsilon}{n} f_{i} \left( a_{1} \cos(\phi_{1} - n\theta), \dots, a_{N} \cos(\phi_{N} - n\theta) \right),$$

$$na_{1} \sin(\phi_{1} - n\theta), \dots, na_{N} \sin(\phi_{N} - n\theta) \right) \sin(\phi_{i} - n\theta) + \mathcal{O}(\epsilon^{2})$$

$$\frac{d\phi_{i}}{d\theta} = \frac{\epsilon}{na_{i}} f_{i} \left( a_{1} \cos(\phi_{1} - n\theta), \dots, a_{N} \cos(\phi_{N} - n\theta) \right),$$

$$na_{1} \sin(\phi_{1} - n\theta), \dots, na_{N} \sin(\phi_{N} - n\theta) \right) \cos(\phi_{i} - n\theta) + \mathcal{O}(\epsilon^{2}). \quad (3.11)$$

We now average the first order terms in the R.H.S. above over one period of the excitation,  $\frac{2\pi}{n}$ . The resulting averaged equations are expressed in terms of the new variables  $r_i$  and  $\varphi_i$ , (that is, the first order averaged quantities of  $a_i$  and  $\phi_i$ , respectively), as follows,

$$\frac{dr_{i}}{d\theta} = \epsilon \left\{ \frac{-1}{2} \tilde{\mu}_{a} r_{i} + \frac{\tilde{\Gamma}_{\theta}}{n} \cos \varphi_{i} F_{1}(r_{i}) + \frac{1}{N} \sum_{j \neq i} \left[ \frac{1}{4} n^{3} r_{i} r_{j}^{2} \sin(2\alpha_{ji}) - n r_{j} G_{1}(r_{i}, r_{j}, \alpha_{ji}) - n (n^{2} + n^{4}) r_{j}^{3} H_{1}(r_{i}, r_{j}, \alpha_{ji}) \right] \right\} 
+ \mathcal{O}(\epsilon^{2}) 
\frac{d\varphi_{i}}{d\theta} = \epsilon \left\{ \frac{-\tilde{\Gamma}_{\theta}}{n r_{i}} \sin \varphi_{i} F_{2}(r_{i}) + \frac{1}{N} \left( \frac{1}{4} n^{5} r_{i}^{2} - \frac{1}{2} n \right) \right. 
\left. + \frac{1}{N} \sum_{j \neq i} \left[ \frac{-1}{4} n^{3} r_{j}^{2} \cos(2\alpha_{ji}) - \frac{n r_{j}}{r_{i}} G_{2}(r_{i}, r_{j}, \alpha_{ji}) - n (n^{2} + n^{4}) \frac{r_{j}^{3}}{r_{i}} H_{2}(r_{i}, r_{j}, \alpha_{ji}) \right] \right\} 
+ \mathcal{O}(\epsilon^{2})$$
(3.12)

where

$$\begin{split} \alpha_{ji} &= \varphi_{j} - \varphi_{i}, \\ F_{1}(r_{i}) &= \frac{1}{2\pi} \int_{0}^{2\pi} \sin^{2}x [1 - (n^{2} + n^{4})r_{i}^{2}\cos^{2}x]^{\frac{1}{2}} dx, \\ F_{2}(r_{i}) &= \frac{1}{2\pi} \int_{0}^{2\pi} \cos^{2}x [1 - (n^{2} + n^{4})r_{i}^{2}\cos^{2}x]^{\frac{1}{2}} dx, \\ G_{1}(r_{i}, r_{j}, \alpha_{ji}) &= \frac{1}{2\pi} \int_{0}^{2\pi} \cos(x) \sin(x - \alpha_{ji}) [1 - (n^{2} + n^{4})r_{j}^{2}\cos^{2}x]^{\frac{1}{2}} \\ & [1 - (n^{2} + n^{4})r_{i}^{2}\cos^{2}(x - \alpha_{ji})]^{\frac{1}{2}} dx, \\ G_{2}(r_{i}, r_{j}, \alpha_{ji}) &= \frac{1}{2\pi} \int_{0}^{2\pi} \cos(x) \cos(x - \alpha_{ji}) [1 - (n^{2} + n^{4})r_{j}^{2}\cos^{2}x]^{\frac{1}{2}} \\ & [1 - (n^{2} + n^{4})r_{i}^{2}\cos^{2}(x - \alpha_{ji})]^{\frac{1}{2}} dx, \\ H_{1}(r_{i}, r_{j}, \alpha_{ji}) &= \frac{1}{2\pi} \int_{0}^{2\pi} \cos(x) \sin^{2}(x) \sin(x - \alpha_{ji}) [\frac{1 - (n^{2} + n^{4})r_{i}^{2}\cos^{2}(x - \alpha_{ji})}{1 - (n^{2} + n^{4})r_{j}^{2}\cos^{2}x}]^{\frac{1}{2}} dx, \\ H_{2}(r_{i}, r_{j}, \alpha_{ji}) &= \frac{1}{2\pi} \int_{0}^{2\pi} \cos(x) \sin^{2}(x) \cos(x - \alpha_{ji}) [\frac{1 - (n^{2} + n^{4})r_{i}^{2}\cos^{2}(x - \alpha_{ji})}{1 - (n^{2} + n^{4})r_{i}^{2}\cos^{2}(x - \alpha_{ji})}]^{\frac{1}{2}} dx. \end{split}$$

These equations govern the first-order, slow-time dynamics of the absorber motions, from which the first-order rotor dynamics can be obtained from equation (3.9). While these equations cover quite general motion, the present interest is in the existence and stability of the important unison motion of the absorbers, to which we now turn.

## 3.3 Stability Criterion

In order to express the unison steady-state solution for the averaged equations (3.12), we introduce new variables r and  $\varphi$  as the steady-state amplitude and phase of unison oscillation, respectively. When the system undergoes unison motions,

$$r_i = r, \qquad \varphi_i = \varphi \qquad \text{for } 1 \le i, j \le N$$
 (3.13)

The steady versions of equations (3.12) can be solved for  $\sin(\varphi)$  and  $\cos(\varphi)$  (since all

 $\alpha_{ji} = 0$ ). Using  $\sin^2(\varphi) + \cos^2(\varphi) = 1$  it can be shown that r and  $\varphi$  must satisfy

$$\tilde{\Gamma}_{\theta} = nr \sqrt{\left(\frac{\tilde{\mu}_a}{2F_1(r)}\right)^2 + \left(\frac{n^5 r^2 - 2n}{4F_2(r)}\right)^2}$$
 and (3.14)

$$\tan \varphi = \left(\frac{n^5 r^2 - 2n}{2\tilde{\mu}_a}\right) \left(\frac{F_1(r)}{F_2(r)}\right). \tag{3.15}$$

The amplitude r can be numerically solved using equation (3.14) and then  $\varphi$  can be easily calculated by equation (3.15). To determine the stability of this response, the Jacobian matrix of the averaged equations (3.12) is evaluated at the unison steady-state solution. Due to the symmetry of the system and this motion, this Jacobian C has the particular form

$$C_{2N\times 2N} = \begin{bmatrix} A_{2\times 2} & B_{2\times 2} & . & B_{2\times 2} \\ B_{2\times 2} & A_{2\times 2} & . & B_{2\times 2} \\ . & . & . & B_{2\times 2} \\ B_{2\times 2} & B_{2\times 2} & B_{2\times 2} & A_{2\times 2} \end{bmatrix}$$
(3.16)

where the entries of the  $2 \times 2$  matrices A and B are given by

$$A_{11} = \frac{-1}{2}\tilde{\mu}_{a} + \frac{1}{2}\tilde{\mu}_{a}rF_{1}(r)^{-1}\frac{\partial F_{1}(r)}{\partial r}$$

$$A_{12} = F_{1}(r)F_{2}(r)^{-1}r\left(\frac{1}{2}n - \frac{1}{4}n^{5}r^{2}\right)$$

$$+ \frac{N-1}{N}\left(\frac{-1}{2}nr - \frac{1}{4}n^{3}r^{3} + \frac{1}{4}n^{5}r^{3} - nr^{3}(n^{2} + n^{4})\frac{\partial H_{1}}{\partial \varphi_{i}}\Big|_{s.s.}\right)$$

$$A_{21} = \left(F_{2}(r)^{-1}\frac{\partial F_{2}(r)}{\partial r} - \frac{1}{r}\right)\left(\frac{1}{2}n - \frac{1}{4}n^{5}r^{2}\right) + \frac{1}{2N}n^{5}r$$

$$+ \frac{N-1}{N}\left(\frac{n}{2r} + \frac{1}{8}n^{3}r + \frac{1}{8}n^{5}r - nr^{2}(n^{2} + n^{4})\frac{\partial H_{2}}{\partial r_{i}}\Big|_{s.s.}\right)$$

$$A_{22} = \frac{-1}{2}\tilde{\mu}_{a}F_{1}(r)^{-1}F_{2}(r)$$

$$B_{11} = 0$$

$$B_{12} = \frac{1}{N}\left(\frac{1}{2}nr + \frac{1}{4}n^{3}r^{3} - \frac{1}{4}n^{5}r^{3} - nr^{3}(n^{2} + n^{4})\frac{\partial H_{1}}{\partial \varphi_{j}}\Big|_{s.s.}\right)$$

$$B_{21} = \frac{1}{N}\left(\frac{-n}{2r} - \frac{1}{8}n^{3}r + \frac{3}{8}n^{5}r - nr^{2}(n^{2} + n^{4})\frac{\partial H_{2}}{\partial r_{j}}\Big|_{s.s.}\right)$$

$$B_{22} = 0,$$

where  $(\cdot)|_{s.s.}$  indicates that the quantity is evaluated at the unison steady state solution. Expressions for  $\frac{\partial H_1}{\partial \varphi_i}|_{s.s.}$ ,  $\frac{\partial H_2}{\partial r_i}|_{s.s.}$ ,  $\frac{\partial H_1}{\partial \varphi_j}|_{s.s.}$  and  $\frac{\partial H_2}{\partial r_j}|_{s.s.}$  are given in Appendix A.

For this structure of C, it can be proved that an eigenvalue of [A-B] is an (N-1) times repeated eigenvalue of C and an eigenvalue of [A+(N-1)B] is also an eigenvalue of C (this is a standard result from bifurcations with symmetry; refer to Section XVIII.4 of (Golubitsky [20] et al, 1988) or Appendix B). Under the assumption that the absorber does not hit the cusp during the unison motion, all eigenvalues of [A+(N-1)B] have negative real parts (see Appendix C for a proof). Thus, the stability of the unison motion is dictated by the eigenvalues of [A-B]. For a  $2 \times 2$  matrix such as [A-B], both eigenvalues have negative real parts if and only if the trace of matrix is negative and the determinant is positive. It can be shown (see Appendix D) that

$$Trace[A - B] = -\tilde{\mu}_a \tag{3.17}$$

so that the trace is always negative. Therefore, [A - B] will have an eigenvalue with positive real part only when its determinant becomes negative. In addition, condition (3.17) indicates that only those bifurcations corresponding to a zero eigenvalue can occur, i.e., Hopf bifurcations cannot occur.

From equation (3.16) one can obtain the determinant of [A-B]. We proceed to solve the condition for the loss of stability in two ways: The first is an "exact" form, using numerical determination of the determinant in terms of the functions  $F_i$  and  $H_i$ . The second approach uses an expansion that is based on the observation that when  $\tilde{\mu}_a \to 0$ , the amplitude at which the instability occurs,  $r^*$ , also approaches zero. By assuming  $\tilde{\mu}_a \ll 1$ , an expansion in  $r^{*2}$  in terms of  $\tilde{\mu}_a$  is carried out for the condition  $\det[A-B]=0$ , which yields

$$r^{*2} = \frac{2}{n^3} \tilde{\mu}_a - \frac{(1+n^2)(14n^2+6n^4)}{8n^6} \tilde{\mu}_a^2 + \mathcal{O}(\tilde{\mu}_a^3). \tag{3.18}$$

Note that based on the computational results shown in equation (3.18),  $r^*$  is not

t

ha ei

m

The the res

ins

Th tha

la t

for 1

It is level

nump

an explicit function of the number of absorbers N, although it may depend on N through  $\tilde{\mu}_a$  if the linear viscous damping described in equation (2.14) is assumed.

The first-order approximation in equation (3.18) gives the simple result

$$r^* \simeq \left(\frac{2\hat{\mu}_a}{n^3\nu}\right)^{\frac{1}{2}}.\tag{3.19}$$

When r exceeds  $r^*$  the determinant of [A-B] becomes negative such that [A-B] has one real eigenvalue with positive real part, and therefore C has (N-1) such eigenvalues.

Recall that condition (3.4) must be satisfied for the absorbers to not reach their maximum amplitude during the unison motion; i.e.,

$$r \le r_{max} = \frac{1}{n\sqrt{n^2 + 1}}. (3.20)$$

This indicates that r will necessarily be small for n > 1. The results regarding the instability and the limiting absorber amplitude, equations (3.19) and (3.20), respectively, can be used to obtain a condition on the system parameters which will insure that the unison motion will be stable over the entire feasible operating range. This holds if  $r^* > r_{max}$ , and provides the following condition on the level of damping that will ensure the stability of the unison motion for all amplitudes up to  $r_{max}$ :

$$\hat{\mu}_a \ge \frac{n\nu}{2(1+n^2)} \ . \tag{3.21}$$

In terms of the dimensional damping coefficients, this yields the following conditions for the cases of viscous and hysteretic damping, respectively:

$$\begin{cases} c_a \ge \frac{m_0^2 R_0^2 \Omega n}{2I_d N (1+n^2)}, & \text{if (2.14) is assumed} \\ c_{a0} \ge \frac{m_0^2 R_0^2 \Omega n}{2I_d (1+n^2)}, & \text{if (2.15) is assumed} \end{cases}$$
(3.22)

It is observed that the only difference in these results is that the minimal damping level required for the viscous model to remain in unison motion decreases as the number of absorbers is increased (while holding the total absorber mass fixed), while for the hysteretic model the damping level required is independent of the number of absorbers.

If condition (3.21) does not hold, then there will exist a critical torque level at which the absorbers, moving in unison, will reach an amplitude of  $r^*$ , and the instability will occur. In order to determine this critical torque we use the relationship between  $\tilde{\Gamma}_{\theta}$  and r given in equation (3.14), expanded for  $r \ll 1$  and  $\tilde{\mu}_a \ll n$ , which yields  $\tilde{\Gamma}_{\theta} \simeq n^2 r$  (this is simply the undamped, linear response relationship, which is a sufficient approximation for motions with amplitudes nearly up to  $r_{max}$ ). With this result, equation (3.19) can be re-expressed in term of the critical level of the disturbing torque as<sup>1</sup>

$$\hat{\Gamma}_{\theta}^* \simeq \sqrt{2\nu n \hat{\mu}_a}. \tag{3.23}$$

The corresponding dimensional forms of the critical torque for the cases of viscous and hysteretic damping are, respectively,

$$\hat{T}_{\theta}^{*} \simeq \begin{cases} \sqrt{2nNc_{a}I_{d}\Omega^{3}R_{0}^{2}}, & \text{if (2.14) is assumed} \\ \sqrt{2nc_{a0}I_{d}\Omega^{3}R_{0}^{2}}, & \text{if (2.15) is assumed.} \end{cases}$$
 (3.24)

This result indicates that the critical torque level for the viscous damping case depends on the number of absorbers N, and is raised by splitting a given total absorber mass into more absorbers. In contrast, for hysteretic damping, the critical torque level is independent of the number of absorbers used. (Recall that this result is valid only if the instability occurs before the absorbers reach the maximum amplitudes of the unison motion.)

For the case of linear viscous damping, the effective damping  $\hat{\mu}_a$  in (2.14) is

See the work by Lee and Shaw (1996) [29] for an alternate derivation of the critical torque level in which a pair of absorbers is considered and one assumes from the outset that the amplitude, r, is small, but allows for arbitrary values of the mass ratio  $\nu$ . In this case, the critical torque level contains a correction term involving  $\nu^2$  — a correction that can be captured in the present analysis only by carrying out second order averaging, a nontrivial task for this system. However, note that their result cannot account for the finite amplitude effects captured here.

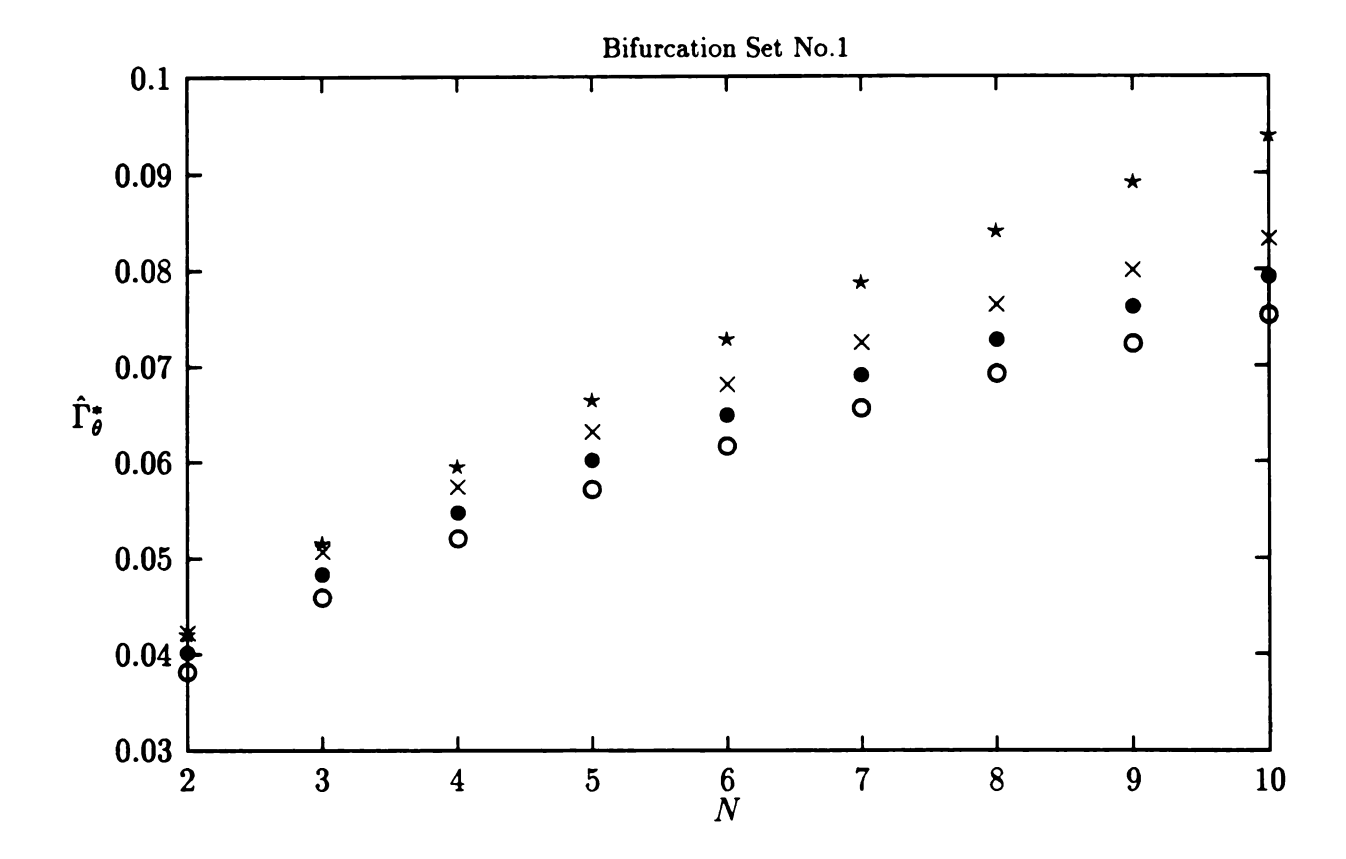


Figure 3.1: The critical torque level,  $\hat{\Gamma}^*_{\theta}$ , versus the number of absorbers, N with  $\frac{c_a}{m_0\Omega} \simeq 0.0013$ . " $\bullet$ " represents the bifurcation point derived from "Det[A-B]=0". " $\star$ " represents the bifurcation point derived from the simplified criterion (3.23). " $\times$ " represents an non-unison motion from numerical simulations. " $\circ$ " represents a unison motion from numerical simulations.

proportional to the number of absorbers and the quantity  $\frac{c_a}{m_0\Omega} = \frac{\mu_a}{N}$  is a fixed physical quantity. Based on this assumption, Figure 3.1 shows the critical disturbing torques levels  $\Gamma_{\theta}^{*}$ 's for different numbers of absorbers, N. The specific numerical values used for parameters are:  $\nu = 0.1662$ , n = 2 (values taken from the 2.5 liter, in-line, four-stroke, four-cylinder engine considered by Denman [16] (1992)), and  $\frac{\tilde{\mu}_a}{N} = \frac{\tilde{\mu}_a}{N} \times \nu = 0.008 \times \nu \simeq 0.0013$ . The symbol '•' in Figure 3.1 denotes the critical torque levels determined by numerically solving Det[A - B] = 0 for the critical r value and using equation (3.14), while '\*' denotes the results derived from the simplified, small-amplitude criterion (3.23). In this figure, we also show simulation results obtained at selected "check points", using a bearing damping level given by  $\hat{\mu}_0 = 0.005$ . Points marked by 'x' denote the upper check points, which lie at torque levels 5% above the critical values; here the absorbers undergo non-unison motions after bifurcation — more on this below. The symbols 'o' denote the lower check points, which lie at torque levels 5% below the critical values; here the absorbers undergo unison motion. The responses near the check points converge very slowly to their respective steady states since they are close to the instability.

One can see that the predicted critical torque levels derived from "Det[A-B] = 0" are within the range bounded by the corresponding upper and lower check points, while the simplified criterion diverges away from the more accurate result as N increases.

Figure 3.2 shows the approximations for the critical disturbing torque level  $\hat{\Gamma}_{\theta}^*$  versus absorber damping  $\hat{\mu}_a$ , as given by the simplified criterion (3.23) and by "Det[A-B]=0". Note that by the results obtained from using equation (3.18), the curves in this figure are independent of the number of absorbers N. The remaining system parameters used are the same as those in Figure 3.1. The upper bound of  $\hat{\mu}_a=0.01$  is chosen to prevent any absorber from hitting a cusp after bifurcation for  $N \leq 10$ , as based on observations from simulations. This figure also shows simulation

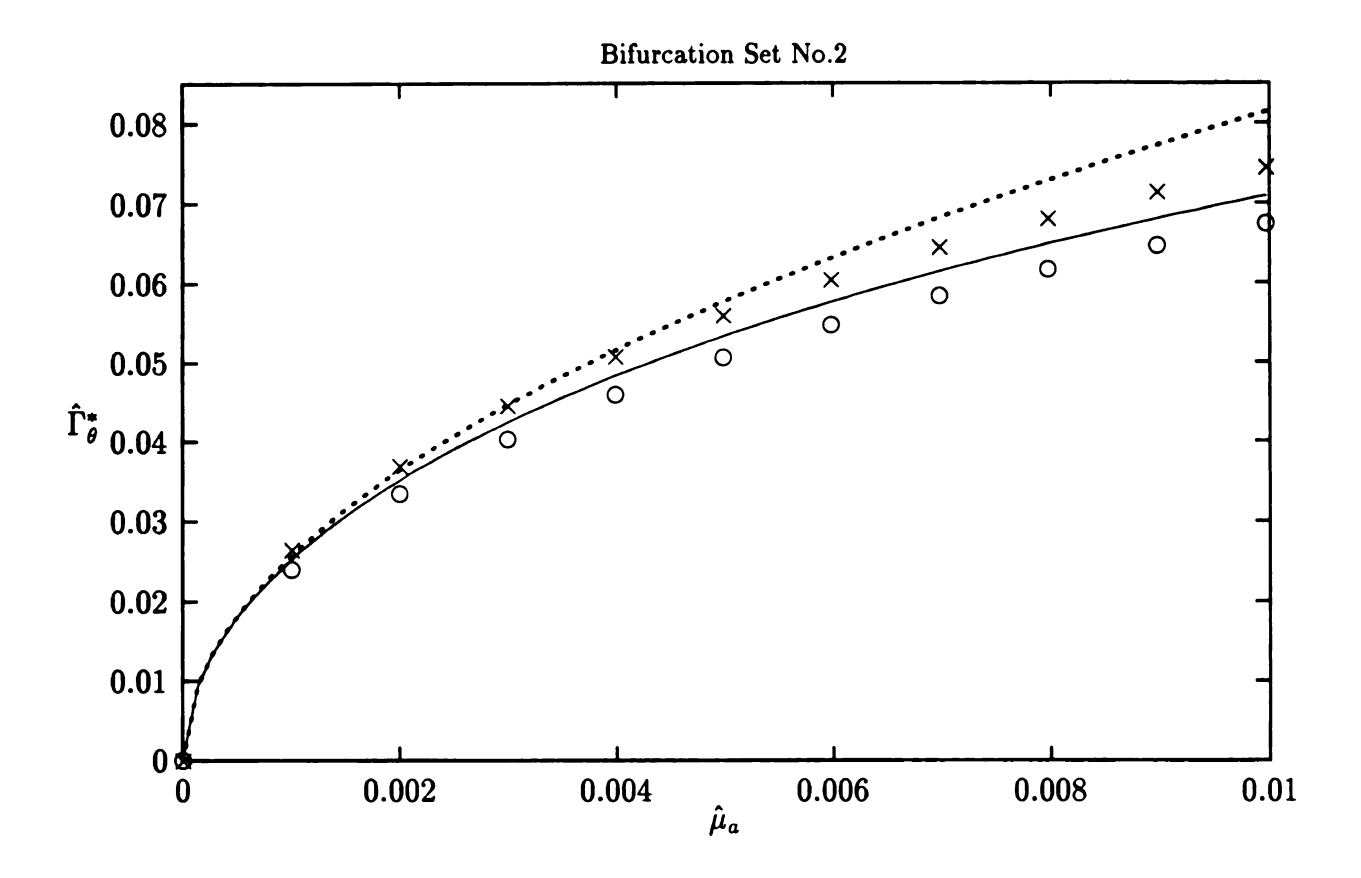


Figure 3.2: The critical torque level,  $\hat{\Gamma}_{\theta}^*$ , versus various absorber damping  $\hat{\mu}_a$ . The solid line represents bifurcation points derived from "Det[A-B]=0". The dashed line represents bifurcation points derived from the simplified criterion (3.23). "×" represents an non-unison motion from numerical simulations. "o" represents a unison motion from numerical simulations.

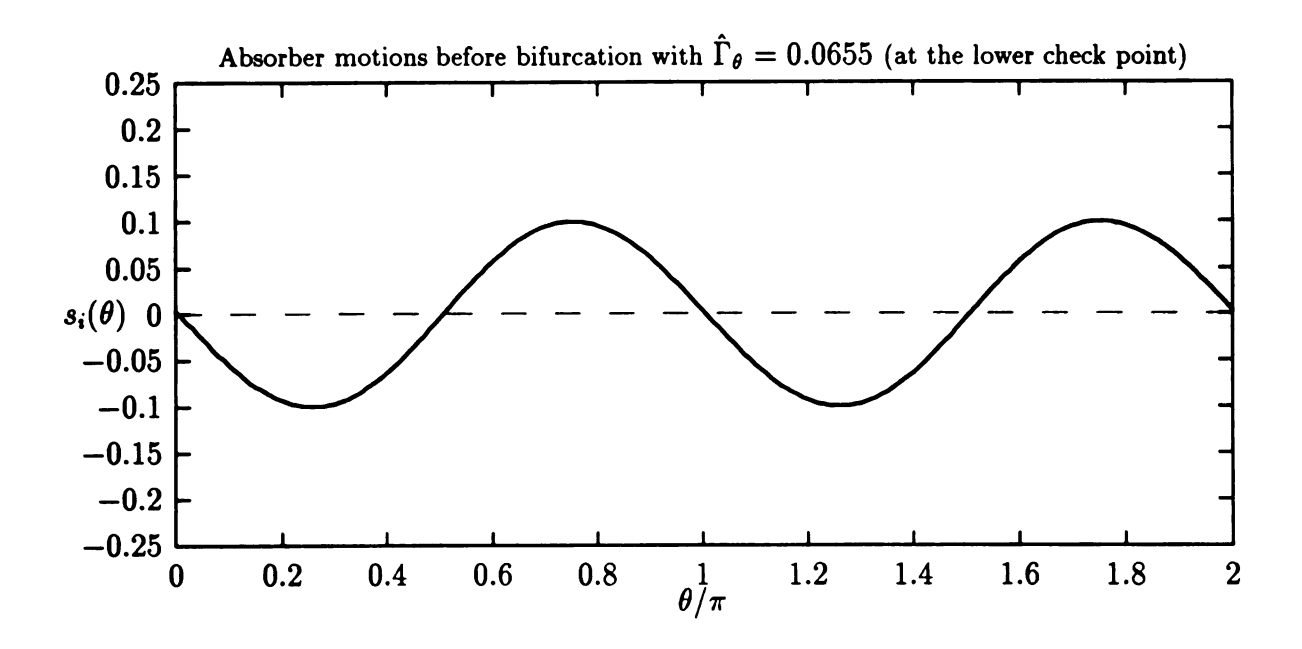
results at check points 'x' and 'o', which indicate that utilizing "Det[A - B] = 0" gives a very accurate prediction of the bifurcation.

Figure 3.3 shows the absorber responses for N=7 at the two check points. The unison motion is obvious. It is interesting to note that the post-critical, non-unison motion involves six absorbers moving together while the seventh has a different motion with a larger amplitude. This super-critical bifurcation was the only type observed in many simulations involving different values of system parameters, different N, and different initial conditions. Note that there will be N such responses possible that are virtually identical, since the symmetry of the problem allows any one of the absorbers to be the one that is "out of step". The specific absorber that steps out is dictated soley by initial conditions. The determination of this response and its effect on the performance of the absorber system is the topic of the next chapter.

#### 3.4 Concluding Remarks

This study investigated the stability of unison motions for multiple identical tautochronic vibration absorbers (CPVA's). This problem has practical importance, as systems of CPVA's are typically divided into N identical masses due to spatial restrictions and in order to balance the rotating system. However, the selection of the total absorber mass is generally done based on the assumption of unison motion. Using the method of averaging, a stability criterion for unison motions was derived in terms of the disturbance torque level and the system parameters. The results indicate that the number of absorbers has an effect on the system stability if the absorber damping is viscous. If the absorber damping is hysteretic, however, the number of absorbers does not affect the instability. In practice, this damping, while critical for good operation, is extremely difficult to determine, either in type or magnitude.

Designers with the aim of improving performance by lowering absorber damping



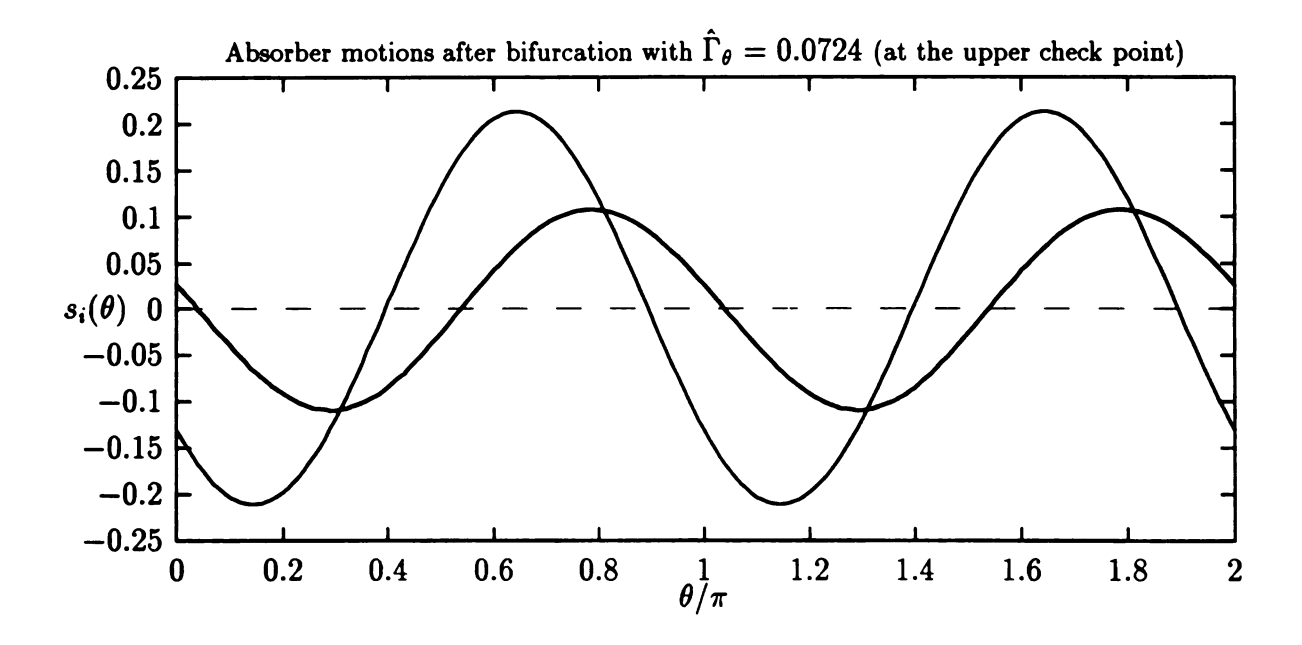


Figure 3.3: Absorber motions before and after the bifurcation point for N=7.

should keep this instability in mind, as it is more likely to occur with smaller damping. The net result of lowering the damping is that the system will have improved performance, but over a smaller operating range, since the post-critical motion of the absorbers will reach amplitude limits at a smaller torque level than the unison motion. This is considered in detail in the next chapter.

in o b fee is to incompatible the

of th

#### CHAPTER 4

# NON-UNISON DYNAMICS OF A ROTATING SYSTEM WITH MULTIPLE TAUTOCHRONIC ABSORBERS

It was shown in the previous chapter that for epicycloidal absorber paths, the unison motion of N identical absorbers may become unstable at a moderate level of the disturbing torque, in which case the performance of the absorbers in the post-bifurcation stage becomes of interest. In addition, it was observed in simulations that the post-critical response involved N-1 absorbers moving in relative unison with the remaining absorber undergoing a larger amplitude motion.

This chapter aims to uncover the source of this response and to determine the effects it has on system performance. To this end, the dynamic response of the model considered in the previous chapter, which consists of a rigid rotor fitted with N identical absorbers using epicycloidal paths and subjected to a harmonic torque, is investigated. The primary goal of this effort is to determine the nature and stabilities of the post-bifurcation, non-unison solutions in order to estimate the effects that the bifurcation has on the two performance measures: the rotor acceleration and the feasible operating torque range. It is determined that the torsional oscillation level is reduced in the post-bifurcation regime, which improves the absorber performance. However, it is also found that the feasible operating torque range is reduced due to the bifurcation, since the absolute peak of all steady state absorbers' motions is increased. It should be noted that the present results are only the first step in such a study, as some important issues must be considered in subsequent work in order for the results to be of any practical use. These matters are taken up in the conclusions of this chapter.

# 4.1 Preparation of Equations of Motion

In the previous chapter, the method of averaging was employed to find a criterion that determines the point at which the unison motion becomes unstable. However, this approach fails to characterize the post-bifurcation dynamics in a convenient form, since the averaged equations are highly nonlinear and coupled in terms of the amplitudes and phases. Essentially, while it is possible to find the post-bifurcation solutions using numerical methods, it is not possible to predict the behavior of the post-bifurcation dynamics in terms of system parameters. To solve this problem, a linear coordinate transformation among absorber displacements is used herein that splits the dynamics into two invariant subspaces, representing the unison motion and its complement, respectively. <sup>1</sup> This transformation is given by

$$\xi_1 = \frac{1}{N} \sum_{j=1}^{N} s_j, \quad \xi_i = \frac{1}{N} (s_1 - s_i) \text{ for } 2 \le i \le N.$$
 (4.1)

#### Remarks:

- This transformation enables one to separate the dynamics in the subspace of the unison mode V, with attendant coordinate  $\xi_1$ , from the dynamics in the complement space W, with coordinates  $\xi_i$ ,  $2 \le i \le N$ . From the structure of the Jacobian C, it is known that when the unison response bifurcates, (N-1) eigenvalues of this system response, which correspond to the system dynamics in W, cross the imaginary axis through zero. Therefore, in order to determine the post-bifurcation behavior, the dynamics in W must be analyzed.
- Note that for a response in which a group of p absorbers move in unison, with  $s_1$  included in that group, there will be (p-1)  $\xi_i$ 's with zero amplitudes and (N-p)  $\xi_i$ 's with nonzero amplitude (for  $2 \le i \le N$ ). Furthermore, if the

A similar transformation was used in [11] in order to put linearized equations in a useful form.

remaining (N-p) absorbers move together, the nonzero  $\xi_i$ 's  $(2 \le i \le N)$  will be equal to one another.

- Each ξ<sub>i</sub> (2 ≤ i ≤ N), is orthogonal to ξ<sub>1</sub> but they are not orthogonal to one another. A standard block diagonalization technique (see [24]) suggests that one choose a set of orthogonal coordinates to characterize the dynamics in W in order to find the linearized solutions near the bifurcation point. In contrast, herein the special transformation (4.1) is chosen for convenience in estimating the feasible operating range of the applied torque.
- The inverse of the transformation exists and is given by

$$s_1 = \sum_{j=1}^{N} \xi_j, \quad s_i = \sum_{j=1}^{N} \xi_j - N \, \xi_i, \quad \text{for } 2 \le i \le N.$$
 (4.2)

• For efficiency of presentation, the matrix **T** is defined such that  $s = T\xi$  where  $s = [s_1, s_2, ..., s_N]^T$  and  $\xi = [\xi_1, \xi_2, ..., \xi_N]^T$ .

The final form for averaging is obtained by applying transformation (4.2) to the equations of motion (3.10) and implementing a transformation to polar coordinates. First, substituting transformation (4.2) into equations (3.10) yields the following transformed equations of motion

$$\xi_1'' + n^2 \xi_1 = \epsilon \hat{f}_1(\boldsymbol{\xi}, \boldsymbol{\xi'}, \theta) + \mathcal{O}(\epsilon^2),$$
  

$$\xi_i'' + n^2 \xi_i = \epsilon \hat{f}_i(\boldsymbol{\xi}, \boldsymbol{\xi'}, \theta) + \mathcal{O}(\epsilon^2), \quad 2 \le i \le N,$$
(4.3)

where

$$\hat{f}_{1}(\boldsymbol{\xi},\boldsymbol{\xi'},\theta) = -\tilde{\mu}_{a}\xi'_{1} + \xi'_{1}Y(\mathbf{T}\boldsymbol{\xi},\theta) 
+ \frac{1}{N} \left[ g\left(\sum_{j=1}^{N} \xi_{j}\right) + \sum_{i=2}^{N} g\left(\sum_{j=1}^{N} \xi_{j} - N \xi_{i}\right) \right] Y(\mathbf{T}\boldsymbol{\xi},\theta), 
\hat{f}_{i}(\boldsymbol{\xi},\boldsymbol{\xi'},\theta) = -\tilde{\mu}_{a}\xi'_{i} + \xi'_{i}Y(\mathbf{T}\boldsymbol{\xi},\theta) 
+ \frac{1}{N} \left[ g\left(\sum_{j=1}^{N} \xi_{j}\right) - g\left(\sum_{j=1}^{N} \xi_{j} - N \xi_{i}\right) \right] Y(\mathbf{T}\boldsymbol{\xi},\theta), 2 \leq i \leq N,$$

$$Y(s,\theta) = \frac{1}{N} \sum_{j=1}^{N} (-2n^2 s_j s_j' - n^2 g(s_j) s_j + \frac{dg(s_j)}{ds_j} s_j'^2) - \tilde{\Gamma}_{\theta} \sin(n\theta).$$

The polar transformation is then given by

$$\xi_{i} = \rho_{i}\cos(\psi_{i} - n\theta), \quad \text{and} \quad \xi'_{i} = n\rho_{i}\sin(\psi_{i} - n\theta), \quad 1 \le i \le N.$$
 (4.4)

Note that this transformation is singular when  $\xi_i$  is zero, and it is therefore not appropriate for determining the stability of the unison mode. However, of interest here is the system dynamics in the post-bifurcation stage. Substituting transformation (4.4) into equations (4.3) results in a set of first-order differential equations which describe the dynamics of  $\rho_i$  and  $\psi_i$ ,  $1 \le i \le N$ , as follows,

$$\rho_i' = \frac{\epsilon}{n} \hat{F}_i(\rho_1, ..., \rho_N, \psi_1, ..., \psi_N, \theta) \sin(\psi_i - n\theta) + \mathcal{O}(\epsilon^2), \tag{4.5a}$$

$$\rho_i\psi_i' = \frac{\epsilon}{n}\hat{F}_i(\rho_1,...,\rho_N,\psi_1,...,\psi_N,\theta)\cos(\psi_i-n\theta) + \mathcal{O}(\epsilon^2), \quad 1 \leq i \leq N, (4.5b)$$

where the function  $\hat{F}_i$  is simply  $\hat{f}_i$  expressed in terms of coordinates  $\rho_i$  and  $\psi_i$ , as obtained by incorporating transformation (4.4) into  $\hat{f}_i$ . Equations (4.5a) and (4.5b) are in the desired form for averaging.

It should be pointed out that, when expressed in terms of the coordinates  $\rho_i$ 's and  $\psi_i$ 's, the subspace of the unison mode **V** is spanned by  $[\rho_1, \psi_1, 0, 0, ...., 0, 0]^T$  and the complement **W** is spanned by  $[0, 0, \rho_2, \psi_2, ...., \rho_N, \psi_N]^T$ .

# 4.2 The Averaged Equations

Considering only the first order terms in  $\epsilon$  in equations (4.5a) and (4.5b), averaging is performed in  $\theta$  over one period of the excitation,  $\frac{2\pi}{n}$ . The resulting averaged equations are expressed in terms of the first-order averaged variables  $\bar{\rho}_i$  and  $\bar{\psi}_i$ ,  $1 \leq i \leq N$ . Due to the complicated nature of the system, this process results in many terms in the forms of integrals, which render closed-form solutions unachievable.

In order to obtain simplified, approximate estimates of the rotor acceleration and the operating torque range, it is assumed that the oscillation amplitudes of the absorbers, that is, the  $\bar{\rho}_i$ 's, are small and of the same order, denoted  $\mathcal{O}(\bar{\rho})$ . Then the averaged equations can be expanded in terms of the  $\bar{\rho}_i$ 's. This yields a set of truncated, averaged equations in terms of  $\bar{\rho}_i$  and  $\bar{\psi}_i$ ,  $1 \leq i \leq N$ , as follows, where each is expanded to the desired order (more on this below):

$$\begin{split} \frac{d\bar{\rho}_{1}}{d\hat{\theta}} &= \frac{-\tilde{\mu}_{a}\bar{\rho}_{1}}{2} + \frac{\tilde{\Gamma}_{\theta}}{2n}\cos\bar{\psi}_{1} + \mathcal{O}(\bar{\rho}^{3}), \qquad (4.6a) \\ \bar{\rho}_{1}\frac{d\bar{\psi}_{1}}{d\hat{\theta}} &= -\frac{\tilde{\Gamma}_{\theta}}{2n}\sin\bar{\psi}_{1} - \frac{n\bar{\rho}_{1}}{2} + \mathcal{O}(\bar{\rho}^{2}), \qquad (4.6b) \\ \frac{d\bar{\rho}_{1}}{d\hat{\theta}} &= -\frac{\tilde{\mu}_{a}\bar{\rho}_{1}}{2} + \frac{n^{3}}{4}\bar{\rho}_{1}^{2}\bar{\rho}_{1}\sin(2\bar{\psi}_{1} - 2\bar{\psi}_{1}) \\ &+ \frac{n^{3}\bar{\rho}_{1}}{4} \sum_{j\neq 1,i} \left\{ 2\bar{\rho}_{1}\bar{\rho}_{j}\sin(\bar{\psi}_{1} - \bar{\psi}_{j}) - (N-1)\bar{\rho}_{j}^{2}\sin[2(\bar{\psi}_{1} - \bar{\psi}_{j})] \right\} \\ &+ \frac{n^{3}\bar{\rho}_{1}}{2} \sum_{j,k\neq 1,i} \sum_{k} \bar{\rho}_{j}\bar{\rho}_{k}\sin(2\bar{\psi}_{1} - \bar{\psi}_{j} - \bar{\psi}_{k}) \\ &+ \frac{(n^{2} + n^{4})\bar{\rho}_{1}}{16n} \left\{ N\tilde{\Gamma}_{\theta}\bar{\rho}_{i}\cos\psi_{i} - \sum_{j=1}^{N} 2\tilde{\Gamma}_{\theta}\bar{\rho}_{j}\cos(2\bar{\psi}_{i} - \bar{\psi}_{j}) \\ &N^{2}\bar{\rho}_{1}\bar{\rho}_{i}\sin(\bar{\psi}_{1} - \bar{\psi}_{i}) - \sum_{j=1}^{N} 2n^{2}\bar{\rho}_{1}\bar{\rho}_{j}\sin(\bar{\psi}_{1} - 2\bar{\psi}_{i} + \bar{\psi}_{j}) \right\} + \mathcal{O}(\bar{\rho}^{5}), \quad (4.6c) \\ \bar{\rho}_{i}\frac{d\bar{\psi}_{i}}{d\hat{\theta}} &= -\frac{n^{3}}{4}\bar{\rho}_{i}\bar{\rho}_{1}^{2}\cos(2\bar{\psi}_{1} - 2\bar{\psi}_{i}) - \frac{(N-1)}{4}n^{3}\bar{\rho}_{i}^{3} \\ &+ \frac{n^{3}\bar{\rho}_{i}}{4} \sum_{j\neq 1,i} \left\{ 2\bar{\rho}_{i}\bar{\rho}_{j}\cos(\bar{\psi}_{i} - \bar{\psi}_{j}) - (N-1)\bar{\rho}_{j}^{2}\cos[2(\bar{\psi}_{i} - \bar{\psi}_{j})] \right\} \\ &+ \frac{n^{3}\bar{\rho}_{i}}{2} \sum_{j,k\neq 1,i} \sum_{k} \bar{\rho}_{j}\bar{\rho}_{k}\cos(2\bar{\psi}_{i} - \bar{\psi}_{j}) - (N-1)\bar{\rho}_{j}^{2}\cos[2(\bar{\psi}_{i} - \bar{\psi}_{j})] \right\} \\ &+ \frac{n^{3}\bar{\rho}_{i}}{16n} \left\{ -3N\tilde{\Gamma}_{\theta}\bar{\rho}_{i}\sin\psi_{i} + \sum_{j=1}^{N} \left[2\tilde{\Gamma}_{\theta}\bar{\rho}_{j}\sin(2\bar{\psi}_{i} - \bar{\psi}_{j}) + 4\tilde{\Gamma}_{\theta}\bar{\rho}_{j}\sin\bar{\psi}_{j} \right] \\ &-3Nn^{2}\bar{\rho}_{1}\bar{\rho}_{i}\cos(\bar{\psi}_{i} - \bar{\psi}_{1}) \\ &+ \sum_{j=1}^{N} \left[ 2n^{2}\bar{\rho}_{1}\bar{\rho}_{j}\cos(2\bar{\psi}_{i} - \bar{\psi}_{1}) + 4n^{2}\bar{\rho}_{1}\bar{\rho}_{j}\cos(\bar{\psi}_{1} - \bar{\psi}_{j}) \right] \right\} + \mathcal{O}(\bar{\rho}^{5}) \quad (4.6d) \end{aligned}$$

where  $2 \le i \le N$  and  $\hat{\theta} \equiv \epsilon \theta$ .

#### 4.3 Steady-State Responses

Note that equations (4.6c) and (4.6d) are expanded out to third order, while terms out to fifth order are retained in the remaining equations. This is consistent for obtaining steady-state solutions, as the  $\mathcal{O}(\bar{\rho}^3)$  terms in the dynamics of  $\bar{\rho}_1$  and  $\bar{\psi}_1$  contribute at  $\mathcal{O}(\bar{\rho}^5)$  in the dynamics of  $\bar{\rho}_i$  and  $\bar{\psi}_i$ ,  $2 \leq i \leq N$ . Since only the first-order nonlinear terms in the dynamics of  $\bar{\rho}_i$  and  $\bar{\psi}_i$ ,  $2 \leq i \leq N$ , are needed to find the desired approximate solutions, the  $\mathcal{O}(\bar{\rho}^3)$  terms in  $\bar{\rho}_1$  and  $\bar{\psi}_1$  are not needed. This fact implies that only the linear dynamics of the unison response are needed in order to determine the first-order nonlinear steady-state solution of the non-unison component (this is most easily seen by making use of the coordinates employed here). In the above suggested method for finding the approximate solutions, it is assumed that the  $\mathcal{O}(\bar{\rho}^3)$  and  $\mathcal{O}(\epsilon)$  terms in the averaged equations will dominate the  $\mathcal{O}(\epsilon^2)$  terms that would result from second order averaging (which is not considered here). The validity of this assumption depends on the actual values of  $\epsilon$  and  $\rho$ , which depend in turn on the level of the disturbing torque. It is shown in the simulations to follow that the present expansion method provides satisfactory results for the system dynamics well beyond the bifurcation.

To find a simple approximation for the steady-state solution for  $\bar{\rho}_1$  and  $\bar{\psi}_1$ , it is assumed that  $\tilde{\mu}_a$  is small compared to n (this is true in most applications), and that the  $\mathcal{O}(\bar{\rho}^3)$  terms in equations (4.6a) and (4.6b) are neglected. Setting equations (4.6a) and (4.6b) equal to zero yields the following approximate steady-state solutions for  $\bar{\rho}_1$  and  $\bar{\psi}_1$ , denoted by  $\tilde{\rho}_1$  and  $\tilde{\psi}_1$ ,

$$\tilde{\bar{\rho}}_1 = \frac{\tilde{\Gamma}_{\theta}}{n^2}$$
 and  $\tilde{\bar{\psi}}_1 = -\frac{\pi}{2}$ . (4.7)

This is nothing more than the linear undamped response, but a reasonable approximation of the unison mode at steady state, even up to amplitudes for which the bifurcation occurs; this is verified in simulations. Substituting the above solutions

into equations (4.6c) and (4.6d), setting their derivatives equal to zero, and ignoring the  $\mathcal{O}(\bar{\rho}^5)$  terms, a set of stationary equations obtains which can be solved for the approximate steady-state solutions of  $\bar{\rho}_i$  and  $\bar{\psi}_i$ ,  $2 \leq i \leq N$ , denoted here as  $\tilde{\bar{\rho}}_i$  and  $\tilde{\bar{\psi}}_i$ , respectively. These equations are

$$0 = \frac{-\tilde{\mu}_{a}\tilde{\tilde{\rho}}_{i}}{2} + \frac{\tilde{\Gamma}_{\theta}^{2}\tilde{\tilde{\rho}}_{i}}{4n}\sin(2\tilde{\tilde{\psi}}_{i})$$

$$+ \frac{n^{3}\tilde{\tilde{\rho}}_{i}}{4}\sum_{j\neq 1,i}\left\{2\tilde{\tilde{\rho}}_{i}\tilde{\tilde{\rho}}_{j}\sin(\tilde{\tilde{\psi}}_{i}-\tilde{\tilde{\psi}}_{j})-(N-1)\tilde{\tilde{\rho}}_{j}^{2}\sin[2(\tilde{\tilde{\psi}}_{i}-\tilde{\tilde{\psi}}_{j})]\right\}$$

$$+ \frac{n^{3}\tilde{\tilde{\rho}}_{i}}{2}\sum_{j,k\neq 1,i}\sum_{k}\tilde{\tilde{\rho}}_{j}\tilde{\tilde{\rho}}_{k}\sin(2\tilde{\tilde{\psi}}_{i}-\tilde{\tilde{\psi}}_{j}-\tilde{\tilde{\psi}}_{k}), \qquad (4.8a)$$

$$0 = \frac{\tilde{\Gamma}_{\theta}^{2}\tilde{\tilde{\rho}}_{i}}{4n}\cos(2\tilde{\tilde{\psi}}_{i}) - \frac{(N-1)n^{3}}{4}\tilde{\tilde{\rho}}_{i}^{3}$$

$$+ \frac{n^{3}\tilde{\tilde{\rho}}_{i}}{4}\sum_{j\neq 1,i}\left\{2\tilde{\tilde{\rho}}_{i}\tilde{\tilde{\rho}}_{j}\cos(\tilde{\tilde{\psi}}_{i}-\tilde{\tilde{\psi}}_{j})-(N-1)\tilde{\tilde{\rho}}_{j}^{2}\cos[2(\tilde{\tilde{\psi}}_{i}-\tilde{\tilde{\psi}}_{j})]\right\}$$

$$+ \frac{n^{3}\tilde{\tilde{\rho}}_{i}}{2}\sum_{j,k\neq 1,i}\sum_{k}\tilde{\tilde{\rho}}_{j}\tilde{\tilde{\rho}}_{k}\cos(2\tilde{\tilde{\psi}}_{i}-\tilde{\tilde{\psi}}_{j}-\tilde{\tilde{\psi}}_{k}), \qquad 2\leq i\leq N. \quad (4.8b)$$

Note that up to this point,  $(\bar{\cdot})$ 's denote the first-order averaged quantities of  $\rho$ 's and  $\psi$ 's and  $(\bar{\cdot})$ 's denote the associated truncated, steady-state quantities of  $(\bar{\cdot})$ 's when the absorber damping is neglected in the unison mode. The post-bifurcation dynamics are investigated using the truncated equations in equations (4.6) and (4.8), as well as their non-truncated version, equations (3.12). The first approach has the advantage of providing explicit results in terms of the system parameters, whereas the second approach is more accurate. (One should note that equations (3.12) express the system dynamics in terms of the s coordinates, which are different from the  $\xi$  coordinates used in this chapter.)

#### 4.4 The Post-Bifurcation Dynamics

In this section a first-order approximation of the post-bifurcation dynamics is examined based on the truncated equations obtained in the previous section. Some general remarks, notational definitions and a brief overview of this section are provided before the detailed results are presented.

It is very difficult to determine all solution branches and their stabilities in a problem with this level of symmetry. However, for the problem at hand, it is possible to estimate certain important features of the response, including the angular acceleration of the rotor and the feasible torque range. Note that the torque range is imposed by the restriction stated in inequality (3.4), the constraint on the amplitude of the absorber motions. Therefore, an estimate for the peak amplitude over the steady state responses of all absorbers, denoted by  $||s||_{ss}$ , is needed.

In section 4.4.1, it is first shown that all possible post-bifurcation, steady-state solutions lie near the surface of an ellipsoid formed by the steady-state amplitudes as expressed by the  $\rho_i$ 's,  $2 \le i \le N$ . Some of the solutions on this ellipsoid are those with the corresponding isotropy subgroups,  $\mathbf{S_p} \times \mathbf{S_{N-p}}$ , for  $1 . For simplicity, such solutions are referred to as "an <math>\mathbf{S_p} \times \mathbf{S_{N-p}}$  solution", or "an  $\mathbf{S_p} \times \mathbf{S_{N-p}}$  branch". A  $\mathbf{S_p} \times \mathbf{S_{N-p}}$  solution simply refers to one with p absorbers moving in relative unison and the other (N-p) absorbers also moving in relative unison, but with a different amplitude and/or phase than the first p.

In section 4.4.2, based on the results obtained in section 4.1, it is shown that among all the possible solution branches, the  $S_1 \times S_{N-1}$  branch leads to the maximum  $||s||_{ss}$  of all possible absorber motions. In section 4.4.3, one of the  $S_1 \times S_{N-1}$  branches is proven to be dynamically stable, based on the truncated equations in (4.6). This information is then used in section 4.5 to estimate the feasible torque range and the amplitude of rotor acceleration (that is, torsional vibration).

# 4.4.1 Approximate Post-bifurcation Solutions

Based on equations (4.8), for each i there exist steady-state solutions with  $\tilde{\bar{\rho}}_i = 0$  or  $\tilde{\bar{\rho}}_i \neq 0$ . As time goes to infinity, some of the  $\tilde{\bar{\rho}}_i$ 's,  $2 \leq i \leq N$ , may converge to  $\tilde{\bar{\rho}}_i = 0$  while the others converge to non-zero steady-state amplitudes, depending on

initial conditions and the stabilities of the various solution branches. In order to distinguish these two types of amplitudes, the following sets of indices are defined

$$\mathcal{Z} \equiv \left\{ i \mid \lim_{\theta \to \infty} \tilde{\bar{\rho}}_i(\theta) = 0, \ 2 \le i \le N \right\},$$

$$\mathcal{N} \equiv \left\{ i \mid \lim_{\theta \to \infty} \tilde{\bar{\rho}}_i(\theta) \ne 0, \ 2 \le i \le N \right\},$$
(4.9)

which contain those indices corresponding to zero and nonzero steady-state amplitudes, respectively. For those  $\tilde{\rho}_i$  with i in  $\mathcal{Z}$ , the solution for the steady-state phase  $\tilde{\psi}_i$  is arbitrary. For the remaining  $\tilde{\rho}_i$ , that is, those with i in  $\mathcal{N}$ , it can be assumed that the corresponding phases are identical; i.e.,  $\tilde{\psi}_i = \tilde{\psi}_j$ ,  $\forall i, j \in \mathcal{N}$  (see Appendix E for a justification of this assumption.) Under this assumption, one can approach equations (4.8) with a method like that used in to obtain equation (3.14). This yields a steady state condition that corresponds to an ellipsoid prescribed by

$$N\sum_{i=2}^{N}\tilde{\bar{\rho}}_{i}^{2}-\sum_{i=2}^{N}\sum_{j=2}^{N}\tilde{\bar{\rho}}_{i}\tilde{\bar{\rho}}_{j}=\left(\frac{\tilde{\Gamma}_{\theta}^{4}}{n^{8}}-\frac{4\tilde{\mu}_{a}^{2}}{n^{6}}\right)^{\frac{1}{2}},$$
(4.10)

such that the steady-state solutions of  $\tilde{\bar{\rho}}_i$ ,  $i \in \mathcal{N}$  lie on this ellipsoid (to a first-order approximation). The formulation of this ellipsoid is independent of number of the nonzero steady-state  $\tilde{\bar{\rho}}_i$ 's, i.e., of the size of  $\mathcal{N}$ , but its dimension depends on the size of  $\mathcal{N}$ .

Note that the ellipsoid exists only for system and excitation parameters satisfying

$$\tilde{\Gamma}_{\theta} \ge \sqrt{2n\tilde{\mu}_{a}},\tag{4.11}$$

which is equivalent to the simplified bifurcation criterion for the unison motion obtained in equation (3.23). Thus, as the torque level is increased, the unison solution, represented by the trivial solution in terms of the variables used here, becomes unstable and spawns an invariant ellipsoid. In fact, this ellipsoid can be shown to be stable based on the truncated averaged equations (4.8), although the full-order dynamics on the surface of the ellipsoid are not know.

Note also that since this ellipsoid results from the truncated equations (4.8); when the non-truncated equations are considered the ellipsoid will be distorted and only a finite number of points on the (distorted) ellipsoid will survive as legitimate steady-state solutions. <sup>2</sup>

Some information about the nature of the solutions on the ellipsoid can be garnered from symmetric bifurcation theory. Consider a case in which p and N-p groups of absorbers move in distinct, but relative unison motions. (Note that in this case (p-1) is the size of  $\mathcal{Z}$ , since the first absorber is not included in  $\mathcal{Z}$ .) As for the other  $\tilde{\rho}_i$ , that is, the N-p with  $i\in\mathcal{N}$ , their steady-state solutions lie on the surface of the ellipsoid (4.10). Based on the "Equivariant Branching Lemma" proposed by Cicogna [10] and Vanderbauwhede [63], when certain conditions are satisfied<sup>3</sup>, the  $\mathbf{S_p}\times\mathbf{S_{N-p}}$  solution branches generically exist for all p,  $1\leq p\leq N$ . Therefore, the existence of the solution branches on the surface of the ellipsoid with identical amplitudes  $\rho_i$  and phases  $\psi_i$  for each  $i\in\mathcal{N}$  is generically ensured for the non-truncated averaged equations. Note that traveling wave types of solutions are also possible in the generic case for this bifurcation, but these have not been observed for the system under consideration. They may not exist, or may be dynamically unstable for this system. Attention is now turned to the most important of these solution branches,  $\mathbf{S_1}\times\mathbf{S_{N-1}}$ .

Working to first nonlinear order predicts the existence of this invariant ellipsoid, but it does not provide the dynamics on it. This could presumably be obtained by using higher order averaging. However, for present purposes this is not necessary.

These two conditions are (also see [20]): (1) The symmetric group  $S_N$  acts on W irreducibly. (2) The critical eigenvalues cross the imaginary axis with non-zero speed as the parameter of interest is varied. These conditions can be verified in the present case. However, one still needs to prove that the present bifurcation problem is *generic*. It is not the author's intention to complete such a rigorous proof here. The "Equivariant Branching Lemma" is simply used as a "road map" to search for possible solution branches, and their existence can be confirmed by numerically solving the non-truncated averaged equations given in equations (3.12).

# **4.4.2 Search for the Solution Branch Leading to the Maximum** $||s||_{ss}$

Instead of finding all possible solution branches, a search for the branch leading to the maximum  $||s||_{ss}$  is conducted in order to estimate the feasible torque range. This is accomplished by substituting the polar form of the absorber responses given in equation (4.4) into the absorber displacements in terms of the  $\xi$  coordinates given in equations (4.2), and assuming identical phases for each absorber during steady-state operation (this is the assumption justified in Appendix E). From this, one can express the steady-state peak value of the first absorber motion by

$$||s_{1}||_{ss} \equiv \max\{ s_{1}(\theta) \mid \theta_{o} \leq \theta \leq \theta_{o} + 2\pi, \ \theta_{o} \to \infty \}$$

$$\simeq \left[ \left( \sum_{i=2}^{N} \tilde{\tilde{\rho}}_{i} \right)^{2} - \frac{2\tilde{\Gamma}_{\theta}}{n^{2}} \sin(\tilde{\tilde{\psi}}_{i}) \left( \sum_{i=2}^{N} \tilde{\tilde{\rho}}_{i} \right) + \frac{\tilde{\Gamma}_{\theta}^{2}}{n^{4}} \right]^{1/2}, \qquad (4.12)$$

which is a square root of a positive quadratic function of  $\sum_{i=2}^{N} \tilde{\rho}_{i}$ . (Note that it is implied from equations (4.8) and Appendix E that  $\sin(\tilde{\psi}_{i})$  is independent of  $\tilde{\rho}_{i}$ ,  $2 \leq i \leq N$ .) Subject to the ellipsoid in equation (4.10),  $||s_{1}||_{ss}$  will reach its maximum value when  $\sum_{i=2}^{N} \tilde{\rho}_{i}$  reaches its extremum. Since  $\sum_{i=2}^{N} \tilde{\rho}_{i} = 0$  is a principal axis for the ellipsoid,  $\sum_{i=2}^{N} \tilde{\rho}_{i}$  reaches its extrema at the direction of the associated eigenvector where  $\tilde{\rho}_{i} = \tilde{\rho}_{j}$ ,  $2 \leq i, j \leq N$ . Hence, among all the possible post-bifurcation solutions, the one with identical  $\tilde{\rho}_{i}$  and  $\tilde{\psi}_{i}$ ,  $2 \leq i \leq N$ , leads to the maximum  $||s_{1}||_{ss}$ . It can be easily shown that the maximum  $||s_{i}||_{ss}$  for all  $2 \leq i \leq N$  is equal to the maximum  $||s_{1}||_{ss}$ , since the results are preserved under different choices of the first absorber ( since all absorbers are identical). As a result, among all the possible post-bifurcation solutions, the one with identical  $\tilde{\rho}_{i}$  and  $\tilde{\psi}_{i}$  for  $2 \leq i \leq N$  leads to the maximum  $||s||_{ss}$  of all possible absorber motions on the steady-state ellipsoid. This solution corresponds to the isotropy subgroup  $\mathbf{S}_{1} \times \mathbf{S}_{N-1}$ , wherein one absorber moves out-of-step relative to all other absorbers, which remain in relative unison. This is also the post-bifurcation solution observed in simulations.

Based on the Equivariant Branching Lemma, at least one such solution branch is

expected to exist (and it contains N identical steady state responses). The Newton-Raphson method was employed to numerically determine from the non-truncated averaged equations (given in equations (3.12)) that such branches indeed exist in the post-bifurcation stage over a wide range of parameter values.

# 4.4.3 Stability of the $S_1 \times S_{N-1}$ Solution Branch

With the existence of the  $S_1 \times S_{N-1}$  solution in hand, a stability analysis is carried out based on the truncated equations (4.6).

Consider equations (4.6a) and (4.6b), in which  $\bar{\rho}_1$  and  $\bar{\psi}_1$  capture the dynamics of the unison mode. The steady-state solutions of  $\bar{\rho}_1$  and  $\bar{\psi}_1$  can be approximated by

$$\bar{\rho}_1 = \hat{\bar{\rho}}_1 + \mathcal{O}(\bar{\rho}^3)$$
 and  $\tan \bar{\psi}_1 = \tan \hat{\bar{\psi}}_1 + \mathcal{O}(\bar{\rho}^3)$  (4.13)

where

$$\hat{\bar{\rho}}_1 = \frac{\tilde{\Gamma}_{\theta}}{n(\tilde{\mu}_a^2 + n^2)^{1/2}} \quad \text{and} \quad \tan \hat{\bar{\psi}}_1 = \frac{-n}{\tilde{\mu}_a}, \tag{4.14}$$

which, when truncated, is simply the linear, damped steady-state unison solution. Note that when compared to the approximate solutions in equation (4.7), here the effect of damping is required since it is crucial to the stability analysis of the  $S_1 \times S_{N-1}$  branch.

This approximate solution is independent of  $\bar{\rho}_i$  and  $\bar{\psi}_i$ ,  $2 \leq i \leq N$ , up to  $\mathcal{O}(\bar{\rho}^3)$  (that is, the unison dynamics are independent of the non-unison dynamics to second nonlinear order). By treating the  $\mathcal{O}(\bar{\rho}^3)$  terms as non-vanishing perturbations in equations (4.6a) and (4.6b), it can be shown (using Lyapunov techniques) that there exists a positive number  $\Theta$ , independent of  $\bar{\rho}_i(\theta)$ ,  $\bar{\psi}_i(\theta)$ ,  $2 \leq i \leq N$ , such that  $[\bar{\rho}_1(\theta), \bar{\psi}_1(\theta)]^T$  is ultimately bounded in an  $\mathcal{O}(\bar{\rho}^3)$  neighborhood of  $[\hat{\bar{\rho}}_1(\theta), \hat{\bar{\psi}}_1(\theta)]^T$  for  $\theta \geq \Theta$ . Hence, the stability of the  $S_1 \times S_{N-1}$  branch can be examined by

incorporating the approximate solution from equation (4.13) in equations (4.6c) and (4.6d), which govern the dynamics of  $\bar{\rho}_i$ ,  $\bar{\psi}_i$ ,  $2 \leq i \leq N$ , and in which the  $\mathcal{O}(\bar{\rho}^3)$  terms in (4.13) only contribute to the terms of  $\mathcal{O}(\bar{\rho}^5)$ .

The subsystem consisting of equations (4.6c) and (4.6d), governing the dynamics of  $\bar{\rho}_i$  and  $\bar{\psi}_i$ ,  $2 \leq i \leq N$ , is considered for the stability analysis. The Jacobian of this subsystem is first derived and evaluated on the  $S_1 \times S_{N-1}$  branch. Due to the symmetry of the subsystem and this solution, this Jacobian, denoted by J, has the form

$$J_{(2N-2)\times(2N-2)} = \begin{bmatrix} A_{2\times2} & B_{2\times2} & . & B_{2\times2} \\ B_{2\times2} & A_{2\times2} & . & B_{2\times2} \\ . & . & . & B_{2\times2} \\ B_{2\times2} & B_{2\times2} & B_{2\times2} & A_{2\times2} \end{bmatrix}.$$
(4.15)

It can be shown that all eigenvalues of J are eigenvalues of one of the  $2 \times 2$  matrices, [A + (N-2)B] or [A-B]. This result is a consequence of the symmetry and does not depend on the actual values of A and B. The nature of the eigenvalues of [A-B] are first determined by the well-known fact that both eigenvalues of a  $2 \times 2$  matrix possess negative real parts if and only if the trace is negative and the determinant is positive. By incorporating approximation (4.13) into the Jacobian J, the determinant and trace of [A-B] are determined to be,

$$Trace[A - B] = -\tilde{\mu}_{a}, \qquad (4.16a)$$

$$Det[A - B] = \frac{N\tilde{\mu}_{a}(n^{2} + n^{4})}{256}\hat{\bar{\rho}}\hat{\bar{\rho}}_{1} \left[ (12 - 5N)(n^{2} + n^{4})\hat{\bar{\rho}}\hat{\bar{\rho}}_{1} + (4N - 12)(n^{2} + n^{4})\hat{\bar{\rho}}\hat{\bar{\rho}}_{1}\cos(2\hat{\bar{\psi}} - 2\hat{\bar{\psi}}_{1}) + 16\cos(\hat{\bar{\psi}} - \hat{\bar{\psi}}_{1}) \right] + \mathcal{O}(\bar{\rho}^{6}) \qquad (4.16b)$$

where  $\hat{\bar{\rho}}$  and  $\hat{\bar{\psi}}$  are used to denote the steady-state amplitudes and phases of  $\bar{\rho}_i$  and  $\bar{\psi}_i$ ,  $2 \leq i \leq N$ , respectively, on the  $S_1 \times S_{N-1}$  branch. Since the trace is always negative, only the sign of Det[A-B] needs to be determined. Letting  $\hat{\bar{\rho}} \to 0^+$ ,

it is

near

bifu

The

bran

near

.

as  $\dot{\bar{\rho}}$ 

-37

bran

4.5

Ir feasil

rotor

4.5.1

As likewis

fore, t

it is found that the sign of Det[A-B] is dominated by the sign of  $\cos(\hat{\psi}-\hat{\psi}_1)$  near the bifurcation point. Based on equations (4.8), it can be shown that near the bifurcation point the phase must satisfy

$$\hat{\bar{\psi}} \simeq \frac{-3\pi}{4} \quad \text{or} \quad \frac{\pi}{4}.$$
 (4.17)

The above two solutions for the phases provide two different  $S_1 \times S_{N-1}$  solution branches. With the approximate value of  $\psi_1$  given in equation (4.7), one has

$$\cos(\hat{\bar{\psi}} - \hat{\bar{\psi}}_1) \simeq \begin{cases} \frac{1}{\sqrt{2}}, & \text{for } \hat{\bar{\psi}} \simeq \frac{-3\pi}{4}, \\ \frac{-1}{\sqrt{2}}, & \text{for } \hat{\bar{\psi}} \simeq \frac{\pi}{4}, \end{cases}$$

near the bifurcation point. The first branch, with  $\hat{\bar{\psi}} \simeq \frac{-3\pi}{4}$ , leads to Det[A-B] > 0 as  $\hat{\bar{\rho}} \to 0^+$  while the other branch similarly leads to Det[A-B] < 0.

As for the [A+(N-2)B] matrix, in Appendix F it is proved that the branch with  $\hat{\bar{\psi}} \simeq \frac{-3\pi}{4}$  leads to Trace[A+(N-2)B] < 0 and Det[A+(N-2)B] > 0 as  $\hat{\bar{\rho}} \to 0^+$  near the bifurcation point. Hence, the  $\mathbf{S_1} \times \mathbf{S_{N-1}}$  branch with  $\hat{\bar{\psi}}$  close to  $-3\pi/4$  is stable. Henceforth, this branch will be designated as "the stable  $\mathbf{S_1} \times \mathbf{S_{N-1}}$  branch."

### 4.5 Absorber Performance

In this section, two important measures of absorber system performance, the feasible operating range of the applied torque and the angular acceleration of the rotor, are estimated.

# 4.5.1 Estimate of the Feasible Torque Range

As the amplitude of the applied torque is increased, the absorbers' amplitudes likewise increase, until a cusp limit (3.4) is reached for one or more absorbers. Therefore, the feasible torque range can be determined if one combines the relationship

between the torque amplitude and  $||s||_{ss}$  with the absorber amplitude limit. This process is described here for both the truncated and non-truncated versions of the equations.

From the analytical results obtained in the previous section, is known that there exists a stable  $S_1 \times S_{N-1}$  solution which yields the maximum  $||s||_{ss}$  (based on the truncated equations). This implies that for any initial conditions, the system will converge to a solution branch that renders an  $||s||_{ss}$  which is less than or equal to that resulting from the stable  $S_1 \times S_{N-1}$  branch. Therefore, this solution branch can be used to predict the maximum  $||s||_{ss}$ , which is used in turn to determine the feasible torque range.

By using the fact that the steady-state amplitudes,  $\rho_i$ ,  $2 \le i \le N$ , are all equal on the stable  $S_1 \times S_{N-1}$  solution branch, the ellipsoid prescribed in equation (4.10) can be used to determine the steady-state amplitudes, yielding

$$\tilde{\tilde{\rho}} \equiv \tilde{\tilde{\rho}}_i = \frac{1}{\sqrt{N-1}} \left( \frac{\tilde{\Gamma}_{\theta}^4}{n^8} - \frac{4\tilde{\mu}_a^2}{n^6} \right)^{\frac{1}{4}}, \quad 2 \le i \le N.$$
(4.18)

Similarly, by using equations (4.8), the equal steady-state phases on this solution branch are found to be

$$\tilde{\bar{\psi}} \equiv \tilde{\bar{\psi}}_i = \frac{1}{2} \left[ \sin^{-1} \left( \frac{2n\tilde{\mu}_a}{\tilde{\Gamma}_{\theta}^2} \right) \right] - \pi, \quad 2 \le i \le N.$$
 (4.19)

It has been shown that  $||s||_{ss}$  can be derived from  $||s_1||_{ss}$ . To determine  $||s_1||_{ss}$ , the expression for  $s_1$  in terms of  $\xi_i$ ,  $1 \le i \le N$ , given in equation (4.2) is utilized. Substituting the angular transformation (4.4) into this expression, using the stable  $\mathbf{S_1} \times \mathbf{S_{N-1}}$  branch and the approximate steady-state unison solution for  $\rho_1$  and  $\psi_1$  given in equations (4.7), one obtains  $||s||_{ss}$ , as follows,

$$||s||_{ss} \equiv \max_{1 \le i \le N} \{ s_i(\theta) \mid \theta_o \le \theta \le \theta_o + 2\pi, \ \theta_o \to \infty \}$$

$$\simeq \left[ \frac{\tilde{\Gamma}_{\theta}^2}{n^4} - \frac{2}{n^2} (N-1) \tilde{\Gamma}_{\theta} \tilde{\bar{\rho}} \sin \tilde{\bar{\psi}} + (N-1)^2 \tilde{\bar{\rho}}^2 \right]^{\frac{1}{2}}$$
(4.20)

where  $\tilde{\bar{\rho}}$  and  $\tilde{\bar{\psi}}$  are given by equations (4.18) and (4.19), respectively.

It is now possible to estimate the feasible operating range of the applied torque level  $\hat{\Gamma}_{\theta}$  by recalling inequality (3.4) and using the approximate expression for  $||s||_{\rm ss}$  in equation (4.20). This can be carried out to an analytical equation, which is not presented here since it is not easily solved for an explicit expression for the maximum torque. Note that since this estimate is based on the truncated equations in equation (4.8), it will deteriorate near the singularity of the absorber path. In order to determine a more accurate estimate for the torque range, one can numerically solve the non-truncated equations (3.12) (as described in section 3.2) for a more accurate estimate of the  $\mathbf{S_1} \times \mathbf{S_{N-1}}$  solution.

Numerical results for the torque range are given in Section 4.6.

## 4.5.2 Estimate of the Rotor Acceleration

An approximate expression for the angular acceleration is first formulated to leading nonlinear order, after which more accurate estimates are computed. Taking the nondimensionalized acceleration  $yy'(\theta)$  stated in equation (3.9), considering only the  $\mathcal{O}(\epsilon)$  terms in  $yy'(\theta)$ , expanding  $yy'(\theta)$  in terms of  $s_i, 1 \leq i \leq N$ , and then using the definition  $\epsilon \equiv \nu$  and the transformation (4.1), yields

$$yy'(\theta) = \nu \left[ \frac{2n^2}{N} \sum_{j=1}^{N} s_j s_j' + n^2 \xi_1 + \tilde{\Gamma}_{\theta} \sin(n\theta) \right] + \mathcal{O}(\rho^3)$$
 (4.21)

where only the first and second order amplitude terms are considered. Utilizing the truncated stationary equations (4.8), a nontrivial calculation (outlined in Appendix G) yields the following lower-order approximation for  $yy'(\theta)$ ,

$$yy'(\theta) \simeq \begin{cases} \epsilon[n^3\tilde{\rho}_1^2\sin(2\tilde{\psi}_1 - 2n\theta)] = \frac{\hat{\Gamma}_{\theta}^2}{\nu n}\sin(2n\theta), & \text{before bifurcation.} \\ \epsilon[2\tilde{\mu}_a\cos(2\tilde{\psi} - 2n\theta)] = 2\hat{\mu}_a\cos(2\tilde{\psi} - 2n\theta), & \text{after bifurcation.} \end{cases}$$
(4.22)

where the approximate solution for  $\tilde{\bar{\rho}}_1$  and  $\tilde{\bar{\psi}}_1$  in equations (4.7) have been used and

where

$$\tilde{\bar{\psi}} = \frac{1}{2} \left[ \sin^{-1} \left( \frac{2n\nu\hat{\mu}_a}{\hat{\Gamma}_{\theta}^2} \right) \right] - \pi.$$

An interesting feature of this result is that the peak value of  $yy'(\theta)$ ; i.e.,  $||yy'||_{ss}$ , is quadratic in terms of the applied torque level in the pre-bifurcation stage — this is due to the fact that the absorber is tuned to eliminate the acceleration at linear order. An even more interesting result is that in the post-bifurcation stage,  $||yy'||_{ss}$  is independent of the torque level; i.e., it saturates after bifurcation. Furthermore, the acceleration  $yy'(\theta)$  vanishes as  $\hat{\mu}_a$  goes to zero. (Recall that the bifurcation torque level also goes to zero as  $\hat{\mu}_a$  goes to zero.) Since the acceleration predicted by equations (4.22) saturates after bifurcation, higher order terms in  $\rho$  will become dominant when the applied torque level begins to go beyond the bifurcation level. In order to obtain a more accurate estimate, one can use the acceleration approximated to the next order, which is given by

$$yy'(\theta) \simeq \nu \left[ \frac{2n^2}{N} \sum_{j=1}^{N} s_j s_j' + n^2 \xi_1 + \tilde{\Gamma}_{\theta} \sin(n\theta) + (n^2 + n^4) \sum_{j=1}^{N} s_j s_j'^2 - \frac{n^2(n^2 + n^4)}{2} \sum_{j=1}^{N} s_j^3 \right]$$
(4.23)

where  $s_i, 1 \leq i \leq N$  are approximated by equations (4.7), (4.18) and (4.19).

An even more accurate estimate can be obtained by numerically solving the non-truncated equations (3.12) given in section 3.2 for the stable  $S_1 \times S_{N-1}$  branch and substituting the resulting  $s_i$ ,  $1 \le i \le N$ , into equation (3.9). These results are found to match simulations very closely over the entire feasible torque range.

#### 4.6 Numerical and Simulation Results

In this section, existence and stability results for steady-state solutions are presented, along with simulation results, which are used to confirm the analytical results and to examine the accuracy of the various levels of approximations used in this study. In addition to the approximate results obtained in the previous sections, included here are numerical solutions of the non-truncated averaged equations (3.12) given in section 3.2. The system parameters used throughout this section are:  $\nu = 0.1662$  and n = 2; these were taken from the 2.5 liter, in-line, four-cylinder, four-stroke engine considered by Denman [16]. Recall that our approximations are based on a small  $\nu$  assumption, and the value considered here is a relatively large ratio for absorber systems; typical values are in the range 0.01-0.1. The absorber damping  $\hat{\mu}_a$  is taken to be independent of the number of the absorbers, N.

The Newton-Raphson method was employed to solve the non-truncated averaged equations (3.12) for the post-bifurcation branches. This process was repeated for the following parameter ranges: N=2 to 10 with increments of one,  $\hat{\mu}_a=0.0013$  to 0.013 with increments of 0.0001,  $\hat{\Gamma}^*_{\theta}=0.03$  to 0.08 with increments of 0.0001. In order to determine as many solutions as possible, several starting points were randomly chosen in the range  $r_i=0$  to 0.22 (the cusp level) and  $\varphi_i=0$  to  $2\pi$ , for each *i*. The associated stability of each solution was determined by numerically evaluating the eigenvalues of the associated Jacobian matrix. Numerical and simulation studies of many  $\mathbf{S_p} \times \mathbf{S_{N-p}}$  solutions were carried out. It was found that in the post-bifurcation stage, for absorber amplitudes below the cusp level, the only stable solution branch is the  $\mathbf{S_1} \times \mathbf{S_{N-1}}$  branch predicted by equations (4.14), (4.18) and (4.19).

Equations (3.2a), (3.2b) and (3.3) were used to directly simulate the system dynamics, using Gear's BDF method [59]. It was found that by utilizing a wide range of initial conditions and the ranges of system parameters described above, the system dynamics always converged to a stable  $S_1 \times S_{N-1}$  response in the post-bifurcation parameter range.

Figure 4.1 shows a typical set of post-bifurcation absorber responses for N=4,  $\hat{\mu}_a=0.0026$  and  $\hat{\Gamma}_\theta=0.048$ . (Note that different values of  $\hat{\mu}_a$  show qualitatively the same system dynamics as the value chosen here, although for higher damping levels

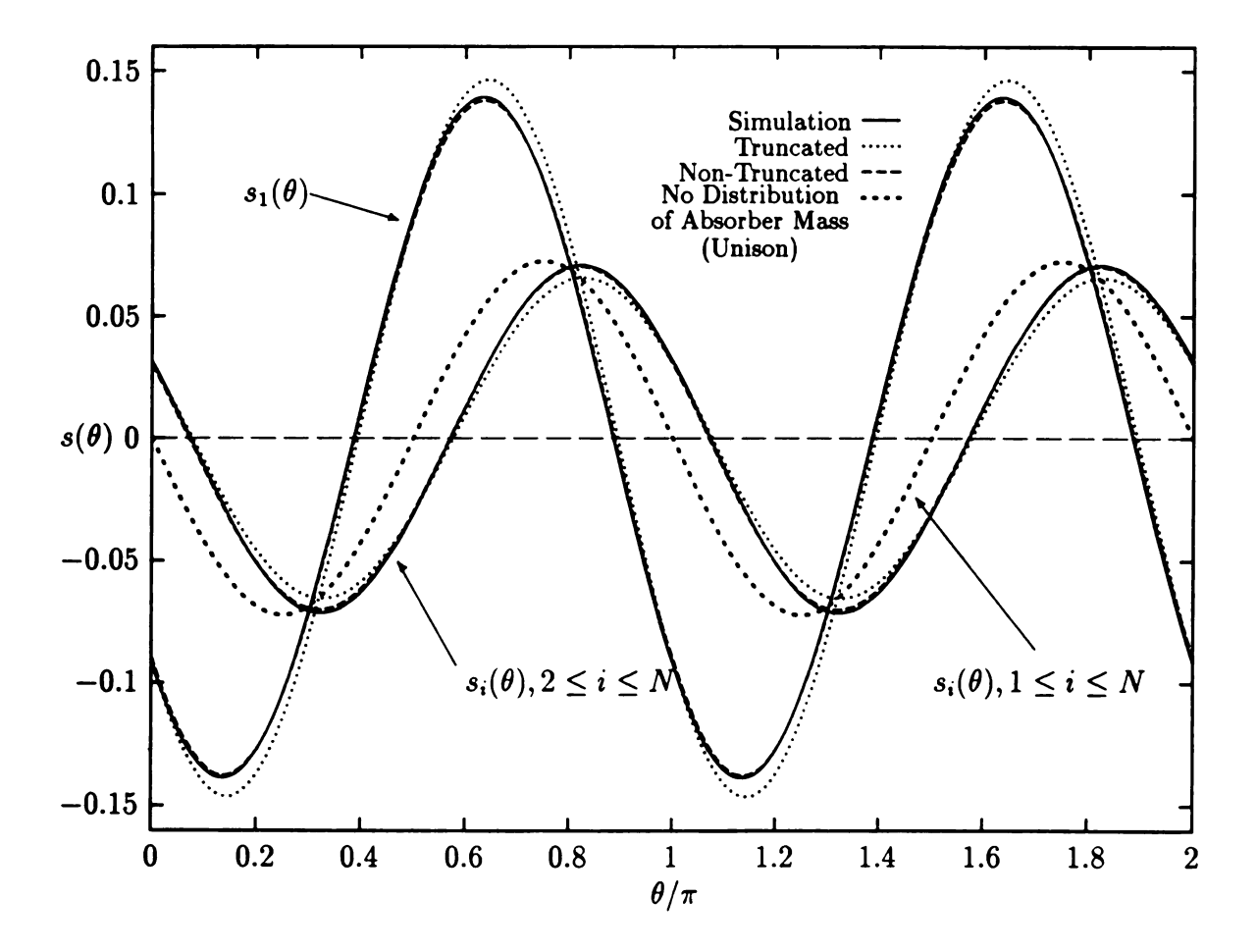


Figure 4.1: Post-bifurcation steady-state responses of the absorbers for N=4 (four absorbers),  $\hat{\mu}_a=0.0026$  and  $\hat{\Gamma}_\theta=0.048$ . Solid lines: Simulation; Dotted lines: Truncated; Dashed lines: Non-truncated; Coarsely dotted lines: Imposed unison response.

the

the

ස්

tic

(=

fo

re

the bifurcation of the unison response occurs nearer the cusp point.) In Figure 4.1, the solid lines represent the simulated response. The dotted lines are derived by estimating the response by truncated equations (4.7), (4.18), (4.19) and transformations (4.2). The dashed lines are obtained by assuming the stable  $S_1 \times S_{N-1}$  solution (= $S_1 \times S_3$  here) and numerically solving the non-truncated averaged equations (3.12) for the absorber responses. The coarse dotted lines represent the simulated absorbers' responses if they are locked into a unison motion (that is, the absorber inertia is a single lumped mass). This shows that the non-truncated equations are very accurate and that the truncated equations are quite satisfactory. Note that the system response, as compared with the corresponding unison motion, has N-1(=3) absorbers with a slight phase shift and little amplitude difference, while one absorber undergoes a motion with drastically different amplitude and phase. It is the localized response of this absorber that will limit the applied torque range. (Initial conditions determine which absorber goes to the large amplitude, but in practice small symmetry-breaking discrepancies may favor localization in a particular absorber.)

Figure 4.2 shows various estimates and simulations of the rotor acceleration for the same case as Figure 4.1. The 2nd-order approximation is derived by the truncated equations and the estimate given in equation (4.22), while the 3rd-order approximation is derived by the truncated equations and the estimate given in equation (4.23). It is seen that the 2nd-order approximation roughly represents the main harmonic component of the simulated acceleration, but offers a poor prediction for  $||yy'||_{ss}$ . This is due to the fact that in the post-bifurcation stage, the terms up to  $\mathcal{O}(\rho^2)$  in equation (3.9) saturate and the higher-order harmonics begin to dominate  $||yy'||_{ss}$ . One remedy to this problem is to use the 3rd-order approximation, from equation (4.23), to estimate  $||yy'||_{ss}$ , which offers a significant improvement over the 2nd-order results. As expected, the numerically-obtained, non-truncated solution is in excellent agreement with the simulated acceleration in all regards.

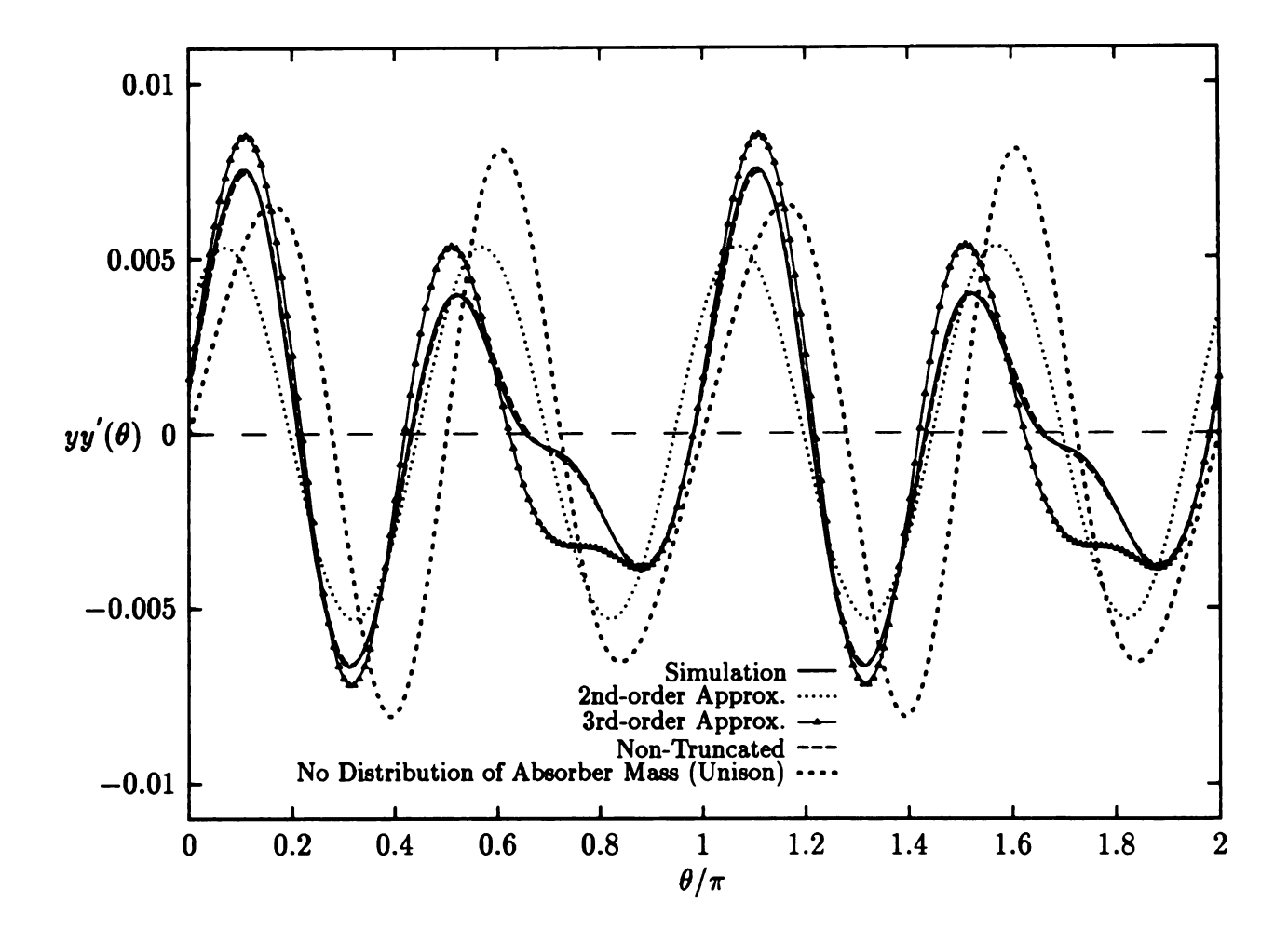


Figure 4.2: Post-bifurcation steady-state responses of the rotor acceleration for N=4 (four absorbers),  $\hat{\mu}_a=0.0026$  and  $\hat{\Gamma}_\theta=0.048$ . Solid lines: Simulation; Dotted lines: The 2nd-order approximation; Triangles: The 3rd-order approximation; Dashed lines: Non-truncated; Coarsely dotted lines: Imposed unison response.

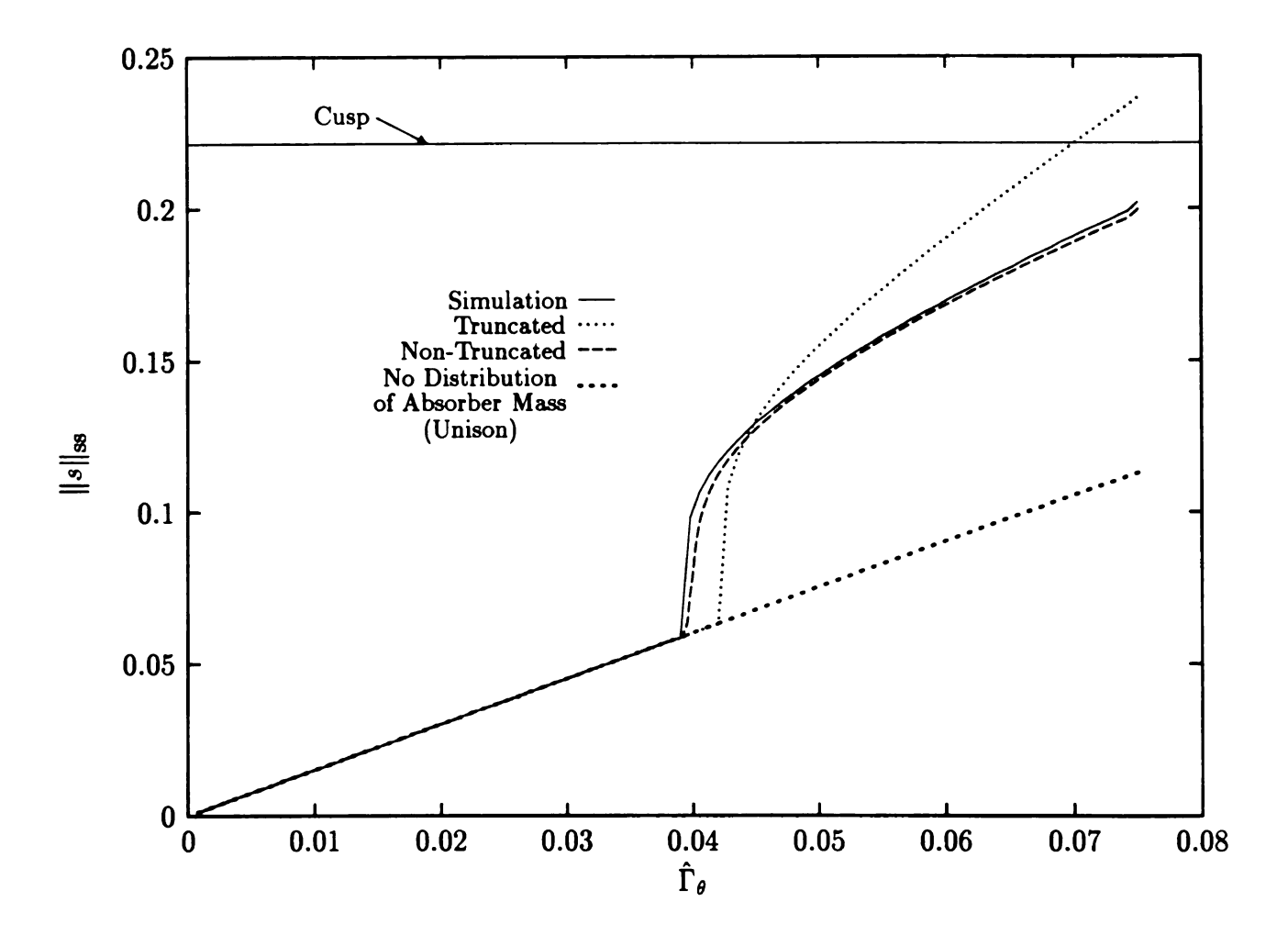


Figure 4.3: The  $||s||_{ss}$ 's derived by different approximations versus the applied torque level. The system parameters used are N=4 (four absorbers) and  $\hat{\mu}_a=0.0026$ . Solid lines: Simulation; Dotted lines: Truncated; Dashed lines: Non-truncated; Coarsely dotted lines: Imposed unison response.

Figure 4.3 shows the peak absorber amplitude  $||s||_{ss}$  versus the applied torque level. The maximum amplitude, which fixes the range of the applied torque, is set by the restriction in equation (3.4) and is marked as "Cusp" in the figure. From this figure, one observes that the truncated equations give a conservative prediction of the feasible torque range while the non-truncated equations give a very accurate estimate. Also, by comparing the unison and non-unison  $||s||_{ss}$ 's, one can see that the distribution of the total absorber mass into several smaller masses significantly decreases the operating torque range. Figure 4.4 shows the percent reduction in this range relative to the unison response for different numbers of absorbers. It is seen that as N increases, the feasible range is dramatically decreased by the bifurcation.

Figure 4.5 shows the rotor angular acceleration  $||yy'||_{ss}$  versus the applied torque level. In this figure, the 2nd-order approximation completely saturates after the bifurcation, which is not observed in the simulations. The 3rd-order results are much improved, and the non-truncated equations again give a very accurate result. By comparing the  $||yy'||_{ss}$ 's for the unison and non-unison responses in the post-bifurcation range, one can see that the distribution of absorber mass slightly improves absorber system performance by decreasing the  $||yy'||_{ss}$  levels. Figure 4.6 shows the ratio of the resulting  $||yy'||_{ss}$  to that for the unison response for various numbers of absorbers with  $\hat{\Gamma}_{\theta} = 0.0555$  and  $\hat{\mu}_{a} = 0.0026$ . It is seen that the  $||yy'||_{ss}$ 's obtained from simulations are well approximated by the non-truncated equations. However, the second and third order results significantly under and over estimate this ratio, respectively. Also, it is seen that the actual ratio approaches unity as N increases.

# 4.7 Concluding Remarks

This study considered the dynamic effects of using several masses to compose the required inertia for a system of tuned absorbers. For usual sizing calculations, one implicitly assumes that these masses move in a unison manner. In chapter 3, it was

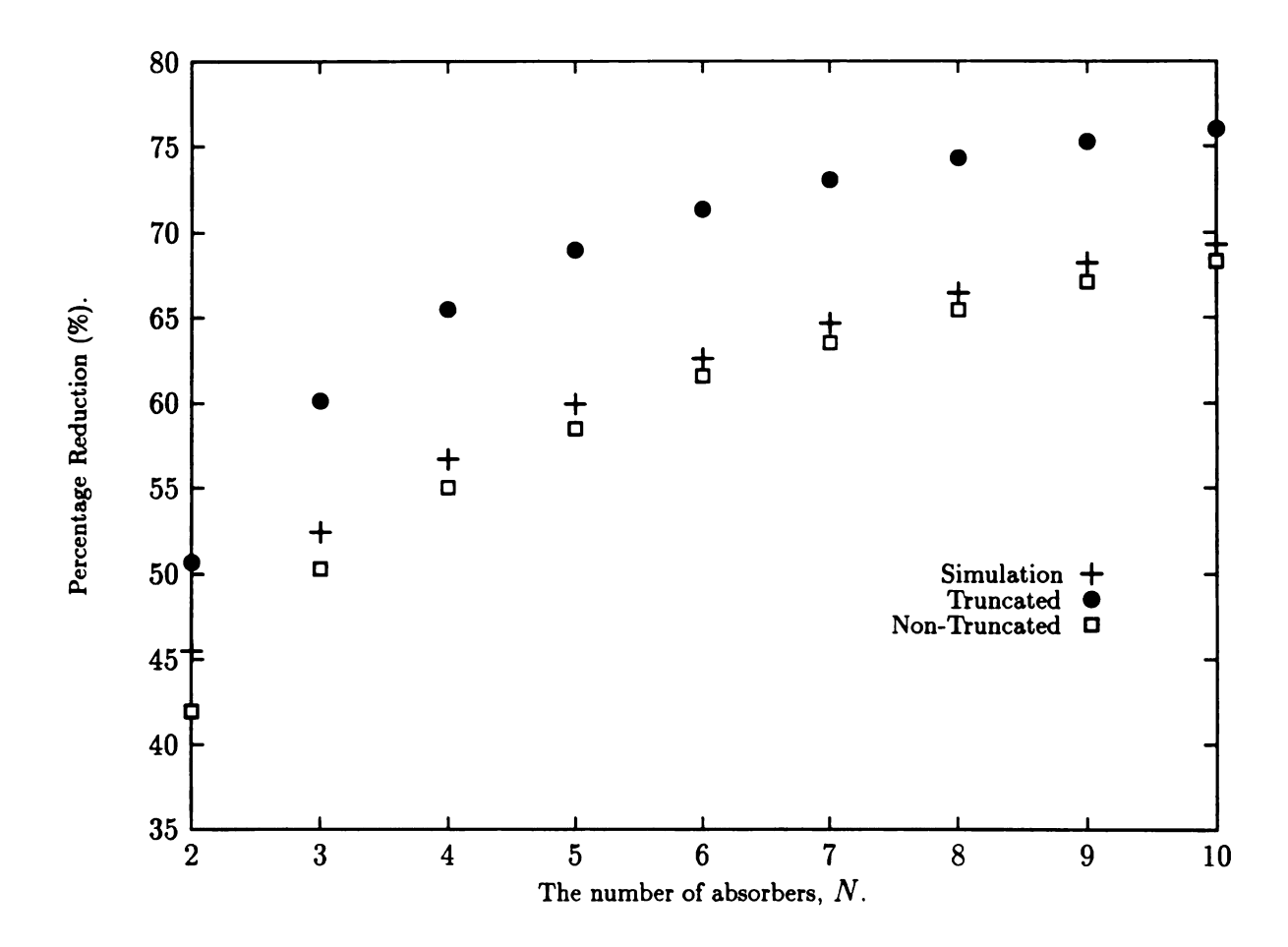


Figure 4.4: The percent reduction in torque range, relative to the unison motion, versus the number of absorbers for  $\hat{\mu}_a = 0.0026$ . "+": Simulation; "•": Truncated; " $\square$ ": Nontruncated.

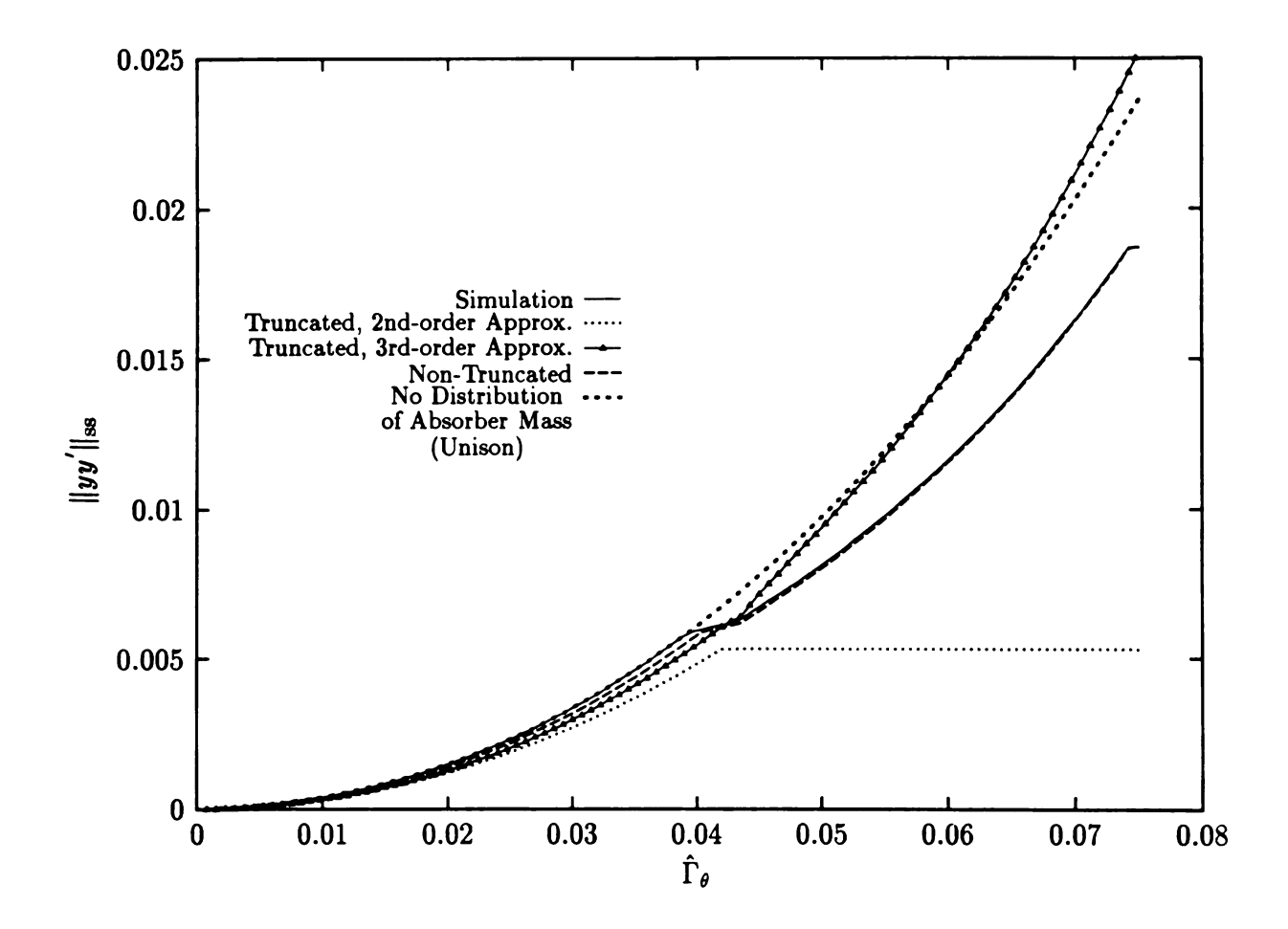


Figure 4.5: The  $||yy'||_{ss}$ 's derived by different approximations versus the applied torque level, for system parameters N=4 (four absorbers) and  $\hat{\mu}_a=0.0026$ . Solid lines: Simulation; Dotted lines: The 2nd-order approximation; Triangles: The 3rd-order approximation; Dashed lines: Nontruncated; Coarsely dotted lines: Imposed unison response.

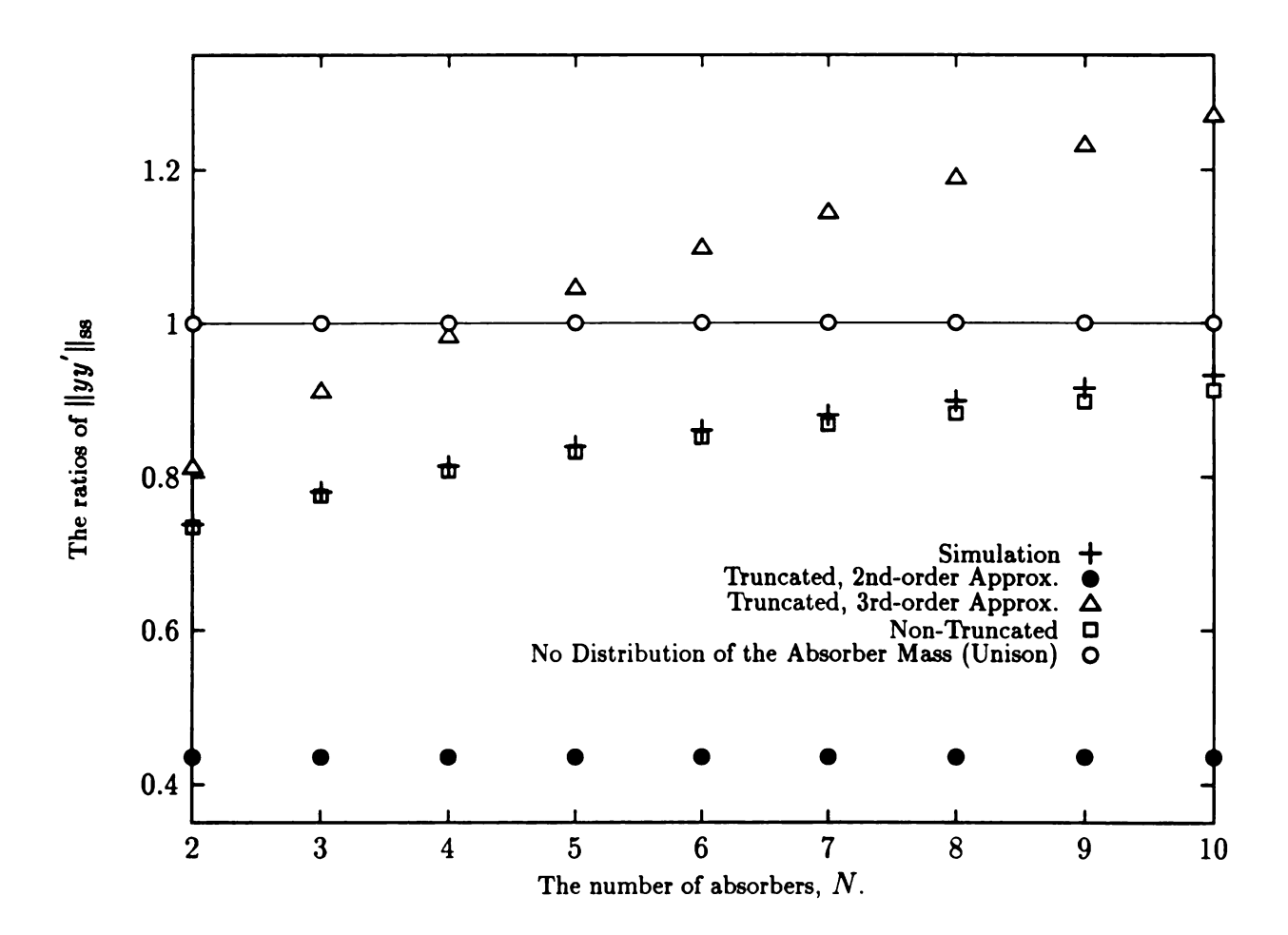


Figure 4.6: The ratio of  $||yy'||_{ss}$  to that for the unison response versus the number of absorbers for  $\hat{\Gamma}_{\theta} = 0.0555$  and  $\hat{\mu}_a = 0.0026$ . "+": Simulation; " $\bullet$ ": The 2nd-order approximation; " $\triangle$ ": The 3rd-order approximation; " $\square$ ": Non-truncated; " $\circ$ ": Imposed unison response.

determined that this motion can become dynamically unstable as the torque level is increased. In the present work the post-bifurcation dynamics are investigated. The results were obtained and verified by employing three methods: (1) low-order truncations of the averaged equations, (2) numerically solving the non-truncated averaged equations, and (3) simulations. The truncated equations offer reliable qualitative results in terms of the dependence on system parameters, but are not very accurate in some respects. In contrast, the non-truncated results, while requiring numerical solutions of the steady-state equations, are very accurate in all respects.

It was found that the post-bifurcation dynamics are dominated by a stable  $S_1 \times S_{N-1}$  steady-state solution branch. This is very reminiscent of *mode localization*, in that one absorber undergoes a much larger amplitude of motion relative to the others (see [62] for relevant work on nonlinear localization). It was also found that this  $S_1 \times S_{N-1}$  branch leads to the maximum  $||s||_{ss}$  and it results in a mild saturation of  $||yy'||_{ss}$  after bifurcation.

Combining the results shown in Figures 4.4 and 4.6 indicates that one does not gain a significant reduction in the level of torsional oscillations by the distribution of the total absorber mass into N masses, but the feasible torque range is drastically reduced.

Designers of absorber systems can refer to the information provided herein in order to obtain refined estimates of system performance before testing. However, it is recognized that other effects may have comparable influence on the overall system behavior. Of particular importance is the level of absorber damping; while generally small in practice, it is difficult to measure and may vary during operation (due to wear, temperature differences, etc.). It is interesting to note that when designing an absorber system, it is desirable to keep this damping as small as possible in order to keep the absorber oscillating in an out-of-phase manner relative to the disturbing torque. This offers optimal torque counteraction if the absorbers move in unison.

However, for a multiple absorber system, a smaller damping level will cause the bifurcation to non-unison response at a smaller level of the disturbing torque level, causing a potentially dramatic decrease in the applicable torque range.

As stated in the introduction, this investigation is only the first step in the study of unison absorber motions. To be of any practical use, the results must be extended to include: other absorber paths, including the widely-used, intentionally mis-tuned circular path; the effects of multiple harmonics in the torque; rotor flexibility and the distribution of torque along the axis of rotation; and mistuning, i.e., symmetry breaking, to name a few. Preliminary simulations that include small mistunings among the absorbers indicate that the individual absorber dynamics can be drastically altered by mistunings on the order of 1%. However, it is also observed that the overall  $||s||_{ss}$ 's and  $||yy'||_{ss}$ 's are quite robust to such changes. An investigation of these effects will bring the research squarely into the active realm of mode localization (Happawana et al [22]; Hodges [25]; Pierre and Dowell [45]; Vakakis and Cetinkaya [62]).

## CHAPTER 5

# THE EFFECTS OF IMPERFECTIONS AND MISTUNING ON THE PERFORMANCE OF THE PAIRED, SUBHARMONIC CPVA SYSTEM

A recent study by Lee et al. [30] has demonstrated a new configuration of centrifugal pendulum vibration absorbers (CPVA's) that is very effective at reducing torsional vibration levels in rotating systems that are subjected to harmonic external torques. This system is composed of a pair of absorbers riding on epicycloidal paths that are tuned to **one-half-order** relative to the frequency of the applied torque. Such a configuration is referred to as the subharmonic absorber system. It was shown in [30] that the restoring torque generated by an ideal, perfectly tuned, undamped pair of subharmonic absorbers is exactly a pure harmonic over a wide range of amplitudes. This has significant potential advantages over conventional designs, since it generates no higher-harmonic torques, even when accounting for nonlinear effects.

The aforementioned results are based the assumption that the absorber paths are perfectly tuned and are manufactured exactly as desired. In practice, however, due to manufacturing tolerances, wear, thermal effects, etc., the absorber paths are never perfect. It was the initial goal of this study to determine the sensitivity of the system response to such small imperfections. During the course of the investigation it was found that a slight mistuning of the linear natural frequencies of the absorbers can actually help to improve some aspects of the absorber performance, although at a price in terms of other measures. In order to account for these effects and to predict the corresponding performance of the absorber system, an extensive analysis

is conducted herein that includes imperfections and intentional mistuning in the mathematical system model.

An evaluation of absorber performance is accomplished by evaluating two performance measures: the angular acceleration of the rotor and the range of the applied torque. The former is used to quantify the level of vibration reduction, which is desired to be as small as possible, while the latter is imposed by the size of the absorbers' masses and their limited range of travel. To calculate these two performance measures, the system dynamic response is approximated using the method of averaging for a particular scaling of the system parameters. The solutions of the averaged equations are derived and considered in light of the system performance goals. Bifurcation diagrams are used to evaluate absorber performance and to distill some guidelines for the design of absorber paths.

## 5.1 The Subharmonic Absorber System

## 5.1.1 The Perfectly-Tuned Absorber System

A subharmonic absorber system was proposed by Lee et al. [30] which is composed of a pair of identical absorbers with individual masses  $m_i = \frac{m_0}{2}$  and identical damping coefficients  $\hat{\mu}_{ai} = \hat{\mu}_a$ , i = 1, 2. These absorbers ride on identical paths specified by

$$x_i^2(s_i) = 1 - \left(\frac{n}{2}\right)^2 s_i^2, \quad i = 1, 2$$
 (5.1)

which is equivalent to  $R_i(S_i) = \sqrt{R_0^2 - \left(\frac{n}{2}\right)^2 S_i^2}$ . This path can be shown to be a particular epicycloid, resulting in absorbers whose natural frequency in the constant rotation rate case is  $n\Omega/2$ , that is, one-half that of the applied torque.

The equations of motion (2.12a) and (2.12b) for N=2 and the identical paths given by equation (5.1) have an exact solution when the absorber damping is zero,

 $\hat{\mu}_a = 0$ , and condition (2.9) (for constant rotor speed) is satisfied. It is given by

$$y(\theta) = 1, (5.2a)$$

$$s_1(\theta) = -s_2(\theta) = \pm \frac{2}{n} \sqrt{\frac{2\hat{\Gamma}_{\theta}}{\nu n}} \cos\left(\frac{n}{2}\theta\right),$$
 (5.2b)

where  $\nu = \frac{m_0 R_0^2}{I_d}$  is the ratio of the total nominal moment inertia of both absorbers about point O to that of the rotor. It is seen from equation (5.2a) that in this response the rotor runs at a constant speed and the absorbers move in an exactly out-of-phase  $(s_1 = -s_2)$  subharmonic response of order two relative to the disturbing torque. In this response the absorbers exactly counteract the applied torque, hence the designation of the subharmonic absorber system. The physics of this absorber response can be seen by observing equation (2.12b), which describes the balance of the torques acting on the rotor. It is seen that the motions of the individual absorbers generate torque harmonics of all odd orders, which, due to their out-of-phase nature, cancel each other in the summation. However, each absorber also generates a single even-order torque, of harmonic n, through the Coriolis term  $\frac{dx_1}{ds_1}s_1'y^2$ . Since even-order torques add together in an out-of-phase motion, these add, creating a purely order n torque that exactly cancels the disturbing torque.

This steady-state operating condition corresponds to a perfectly constant rotor speed, which is the ultimate design goal of such an absorber system. Note also that this solution, while not absolutely global due to the limited range of absorber motion imposed by the cusps, is valid and exact over a wide range of torque amplitudes (described in more detail below). When the system possesses small, nonzero absorber damping, it was shown in [30] that this pair of subharmonic absorbers is able to limit the rotor acceleration  $\theta$  to a level that is of the same order as the absorber damping, and that this acceleration saturates at a fixed, small level as the torque amplitude is increased over a wide torque range.

## 5.1.2 Absorber Imperfections, Mistuning and Limitations

The dynamically favorable property described in the previous section can only be approximated in practice. Several effects will come into play that limit the ideal solution, including tolerances in the cutting process used for generating the absorber paths, the presence of rollers in the bifilar configuration (whose dynamics do not follow the absorbers' motions [16]), and deformations due to wear, elasticity or thermal effects. In order to account for these imperfections, the absorber path functions (5.1) are generalized to the following,

$$x_{i}(s_{i}; \varrho_{ij}) = 1 - \left(\frac{n}{2}\right)^{2} s_{i}^{2} - \sum_{j} \varrho_{ij} s_{i}^{j}, \quad i = 1, 2$$
 (5.3)

where the  $\varrho$ 's are used to quantify the the deviations from the ideal path. Note that all  $\varrho$ 's are assumed to be small in magnitude in the following analysis. In order to have control on the system dynamics, it is also worthwhile to examine the effect of intentionally mistuning the linear frequencies of the absorbers relative to their design value of n/2. To incorporate this mistuning, the absorber path describing functions are reformulated as

$$x_i(s_i; \varrho_{ij}, \Delta\omega_i) = 1 - \left[ \left( \frac{n}{2} \right)^2 + \Delta\omega_i \right] s_i^2 - \sum_j \varrho_{ij} s_i^j, \quad i = 1, 2$$
 (5.4)

where the  $\Delta\omega$ 's represent the intentional mistuning for each path. For simplification equation (5.4) is re-expressed as

$$x_i(s_i; \hat{\delta}_{ij}) = 1 - \left(\frac{n}{2}\right)^2 s_i^2 - \sum_j \hat{\delta}_{ij} s_i^j, \quad i = 1, 2,$$
 (5.5)

where  $\hat{\delta}_{ij} = \varrho_{ij}$  for all i, j, except  $\hat{\delta}_{i2} = \varrho_{i2} + \Delta \omega_i$  for i=1, 2. This split may appear to be artificial, but the idea is that the parameters  $\Delta \omega_i$  are to be designed into the path, whereas the  $\varrho_{ij}$ 's are small and generally unknown perturbations in the path.

From equation (2.8), it should be noted that the value of the function  $g_i(s_i)$  must be kept real during absorber motions. This leads to a restriction on the amplitudes

of the absorber motions. For the case when all mistunings and imperfections are small,  $\hat{\delta}_{ij} \ll 1$ , the aforementioned restriction is approximated by

$$s_i(\theta) \le s_{\max} + \mathcal{O}(\hat{\delta}), \quad \forall \ \theta \text{ and } i, \quad \text{where } s_{\max} = \frac{4}{n\sqrt{n^2 + 4}}.$$
 (5.6)

This restriction, derived by maintaining the g(s)'s real, keeps the absorbers from passing the cusp points of the epicycloidal paths. This also imposes a finite operating range on the disturbing torque level  $\hat{\Gamma}_{\theta}$ . For the case of perfect absorber paths it is given by

$$\hat{\Gamma}_{\theta} \le \bar{\hat{\Gamma}}_{\theta,0} = \frac{2n\nu}{n^2 + 4},\tag{5.7}$$

over which the desired system response given in equations (5.2) can be maintained. (Note that these explicit forms can be given for the subharmonic absorber since the desired ideal steady state response is known exactly.)

## 5.2 Measures of Performance

Two performace measures will be used to quantify the effectiveness of an absorber system. The first is the amplitude of torsional oscillations here represented by its peak angular acceleration at steady state, denoted by  $||yy'||_{ss}$ . The second performance measure is the range of the applied torque amplitude over which the absorber can operate, denoted by  $\tilde{\Gamma}_{\theta}$ . A complete description of these two performance measures was provided in section 2.6. Note that for the perfect, undamped subharmonic absorber,  $||yy'||_{ss} = 0$  and the corresponding torque range is given by  $\tilde{\Gamma}_{\theta,0}$  in equation (5.7). One of the main goals of this work is to determine  $||yy'||_{ss}$  and the generalization for condition (5.7) for the damped, imperfect system. These results will point out some limitations that are imposed on the subharmonic absorber system by parameter uncertainties, but it will also offer the designer some flexibility in designing the path to achieve certain goals.

## 5.3 Scaling and Reduction of the Equations of Motion

Approximate solutions are sought for the damped and imperfect system by making some scaling assumptions and employing asymptotic analysis techniques. This is accomplished by first utilizing the definition of the small parameter  $\epsilon$  in equation (3.5) and the scaling (3.6) used for a different case in section 3.1.1. With the definition of  $\epsilon \equiv \nu$ , the small imperfections and mistunings can be scaled by

$$\hat{\delta}_{ij} = \epsilon \tilde{\delta}_{ij}, \quad \forall j, \quad \text{and} \quad i = 1, 2.$$
 (5.8)

Note that typical values of the  $\tilde{\delta}_{ij}$ 's are less than one percent, whereas  $\nu$  may range from one to ten percent. The conservative assumption (5.8) is made in order to incorporate the effects of imperfections and mistunings in the first order analysis.

The unperturbed system dynamics for this scaling are determined by considering equation (2.12b) with  $\epsilon = 0$ , that is,  $\nu = 0$ , which yields y = 1. Using this in equation (2.12a) with  $\hat{\mu}_a = 0$  yields a linear oscillator with frequency n/2 for the absorber motion. Thus, the steady-state solution of the unperturbed system is simply a constant rotor speed, y = 1, and the absorber motion is harmonic with frequency n/2 and arbitrary amplitude.

The rotor acceleration can be derived by following the same procedure used for the case with N tautochronic absorbers described in section 3.1.2. This gives the following expression for the acceleration,

$$yy'(\theta) = -\epsilon \left\{ \frac{1}{2} \sum_{j=1}^{2} \left( -\frac{n^{2}}{2} s_{j} s_{j}' - \left( \frac{n}{2} \right)^{2} g^{0}(s_{j}) s_{j} + \frac{dg^{0}(s_{j})}{ds_{j}} s_{j}'^{2} \right) - \tilde{\Gamma}_{\theta} \sin(n\theta) \right\} + \mathcal{O}(\epsilon^{2}).$$
(5.9)

where

$$g^{0}(s_{i}) = g_{i}(s_{i}; \hat{\delta}_{ij} = 0) = \sqrt{1 - \left(\frac{4n^{2} + n^{4}}{16}\right) s_{i}^{2}}, \quad i = 1, 2.$$

Likewise, a set of weakly coupled, weakly nonlinear oscillators for the absorber dynamics can be obtained, given by

$$s_{i}'' + \left(\frac{n}{2}\right)^{2} s_{i} = \epsilon f_{i}(s_{1}, s_{2}, s_{1}', s_{2}', \theta) + \mathcal{O}(\epsilon^{2}), \qquad i = 1, 2$$
 (5.10)

where

$$f_{i}(s_{1}, s_{2}, s'_{1}, s'_{2}, \theta) = -\tilde{\mu}_{a}s'_{i} - h_{i}(s_{i})$$

$$+[s'_{i} + g^{0}(s_{i})][\frac{1}{2}\sum_{j=1}^{2}(-\frac{n^{2}}{2}s_{j}s'_{j} - \left(\frac{n}{2}\right)^{2}g^{0}(s_{j})s_{j} + \frac{dg^{0}(s_{j})}{ds_{j}}s'_{j}^{2})$$

$$-\tilde{\Gamma}_{\theta}\sin(n\theta)],$$

$$h_{i}(s_{i}) = \frac{1}{2}\sum_{i}j\tilde{\delta}_{ij}s_{i}^{j-1}.$$

## Remarks:

- This system has two degrees of freedom with a 1:1 internal resonance. In addition, the excitation is in a 2:1 resonance with respect to the absorbers, and it is of parametric form. In this regard, the system is very similar to that considered by Yang and Sethna [67].
- The effects of the imperfections and intentional mistunings are present in the function h's which results from the term  $\frac{1}{2}\frac{dx_1}{ds_1}y$  in the equation of motion (2.12a).

# 5.4 The Averaged Equations

In this section some standard coordinate changes are first carried out which put the equations in the desired form. Averaging is then applied, and this followed by a discussion of the system parameters which appear in the averaged equations and by a presentation of a modified form of the equations for a special scaling of the imperfections. With these forms of the averaged equations in hand, the search for approximate steady-state solutions is carried out in the following sections, the results of which are used for performance evaluation.

#### 5.4.1 The Periodic Standard Form

A linear coordinate transformation between absorber displacements is first used to simplify the ensuing analysis. This transformation splits the leading order system dynamics into two invariant subspaces, representing the unison motion and its complement. A subsequent transformation to amplitude/phase coordinates will render the desired form.

The first transformation is given by

$$\xi = \frac{s_1 + s_2}{2}$$
 and  $\eta = \frac{s_1 - s_2}{2}$ . (5.11)

Substituting transformation (5.11) into equations (5.10) yields the following transformed equations of motion

$$\xi'' + \left(\frac{n}{2}\right)^{2} \xi = \epsilon \hat{f}_{\xi}(\xi, \xi', \eta, \eta', \theta) + \mathcal{O}(\epsilon^{2}),$$

$$\eta'' + \left(\frac{n}{2}\right)^{2} \eta = \epsilon \hat{f}_{\eta}(\xi, \xi', \eta, \eta', \theta) + \mathcal{O}(\epsilon^{2}), \quad 2 \leq i \leq N, \quad (5.12)$$

where

$$\hat{f}_{\xi}(\xi,\xi',\eta,\eta',\theta) = -\tilde{\mu}_{a}\xi' - \frac{1}{2}h_{1}(\xi+\eta) - \frac{1}{2}h_{2}(\xi-\eta) 
+ \left[\xi' + \frac{1}{2}g^{0}(\xi+\eta) + \frac{1}{2}g^{0}(\xi-\eta)\right]Y(\xi+\eta,\xi-\eta,\theta), 
\hat{f}_{\eta}(\xi,\xi',\eta,\eta',\theta) = -\tilde{\mu}_{a}\eta' - \frac{1}{2}h_{1}(\xi+\eta) + \frac{1}{2}h_{2}(\xi-\eta) 
+ \left[\eta' + \frac{1}{2}g^{0}(\xi+\eta) - \frac{1}{2}g^{0}(\xi-\eta)\right]Y(\xi+\eta,\xi-\eta,\theta), 
Y(s_{1},s_{2},\theta) = \frac{1}{2}\sum_{j=1}^{2}(-\frac{n^{2}}{2}s_{j}s_{j}' - \left(\frac{n}{2}\right)^{2}g^{0}(s_{j})s_{j} + \frac{dg^{0}(s_{j})}{ds_{j}}s_{j}'^{2}) 
-\tilde{\Gamma}_{\theta}\sin(n\theta).$$
(5.13a)

Next, the polar coordinate transformation given by

$$\xi = r_{\xi} \cos(\varphi_{\xi} - \frac{n\theta}{2}), \qquad \xi' = nr_{\xi} \sin(\varphi_{\xi} - \frac{n\theta}{2}),$$

$$\eta = r_{\eta} \cos(\varphi_{\eta} - \frac{n\theta}{2}), \qquad \eta' = nr_{\eta} \sin(\varphi_{\eta} - \frac{n\theta}{2}). \tag{5.14}$$

is applied. Substituting the above transformations into equations (5.12) yields a set of first-order differential equations which describe the dynamics of  $r_{\xi}$ ,  $\varphi_{\xi}$ ,  $r_{\eta}$  and  $\varphi_{\eta}$  in the periodic standard form [39], as follows,

$$r'_{\xi} = \frac{2\epsilon}{n} \hat{F}_{\xi}(r_{\xi}, \varphi_{\xi}, r_{\eta}, \varphi_{\eta}, \theta) \sin(\varphi_{\xi} - \frac{n\theta}{2}) + \mathcal{O}(\epsilon^{2}),$$
 (5.15a)

$$r_{\xi}\varphi_{\xi}' = \frac{2\epsilon}{n}\hat{F}_{\xi}(r_{\xi}, \varphi_{\xi}, r_{\eta}, \varphi_{\eta}, \theta)\cos(\varphi_{\xi} - \frac{n\theta}{2}) + \mathcal{O}(\epsilon^{2}), \tag{5.15b}$$

$$r'_{\eta} = \frac{2\epsilon}{n} \hat{F}_{\eta}(r_{\xi}, \varphi_{\xi}, r_{\eta}, \varphi_{\eta}, \theta) \sin(\varphi_{\eta} - \frac{n\theta}{2}) + \mathcal{O}(\epsilon^{2}),$$
 (5.15c)

$$r_{\eta}\varphi'_{\eta} = \frac{2\epsilon}{n}\hat{F}_{\eta}(r_{\xi},\varphi_{\xi},r_{\eta},\varphi_{\eta},\theta)\cos(\varphi_{\eta}-\frac{n\theta}{2}) + \mathcal{O}(\epsilon^{2}),$$
 (5.15d)

where the functions  $\hat{F}_{\xi}$  and  $\hat{F}_{\eta}$  are simply  $\hat{f}_{\xi}$  and  $\hat{f}_{\eta}$  expressed, respectively, in terms of coordinates  $r_{\xi}$ ,  $\varphi_{\xi}$ ,  $r_{\eta}$  and  $\varphi_{\eta}$ , as obtained by incorporating transformation (5.14) into  $\hat{f}_{\xi}$  and  $\hat{f}_{\eta}$ . Equations (5.15a) to (5.15d) are in the desired form for averaging.

## 5.4.2 Application of Averaging

Considering only the first order terms in  $\epsilon$  in equations (5.15), averaging is performed in  $\theta$  over one period of the excitation,  $\frac{4\pi}{n}$ . The resulting averaged equations are expressed in terms of the first-order averaged variables  $\bar{r}_{\xi}$ ,  $\bar{\varphi}_{\xi}$ ,  $\bar{r}_{\eta}$  and  $\bar{\varphi}_{\eta}$ . Due to the complicated nature of the system, this process results in many terms in the form of integrals which do not yield closed-form expressions.

In order to obtain simplified, approximate estimates of the rotor acceleration and the operating torque range, it is assumed that the oscillation amplitudes of the absorbers, that is,  $\bar{r}_{\xi}$  and  $\bar{r}_{\eta}$ , are small and of the same order, denoted by  $\mathcal{O}(\bar{r})$ . The averaged equations are then expanded in terms of  $\bar{r}_{\xi}$  and  $\bar{r}_{\eta}$ . This yields the following set of truncated, averaged equations, where each has been expanded to the desired order,  $\mathcal{O}(\bar{r}^3)$ ,

$$\frac{d\bar{r}_{\xi}}{d\hat{\theta}} = \frac{-1}{2}\tilde{\mu}_{a}\bar{r}_{\xi} - \left(\frac{\tilde{\delta}_{\eta 2}\bar{r}_{\eta}}{n} + \frac{3\tilde{\delta}_{\eta 4}\bar{r}_{\eta}^{3}}{2n} + \frac{3\tilde{\delta}_{\eta 4}\bar{r}_{\xi}^{2}\bar{r}_{\eta}}{2n}\right)\sin(\bar{\varphi}_{\xi} - \bar{\varphi}_{\eta}) + \frac{1}{4}\tilde{\Gamma}_{\theta}\bar{r}_{\xi}\sin2\bar{\varphi}_{\xi} + c_{n1}\bar{r}_{\xi}\bar{r}_{\eta}^{2}\sin(2\bar{\varphi}_{\xi} - 2\bar{\varphi}_{\eta}) + \mathcal{O}(\bar{r}^{5}),$$
(5.16a)

$$\bar{r}_{\xi} \frac{d\bar{\varphi}_{\xi}}{d\hat{\theta}} = \left(-\frac{\tilde{\delta}_{\xi^{2}}}{n} - \frac{n}{4}\right) \bar{r}_{\xi} - \left(\frac{\tilde{\delta}_{\eta^{2}}\bar{r}_{\eta}}{n} + \frac{3\tilde{\delta}_{\eta^{4}}\bar{r}_{\eta}^{3}}{2n} + \frac{9\tilde{\delta}_{\eta^{4}}\bar{r}_{\xi}^{2}\bar{r}_{\eta}}{2n}\right) \cos(\bar{\varphi}_{\xi} - \bar{\varphi}_{\eta})$$

$$+ \frac{1}{4}\tilde{\Gamma}_{\theta}\bar{r}_{\xi}\cos2\bar{\varphi}_{\xi} + c_{n1}\bar{r}_{\xi}\bar{r}_{\eta}^{2}\cos(2\bar{\varphi}_{\xi} - 2\bar{\varphi}_{\eta}) + c_{n2}\bar{r}_{\xi}^{3} + c_{n3}\bar{r}_{\xi}\bar{r}_{\eta}^{2}$$

$$+ \mathcal{O}(\bar{r}^{5}), \qquad (5.16b)$$

$$\frac{d\bar{r}_{\eta}}{d\hat{\theta}} = \frac{-1}{2}\tilde{\mu}_{a}\bar{r}_{\eta} - \left(\frac{\tilde{\delta}_{\eta^{2}}\bar{r}_{\xi}}{n} + \frac{3\tilde{\delta}_{\eta^{4}}\bar{r}_{\xi}^{3}}{2n} + \frac{3\tilde{\delta}_{\eta^{4}}\bar{r}_{\eta}^{2}\bar{r}_{\xi}}{2n}\right) \sin(\bar{\varphi}_{\eta} - \bar{\varphi}_{\xi}) + \frac{1}{4}\tilde{\Gamma}_{\theta}\bar{r}_{\eta}\sin2\bar{\varphi}_{\eta}$$

$$+ c_{n1}\bar{r}_{\eta}\bar{r}_{\xi}^{2}\sin(2\bar{\varphi}_{\eta} - 2\bar{\varphi}_{\xi}) + \mathcal{O}(\bar{r}^{5}), \qquad (5.16c)$$

$$\bar{r}_{\eta}\frac{d\bar{\varphi}_{\eta}}{d\hat{\theta}} = -\frac{\tilde{\delta}_{\xi^{2}}}{n}\bar{r}_{\eta} - \left(\frac{\tilde{\delta}_{\eta^{2}}\bar{r}_{\xi}}{n} + \frac{3\tilde{\delta}_{\eta^{4}}\bar{r}_{\xi}^{3}}{2n} + \frac{9\tilde{\delta}_{\eta^{4}}\bar{r}_{\eta}^{2}\bar{r}_{\xi}}{2n}\right)\cos(\bar{\varphi}_{\eta} - \bar{\varphi}_{\xi}) + \frac{1}{4}\tilde{\Gamma}_{\theta}\bar{r}_{\eta}\cos2\bar{\varphi}_{\eta}$$

$$+ c_{n1}\bar{r}_{\eta}\bar{r}_{\xi}^{2}\cos(2\bar{\varphi}_{\eta} - 2\bar{\varphi}_{\xi}) - c_{n4}\bar{r}_{\eta}^{3} + c_{n3}\bar{r}_{\eta}\bar{r}_{\xi}^{2} + \mathcal{O}(\bar{r}^{5}), \qquad (5.16d)$$

and where

$$\hat{\theta} \equiv \epsilon \theta, \quad \tilde{\delta}_{\xi 2} = \frac{\tilde{\delta}_{12} + \tilde{\delta}_{22}}{2}, \quad \tilde{\delta}_{\eta 2} = \frac{\tilde{\delta}_{12} - \tilde{\delta}_{22}}{2}, \quad \tilde{\delta}_{\xi 4} = \frac{\tilde{\delta}_{14} + \tilde{\delta}_{24}}{2}, \quad \tilde{\delta}_{\eta 4} = \frac{\tilde{\delta}_{14} - \tilde{\delta}_{24}}{2}, \\
c_{n1} = \frac{4n^3 - n^5}{256} - \frac{3\tilde{\delta}_{\xi 4}}{2n}, \quad c_{n2} = \frac{n^5}{128} - \frac{3\tilde{\delta}_{\xi 4}}{2n}, \quad c_{n3} = \frac{4n^3 + n^5}{128} - \frac{3\tilde{\delta}_{\xi 4}}{2n} \\
\text{and} \quad c_{n4} = \frac{n^3}{32} + \frac{3\tilde{\delta}_{\xi 4}}{2n}. \tag{5.17}$$

These equations contain the essential dynamics that arise from the resonant structure of this system. The stationary solutions of equations (5.16) represent the amplitudes and phases of the periodic steady-state responses of the absorbers, as represented by the unison and opposition modal coordinates. Non-stationary steady-state solutions are represented by amplitude and phase modulated oscillations of the averaged equations.

The averaged equations (5.16) as derived using the polar transformation (5.14) are singular when either  $\xi$  or  $\eta$  is zero. Therefore, they cannot be used for determining the stability of any trivial solutions that may exist. When faced with this problem, the following transformation is employed,

$$A_{\xi} = \bar{r}_{\xi} \cos \bar{\varphi}_{\xi}, \quad B_{\xi} = \bar{r}_{\xi} \sin \bar{\varphi}_{\xi}, \quad A_{\eta} = \bar{r}_{\eta} \cos \bar{\varphi}_{\eta}, \quad \text{and} \quad B_{\eta} = \bar{r}_{\eta} \sin \bar{\varphi}_{\eta}, \quad (5.18)$$
  
which yields an equivalent set of truncated, averaged equations expressed in Cartesian

coordinates. These are given in Appendix H.

## 5.4.3 System Parameters

The averaged equations (5.16) depend on seven dimensionless parameters:  $\tilde{\mu}_a$ ,  $\tilde{\Gamma}_{\theta}$ , n,  $\tilde{\delta}_{\xi 2}$ ,  $\tilde{\delta}_{\eta 2}$   $\tilde{\delta}_{\xi 4}$  and  $\tilde{\delta}_{\eta 4}$ .

Note that the effects of imperfections are present in the truncated averaged equations only through the second and fourth order terms as they are defined in terms of the path formulations given in equation (5.5). The coefficients of odd powers of s in the path formulation, that is,  $\hat{\delta}_{\xi 1}$ ,  $\hat{\delta}_{\eta 1}$ ,  $\hat{\delta}_{\xi 3}$  and  $\hat{\delta}_{\eta 3}$ , do not appear in the averaged equations (5.16). Thus, the analysis indicates that such terms, which measure the deviation of the path's symmetry about its vertex, do not contribute to the resonant responses. As defined in equation (5.17), the parameters  $\tilde{\delta}_{\xi 2}$  and  $\tilde{\delta}_{\eta 2}$  are the sum and difference of  $\tilde{\delta}_{12}$  and  $\tilde{\delta}_{22}$ , respectively, and these result from the net effects of frequency mistuning and linear imperfections in the dynamics of each absorber. The parameters  $\tilde{\delta}_{\xi 4}$  and  $\tilde{\delta}_{\eta 4}$  result from fourth-order imperfections in the absorber path realization, that is, they capture the leading-order nonlinear imperfections that are symmetric about the path vertex.

Of the other system parameters,  $\tilde{\mu}_a$  is the absorber damping which, in practice, is designed to be small and will be regarded as fixed in the bifurcation analysis of this chapter.  $\tilde{\Gamma}_{\theta}$  is the amplitude of the main harmonic of the disturbing torque, and this is used as the primary bifurcation parameter. Since the absorber motions are prevented from reaching the cusps on their paths, the applicable range for  $\tilde{\Gamma}_{\theta}$  is finite for each steady-state solution branch of the averaged equations (5.16). The value of n is fixed by the loading condition, e.g., in an M-cylinder, four-stroke internal combustion engine, n = M/2. Note that the value of n affects the signs of the  $c_n$ 's, and can even render them zero if  $\tilde{\delta}_{\xi 4} = 0$ . These differences can result in qualitatively different bifurcation diagrams, as shown below.

Note also that the term  $-n\bar{r}_{\xi}/4$  in equation (5.16b) results from expansion of

the term  $(n/2)^2 g^0(s_i) s_i$  in the  $\epsilon$ -order function Y in equation (5.13). This term characterizes the difference between the linear frequencies of the two modes, that is,  $-n\bar{r}_{\xi}/4$  plays the role of internal mistuning on the system dynamics. When this term is nonzero, the system dynamics are not invariant under the exchange of the two modes. It will be seen in the analysis presented below that this term is a key factor in obtaining the desired performance of the subharmonic absorber system.

## 5.4.4 Averaged Equations for Nearly Identical Absorber Paths

In order to evaluate absorber performance in terms of the two performance measures defined above, the steady-state solutions of the truncated averaged equations (5.16) must be determined. However, due to the complexity of the expanded averaged equations (5.16), it is impossible to find steady-state solutions in closed form. In order to determine some approximate solutions an additional scaling assumption on the mistuning parameters is employed.

It is assumed that one can manufacture the curves for the absorbers such that the relative precision between the curves is much higher than their absolute precision. This assumption leads to the following scaling of the imperfection parameters,

$$\frac{\tilde{\delta}_{\eta i}}{\tilde{\delta}_{\xi i}} = \mathcal{O}(\epsilon) \quad \text{for } i = 1, 2, \dots$$
 (5.19)

This scaling allows the designer to intentionally mistune the absorbers relative to the order of the applied torque, and it accounts for some imperfection in the paths, but it does assume that the two paths are nearly identical. With scaling (5.19) adopted, the terms involving the  $\tilde{\delta}_{\eta}$ 's in the averaged equations (5.16) are pushed out to  $\mathcal{O}(\epsilon^2)$ , and thus have no influence on the dynamics at this level of approximation. This scaling assumption will be revisited near the end of this chapter.

The resulting modified, truncated averaged equations are given by,

$$\frac{d\bar{r}_{\xi}}{d\hat{\theta}} = \frac{-1}{2}\tilde{\mu}_{\alpha}\bar{r}_{\xi} + \frac{1}{4}\tilde{\Gamma}_{\theta}\bar{r}_{\xi}\sin 2\bar{\varphi}_{\xi} - c_{n1}\bar{r}_{\xi}\bar{r}_{\eta}^{2}\sin(2\bar{\varphi}_{\xi} - 2\bar{\varphi}_{\eta}), \qquad (5.20a)$$

$$\bar{r}_{\xi} \frac{d\bar{\varphi}_{\xi}}{d\hat{\theta}} = \left(\frac{-\tilde{\delta}_{\xi 2}}{n} - \frac{n}{4}\right) \bar{r}_{\xi} + \frac{1}{4} \tilde{\Gamma}_{\theta} \bar{r}_{\xi} \cos 2\bar{\varphi}_{\xi} + c_{n1} \bar{r}_{\xi} \bar{r}_{\eta}^{2} \cos(2\bar{\varphi}_{\xi} - 2\bar{\varphi}_{\eta}) + c_{n2} \bar{r}_{\xi}^{3} + c_{n3} \bar{r}_{\xi} \bar{r}_{\eta}^{2},$$

$$(5.20b)$$

$$\frac{d\bar{r}_{\eta}}{d\hat{\theta}} = \frac{-1}{2}\tilde{\mu}_{a}\bar{r}_{\eta} + \frac{1}{4}\tilde{\Gamma}_{\theta}\bar{r}_{\eta}\sin 2\bar{\varphi}_{\eta} - c_{n1}\bar{r}_{\eta}\bar{r}_{\xi}^{2}\sin(2\bar{\varphi}_{\eta} - 2\bar{\varphi}_{\xi}), \qquad (5.20c)$$

$$\bar{r}_{\eta} \frac{d\bar{\varphi}_{\eta}}{d\hat{\theta}} = \frac{-\tilde{\delta}_{\xi 2}}{n} \bar{r}_{\eta} + \frac{1}{4} \tilde{\Gamma}_{\theta} \bar{r}_{\eta} \cos 2\bar{\varphi}_{\eta} + c_{n1} \bar{r}_{\eta} \bar{r}_{\xi}^{2} \cos(2\bar{\varphi}_{\eta} - 2\bar{\varphi}_{\xi}) - c_{n4} \bar{r}_{\eta}^{3} + c_{n3} \bar{r}_{\eta} \bar{r}_{\xi}^{2}$$

$$(5.20d)$$

where  $\hat{\theta}$ ,  $c_{n1}$ ,  $c_{n2}$ ,  $c_{n3}$  and  $c_{n4}$  are the same as defined in equations (5.17). Utilizing transformation (5.18), the corresponding averaged equations (5.20) in terms of Cartesian coordinates are determined, and these are given by equations (H.2) in Appendix H.

It is seen from equations (5.20) that in this case  $\tilde{\Gamma}_{\theta}$ , n,  $\tilde{\delta}_{\xi 2}$  and  $\tilde{\delta}_{\xi 4}$  are the important parameters to be considered in the bifurcation analysis.  $\tilde{\delta}_{\xi 2}$  enters the averaged equations as a linear frequency detuning, while  $\tilde{\delta}_{\xi 4}$  affects the coefficients of the first-order nonlinear terms. If  $\tilde{\delta}_{\xi 4}$  is very small, the value of n will dictate the coefficients of the nonlinear terms, thus fixing the nature of the bifurcation diagram.

It is interesting to point out that the truncated, averaged equations (5.20) have the same structure as those analyzed by Yang and Sethna [67] in a study of the flexural vibrations of nearly square plates subjected to parametric in-plane excitation. In that study, two detuning parameters with respect to the flatural frequencies of each individual oscillator are considered as primary bifurcation parameters, and local and global bifurcation analyses are carried out. Herein, in addition to the imperfection and mistuning parameters, the disturbing torque level  $\tilde{\Gamma}_{\theta}$  is considered as a primary bifurcation parameter in order to evaluate the absorber performance under various levels of the disturbing torque.

For more related works on bifurcation analyses for dynamical systems composed of weakly-coupled oscillators and subject to internal and/or external resonances, one can refer to Bajaj et al. [2], and Ariaratnam and Sri Namachchivaja [1].

## 5.5 Approximate Steady-State Solutions

This section begins with a brief discussion about the types of steady-state responses that can occur, followed by a detailed analysis of each type. Of particular interest are the existence, stability, and range of validity for each type of response. These results are used for the performance evaluation described in the section 5.6.

## 5.5.1 Solution Types

With assumption (5.19) adopted, it is evident from the averaged equations (5.20) that for any given system parameters there exists a trivial solution which leads to no motion for the absorbers; i.e.,  $\bar{r}_{\xi} = \bar{r}_{\eta} = 0$ . Also, there are solutions with  $\bar{r}_{\xi} = 0, \bar{r}_{\eta} \neq 0$  and with  $\bar{r}_{\eta} = 0, \bar{r}_{\xi} \neq 0$ . These are single-mode solutions and are denoted by "SM" in the following. Solutions with  $\bar{r}_{\xi} \neq 0$  and  $\bar{r}_{\eta} = 0$  are unison mode solutions. Such synchronized motions of the two absorbers are denoted as "SM1". Solutions with  $\bar{r}_{\xi} = 0$  and  $\bar{r}_{\eta} \neq 0$  correspond to motions in which the two absorbers undergo oscillations with the same amplitude but are  $\pi$  out-of-phase, and these are denoted as "SM2". In addition, there exist couple-mode solutions with  $\bar{r}_{\xi}$  and  $\bar{r}_{\eta}$  both non-zero, denoted by "CM." Note that for certain values of the system parameters, periodic solutions arising from Hopf bifurcations may exist for the averaged equations, and these represent amplitude and phase modulated oscillations of the absorbers. However, it will be shown that such motions are not physically possible for this system, due to the finite physical limits of the absorber paths.

As each solution type is considered, results are presented in the form of bifurcation diagrams depicted by plotting the amplitudes of the two modes versus the torque amplitude  $\tilde{\Gamma}_{\theta}$ . For this study the value of the absorber damping  $\tilde{\mu}_{a}$  is fixed, whereas several possible values for n,  $\tilde{\delta}_{\xi 2}$  and  $\tilde{\delta}_{\xi 4}$  are considered. The solution branches are

represented in closed form whenever possible, and are otherwise determined using numerical tools such as AUTO [17] and the Newton-Raphson method. Figure 5.1 shows a representative bifurcation diagram for the system with n=2,  $\tilde{\mu}_a=0.05$ ,  $\tilde{\delta}_{\xi 2}=0.06$  and  $\tilde{\delta}_{\xi 4}=0$ . This diagram is typical and depicts the general features that appear in the following analyses. However, most of the solution branches shown will be shown to be non-physical, thus significantly simplifying the picture of the actual steady-state response.

## 5.5.2 The Zero Solution

It is evident from the averaged equations (5.20) that the zero solution; i.e.,  $\bar{r}_{\xi} = \bar{r}_{\eta} = 0$ , exists for any set of system parameters. Its stability can be determined by the eigenvalues of the corresponding Jacobian matrix of equations (H.2) evaluated at the origin. It is found that this matrix has the following form,

$$J_{4\times 4} = \begin{bmatrix} A_{2\times 2} & O_{2\times 2} \\ O_{2\times 2} & B_{2\times 2} \end{bmatrix}$$
 (5.21)

where  $O_{2\times 2}$  represents the two-by-two zero matrix. The eigenvalues of J thus coincide with the eigenvalues of A and B, which are

$$\lambda_{1,2} = \frac{-\tilde{\mu}_a}{2} \pm \frac{1}{4n} \sqrt{-16\tilde{\delta}_{\xi 2}^2 + \tilde{\Gamma}_{\theta}^2 n^2},$$
 (5.22a)

$$\lambda_{3,4} = \frac{-\tilde{\mu}_a}{2} \pm \frac{1}{4n} \sqrt{-(n^2 + 4\tilde{\delta}_{\xi^2})^2 + \tilde{\Gamma}_{\theta}^2 n^2}.$$
 (5.22b)

Based on these eigenvalues, it is easy to show that for nonzero damping ( $\tilde{\mu}_a \neq 0$ ) there are no Hopf bifurcations from the zero solution. The bifurcation sets on which an eigenvalue becomes zero are shown in Figure 5.2, which is depicted for the system parameters, n=2 and  $\tilde{\mu}_a=0.05$ . In this figure, the zero solution is stable under the curve AOB and unstable above AOB. Note that a double zero eigenvalue condition holds at the point labeled O. All bifurcations from the zero solution are pitchfork

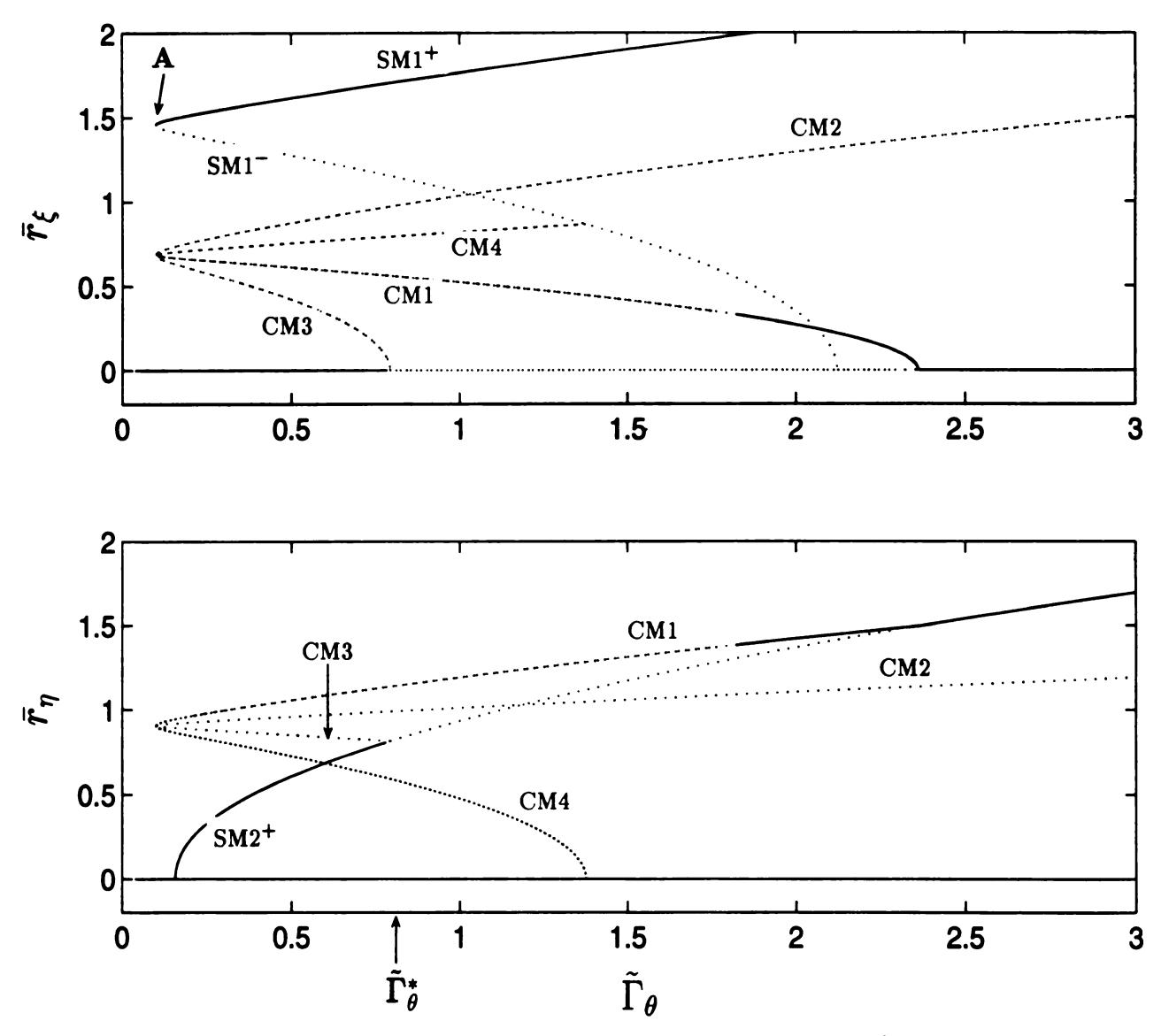


Figure 5.1: The bifurcation diagram for n=2,  $\tilde{\mu}_a=0.05$ ,  $\tilde{\delta}_{\xi 2}=0.06$ ,  $\tilde{\delta}_{\xi 4}=0$ ,  $\tilde{\delta}_{\eta 2}=0$ ,  $\tilde{\delta}_{\eta 4}=0$ . The solid lines represent stable solutions and the dashed lines represent unstable solutions.

bifurcations, and both the super- and sub-critical cases occur for various system parameters.

Of course, this solution is not affected by the limitations imposed on absorber motion.

## 5.5.3 Single-Mode Solutions

#### 5.5.3.1 Solution Branches

There exist two types of single-mode solutions, defined above and labeled as SM1 and SM2.

For **SM1**, the synchronous responses, the solutions with  $\bar{r}_{\xi} \neq 0$  can be determined by equations (5.20a) and (5.20b), yielding

$$\bar{r}_{\xi+}^{2} = \frac{1}{4c_{n2}} \left( \frac{4\tilde{\delta}_{\xi2}}{n} + n + \sqrt{\tilde{\Gamma}_{\theta}^{2} - 4\tilde{\mu}_{a}^{2}} \right), \quad \bar{r}_{\xi-}^{2} = \frac{1}{4c_{n2}} \left( \frac{4\tilde{\delta}_{\xi2}}{n} + n - \sqrt{\tilde{\Gamma}_{\theta}^{2} - 4\tilde{\mu}_{a}^{2}} \right) (5.23)$$

$$\tan 2\bar{\varphi}_{\xi+} = \frac{2\tilde{\mu}_{a}}{\sqrt{\tilde{\Gamma}_{\theta}^{2} - 4\tilde{\mu}_{a}^{2}}}, \quad \tan 2\bar{\varphi}_{\xi-} = \frac{-2\tilde{\mu}_{a}}{\sqrt{\tilde{\Gamma}_{\theta}^{2} - 4\tilde{\mu}_{a}^{2}}}. \quad (5.24)$$

The solution branches with  $\bar{r}_{\xi+}$  and  $\bar{r}_{\xi-}$  on SM1 are denoted by SM1<sup>+</sup> and SM1<sup>-</sup>, respectively.

Utilizing the same procedure and notation, the solutions for SM2, the out-ofphase responses, are found to be

$$\bar{r}_{\eta+}^{2} = \frac{1}{4c_{n4}} \left( -\frac{4\tilde{\delta}_{\xi2}}{n} + \sqrt{\tilde{\Gamma}_{\theta}^{2} - 4\tilde{\mu}_{a}^{2}} \right), \quad \bar{r}_{\eta-}^{2} = \frac{1}{4c_{n4}} \left( -\frac{4\tilde{\delta}_{\xi2}}{n} - \sqrt{\tilde{\Gamma}_{\theta}^{2} - 4\tilde{\mu}_{a}^{2}} \right), \quad (5.25)$$

$$\tan 2\bar{\varphi}_{\eta+} = \frac{2\tilde{\mu}_{a}}{\sqrt{\tilde{\Gamma}_{\theta}^{2} - 4\tilde{\mu}_{a}^{2}}}, \quad \tan 2\bar{\varphi}_{\eta-} = \frac{-2\tilde{\mu}_{a}}{\sqrt{\tilde{\Gamma}_{\theta}^{2} - 4\tilde{\mu}_{a}^{2}}}. \quad (5.26)$$

The existence of SM1<sup>-</sup> and SM2<sup>-</sup> depend on the signs of  $\left[\frac{4\tilde{\delta}_{\xi2}}{n} + n\right]$  and  $\left[\frac{-4\tilde{\delta}_{\xi2}}{n}\right]$ , respectively. Since  $|\tilde{\delta}_{\xi2}| << 1$ , it follows that  $|\frac{4\tilde{\delta}_{\xi2}}{n}| \ll n$ , and therefore SM1<sup>-</sup> always exists for the parameter ranges of interest. However, the existence of SM2<sup>-</sup> depends critically on the sign of  $\tilde{\delta}_{\xi2}$ . When SM1<sup>-</sup> and SM2<sup>-</sup> exist, they arise

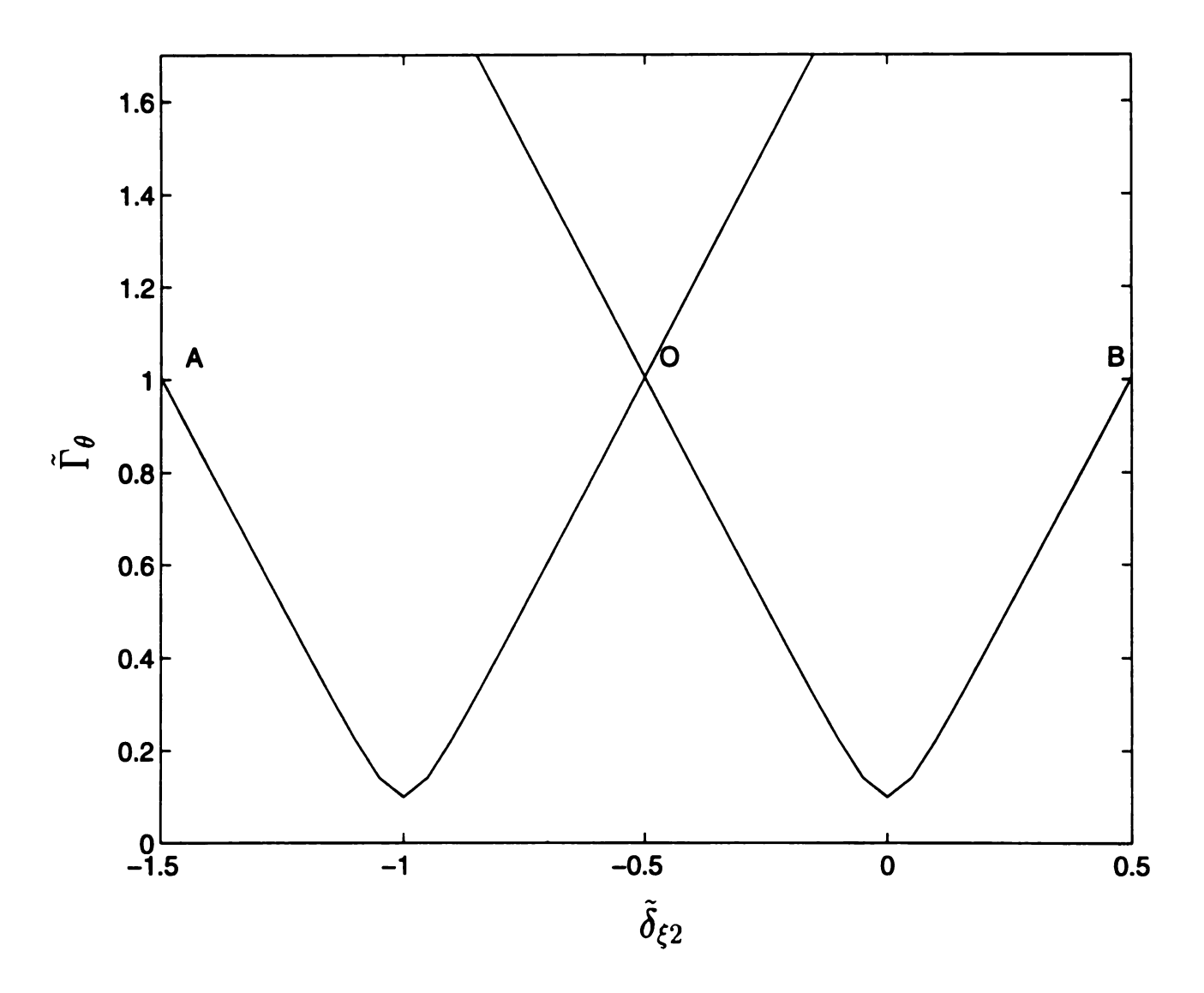


Figure 5.2: The bifurcation set of the zero solution for  $\tilde{\delta}_{\eta 2} = \tilde{\delta}_{\eta 4} = 0$  and  $\tilde{\mu}_a = 0.05$ .

from the zero solution via pitchfork bifurcations and then merge with SM1<sup>+</sup> and SM2<sup>+</sup>, respectively, in saddle-node bifurcations. If SM2<sup>-</sup> does not exist, SM2<sup>+</sup> arises directly from the zero solution through a pitchfork bifurcation. Note that the internal mistuning plays an important role in determining the nature of these single-mode solutions.

## 5.5.3.2 Stability

With these solutions in hand, a stability analysis is conducted by evaluating the corresponding Jacobian matrix on the various single-mode solutions. It is found, as in the case for the zero solution, that the Jacobian matrix possesses the structure stated in equation (5.21). Hence, the eigenvalues of this Jacobian matrix satisfy two second-order polynomials of the form

$$\lambda^2 + \tilde{\mu}_a \lambda + D_A = 0, \quad \lambda^2 + \tilde{\mu}_a \lambda + D_B = 0, \tag{5.27}$$

where the first and second polynomials are derived from the the block matrices A and B, respectively, in equation (5.21). Since  $\tilde{\mu}_a > 0$ , the stability of the **SM1** and **SM2** solutions can be determined entirely by the signs of  $D_A$  and  $D_B$ . Furthermore, due to the fact that  $\tilde{\mu}_a > 0$  no Hopf bifurcations occur from **SM1** or **SM2**. The stability for each branch on **SM1** and **SM2** is now determined.

Utilizing transformations (5.18) when necessary,  $D_A$  and  $D_B$  can be derived. For SM1,

$$D_{A1\pm} = \pm c_{n2} \bar{r}_{\xi\pm}^2 \sqrt{\tilde{\Gamma}_{\theta}^2 - 4\tilde{\mu}_a^2}. \tag{5.28}$$

Since  $D_{A1-}$  is negative on the branch SM1<sup>-</sup>, this leads to one positive eigenvalue, and thus SM1<sup>-</sup> is always unstable. For the branch SM1<sup>+</sup>,  $D_{A1+}$  is positive and this leads to negative eigenvalues. Thus, the stability of SM1<sup>+</sup> must be determined by the sign of  $D_{B1+}$ , which is given in Appendix I. It can be shown that for  $\tilde{\delta}_{\xi}$  small,  $D_{B1+}$  is positive. Hence, the branch SM1<sup>+</sup> is stable.

For SM2,

$$D_{B2\pm} = \pm c_{n4} \bar{r}_{n\pm}^2 \sqrt{\tilde{\Gamma}_{\theta}^2 - 4\tilde{\mu}_a^2}. \tag{5.29}$$

Applying the same approach used for SM1 yields the following results. The branch SM2<sup>-</sup> is always unstable and the stability of the branch SM2<sup>+</sup> is determined by the sign of  $D_{A2+}$ , which is given in Appendix J. It can be shown that for  $\tilde{\delta}_{\xi}$  small,  $D_{A2+}$  becomes negative at a level of  $\tilde{\Gamma}_{\theta}$  denoted by  $\tilde{\Gamma}_{\theta}^*$ , at which point a secondary bifurcation occurs. An example of this is shown in Figure 5.1, where SM2<sup>+</sup> is unstable for  $\tilde{\Gamma}_{\theta} > \tilde{\Gamma}_{\theta}^*$ .

# 5.5.3.3 Range of Validity

Based on condition (5.6), only a finite torque range is valid for each branch, in order to keep the motions of the absorbers below the cusps. Only stable solution branches are considered, since these will dictate the steady-state system behavior.

For the solutions on SM1, only the stable branch SM1<sup>+</sup> is of interest. Using equations (5.23), a condition can be determined such that point A in Figure 5.1 is above the cusp amplitude, thus violating condition (5.6). This condition is given by

$$\tilde{\delta}_{\xi 2} > 2nc_{n2} - \frac{n^2}{4},\tag{5.30}$$

which, if satisfied, implies that no stable **SM1** solutions are valid. For the case with n=2 and small  $\tilde{\delta}_{\xi 4}$ , the R.H.S. of the above equation is approximately -3/4, and thus the condition is satisfied for any realistic value of  $\tilde{\delta}_{\xi 2}$ . The same argument sustains for different values of n.

It is thus concluded that for small  $\tilde{\delta}_{\xi}$ , the stable solutions on the branch SM1 do not correspond to legitimate steady-state responses for the equations of motion (2.12). This result is largely due to the "internal mistuning" mentioned in section 5, since the term " $-n^2/4$ " in the R.H.S of inequality (5.30) results from the effect of internal mistuning.

On the other hand, it is seen from equations (5.25), representing the **SM2** single-mode solutions, that internal mistuning has no effect (to leading order) on the out-of-phase responses. This fact actually allows the stable solution **SM2**<sup>+</sup> to be valid up to a torque level denoted by  $\tilde{\Gamma}_{\theta}$ , at which the absorbers hit the cusps. (Note that  $\tilde{\Gamma}_{\theta}$  herein is a rescaled version of  $\tilde{\Gamma}_{\theta}$  defined in equation (5.7); i.e.,  $\tilde{\Gamma}_{\theta} = \epsilon \tilde{\Gamma}_{\theta}$ ). Based on the solutions given in equations (5.25) and the restriction on the the absorber motions given by the approximation in equation (5.6),  $\tilde{\Gamma}_{\theta}$  can be approximated by

$$\bar{\tilde{\Gamma}}_{\theta} \simeq \left[ \left( \frac{2n}{n^2 + 4} + \frac{96\tilde{\delta}_{\xi 4}}{n^3(n^2 + 4)} + \frac{4\tilde{\delta}_{\xi 2}}{n} \right)^2 + 4\tilde{\mu}_a^2 \right]^{\frac{1}{2}}.$$
 (5.31)

This limit is now compared against the secondary bifurcation torque amplitude,  $\tilde{\Gamma}_{\theta}^{*}$ , described in the previous section. Utilizing the information given in Appendix J, this torque can be numerically computed and compared with equation (5.31). It is determined that  $\tilde{\Gamma}_{\theta}^{*} > \bar{\tilde{\Gamma}}_{\theta}$  over the following ranges of the mistuning parameters:  $\hat{\delta}_{\xi 2} \in [-0.03, 0.03]$  and  $\hat{\delta}_{\xi 4} \in [-0.03, 0.03]$ . Therefore, the important conclusion is reached that the SM2<sup>+</sup> responses are stable all the way out to the cusp amplitude for realistic values of imperfections.

The stable SM2<sup>+</sup> branch is central to the effectiveness of the subharmonic vibration absorber system, as described in section 5.6.

## 5.5.4 Coupled-Mode Solutions

The existence, stability and range of validity of the coupled-mode solutions are now considered.

### 5.5.4.1 Solution Branches and Their Stability

Observing the averaged equations (5.20), one can first classify all possible steadystate solutions into two distinct groups: the first satisfies  $\sin(2\bar{\varphi}_{\xi} - 2\bar{\varphi}_{\eta}) = 0$  and the other does not. Solutions in the group with the property  $\sin(2\bar{\varphi}_{\xi} - 2\bar{\varphi}_{\eta}) = 0$  are sought first. This property implies  $\cos(2\bar{\varphi}_{\xi} - 2\bar{\varphi}_{\eta}) = \pm 1$ , which enables one to solve the averaged equations (5.20) for steady-state solutions. As a result, eight steady-state solutions are found, given by

$$\begin{split} & \bar{r}_{\xi15}^2 = \left[\frac{c_{n4}}{4(c_{n2}c_{n4} + (c_{n3} \pm c_{n1})^2)}\right] \left[n + \frac{4\tilde{\delta}_{\xi2}}{n} + \frac{4(c_{n3} \pm c_{n1})}{c_{n4}n} \tilde{\delta}_{\xi2} + \left(\frac{-c_{n3} \mp c_{n1}}{c_{n4}} + 1\right) \left(\tilde{\Gamma}_{\theta}^2 - 4\tilde{\mu}_{a}^2\right)^{\frac{1}{2}}\right], \\ & \bar{r}_{\eta15}^2 = \left[\frac{c_{n2}}{4(c_{n2}c_{n4} + (c_{n3} \pm c_{n1})^2)}\right] \left[\frac{-4\tilde{\delta}_{\xi2}}{n} + \frac{(c_{n3} \pm c_{n1})}{c_{n2}} (n + \frac{4\tilde{\delta}_{\xi2}}{n}) + \left(\frac{c_{n3} \pm c_{n1}}{c_{n2}} + 1\right) \left(\tilde{\Gamma}_{\theta}^2 - 4\tilde{\mu}_{a}^2\right)^{\frac{1}{2}}\right], \\ & \bar{r}_{\xi26}^2 = \left[\frac{c_{n4}}{4(c_{n2}c_{n4} + (c_{n3} \pm c_{n1})^2)}\right] \left[n + \frac{4\tilde{\delta}_{\xi2}}{n} + \frac{4(c_{n3} \pm c_{n1})}{c_{n4}n} \tilde{\delta}_{\xi2} + \left(\frac{c_{n3} \pm c_{n1}}{c_{n4}} + 1\right) \left(\tilde{\Gamma}_{\theta}^2 - 4\tilde{\mu}_{a}^2\right)^{\frac{1}{2}}\right], \\ & \bar{r}_{\eta26}^2 = \left[\frac{c_{n2}}{4(c_{n2}c_{n4} + (c_{n3} \pm c_{n1})^2)}\right] \left[\frac{-4\tilde{\delta}_{\xi2}}{n} + \frac{(c_{n3} \pm c_{n1})}{c_{n2}} (n + \frac{4\tilde{\delta}_{\xi2}}{n}) + \left(\frac{c_{n3} \pm c_{n1}}{c_{n2}} - 1\right) \left(\tilde{\Gamma}_{\theta}^2 - 4\tilde{\mu}_{a}^2\right)^{\frac{1}{2}}\right], \\ & \bar{r}_{\xi37}^2 = \left[\frac{c_{n4}}{4(c_{n2}c_{n4} + (c_{n3} \pm c_{n1})^2)}\right] \left[n + \frac{4\tilde{\delta}_{\xi2}}{n} + \frac{4(c_{n3} \pm c_{n1})}{c_{n4}n} \tilde{\delta}_{\xi2} + \left(\frac{-c_{n3} \mp c_{n1}}{c_{n4}} - 1\right) \left(\tilde{\Gamma}_{\theta}^2 - 4\tilde{\mu}_{a}^2\right)^{\frac{1}{2}}\right], \\ & \bar{r}_{\eta37}^2 = \left[\frac{c_{n2}}{4(c_{n2}c_{n4} + (c_{n3} \pm c_{n1})^2)}\right] \left[n + \frac{4\tilde{\delta}_{\xi2}}{n} + \frac{4(c_{n3} \pm c_{n1})}{c_{n4}n} \tilde{\delta}_{\xi2} + \left(\frac{-c_{n3} \mp c_{n1}}{c_{n4}} - 1\right) \left(\tilde{\Gamma}_{\theta}^2 - 4\tilde{\mu}_{a}^2\right)^{\frac{1}{2}}\right], \\ & \bar{r}_{\xi48}^2 = \left[\frac{c_{n4}}{4(c_{n2}c_{n4} + (c_{n3} \pm c_{n1})^2)}\right] \left[n + \frac{4\tilde{\delta}_{\xi2}}{n} + \frac{4(c_{n3} \pm c_{n1})}{c_{n4}n} \tilde{\delta}_{\xi2} + \left(\frac{-c_{n3} \mp c_{n1}}{c_{n4}} - 1\right) \left(\tilde{\Gamma}_{\theta}^2 - 4\tilde{\mu}_{a}^2\right)^{\frac{1}{2}}\right], \\ & \bar{r}_{\eta48}^2 = \left[\frac{c_{n2}}{4(c_{n2}c_{n4} + (c_{n3} \pm c_{n1})^2)}\right] \left[n + \frac{4\tilde{\delta}_{\xi2}}{n} + \frac{4(c_{n3} \pm c_{n1})}{c_{n4}n} \tilde{\delta}_{\xi2} + \left(\frac{-c_{n3} \mp c_{n1}}{c_{n4}} - 1\right) \left(\tilde{\Gamma}_{\theta}^2 - 4\tilde{\mu}_{a}^2\right)^{\frac{1}{2}}\right], \\ & \bar{r}_{\eta48}^2 = \left[\frac{c_{n2}}{4(c_{n2}c_{n4} + (c_{n3} \pm c_{n1})^2)}\right] \left[n + \frac{4\tilde{\delta}_{\xi2}}{n} + \frac{4(c_{n3} \pm c_{n1})}{c_{n4}n} \tilde{\delta}_{\xi2} + \left(\frac{-c_{n3} \mp c_{n1}}{c_{n4}} - 1\right) \left(\tilde{\Gamma}_{\theta}^2 - 4\tilde{\mu}_{a}^2\right)^{\frac{1}{2}}\right], \\ & \bar{r}_{\eta48}^2 = \left[\frac{c_{n3}}{4(c_{n2}c_{n4} + (c_{n3} \pm c_{n1})^2}\right$$

with phases given by

$$\sin(2\bar{\varphi}_{\xi i}) = \sin(2\bar{\varphi}_{\eta i}) = \frac{2\tilde{\mu}_a}{\tilde{\Gamma}_{\theta}}, \quad 1 \le i \le 8.$$
 (5.33)

The stabilities of these coupled-mode solutions can be determined by evaluating the corresponding Jacobian matrix on the corresponding solution branches and examining their eigenvalues. In this case, the characteristic equation is fourth order. Due to the complexity involved in the expressions for the stability criteria, results are not explicitly given here.

The solutions in the other group, which satisfy  $\sin(2\bar{\varphi}_{\xi} - 2\bar{\varphi}_{\eta}) \neq 0$ , are obtained by utilizing the computational algorithm outlined in Appendix K. The corresponding stability is then determined by numerically evaluating the Jacobian matrix on the solution branches.

By comparing the single-mode and coupled solutions (denoted by CM1 to CM4),

one finds that all coupled-mode solutions bifurcate from single-mode solution through pitchfork bifurcations. Also, no isolated solution branches are found to exist.

# 5.5.4.2 Range of Validity

It is of practical importance to identify the set of stable coupled-mode solutions which satisfy condition (5.6), that is, those that are physically possible. It turns out that no such solutions are valid, and this is shown by a simple argument, and backed up by detailed calculations.

First, it is known that all coupled-mode solutions bifurcate from single-mode solutions. Furthermore, in section 5.5.3.3 it was determined that all single-mode branches are beyond their range of validity when they bifurcate to coupled-mode solutions. Therefore, no coupled-mode solutions are valid for the range of parameters of interest.

A more detailed calculation follows that allows one to directly check condition (5.6) for all coupled-mode solutions at once over a range of parameters. To facilitate the method, a relationship between the two modal amplitudes,  $\bar{r}_{\xi}$  and  $\bar{r}_{\eta}$ , is first derived. Setting the R.H.S. of the averaged equations (5.20) equal to zero yields

$$0 = -2\tilde{\mu}_a + \tilde{\Gamma}_\theta \sin 2\bar{\varphi}_\xi - 4c_{n1}\bar{r}_\eta^2 \sin(2\bar{\varphi}_\xi - 2\bar{\varphi}_\eta), \qquad (5.34a)$$

$$0 = \left(\frac{-4\tilde{\delta}_{\xi 2}}{n} - n\right) + \tilde{\Gamma}_{\theta} \cos 2\bar{\varphi}_{\xi} + 4c_{n1}\bar{r}_{\eta}^{2} \cos(2\bar{\varphi}_{\xi} - 2\bar{\varphi}_{\eta}) + 4c_{n2}\bar{r}_{\xi}^{2} + 4c_{n3}\bar{r}_{\eta}^{2}, \tag{5.34b}$$

$$0 = -2\tilde{\mu}_a + \tilde{\Gamma}_\theta \sin 2\bar{\varphi}_\eta - 4c_{n1}\bar{r}_\xi^2 \sin(2\bar{\varphi}_\eta - 2\bar{\varphi}_\xi), \qquad (5.34c)$$

$$0 = \frac{-4\tilde{\delta}_{\xi 2}}{n} + \tilde{\Gamma}_{\theta}\cos 2\bar{\varphi}_{\eta} + 4c_{n1}\bar{r}_{\xi}^{2}\cos(2\bar{\varphi}_{\eta} - 2\bar{\varphi}_{\xi}) - 4c_{n4}\bar{r}_{\eta}^{2} + 4c_{n3}\bar{r}_{\xi}^{2}. (5.34d)$$

Combining equations (5.34b) and (5.34d) gives

$$\left(\frac{-4\tilde{\delta}_{\xi 2}}{n}-n\right)\bar{r}_{\xi}^{2}+\frac{4\tilde{\delta}_{\xi 2}}{n}\bar{r}_{\eta}^{2}-\tilde{\Gamma}_{\theta}\left(\bar{r}_{\eta}^{2}\cos 2\bar{\varphi}_{\eta}-\bar{r}_{\xi}^{2}\cos 2\bar{\varphi}_{\xi}\right)+4c_{n2}\bar{r}_{\xi}^{4}+4c_{n4}\bar{r}_{\eta}^{4}=0(5.35)$$

Next, incorporating equations (5.34a) and (5.34c) into equations (5.34b) and (5.34d),

respectively, one can represent  $\cos 2\bar{\varphi}_{\xi}$  and  $\cos 2\bar{\varphi}_{\eta}$  as functions of  $\tilde{\Gamma}_{\theta}$ ,  $\tilde{\mu}_{a}$ ,  $\tilde{\delta}_{\xi 2}$ , n,  $\bar{r}_{\xi}^{2}$  and  $\bar{r}_{\eta}^{2}$ , as follows,

$$\cos 2\bar{\varphi}_{\xi} = \frac{-1}{8c_{n1}\tilde{\Gamma}_{\theta}\bar{r}_{\xi}^{2}} \left[ \tilde{\Gamma}_{\theta}^{2} + 16c_{n1}^{2}\bar{r}_{\xi}^{4} - 4\tilde{\mu}_{a}^{2} - \left( \frac{4\tilde{\delta}_{\xi2}}{n} + 4c_{n4}\bar{r}_{\eta}^{2} - 4c_{n3}\bar{r}_{\xi}^{2} \right)^{2} \right],$$

$$\cos 2\bar{\varphi}_{\eta} = \frac{-1}{8c_{n1}\tilde{\Gamma}_{\theta}\bar{r}_{\eta}^{2}} \left[ \tilde{\Gamma}_{\theta}^{2} + 16c_{n1}^{2}\bar{r}_{\eta}^{4} - 4\tilde{\mu}_{a}^{2} - \left( \frac{4\tilde{\delta}_{\xi2}}{n} + n - 4c_{n2}\bar{r}_{\xi}^{2} - 4c_{n3}\bar{r}_{\eta}^{2} \right)^{2} \right].$$

$$(5.36a)$$

$$(5.36b)$$

Substituting the above equations into equation (5.35) yields the following fourthorder polynomial which governs a relationship between the two modal amplitudes on any coupled-mode, periodic, steady-state response,

$$\alpha_1 \bar{r}_{\ell}^4 + \alpha_2 \bar{r}_{\eta}^4 + \alpha_3 \bar{r}_{\ell}^2 \bar{r}_{\eta}^2 + \alpha_4 \bar{r}_{\ell}^2 + \alpha_5 \bar{r}_{\eta}^2 + \alpha_6 = 0, \tag{5.37}$$

where

$$\alpha_{1} = 2c_{n1}c_{n2} - c_{n1}^{2} - c_{n2}^{2} + c_{n3}^{2}, \quad \alpha_{2} = 2c_{n1}c_{n4} + c_{n1}^{2} - c_{n3}^{2} + c_{n4}^{2},$$

$$\alpha_{3} = -2(c_{n2}c_{n3} + c_{n4}c_{n3}), \quad \alpha_{4} = (c_{n2} - c_{n1})\left(\frac{2\tilde{\delta}_{\xi 2}}{n} + \frac{n}{2}\right) - \frac{2\tilde{\delta}_{\xi 2}}{n}c_{n3},$$

$$\alpha_{5} = 2(c_{n1} + c_{n3} + c_{n4})\left(\frac{\tilde{\delta}_{\xi 2}}{n}\right) + \frac{nc_{n3}}{2} \quad \text{and} \quad \alpha_{6} = \frac{\tilde{\delta}_{\xi 2}^{2}}{n^{2}} - \left(\frac{\tilde{\delta}_{\xi 2}}{n} + \frac{n}{4}\right)^{2}. \quad (5.38)$$

Note that this polynomial does not depend on the torque amplitude  $\tilde{\Gamma}_{\theta}$ . Thus, for fixed values of n and the system parameters, this constraint represents two curves in the  $\bar{r}_{\xi}$ - $\bar{r}_{\eta}$  plane. An example for n=2,  $\tilde{\delta}_{\xi 2}=0.05$  and  $\tilde{\delta}_{\xi 4}=0$  is shown in Figure 5.3. Also shown in this figure is the set of amplitudes that satisfy condition (5.6), represented by the interior of the triangle OAB. It is seen that all points on the two curves generated by the polynomial (5.37) are outside the triangle OAB. Thus, no coupled-mode solutions are physically possible for this set of parameters. One can generate such graphical information for any values of n,  $\tilde{\delta}_{\xi 2}$  and  $\tilde{\delta}_{\xi 4}$  in order to check the feasibility of the coupled-mode solutions.

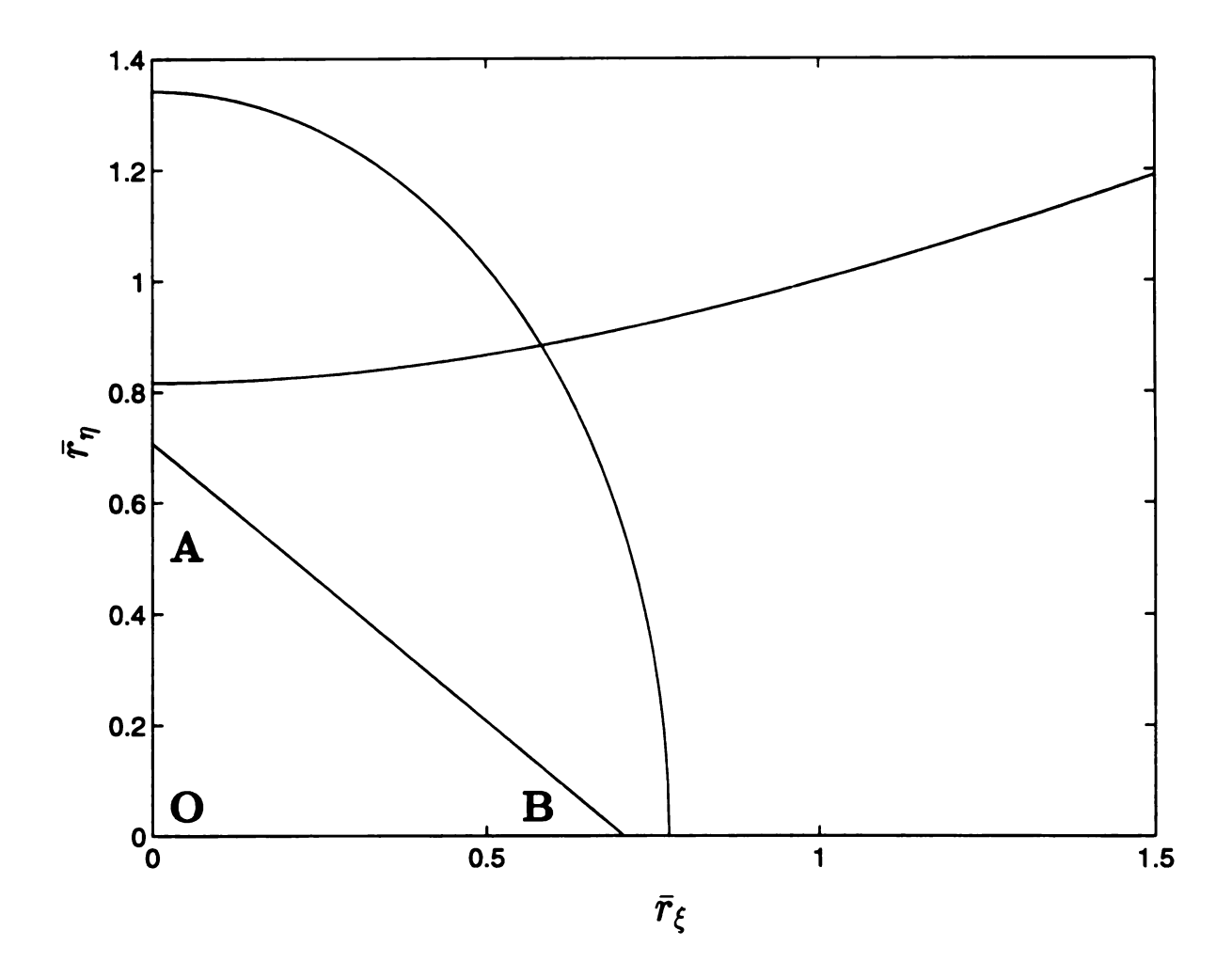


Figure 5.3: The curves represent the relationship between  $\bar{r}_{\eta}$  and  $\bar{r}_{\xi}$  in coupled-mode solutions for n=2,  $\tilde{\delta}_{\xi 2}=0.05$  and  $\tilde{\delta}_{\xi 4}=0$ . The feasible absorber motions lie inside of triangle **OAB** 

### 5.5.5 Remarks

With all possible solution branches and corresponding stabilities in hand, bifurcation diagrams showing all periodic steady-state responses and their stabilities can be generated. Figure 5.1 shows a typical bifurcation diagram for  $\tilde{\delta}_{\xi} = 0.06$ ,  $\tilde{\delta}_{\eta} = 0$  and n = 2. However, as shown above, many of the solution branches are non-physical.

AUTO [17] was utilized to confirm the results obtained above, and consistency was found in every case checked. In addition, AUTO also found some non-physical periodic solutions to equations (5.20), all of which arise from the coupled-mode solutions via Hopf bifurcations.

Based on the results obtained in this section, the following conclusion is drawn. For reasonable ranges of the system parameters, the only viable steady-state system responses are the trivial solution and those on the branch SM2<sup>+</sup>. To ensure this conclusion for a given system, one can use the criterion in equation (5.30) and the method provided in section 5.5.4.2 to confirm that SM2<sup>+</sup> is the only nontrivial solution that satisfies condition (5.6).

When the system is undamped and the paths are perfect, the solution SM2<sup>+</sup> reduces to the idealized subharmonic absorber system response given in equations (5.2a) and (5.2b). It is therefore not too surprising that this solution will persist in the face of imperfections, and that it will offer good performance as a torsional vibration absorber. The details of this performance are considered next.

## 5.6 Absorber Performance and Design Guidelines

This section contains the main results of this chapter. Here the desired steadystate solution is considered in terms of the system's effectiveness as a vibration absorber. Considered in turn are the following: some general features of the response, expressions for the two measures of system performance, details of the effects of imperfections and mistuning, a summary of results in the form of design guidelines, and verification by simulations.

### 5.6.1 The Desired Solution

In this section it is shown that the stable branch SM2<sup>+</sup> is very favorable in terms of meeting the two goals outlined in section 5.2.

For a given disturbing torque level,  $\hat{\Gamma}_{\theta}$ , the absorber dynamics can converge to any stable steady-state solution. Utilizing the expression for the angular acceleration " $yy'(\theta)$ " provided in equation (5.9) and the solution branches obtained by the averaged equations, one can compute the rotor acceleration on each branch. The main conclusion of these results is the following: for various values of n, small  $\tilde{\delta}_{\xi}$ 's and zero  $\tilde{\delta}_{\eta}$ , among all branches, the **SM2** branches lead to the smallest  $\|yy'\|_{ss}$  over the feasible range of the disturbing torque. This result can be explained in terms of the harmonics contained in yy', as follows. First,  $yy'(\theta)$  given in equation (5.9) is expanded in terms of the s's. Next, it is observed that each steady-state absorber response  $s(\theta)$  is dominated by a harmonic of order n/2 (since they are nearly linear). From these facts it is determined that the net rotor acceleration yy' is generally composed of all odd harmonics, but only one even harmonic, which comes from the term  $-2n^2s_js_j'$  in the summation. Now, suppose there is a non-zero  $\bar{r}_{\xi}$  for the steady-state solution. In equation (5.9) it renders the summation of all odd harmonics nonzero and thus the higher-order harmonics will be amplified. This leads to a large value of  $||yy'||_{ss}$ . Contrarily, if  $\bar{r}_{\xi} = 0$  for a steady-state solution, that is, if the two absorbers simply move in an out-of-phase manner with the same amplitude, the odd harmonics resulting from the motion of the two absorbers will cancel each other in the summation and only the even harmonic term survives. In fact, it is a pure harmonic of order n, and it is precisely this effect which is used to counteract the harmonic disturbing torque. This is the crux of the subharmonic absorber system.

Since the solution branch SM2<sup>+</sup> is the desirable solution in terms of rotor acceleration, it is useful to ensure that it is the only possible stable steady-state response. For a given set or range of parameters, one can employ the criterion given by equation (5.30) and the method provided in section 5.5.4.2 to verify that the other potential solutions are not viable. After this is accomplished, one can be quite certain that the absorber performance as evaluated in the following section will be achieved.

## 5.6.2 Absorber Performance on SM2<sup>+</sup>

The peak rotor acceleration  $||yy'||_{ss}$  is first derived. On SM2<sup>+</sup>, the absorber motions are represented by the single-mode solution given in equations (5.25) and (5.26). These solutions are incorporated in expression (5.9) for the rotor acceleration, the scalings in equations (5.8) and (3.6) are employed, and terms up to  $\mathcal{O}(\epsilon)$  are retained, yielding

$$||yy'||_{ss} = \left[ (2\hat{\mu}_a)^2 + \left( \frac{4\hat{\delta}_{\xi 2}}{n} + \frac{6\hat{\delta}_{\xi 4}\bar{r}_{\eta+}^2}{n} \right)^2 \right]^{\frac{1}{2}} \quad \text{on } \mathbf{SM2}^+,$$
 (5.39)

where  $\bar{r}_{\eta+}^2$  is given by equation (5.25). Note that the exact saturation exhibited by the ideal absorber system is lost when the nonlinear mistuning parameter  $\hat{\delta}_{\xi 4}$  is non-zero, since  $\bar{r}_{\eta+}^2$  depends on the torque level. However, exact saturation at different levels can be obtained when  $\hat{\delta}_{\xi 4} = 0$ . This is discussed more fully in section 5.6.3.

The applied torque range  $\hat{\Gamma}_{\theta}$  is simply set by the upper torque limit at which the absorbers hit the cusps on the **SM2**<sup>+</sup> branch, given by equation (5.31). Utilizing the scaling assumptions, one can obtain  $\hat{\Gamma}_{\theta}$  by scaling equation (5.31), as follows:

$$\bar{\hat{\Gamma}}_{\theta} \simeq \left[ \left( \frac{2n\nu}{n^2 + 4} + \frac{96\hat{\delta}_{\xi 4}}{n^3(n^2 + 4)} + \frac{4\hat{\delta}_{\xi 2}}{n} \right)^2 + 4\hat{\mu}_a^2 \right]^{\frac{1}{2}}.$$
 (5.40)

This result is the generalization of the result given in equation (5.7) for the ideal system, accounting for the effects of absorber damping, mistuning and imperfections.

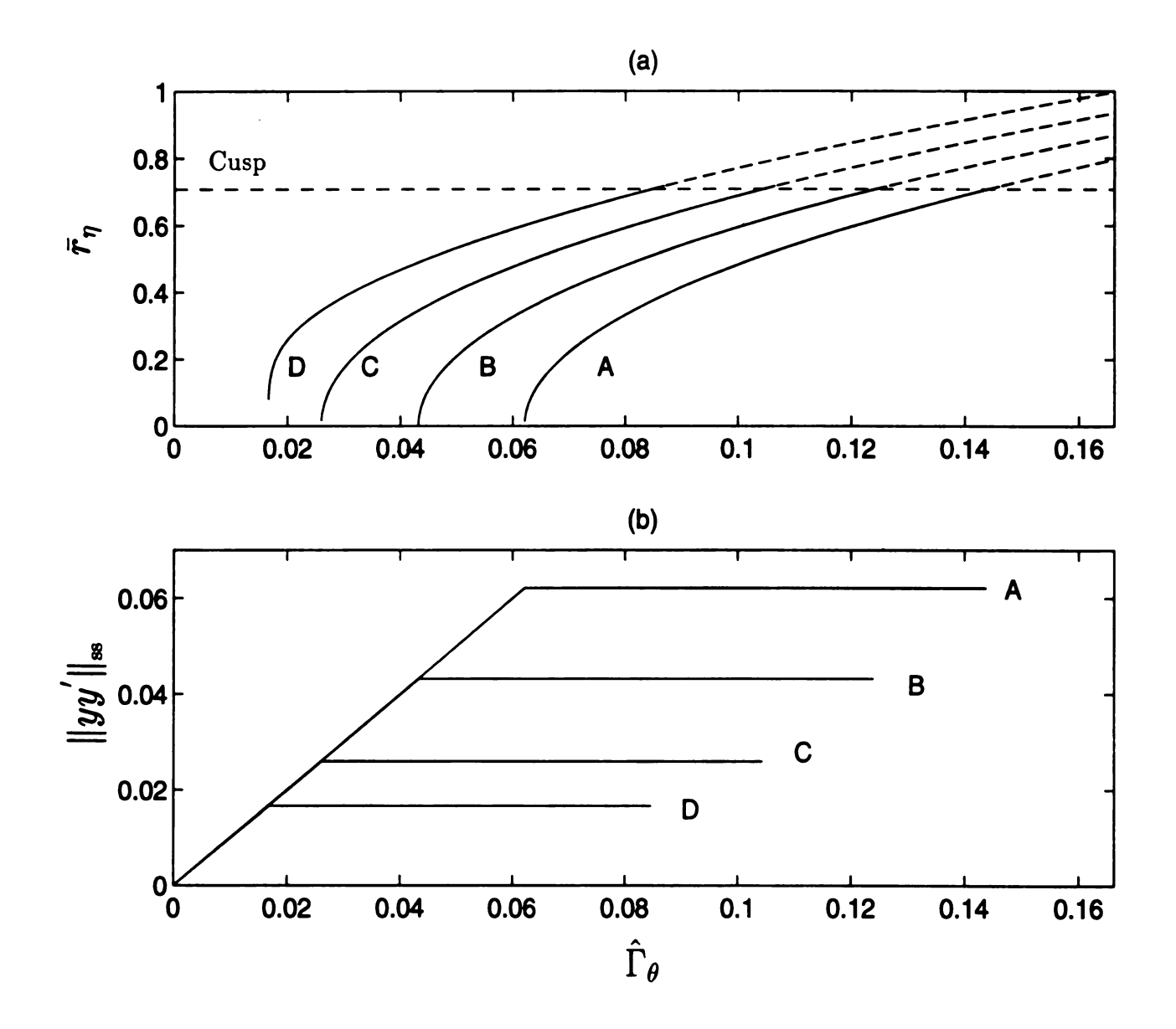
Note that this result assumes that the cusp is reached before a secondary bifurcation takes place, and this can be checked for each case by the procedure outlined in section 5.5.3.3.

## 5.6.3 Effects of Imperfections and Mistuning

The effects of  $\hat{\delta}_{\xi 2}$ ,  $\hat{\delta}_{\xi 4}$ ,  $\hat{\delta}_{\eta 2}$  and  $\hat{\delta}_{\eta 4}$  are considered in turn in this section. Recall that these scaled parameters capture the effects of mistunings and imperfections associated with the second and fourth order coefficients in the path function (5.5).

Observing the solutions for SM2<sup>+</sup> given by equation (5.25), one sees that a small non-zero value of  $\hat{\delta}_{\xi 4}$  does not qualitatively change system behavior since it only affects the magnitude of the coefficient  $c_{n4}$ . Based on this fact, the effects of  $\hat{\delta}_{\xi 2}$  on absorber performance are first considered for the case when  $\hat{\delta}_{\xi 4}$  is zero. It is seen from equation (5.39) that  $||yy'||_{\text{SS}}$  depends on the parameters  $\hat{\mu}_a$ , n, and  $\hat{\delta}_{\xi 2}$  (for  $\hat{\delta}_{\xi 4} = 0$ ). It is independent of the disturbing torque level and independent of the absorbers' amplitudes. This indicates that the rotor acceleration saturates after the bifurcation point, a result that is valid until  $\hat{\Gamma}_{\theta}$  reaches  $\bar{\hat{\Gamma}}_{\theta}$ .

In order to demonstrate the main results, bifurcation diagrams for various values of  $\hat{\delta}_{\xi 2}$  with n=2,  $\hat{\mu}_a=0.0083$  ( $\tilde{\mu}_a=0.05$ ) and  $\hat{\delta}_{\xi 4}=0$  are now described. Figures 5.4(a) and 5.4(c) show the response of  $\bar{r}_{\eta}$  for positive and negative values of  $\hat{\delta}_{\xi 2}$ , respectively (recall that  $\bar{r}_{\xi}=0$  on the branch being considered). Figures 5.4(b) and 5.4(d) show the corresponding rotor accelerations up to the torque level  $\bar{\Gamma}_{\theta}$ , where the absorber motions hit the cusps. It can be seen from these figures that the level of rotor acceleration is smallest for zero mistuning, case D (as expected). However, the largest torque range is obtained for the largest positive value of mistuning considered here, case A. It is also observed that the amplitudes of the absorber motions are much larger for negative values of  $\hat{\delta}_{\xi 2}$  than for positive values. Furthermore, for negative values of  $\hat{\delta}_{\xi 2}$ , a highly undesirable subcritical bifurcation takes the system to the



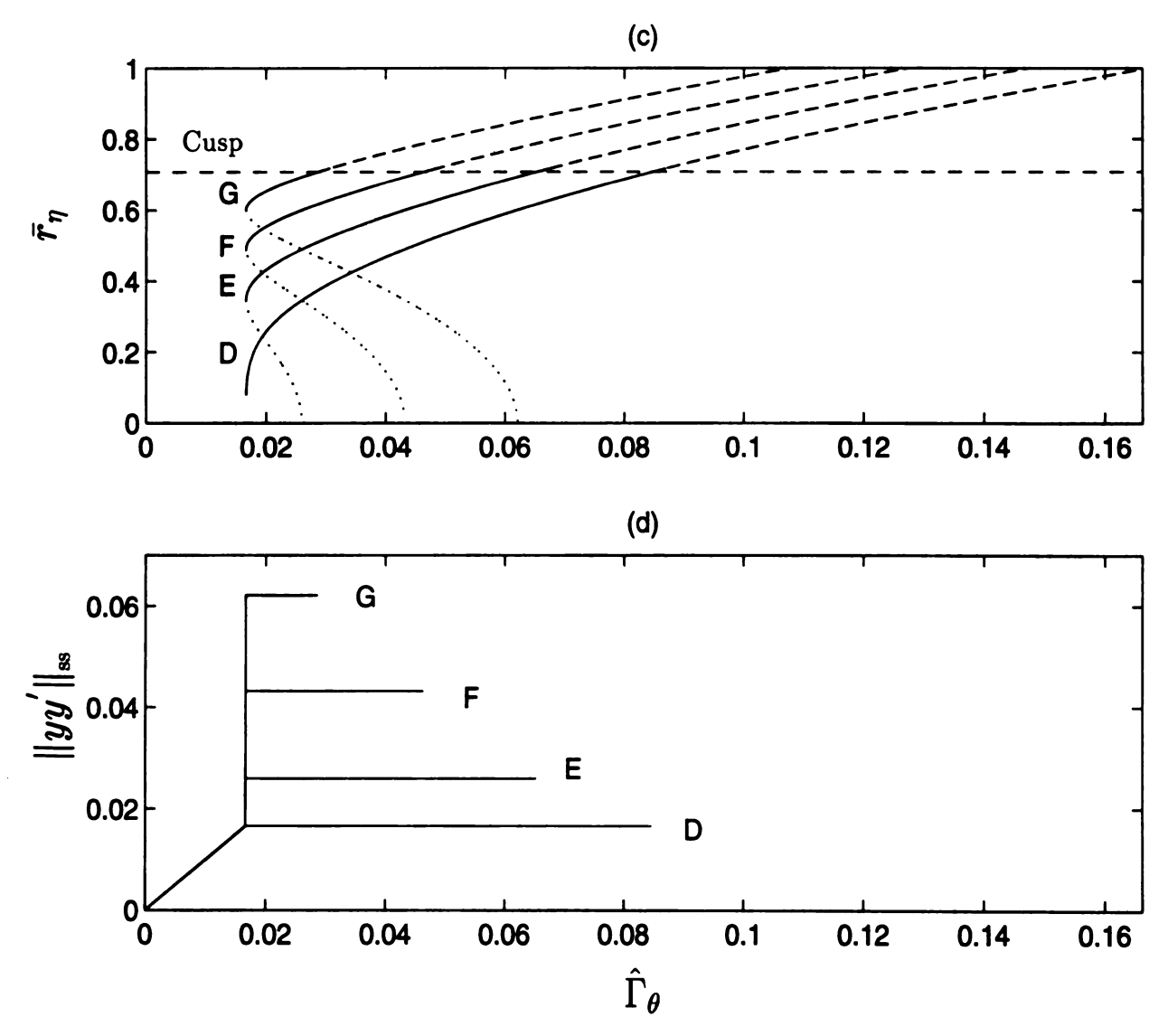


Figure 5.4: The response bifurcation diagram for **SM2** with n=2,  $\hat{\delta}_{\xi 4}=0$ ,  $\tilde{\delta}_{\eta 2}=0$ ,  $\tilde{\delta}_{\eta 4}=0$ ,  $\hat{\mu}_{a}=0.0083$  and various  $\hat{\delta}_{\xi 2}$ : (A) 0.03 (B) 0.02 (C) 0.01 (D) 0.00 (E) -0.01 (F) -0.02 (G) -0.03.

desired subharmonic solution. Therefore, in order to ensure a large torque range, to avoid jump behaviors, and to keep  $||yy'||_{ss}$  small, it is suggested that the absorber paths be designed such that  $\hat{\delta}_{\xi 2}$  is either zero or small and positive. The selection of a specific value for  $\hat{\delta}_{\xi 2}$  will depend on the criteria at hand, as tradeoffs between the torque range and torsional vibration amplitudes can be made.

The effects of nonzero  $\hat{\delta}_{\xi 4}$ 's on absorber performance are considered next. Throughout this discussion it is assumed that  $\hat{\delta}_{\xi 2}$  is positive and small. As pointed out above, the presence of this nonlinear imperfection destroys the perfect saturation of the rotor acceleration beyond the bifurcation point. Utilizing equations (5.39) and (5.40), bifurcation diagrams can be generated for various values of  $\hat{\delta}_{\xi 4}$ . An example for n=2,  $\hat{\mu}_a=0.0083$  and  $\hat{\delta}_{\xi 2}=0.02$  is shown in Figure 5.5. By comparing the responses with positive and negative values of  $\hat{\delta}_{\xi 4}$ , it is seen that negative values offer better performance in terms of the rotor acceleration, but they also reduce the applied torque range. On the other hand, although positive values of  $\hat{\delta}_{\xi 4}$  lead to a larger torque range, they cause an increase in the level of rotor acceleration. Also note that this parameter does not affect the torque level at which the bifurcation occurs.

The results given above are based on scaling assumption (5.19), which says that the differences in the paths are even smaller than the general level of imperfections and mistunings. This condition is now relaxed in order to consider the effects of nonzero, small  $\hat{\delta}_{\eta}$ 's. Due to the complexity of the resulting averaged equations, bifurcation diagrams can only be generated numerically, in this case using AUTO. The effects of the imperfection parameter  $\hat{\delta}_{\eta 2}$  are considered first. Figure 5.6 shows the bifurcation diagram with the same system parameters used in Figure 5.1, but with  $\hat{\delta}_{\eta 2} = 0.01$  and  $\hat{\delta}_{\eta 4} = 0$ . Comparing Figure 5.1 and Figure 5.6, it is seen that they are qualitatively the same, except that the zero amplitude parts of the solutions in the two single-mode responses are replaced by nonzero, but very small amplitudes. Note that the solutions denoted by SM1<sup>+</sup>, SM1<sup>-</sup> and SM2<sup>+</sup> in the

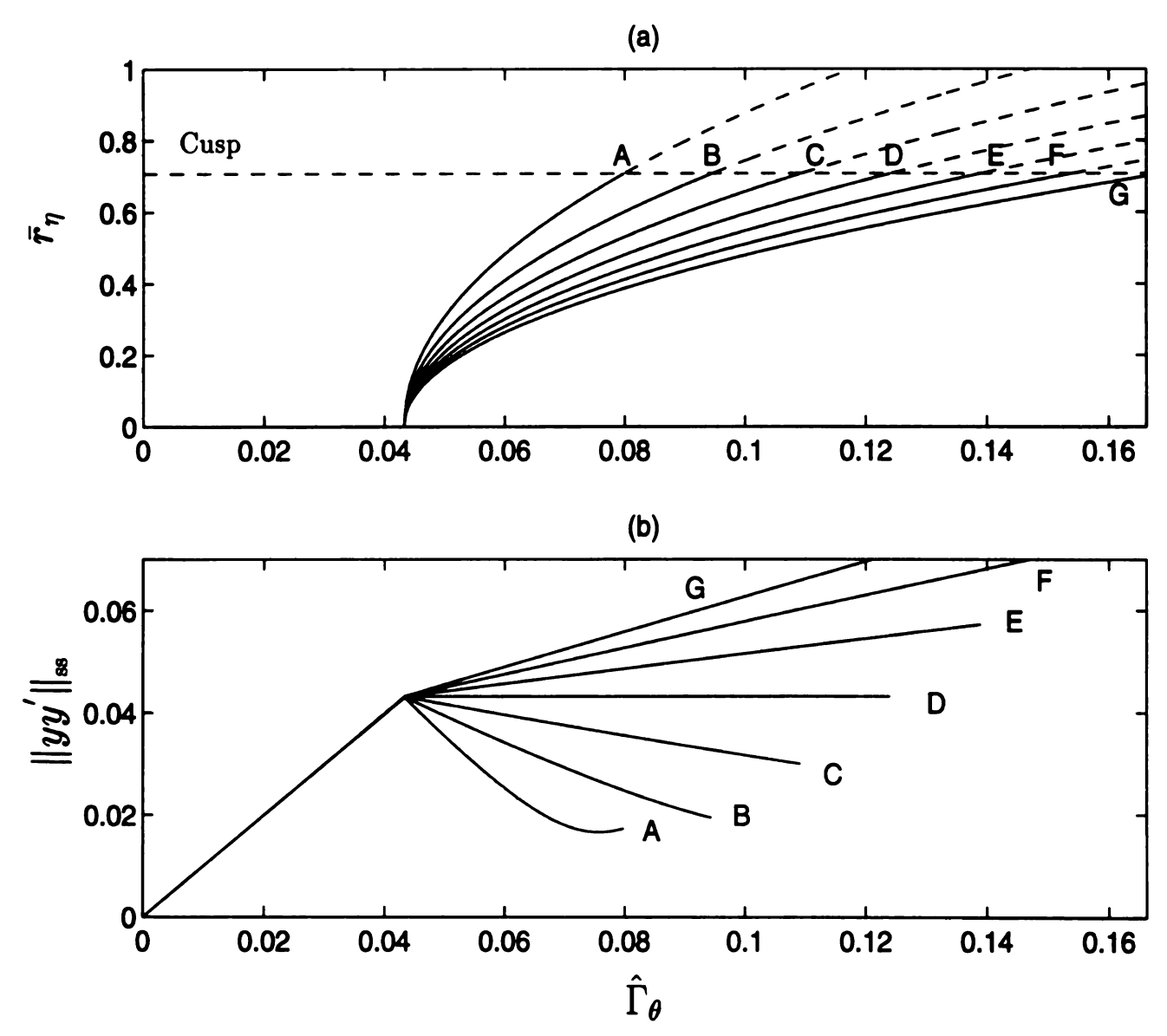


Figure 5.5: The response bifurcation diagram for SM2 with n=2,  $\hat{\delta}_{\xi 2}=0.02,~\tilde{\delta}_{\eta 2}=0,~\tilde{\delta}_{\eta 4}=0,~\hat{\mu}_a=0.0083$  and various  $\hat{\delta}_{\xi 4}$ : (A) -0.03 (B) -0.02 (C) -0.01 (D) 0.00 (E) 0.01 (F) 0.02 (G) 0.03.

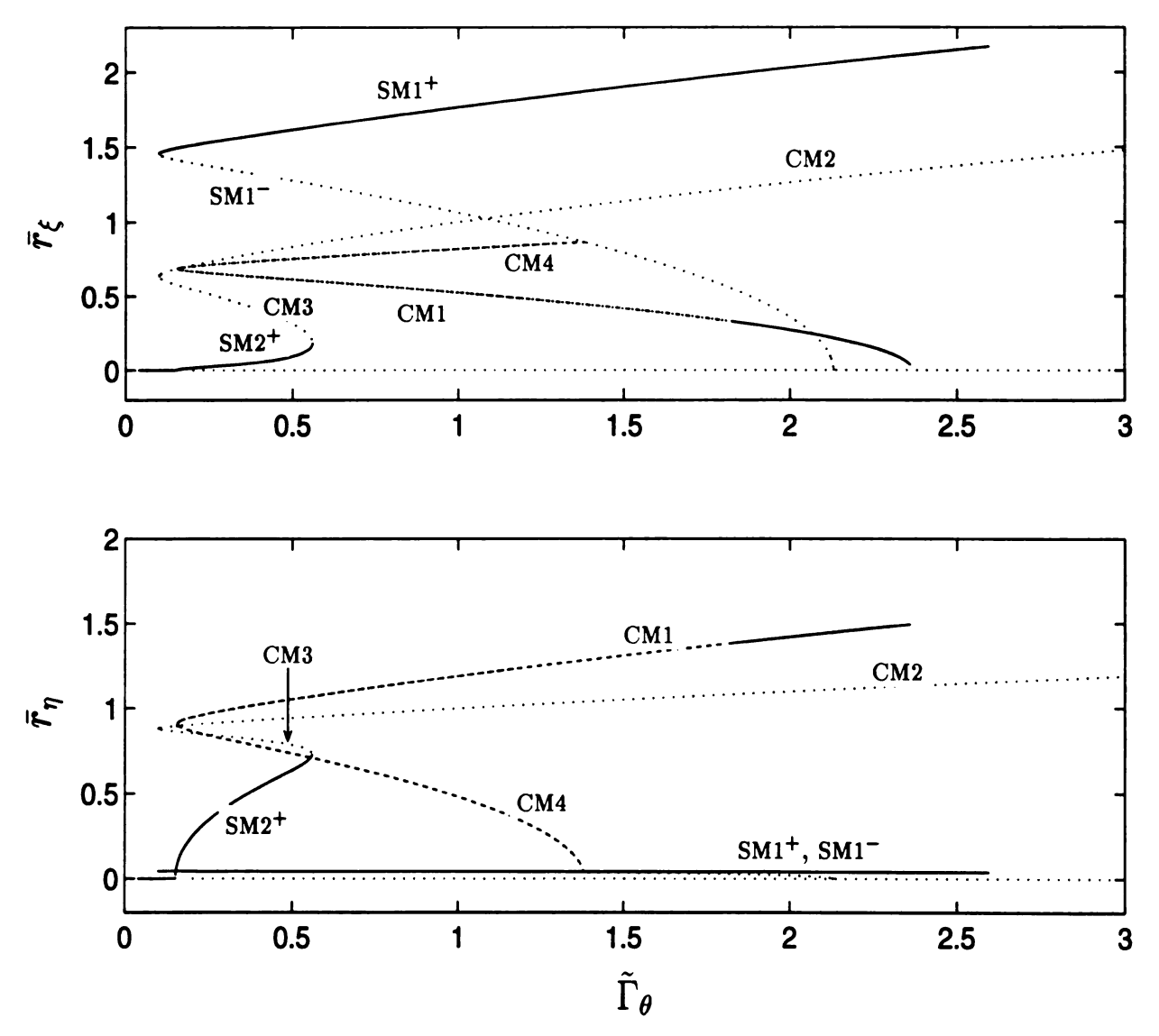


Figure 5.6: The response bifurcation diagram for n=2,  $\tilde{\mu}_a=0.05$ ,  $\hat{\delta}_{\xi 2}=0.01$ ,  $\hat{\delta}_{\eta 2}=0.01$ ,  $\hat{\delta}_{\xi 4}=0$  and  $\hat{\delta}_{\eta 4}=0$ . The solid lines represent stable solutions and the dashed lines represent unstable solutions.

figure are labeled so for convenience and for comparison purposes only, since they are in fact coupled-mode solutions in this case. Figure 5.7 shows the solutions for  $\bar{r}_{\xi}$ ,  $\bar{r}_{\eta}$ , and the corresponding rotor accelerations on the branch  $SM2^+$  for  $\hat{\delta}_{\xi 2} = 0.02$ ,  $\hat{\delta}_{\xi 4} = 0.01$ ,  $\hat{\delta}_{\eta 4} = 0$  and various values of  $\hat{\delta}_{\eta 2}$ . It is seen that the existence of a nonzero component of  $\bar{r}_{\xi}$  decreases the applicable torque range and increases the rotor acceleration as the magnitude of  $\hat{\delta}_{\eta 2}$  becomes larger. Both effects deteriorate absorber performance. In addition, the parameter  $\hat{\delta}_{\eta 4}$  is found to have the same qualitative effect on the system behavior as  $\hat{\delta}_{\eta 2}$ .

## 5.6.4 Design Guidelines

In summary, the above results indicate that the following general guidelines be followed when designing the paths for a subharmonic absorber system:

- The absorber paths should be kept as identical as possible.
- The linear mistuning parameter  $\hat{\delta}_{\xi 2}$  should be selected to be small and positive, in order to be safe and avoid it becoming negative due to unforeseen changes.
- ullet The nonlinear imperfection parameter  $ilde{\delta}_{\xi 4}$  should made as small as possible.
- One can refer to the predicted dynamics in order to choose values of  $\tilde{\delta}_{\xi 4}$  and  $\tilde{\delta}_{\xi 2}$  for a particular specification in terms of vibration level or torque range. This would most likely be implemented experimentally by a trial-and-error approach.

## 5.6.5 Simulation Results

Numerical simulations for the equations of motion (2.12) are carried out in order to verify the system dynamics as predicted by the averaged equations. The system

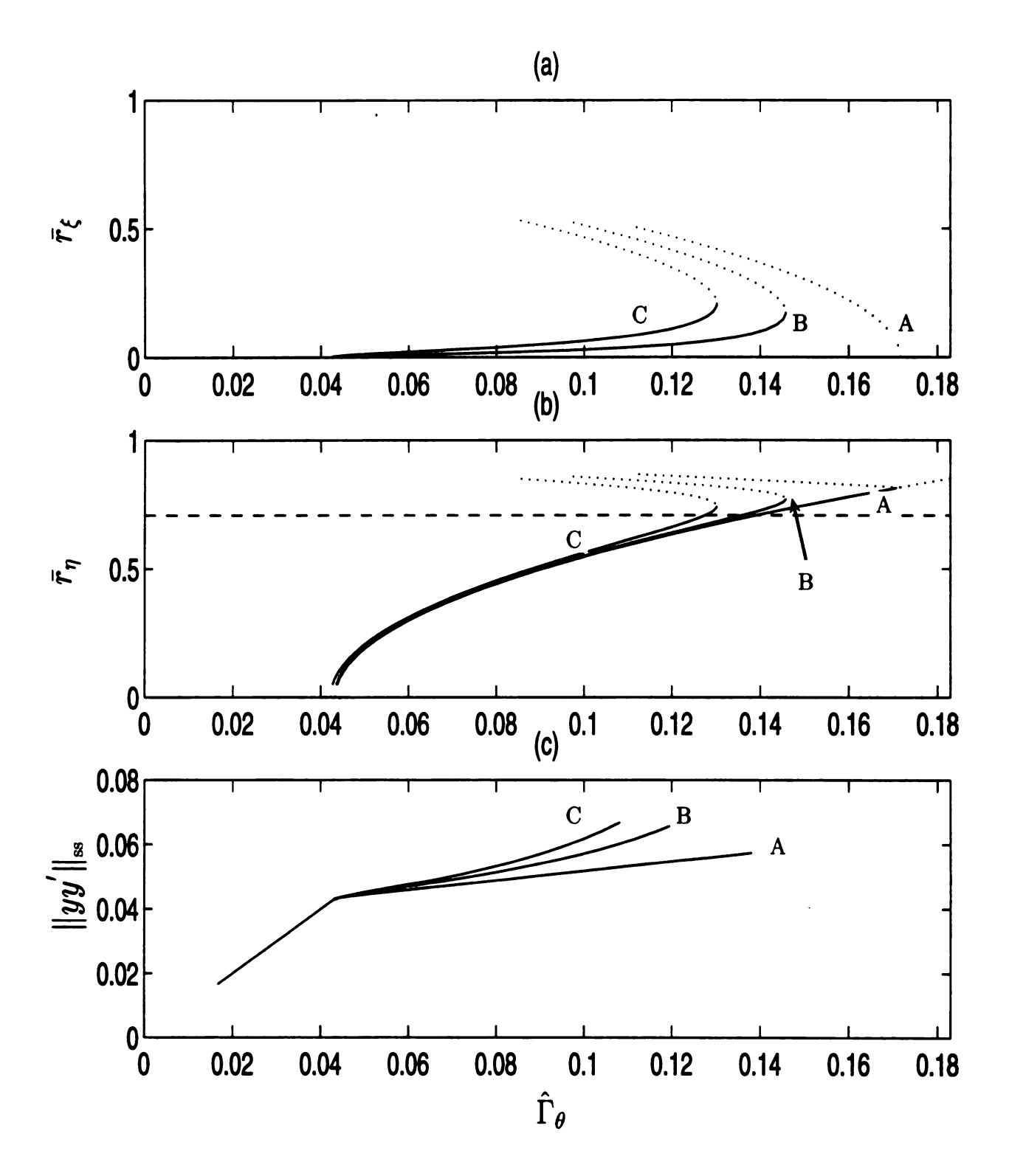


Figure 5.7: The response bifurcation diagram of **SM2** for n=2,  $\hat{\mu}_a=0.0083,\ \hat{\delta}_{\xi 2}=0.02$  and  $\hat{\delta}_{\xi 4}=0.01,\ \hat{\delta}_{\eta 4}=0$  and various  $\hat{\delta}_{\eta 2}$ : (A) 0.0 (B) 0.01 (C) 0.02.

parameters used throughout this section are  $\nu=0.166$  and n=2. These are values taken from the 2.5 liter, in-line, four stroke, four cylinder engine considered by Denman [16]. The damping coefficients are taken to be  $\hat{\mu}_0=0.05$  and  $\hat{\mu}_a=0.0083$  ( $\tilde{\mu}_a=0.05$ ). The following truncated absorber path formulation, expressed in terms of the  $\hat{\delta}$ 's, is employed, (5.5) given by

$$x_i(s_i; \hat{\delta}_{ij}) = 1 - \hat{\delta}_{i1}s_i - \left[ \left( \frac{n}{2} \right)^2 + \hat{\delta}_{i2} \right] s_i^2 - \hat{\delta}_{i3}s_i^3 - \hat{\delta}_{i4}s_i^4, \quad i = 1, 2.$$
 (5.41)

Higher-order imperfections are not included here since it is evident that they will not contribute to the first-order nonlinear resonant responses. In all cases the coefficients of odd powers of s,  $\hat{\delta}_{\xi 1}$ ,  $\hat{\delta}_{\eta 1}$ ,  $\hat{\delta}_{\xi 3}$  and  $\hat{\delta}_{\eta 3}$ , are assumed to be small. The simulations show no sign of any effects from these  $\hat{\delta}$ 's, as predicted by the analysis.

Overall, excellent consistency is found between the analytical results derived from the non-truncated averaged equations (5.16) and the simulations.

A representative case is chosen to demonstrate the simulation results and their comparison with the analysis. Imperfection parameters for this case are,

$$\hat{\delta}_{\xi 1} = 0.01, \quad \hat{\delta}_{\eta 1} = 0.01, \quad \hat{\delta}_{\xi 2} = 0.02, \quad \hat{\delta}_{\eta 2} = 0.005,$$

$$\hat{\delta}_{\xi 3} = 0.01, \quad \hat{\delta}_{\eta 3} = 0.01, \quad \hat{\delta}_{\xi 4} = 0.01, \quad \hat{\delta}_{\eta 4} = 0.005. \tag{5.42}$$

Here the linear frequency mistuning for the two absorbers is  $\Delta\omega_1 = \Delta\omega_2 = 0.02$  (2% mistuning for n=2) with a deviation represented by  $\hat{\delta}_{\eta 2} = 0.005$ . A small, positive  $\hat{\delta}_{\xi 4} = 0.01$  is chosen, which enlarges the range of the disturbing torque but also increases rotor acceleration amplitudes. A small deviation  $\hat{\delta}_{\eta 4} = 0.005$  is chosen to demonstrate its influence on the system response. The bifurcation diagram using this set of values is shown in Figure 5.8. The solid lines represent the absorber amplitude solutions, as computed by AUTO using the non-truncated averaged equations (5.16), and the corresponding rotor acceleration, which is calculated by the  $\mathcal{O}(\epsilon)$  term of  $yy'(\theta)$  given in equation (5.9). The circles are the results obtained from simulations, after allowing the system to settle into its steady-state response. It is seen from this

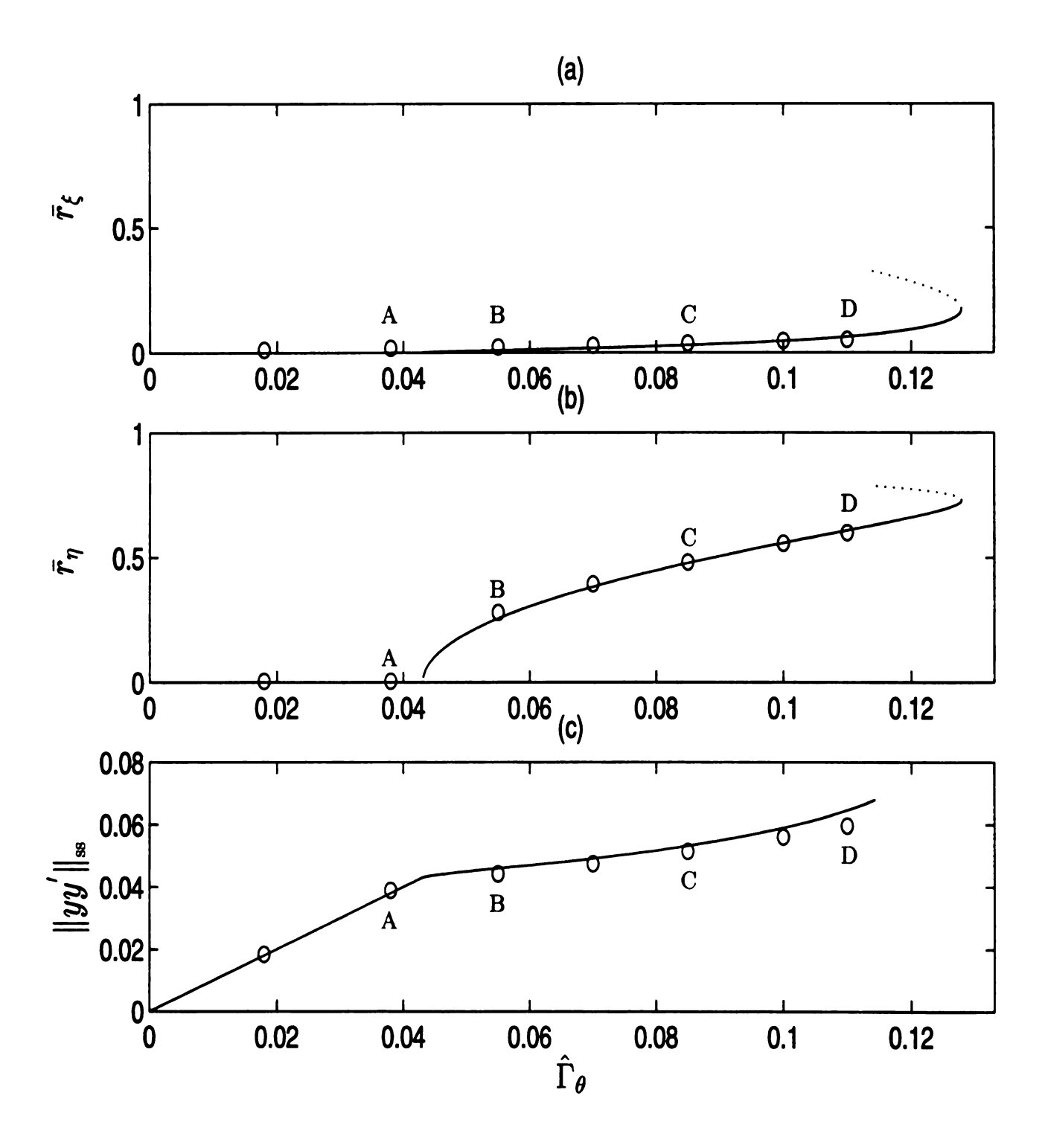


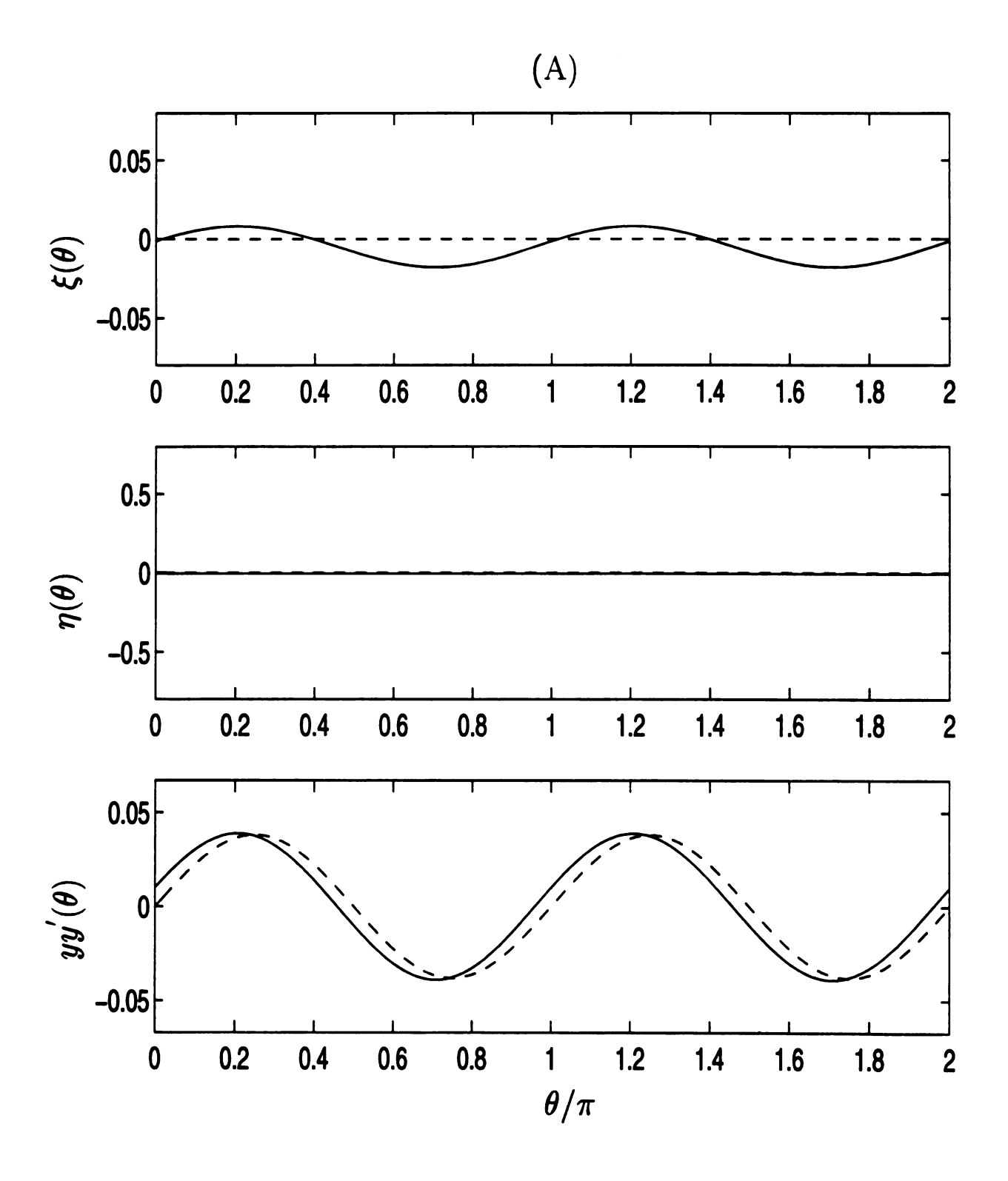
Figure 5.8: The simulated and analytical responses on SM2 for n=2,  $\hat{\mu}_a=0.0083$ ,  $\hat{\delta}_{\xi 2}=0.02$ ,  $\hat{\delta}_{\xi 4}=0.01$ ,  $\hat{\delta}_{\eta 2}=0.005$  and  $\hat{\delta}_{\eta 4}=0.005$ .

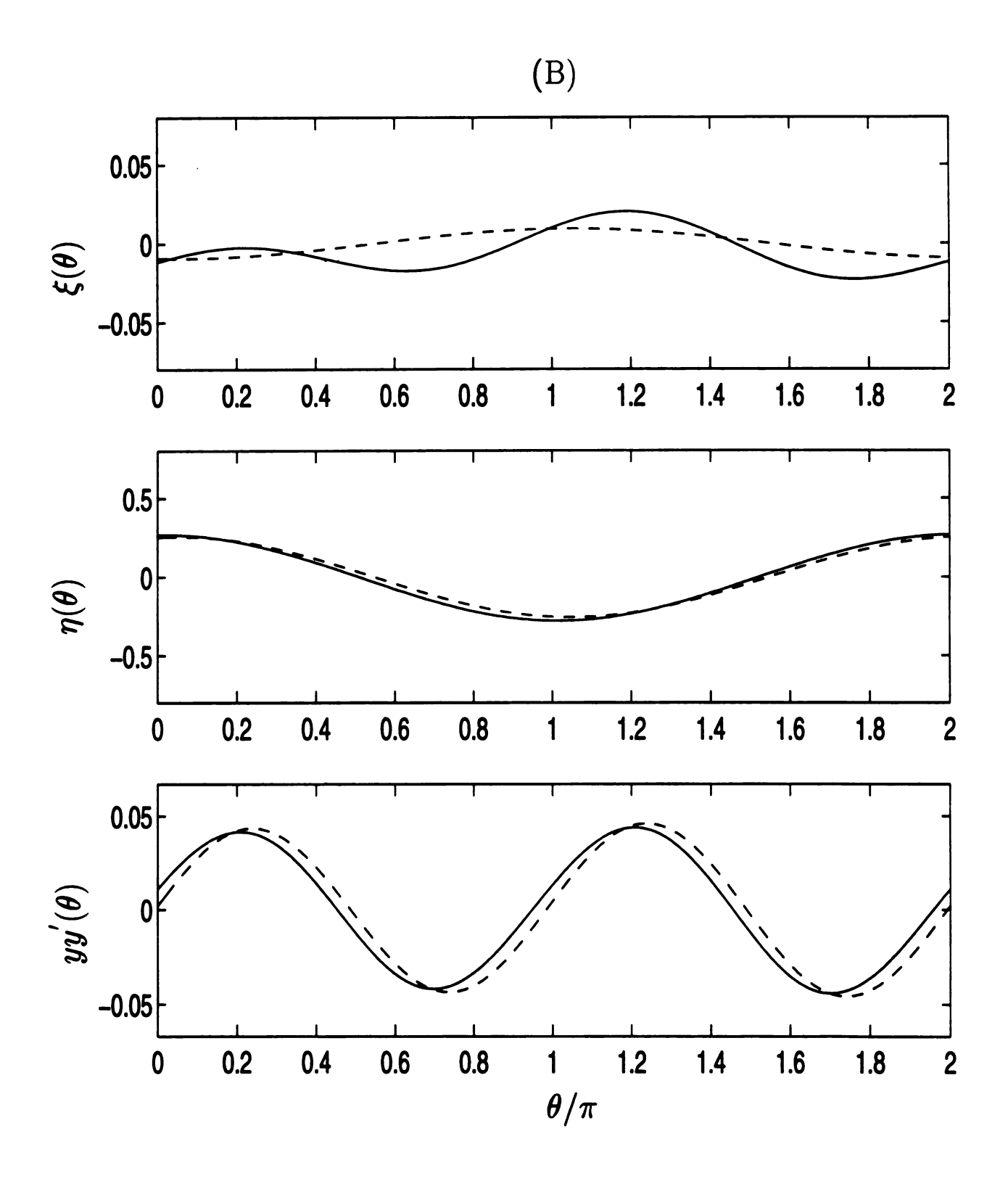
figure that the averaged equations (5.16) offer a very satisfactory prediction of the system dynamics, even for this value of the perturbation parameter,  $\epsilon = 0.166$ .

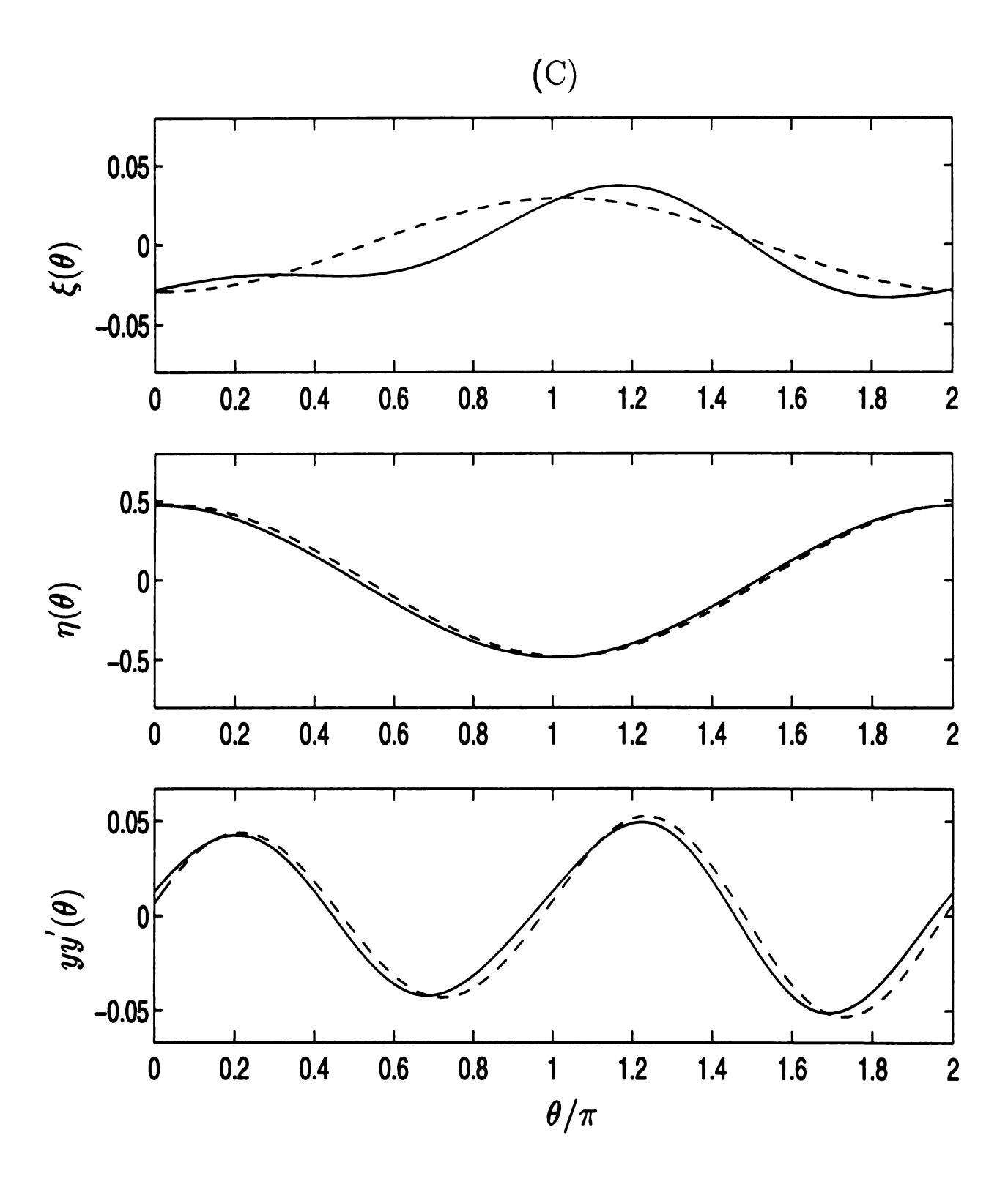
Figure 5.9 shows the system responses and the angular accelerations of the rotor at points A, B, C, and D indicated in Figure 5.8. Solid lines represent the simulated responses while the dashed lines represent the responses predicted by the nontruncated averaged equations (5.16). Note that the scale used to depict the  $\xi(\theta)$  response in Figure 5.9 (A) - (D) is expanded for greater clarity. It is seen from (A) - (D) that the approximations obtained from averaging for the crucial response variables  $yy'(\theta)$  and  $\eta(\theta)$  are very accurate.

At point A, the simulations show that the absorber motions are dictated by the non-resonant responses, that is, the absorbers respond in a synchronized manner at the frequency of the disturbing torque (the linear system response). For this case the averaged equations predict zero resonant responses for both  $\xi(\theta)$  and  $\eta(\theta)$ . At point B, as predicted by the averaged equations, a subharmonic resonant response with frequency half that of the disturbing torque has appeared. This response possesses a nonzero component in the difference coordinate  $\eta(\theta)$  and a very small component in the sum coordinate  $\xi(\theta)$ . Figure 5.9(B) shows that the simulated  $\eta(\theta)$  matches well with the analysis, while the simulated  $\xi(\theta)$  is approximately a superposition of the non-resonant response shown in Figure 5.9(A) (not predicted) and the resonant response (predicted). In this case, the absorber motions are dominated by the out-of-phase component  $\eta(\theta)$ . From (C) to (D), as  $\hat{\Gamma}_{\theta}$  is increased, the response of  $\xi(\theta)$  grows and begins to influence the rotor acceleration. In addition, higher harmonics start to creep into the response.

Using the simulations, one also finds consistency between the predicted and simulated torque ranges. This follows since in the large torque range the absorber motion is dominated by  $\eta(\theta)$ , which is well approximated by the analytical results.







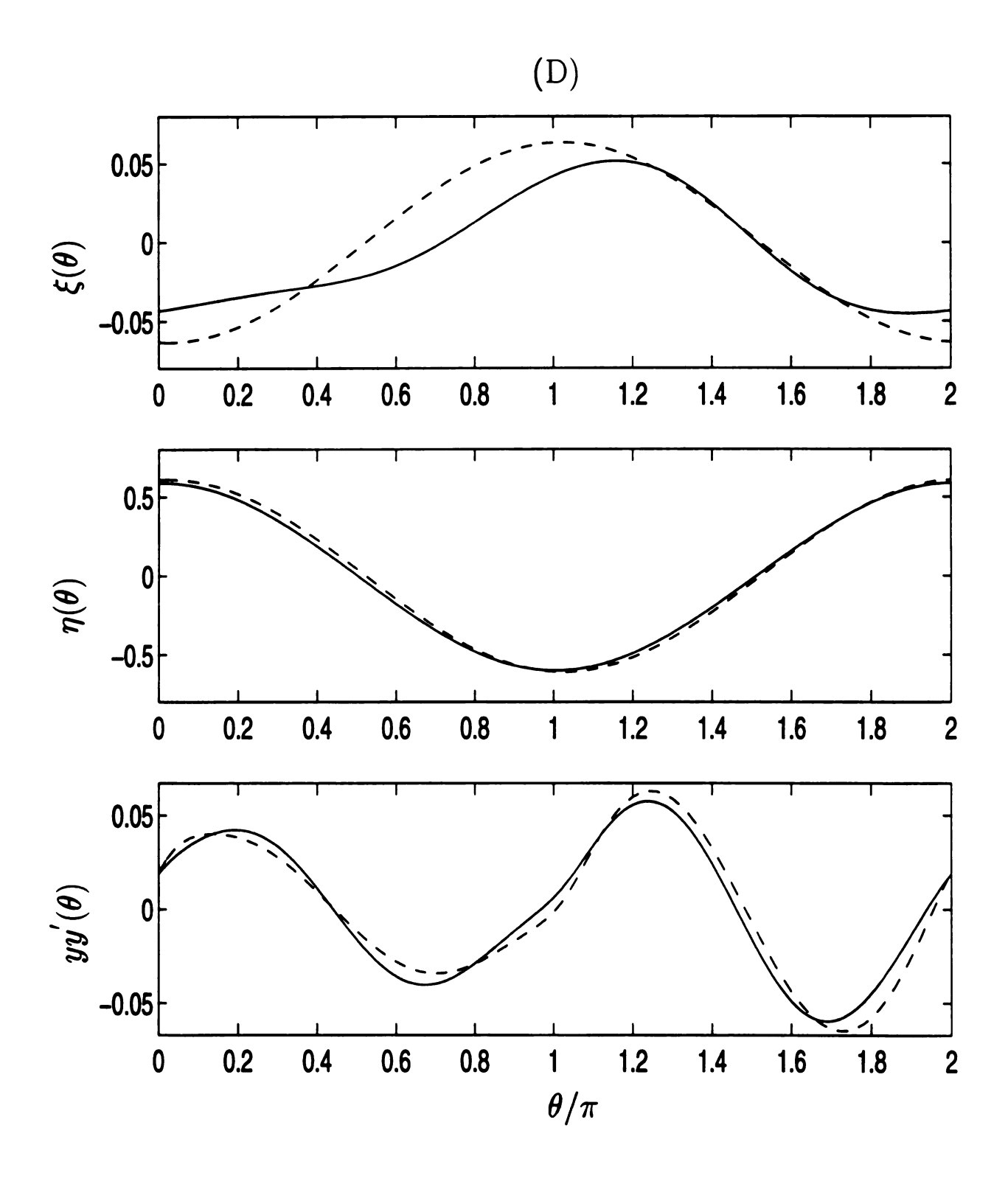


Figure 5.9: The absorber responses and rotor accelerations for  $\hat{\Gamma}_{\theta} = 0.038, 0.055, 0.085, 0.11$ , corresponding to points (A), (B), (C) and (D) in Figure 5.8, respectively.

## 5.7 Concluding Remarks

The performance of a pair of subharmonic absorbers as proposed by Lee and Shaw [30] has been re-assessed by incorporating imperfections and intentional mistuning into the absorber paths. Based on approximate solutions obtained by scaling the system parameters and applying the method of averaging, it is found that the mistunings and imperfections entering the path function at even orders of the path variable s play an important role in the resonant responses of the system. It is also found that differences between the two paths of the absorbers have a generally deleterious effect on system performance. On the other hand, mistunings and imperfections that are identical to the two paths can be used to trade off between the operating range of the system and the level of torsional vibration.

This work only considers a rotating system with a single pair of subharmonic absorbers. In practice, one needs to choose the total absorber inertia to be sufficiently large such that the absorbers' amplitudes remain below some specified level even under severe operating conditions. This is typically accomplished by stationing several absorber masses along and around the axis of rotation. These multi-mass arrangements are also used for balancing and/or due to restricted space around the rotor. In many cases, these absorbers are of identical mass and have identical path tuning. In the next chapter the performance of systems with multiple pairs of subharmonic absorbers are considered, and bifurcations are found to occur. It will be shown that the desired torsional vibration reduction is maintained, and that one must include imperfections in the model in order to obtain a realistic estimate of the torque range.

# CHAPTER 6

# NONLINEAR DYNAMICS OF A MULTIPLE SUBHARMONIC CPVA SYSTEM

The study presented in the previous chapter considers a rotating system with a single pair of subharmonic absorbers. In practice, one needs to choose the total absorber inertia to be sufficiently large such that the absorbers' amplitudes remain below some specified level even under severe operating conditions. This is typically accomplished by stationing several absorber masses along and around the axis of rotation. These multi-mass arrangements are also used for balancing and/or due to restricted space around the rotor. In many cases, these absorbers are of identical mass and have identical path tuning.

In this chapter, a system consisting of a rotor and multiple identical subharmonic absorbers is considered. Due to balancing considerations, only the cases with multiple pairs of subharmonic absorbers are investigated herein. Some general features of the equations of motion for such a system are first described and they are massaged into a form where averaging can be applied. For simplicity, an asymptotic analysis utilizing special scaling and the method of averaging is first carried out for a system with two pairs of absorbers to predict the bifurcation point of the desired (unison) motion and the post-bifurcation responses. Under the assumption that each absorber path is identical and possesses the same mistuning and imperfections, the absorber performance can be re-evaluated with respect to various imperfection and mistuning parameters by computing two performance measures. Design guidelines for the absorber paths are distilled from the results. Based on some preliminary analyses and simulations, it can be shown that the generic design guidelines found for the case

with two pairs of absorbers are applicable to the case with an arbitrary numbers of pairs of absorbers.

The analytical and simulation results show that compared to the idealized system composed of a single pair of subharmonic absorbers, an increase of absorber number may lead to a drastic decrease on the torque range due to the possibility that the system dynamics converges to a non- $S_{N/2} \times S_{N/2}$  branch in the post-bifurcation stage for some parameter ranges of mistuning and imperfections. (The  $S_{N/2} \times S_{N/2}$  branch is the response in which half of the absorbers move, exactly, out-of-phase relative to the other half, with the same amplitudes, leading to equivalent system dynamics as that for the system with a single pair of absorbers.) Based on evaluations of the performance measures, general design guidelines for absorber paths for arbitrary pairs of absorbers can be outlined to trade off between the increase of the torque range and the reduction of torsional vibration.

# 6.1 The Multiple Subharmonic Absorber System

### 6.1.1 The Perfectly Tuned Absorber System

A subharmonic absorber system was proposed by Lee et al. [30] which is composed of a pair of absorbers with identical individual masses and dampings. Due to spatial restrictions and balancing requirements, a system consisting of N/2 (N even) pairs of identical absorbers with individual masses  $m_i = \frac{m_0}{N}$  and identical damping coefficients  $\hat{\mu}_{ai} = \hat{\mu}_a$ , i = 1, ..., N, is considered here.

These absorbers ride on identical paths specified by

$$x_i^2(s_i) = 1 - \left(\frac{n}{2}\right)^2 s_i^2, \quad 1 \le i \le N,$$
 (6.1)

which is equivalent to  $R_i(S_i) = \sqrt{R_0^2 - \left(\frac{n}{2}\right)^2 S_i^2}$ . This path is a particular epicycloid [16]. It was shown in section 5.1.3. that these paths tune the nondimension-

alized natural frequency of each absorber to be n/2, that is, one-half that of the applied torque.

The equations of motion (2.12a) and (2.12b) and the identical paths given by equation (6.1) have an exact solution when the absorber damping is zero,  $\hat{\mu}_a = 0$ , and the steady rotation condition (2.9) is satisfied. It is given by

$$y(\theta) = 1, (6.2a)$$

$$s_i(\theta) = -s_j(\theta) = \pm \frac{2}{n} \sqrt{\frac{2\hat{\Gamma}_{\theta}}{\nu n}} \cos\left(\frac{n}{2}\theta\right),$$
 (6.2b)

where  $i=1,3,...,(N-1),\ j=2,4,...,N$  and  $\nu=\frac{m_0R_0^2}{I_d}$  is the ratio of the total nominal moment inertia of all absorbers about point O to that of the rotor. The solution described in equation (6.2) represents a response with a constant speed of the rotor and half of the absorbers moving out-of-phase relative to the other half, which is denoted by the  $\mathbf{S_{N/2}} \times \mathbf{S_{N/2}}$  solution. One can refer to section 5.1.1 for a description of this type of response.

### 6.1.2 Imperfections, Mistuning and Limitations

The steady-state solution in equations (6.2) corresponds to perfectly constant rotor speed, which is the ultimate design goal of such an absorber system; However, as absorber damping, mistuning and imperfections enter the absorber path configuration, a constant rotor speed is unachievable. To account for the aforementioned effects, the absorber path functions are generalized following the same steps used in section 5.1.2., yielding

$$x_i(s_i; \hat{\delta}_{ij}) = 1 - \left(\frac{n}{2}\right)^2 s_i^2 - \sum_j \hat{\delta}_{ij} s_i^j, \quad i = 1, 2, ..., N.$$
 (6.3)

where the  $\hat{\delta}_{ij}$ 's are imperfections at various orders of the path functions, and the  $\hat{\delta}_{i2}$ 's incorporate both the effects of intentional mistuning and imperfections.

Keeping the function  $g_i(s_i)$  real during absorber motions leads to a restriction

on the amplitudes of the absorber motions. For the case when all mistuning and imperfections are small,  $\hat{\delta}_{ij} \ll 1$ , the aforementioned restriction is approximated by

$$s_i(\theta) \le s_{\max} + \mathcal{O}(\hat{\delta}), \quad \forall \ \theta \text{ and } i, \quad \text{where } s_{\max} = \frac{4}{n\sqrt{n^2 + 4}}.$$
 (6.4)

The above restriction will impose a finite operating range on the disturbing torque level  $\hat{\Gamma}_{\theta}$ .

## 6.2 Reduction of the Equations of Motion

Approximations of the steady-state solutions are sought in the next section through an asymptotic analysis in order to evaluate absorber performance measures. To this end, a re-arrangement and series approximation for the equations of motion is conducted in section 6.2.1, followed by two proposed transformations which allow one to re-formulate the system dynamics in a periodic form which is amenable for averaging.

## 6.2.1 The Rotor Acceleration and Absorber Dynamics

The scaling of parameters and the series approximation for the equations of motion employed in sections 3.1.2 and 5.3 are utilized herein to derive an approximation of the rotor acceleration, given by

$$yy'(\theta) = -\epsilon \left\{ \frac{1}{N} \sum_{j=1}^{N} \left( -\frac{n^2}{2} s_j s_j' - \left( \frac{n}{2} \right)^2 g^0(s_j) s_j + \frac{dg^0(s_j)}{ds_j} s_j'^2 \right) - \tilde{\Gamma}_{\theta} \sin(n\theta) \right\} + \mathcal{O}(\epsilon^2).$$
(6.5)

where

$$g^{0}(s_{i}) = g_{i}(s_{i}; \hat{\delta}_{ij} = 0) = \sqrt{1 - \left(\frac{4n^{2} + n^{4}}{16}\right) s_{i}^{2}}, \quad i = 1, ..., N,$$

and a set of weakly coupled, weakly nonlinear oscillators for the absorber dynamics, which are described by a set of 2nd order ODE's, as follows,

$$s_i'' + \left(\frac{n}{2}\right)^2 s_i = \epsilon f_i(s_1, s_2, s_1', s_2', \theta) + \mathcal{O}(\epsilon^2), \qquad i = 1, ..., N$$
 (6.6)

where

$$\begin{split} f_{i}(s_{1},s_{2},s_{1}^{'},s_{2}^{'},\theta) &= -\tilde{\mu}_{a}s_{i}^{'}-h_{i}(s_{i}) \\ &+[s_{i}^{'}+g^{0}(s_{i})][\frac{1}{N}\sum_{j=1}^{N}(-\frac{n^{2}}{2}s_{j}s_{j}^{'}-\left(\frac{n}{2}\right)^{2}g^{0}(s_{j})s_{j}+\frac{dg^{0}(s_{j})}{ds_{j}}s_{j}^{'2}) \\ &-\tilde{\Gamma}_{\theta}\sin(n\theta)], \\ h_{i}(s_{i}) &= \frac{1}{2}\sum_{j}j\tilde{\delta}_{ij}s_{i}^{j-1}. \end{split}$$

### Remarks:

- It can be recognized in the above equations that the linear oscillating frequencies of the absorbers are identical to each other. Thus, there exist 1:1 internal resonances between each absorber dynamics. In addition, the excitation is in a 2:1 resonance with respect to each absorber, and it is of parametric form. Note that the types and structures of resonances appearing hererin is the same as those for the case with a single pair of absorbers, except that there are multiple 1:1 resonances in this case.
- In the case with multiple absorbers tuned to the the order of the external torque, which is the system analyzed in chapter 4, the excitation is in a 1:1 resonance with respect to each absorber (different from the present case), and there exist 1:1 internal resonances between each absorber dynamics (the same as the present case).
- Non-zero, distinct imperfections and mistuning undermine the embedding symmetry of the system,  $S_N$ .

### 6.2.2 The Periodic Standard Form

Averaging on the system dynamics is conducted in the following sections in order to obtain approximate steady-state responses. This is accomplished by first arranging the system equations (6.6) into amenable form for averaging, the periodic form, through two stages of transformation. The first transformation is given by

$$\xi_1 = \frac{1}{N} \sum_{j=1}^{N} s_j, \quad \xi_i = \frac{1}{N} (s_1 - s_i) \text{ for } 2 \le i \le N.$$
 (6.7)

The above linear coordinate transformation among absorber displacements is used to split the dynamics into two invariant subspaces, representing the unison motion and its complement, respectively. For more insight into the physics of this transformation, one can refer to section 4.1.

The second transformation is the polar coordinate transformation which is given by

$$\xi_i = r_i \cos(\varphi_i - \frac{n\theta}{2}), \quad \xi_i' = nr_i \sin(\varphi_i - \frac{n\theta}{2}), \quad \text{for } 1 \le i \le N.$$
 (6.8)

Utilizing the transformations in equations (6.7) and (6.8) and following the steps used in section 5.4.1, one can transform equations (6.6) into the standard periodic form, as follows,

$$r'_{i} = \frac{2\epsilon}{n}\hat{F}_{i}(r_{1},....,r_{N},\varphi_{1},....,\varphi_{N},\theta)\sin(\varphi_{i}-\frac{n\theta}{2})+\mathcal{O}(\epsilon^{2}),$$
 (6.9a)

$$r_i \varphi_i' = \frac{2\epsilon}{n} \hat{F}_i(r_1, \dots, r_N, \varphi_1, \dots, \varphi_N, \theta) \cos(\varphi_i - \frac{n\theta}{2}) + \mathcal{O}(\epsilon^2)$$
 (6.9b)

where  $1 \leq i \leq N$ , and the functions  $\hat{F}_i$ 's result from incorporating transformations (6.7) and (6.8) into  $f_i$ ,  $1 \leq i \leq N$ , which are listed in equations (6.6).

## 6.3 The Averaged Equations

Considering only the first-order terms in  $\epsilon$  in equations (6.9), first-order averaging is performed over one period of excitation  $\frac{4\pi}{n}$ . The resulting averaged equations can be expressed in terms of the first-order averaged variables,  $\bar{r}_i$ , and  $\bar{\varphi}_i$ ,  $1 \leq i \leq N$ . Due to the complicated nature involved in the functions  $f_i$ 's in equation (6.6), the averaging process does not yield closed-form expressions for each term in the

averaged equations. To solve this problem, several assumptions are made. First, the oscillation amplitudes of absorbers, that is,  $\bar{r}_i$ ,  $1 \leq i \leq N$ , are assumed to be small and of the same order, denoted by  $\mathcal{O}(\bar{r})$ . Second, the resulting averaged equations are expanded in terms of  $\bar{r}_i$ ,  $1 \leq i \leq N$  up to  $\mathcal{O}(\bar{r}^3)$ , the first nonlinear-order terms, in order to capture the resonant solutions in the post-bifurcation stage. Third, it is assumed that the relative precision between the curves manufactured for the absorber paths is much higher than their absolute precision, which renders nearly identical absorber paths, yielding

$$\frac{\tilde{\sigma}_{ij}}{\tilde{\sigma}_{1j}} = \mathcal{O}(\epsilon) \quad \text{for } 2 \le i \le N, \quad j = 1, 2, \dots,$$

$$(6.10)$$

where

$$\tilde{\sigma}_{1j} = \frac{1}{N} \sum_{i=1}^{4} \tilde{\delta}_{ij}, \ j = 1, 2, \dots,$$

$$\tilde{\sigma}_{ij} = \frac{1}{N} (\tilde{\delta}_{1j} - \tilde{\delta}_{ij}), \ 2 \le i \le N, \ j = 1, 2, \dots.$$

The aforementioned steps result in a set of averaged equations of the form

$$\frac{d\bar{r}_{1}}{d\hat{\theta}} = \frac{-1}{2}\tilde{\mu}_{a}\bar{r}_{1} + \frac{1}{4}\tilde{\Gamma}_{\theta}\bar{r}_{1}\sin 2\bar{\varphi}_{1} \\
+\hat{G}_{1}(r_{1},.....,r_{N},\varphi_{1},.....,\varphi_{N}) + \mathcal{O}(\bar{r}^{5}), \qquad (6.11a)$$

$$\bar{r}_{1}\frac{d\bar{\varphi}_{1}}{d\hat{\theta}} = \left(-\frac{\tilde{\sigma}_{12}}{n} - \frac{n}{4}\right)\bar{r}_{1} + \frac{1}{4}\tilde{\Gamma}_{\theta}\bar{r}_{1}\cos 2\bar{\varphi}_{1} \\
+\hat{H}_{1}(r_{1},.....,r_{N},\varphi_{1},.....,\varphi_{N}) + \mathcal{O}(\bar{r}^{5}), \qquad (6.11b)$$

$$\frac{d\bar{r}_{i}}{d\hat{\theta}} = \frac{-1}{2}\tilde{\mu}_{a}\bar{r}_{i} + \frac{1}{4}\tilde{\Gamma}_{\theta}\bar{r}_{i}\sin 2\bar{\varphi}_{i} \\
+\hat{G}_{i}(r_{1},.....,r_{N},\varphi_{1},.....,\varphi_{N}) + \mathcal{O}(\bar{r}^{5}), \qquad (6.11c)$$

$$\bar{r}_{i}\frac{d\bar{\varphi}_{i}}{d\hat{\theta}} = -\frac{\tilde{\sigma}_{12}}{n}\bar{r}_{i} + \frac{1}{4}\tilde{\Gamma}_{\theta}\bar{r}_{i}\cos 2\bar{\varphi}_{i} \\
+\hat{H}_{i}(r_{1},.....,r_{N},\varphi_{1},.....,\varphi_{N}) + \mathcal{O}(\bar{r}^{5}), \qquad (6.11d)$$

where  $2 \leq i \leq N$ ,  $\hat{\theta} \equiv \epsilon \theta$ , and the functions  $\hat{G}$ 's,  $\hat{H}$ 's contain the  $\mathcal{O}(\bar{r}^3)$  terms resulting from averaging. Due to the complexity involved and the dependence on

the number of absorbers, they are not listed explicitly here; however, they can be derived easily by following the procedure stated above.

Note that with the scaling assumptions (6.10), which forces near-identity of imperfections and mistuning in each absorber, the averaged equations (6.11) up to  $\mathcal{O}(\bar{r}^3)$  possesses the isotropy subgroup  $S_N$ . It is also seen in these averaged equations that the internal mistuning is evident through the presence of the term  $-n\bar{r}_1/4$  in equation (6.11b), which represents the discrepancy between the frequencies of two normal response modes. This will be shown to be a key factor in predicting the approximate post-bifurcation responses of the system in the next section.

### 6.4 Case Studies

In section 6.4.1, a system with **two** pairs of subharmonic absorbers (N=4) is first considered. In section 6.4.1.1, these equations are analyzed to find approximate steady-state solution branches and the corresponding stabilities. In section 6.4.1.2 two performance measures are evaluated based on the solution branches found and their associated stabilities are detected. It is found that only solutions with isotropy subgroups  $S_2 \times S_2$  and  $S_1 \times S_3$  are possible as stable steady states.

Next, the studies are extended to the cases with arbitrary pairs of absorbers, described in section 6.4.2. Based on some preliminary analysis and simulations, it is found that for a system of N absorbers (N/2 pairs), only the solutions with isotropy subgroups  $S_{N/2} \times S_{N/2}$  and  $S_1 \times S_{N-1}$  survive as stable and feasible solutions without vulnerability of violating the cusp condition. This result is consistent to those found in the case with two pairs of absorbers.

### 6.4.1 Two Pairs of Absorbers

## 6.4.1.1 Steady-State Solution Branches

It is very difficult to determine all solution branches due to the high level of symmetry and dimensions involved in the system's averaged equations (6.11). However, the restriction on the absorber motions described in equations (6.4) impose an upper limit on the feasible torque range. This condition facilitates the search for the post-bifurcation, steady-state solution branches near the first bifurcation point. In the following, the post-bifurcation, steady-state solution branches are sought near the first bifurcation point. Then, the corresponding stabilities are detected by evaluating the corresponding Jacobians.

It can be shown by evaluating the Jacobian of equations (6.11) that by assuming  $\tilde{\sigma}_{12}$  to be small, the trivial solution becomes unstable as  $\tilde{\Gamma}_{\theta}$  approaches  $2\tilde{\mu}_a$ ; thus,  $\tilde{\Gamma}_{\theta}^* \simeq 2\tilde{\mu}_a$  where  $\tilde{\Gamma}_{\theta}^*$  denotes the critical torque level at the first bifurcation point. Based the structure of equations (6.11a) and (6.11b), one can show that  $\bar{r}_1 \simeq 0$  as  $\tilde{\Gamma}_{\theta} \to (2\tilde{\mu}_a)^+$ , due to the effect of the internal mistuning. In the following, " $\bar{r}_1 \simeq 0$ " will be applied to find possible post-bifurcation solutions.

In the post-bifurcation stage, the system might converge to any steady-state solution with non-zero components of  $\bar{r}_i$ ,  $2 \le i \le 4$ . To classify these solutions, the following sets of indices are defined

$$\hat{\mathcal{Z}} \equiv \left\{ i \mid \lim_{\theta \to \infty} \bar{r}_i(\theta) = 0, \ 2 \le i \le 4 \right\}, \text{ and}$$

$$\hat{\mathcal{N}} \equiv \left\{ i \mid \lim_{\theta \to \infty} \bar{r}_i(\theta) \ne 0, \ 2 \le i \le 4 \right\}, \tag{6.12}$$

which contains those indices corresponding to zero and nonzero steady-state amplitudes, respectively. For those  $\bar{r}_i$  with i in  $\hat{\mathcal{Z}}$ , the solution for the steady-state phase  $\bar{\varphi}_i$  is arbitrary. For the remaining  $\bar{r}_i$ 's, that is, those with i in  $\hat{\mathcal{N}}$ , it can be assumed

that the corresponding phases are identical; i.e.,  $\bar{\varphi}_i = \bar{\varphi}_j$ ,  $\forall i, j \in \hat{\mathcal{N}}$  (one can utilize a procedure similar to that given in Appendix E to justify this assumption). Applying the above results and " $\bar{r}_1 \simeq 0$ " to equations (6.11c) and (6.11d) yields that the post-bifurcation solutions must satisfy

$$0 = \frac{-1}{2}\tilde{\mu}_a + \frac{1}{4}\tilde{\Gamma}_\theta \sin 2\bar{\varphi}, \qquad (6.13a)$$

$$0 = \frac{-\tilde{\sigma}_{12}}{n} + \frac{1}{4}\tilde{\Gamma}_{\theta}\cos 2\bar{\varphi} - \frac{1}{32n}\Psi(\bar{r}_{i}; \bar{r}_{2}, \bar{r}_{3}, \bar{r}_{4}, \tilde{\sigma}_{14}), i \in \hat{\mathcal{N}}, \qquad (6.13b)$$

where

$$\bar{\varphi} = \bar{\varphi}_{i}, \quad i \in \hat{\mathcal{N}}, \text{ and}$$

$$\Psi(\bar{r}_{i}; \bar{r}_{2}, \bar{r}_{3}, \bar{r}_{4}, \tilde{\sigma}_{14}) = 3n^{4}\bar{r}_{2}^{2} + 3n^{4}\bar{r}_{3}^{2} + 3n^{4}\bar{r}_{4}^{2} - 2n^{4}\bar{r}_{2}\bar{r}_{3} - 2n^{4}\bar{r}_{3}\bar{r}_{4} - 2n^{4}\bar{r}_{2}\bar{r}_{4}$$

$$+192\tilde{\sigma}_{14}(4\bar{r}_{i}^{2} - 3\bar{r}_{2}\bar{r}_{i} - 3\bar{r}_{3}\bar{r}_{i} - 3\bar{r}_{4}\bar{r}_{i})$$

$$+144\tilde{\sigma}_{14}(\bar{r}_{2}^{2} + \bar{r}_{3}^{2} + \bar{r}_{4}^{2} + 2\bar{r}_{2}\bar{r}_{3} + 2\bar{r}_{2}\bar{r}_{4} + 2\bar{r}_{3}\bar{r}_{4}). \quad (6.14b)$$

Equations (6.13) lead to

$$\Psi(\bar{r}_i; \bar{r}_2, \bar{r}_3, \bar{r}_4, \tilde{\sigma}_{14}) = \Psi(\bar{r}_j; \bar{r}_2, \bar{r}_3, \bar{r}_4, \tilde{\sigma}_{14}), \quad i, j \in \hat{\mathcal{N}}.$$
(6.15)

Note that equation (6.15) is automatically satisfied for a system with zero fourthorder imperfection (that is,  $\tilde{\sigma}_{14} = 0$ ) due to the invariance of the function  $\Psi(\bar{r}_i; \bar{r}_2, \bar{r}_3, \bar{r}_4, 0)$ under arbitrary exchanges of  $[\bar{r}_2, \bar{r}_3, \bar{r}_4]$ . In this case, there exist an infinite number of steady state solutions (at this level of approximation) which lie on an ellipsoid prescribed by

$$\mathcal{E}^{0} = \{ [\bar{r}_{2}, \bar{r}_{3}, \bar{r}_{4}] | \Phi(\bar{r}_{i}; \bar{r}_{2}, \bar{r}_{3}, \bar{r}_{4}, 0) = 0 \}, \qquad (6.16)$$

where

$$\Phi(\bar{r}_i; \bar{r}_2, \bar{r}_3, \bar{r}_4, \tilde{\sigma}_{14}) = -32\tilde{\sigma}_{12} + 8n(\tilde{\Gamma}_{\theta}^2 - 4\tilde{\mu}_{\theta}^2)^{\frac{1}{2}} - \Psi(\bar{r}_i; \bar{r}_2, \bar{r}_3, \bar{r}_4, \tilde{\sigma}_{14}). \tag{6.17}$$

However, in practice, the fourth-order imperfection  $\tilde{\sigma}_{14}$  is always a small, nonzero quantity. In the following, the possible steady-state solutions are sought by solving

equations (6.13) with assistance from a graphical interpretation in the phase space of the dynamical system.

For each i, equations (6.13) are satisfied for any solutions on the ellipsoid

$$\mathcal{E}^{i} = \{ [\bar{r}_{2}, \bar{r}_{3}, \bar{r}_{4}] | \Phi(\bar{r}_{i}; \bar{r}_{2}, \bar{r}_{3}, \bar{r}_{4}, \tilde{\sigma}_{14}) = 0 \}.$$
(6.18)

One should note that for any steady-state solution, it must satisfy equations (6.13) for all  $i \in \hat{\mathcal{N}}$  simultaneously. Hence, all possible steady-state solutions are the intersection points of the  $\mathcal{E}^i, i \in \hat{\mathcal{N}}$ ; i.e., the set

$$S = \bigcap_{i \in \hat{\mathcal{N}}} \mathcal{E}^i \tag{6.19}$$

contains all possible steady-state solutions. Figure 6.1 interprets the graphical relationship among the aforementioned ellipsoids, where the case with  $\hat{\mathcal{N}} = \{2,3\}$  is used for the sake of a clear presentation. It is seen from this figure that with a small, nonzero  $\tilde{\sigma}_{14}$ , each ellipsoid  $\mathcal{E}^i$  is slightly distorted away form  $\mathcal{E}^0$  but in a different preferable direction for different i. This results in only finite number of steady-state solutions, which lie at the intersection points of the  $\mathcal{E}^i$ ,  $i \in \hat{\mathcal{N}}$ , denoted by points  $I_j$ ,  $1 \leq j \leq 4$ , in the figure.

Based on equations (6.18) and (6.19), the aforementioned intersections, i.e., the steady-state solutions, can be found by solving

$$\Phi(\bar{r}_i; \bar{r}_2, \bar{r}_3, \bar{r}_4, \tilde{\sigma}_{14}) = \Phi(\bar{r}_j; \bar{r}_2, \bar{r}_3, \bar{r}_4, \tilde{\sigma}_{14}) = 0, \quad i, j \in \hat{\mathcal{N}}, \tag{6.20}$$

which automatically satisfies equation (6.15). It can be shown that the mode shapes for all solutions in the set S can be found by examining equation (6.15). They are listed in Table 6.1, where the corresponding isotropy subgroup is used for classification. It is seen from this table that there exist only three distinct types of solutions:  $S_2 \times S_2$ ,  $S_1 \times S_3$ ,  $S_1 \times S_1 \times S_2$ . The existence of two different mode shapes for the  $S_1 \times S_3$  and  $S_1 \times S_1 \times S_2$  solution branches is due to different choices of  $s_1$ . In fact,

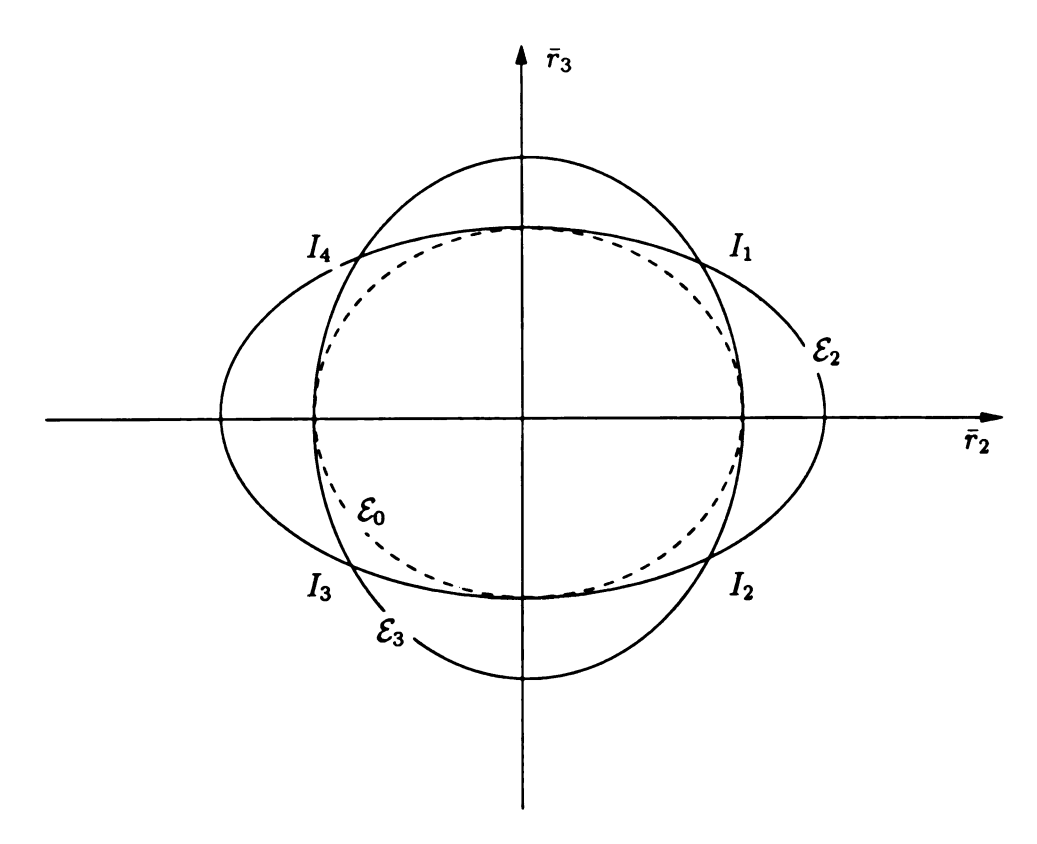


Figure 6.1: The graphical interpretation of the distorted ellipsoids.

Isotropy Subgroup	Mode Shapes of $[\bar{r}_2, \bar{r}_3, \bar{r}_4]$		
$S_2 \times S_2$	$[ar{r},ar{r},0]$		
$S_1 \times S_3$	$[ar{r},ar{r},ar{r}]  ext{ or } [ar{r},0,0]$		
$S_1 \times S_1 \times S_2$	$[ar{r},-ar{r},0]$ or $[ar{r},ar{r},2ar{r}]$		

Table 6.1: The solutions branches classified by their isotropy subgroups and their mode shapes.

they are dynamically equivalent. Figure 6.2 depicts the typical responses in the time domain for these solutions.

With the mode shapes in hand, the steady-state solutions can be obtained by solving equations (6.20). Furthermore, by numerically evaluating the Jacobian of the truncated, averaged equations (6.11) numerically at these solutions, one can

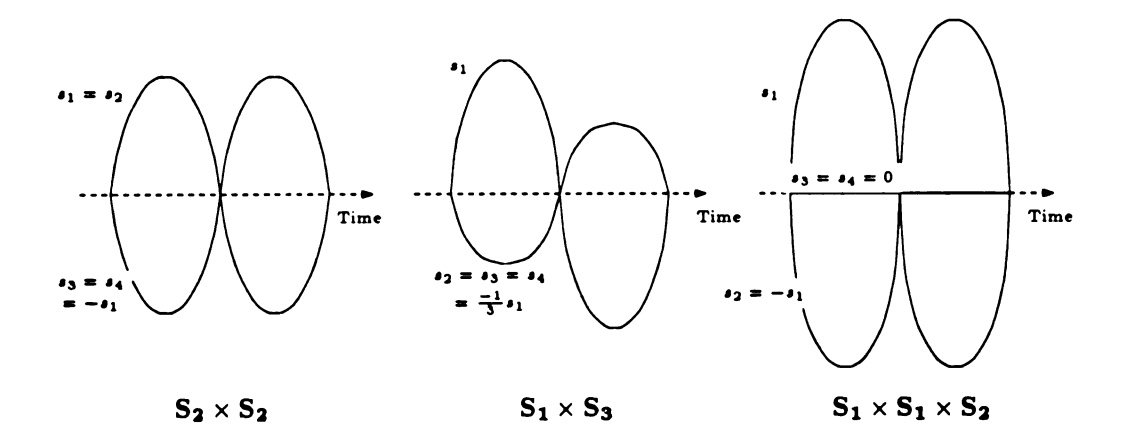


Figure 6.2: The mode shapes of the steady-state solutions with various isotropy groups

detect the corresponding stabilities for each steady-state solution.

#### 6.4.1.2 Absorber Performance and Design Guidelines

In this section, the absorber performance will be evaluated by computing two performance measures based on the solution branches and their stabilities. Furthermore, generic design guidelines for the absorber paths are given based on the predicted performance. However, due to the high multiplicity of the post-bifurcation solutions and the complexity of the corresponding stability boundaries, closed-form representations of the two performance measures are not pursued in detail. The design guidelines are distilled through a general discussion based on a representative case study. Based on a number of simulations, the design guidelines presented later are robust over a wide range of system parameters.

Figures 6.3 to 6.5 show the stability and feasibility boundaries for the representative case, for the solutions with the three different mode shapes, as functions of the two imperfection parameters,  $\hat{\sigma}_{12}$  and  $\hat{\sigma}_{14}$  ( $\hat{\sigma}_{12}$  and  $\hat{\sigma}_{14}$  denote the unscaled quantities of  $\tilde{\sigma}_{12}$  and  $\tilde{\sigma}_{14}$ ; i.e.,  $\hat{\sigma}_{ij} = \epsilon \tilde{\sigma}_{ij}$ ). The common system parameters used for this study are  $\hat{\Gamma}_{\theta} = 0.035$ ,  $\hat{\mu}_{a} = 0.005$ , n = 2 and  $\nu = 0.1662$  (The latter two parameters are taken from the 2.5 liter, in-line, four-stroke, four cylinder engine considered by Denman [16]). In this figure, "S" and "U" denote stable and unstable regions respectively. Also, the dashed line divides the feasible and infeasible regions, where the corresponding absorber motions hit or not hit the cusps. It is seen that among the three types of solutions, a large set of the  $S_2 \times S_2$  solutions survive as stable and feasible; a small set of the  $S_1 \times S_3$  solutions lead to stable and feasible motions; only a tiny set of the  $S_1 \times S_1 \times S_2$  solutions are stable and feasible. Based on simulations, all the stable and feasible steady-state solutions in areas "abc" and "def" in Figure 6.4 and 6.5, respectively, are unrealistic since the absorber motions will most likely hit the cusps during the transient responses. Thus, they will not be considered for absorber performance evaluation. As results, only stable, feasible  $S_2 \times S_2$  and  $S_1 \times S_3$  solutions in Figure 6.3 and 6.4 are the candidates for performance evaluation in the following.

Figure 6.6 show the contours of the rotor accelerations with a fixed  $\tilde{\Gamma}_{\theta} = 0.035$ , for all stable and feasible solutions, except for those in areas "abc" and "def" in Figure 6.4 and 6.5. Figure 6.7 and 6.8 show the feasible ranges of the disturbing torque for the  $S_2 \times S_2$  and  $S_1 \times S_3$  solution branches respectively. Note that the expression of the rotor acceleration in equation (6.5) and the limitation of absorber motions in inequality (6.4) are used to here generate these figures. It is seen from Figure 6.6 to 6.8 that small, positive  $\hat{\sigma}_{12}$ 's and  $\hat{\sigma}_{14}$ 's, leading to the  $S_2 \times S_2$  branches, have good balance between achieving small rotor accelerations and rendering larger feasible ranges of the disturbing torque, while small, positive  $\hat{\sigma}_{12}$ 's and small, negative  $\hat{\sigma}_{14}$ 's, leading to the stable, feasible  $S_1 \times S_3$  branches, render larger rotor accelerations, smaller torque ranges and vulnerability for absorbers to hit the cusps during the transient response.

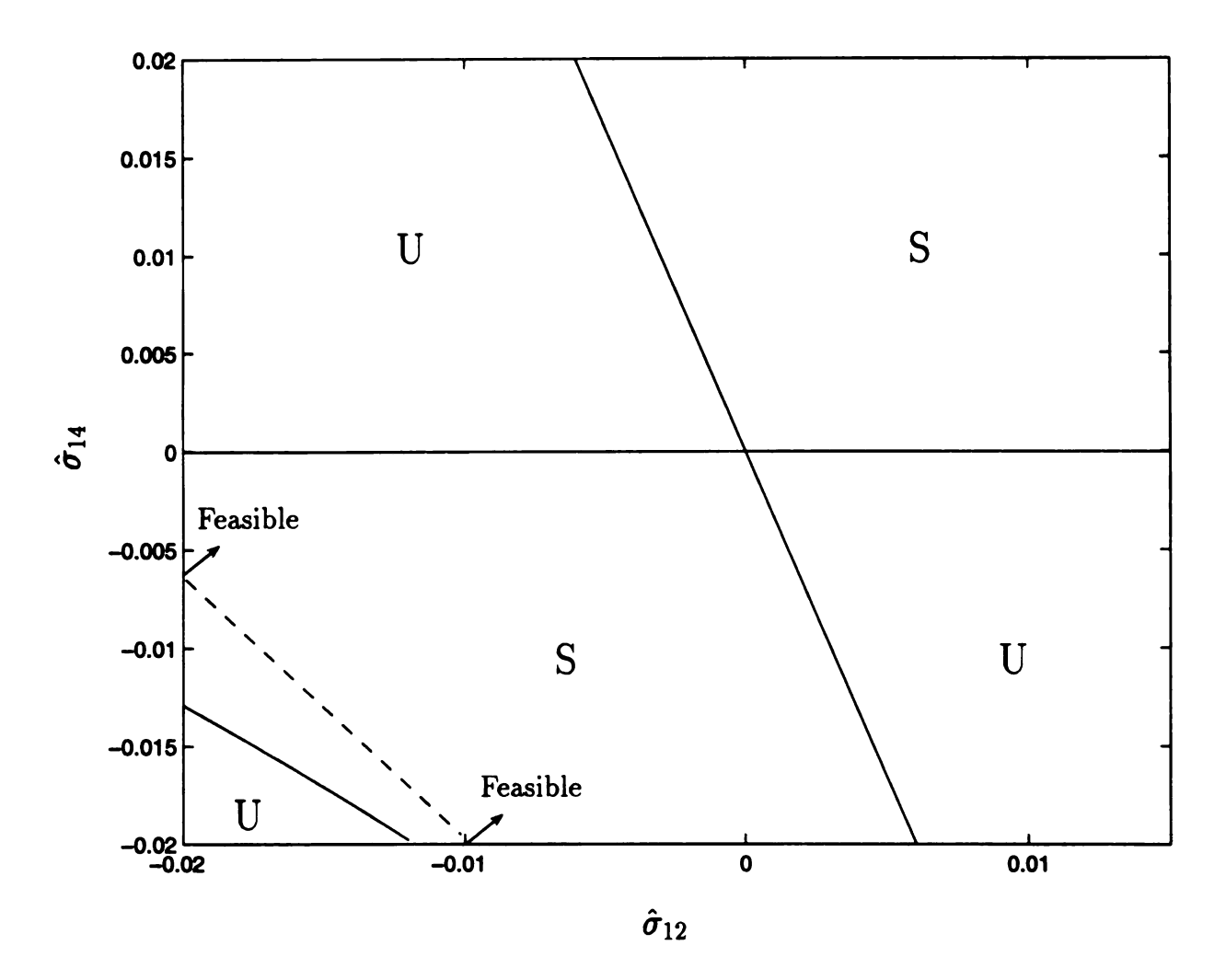


Figure 6.3: The stability and feasibility boundaries of the solutions with isotropy subgroup  $S_2 \times S_2$  for  $\hat{\Gamma}_{\theta} = 0.035$ ,  $\hat{\mu}_a = 0.005$ , n = 2 and  $\nu = 0.1662$ .

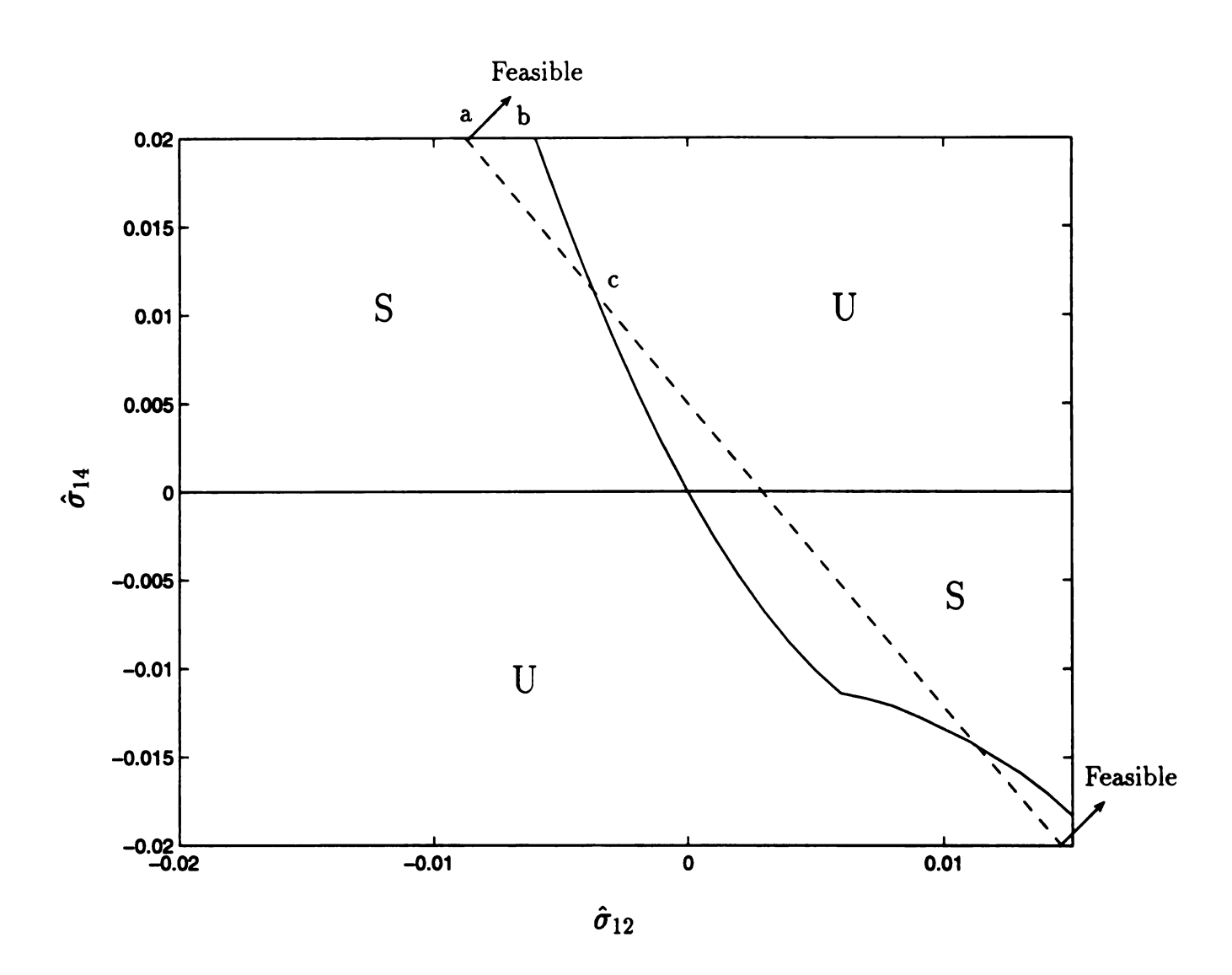


Figure 6.4: The stability and feasibility boundaries of the solutions with isotropy subgroup  $S_1 \times S_3$  for  $\hat{\Gamma}_{\theta} = 0.035$ ,  $\hat{\mu}_a = 0.005$ , n = 2 and  $\nu = 0.1662$ .

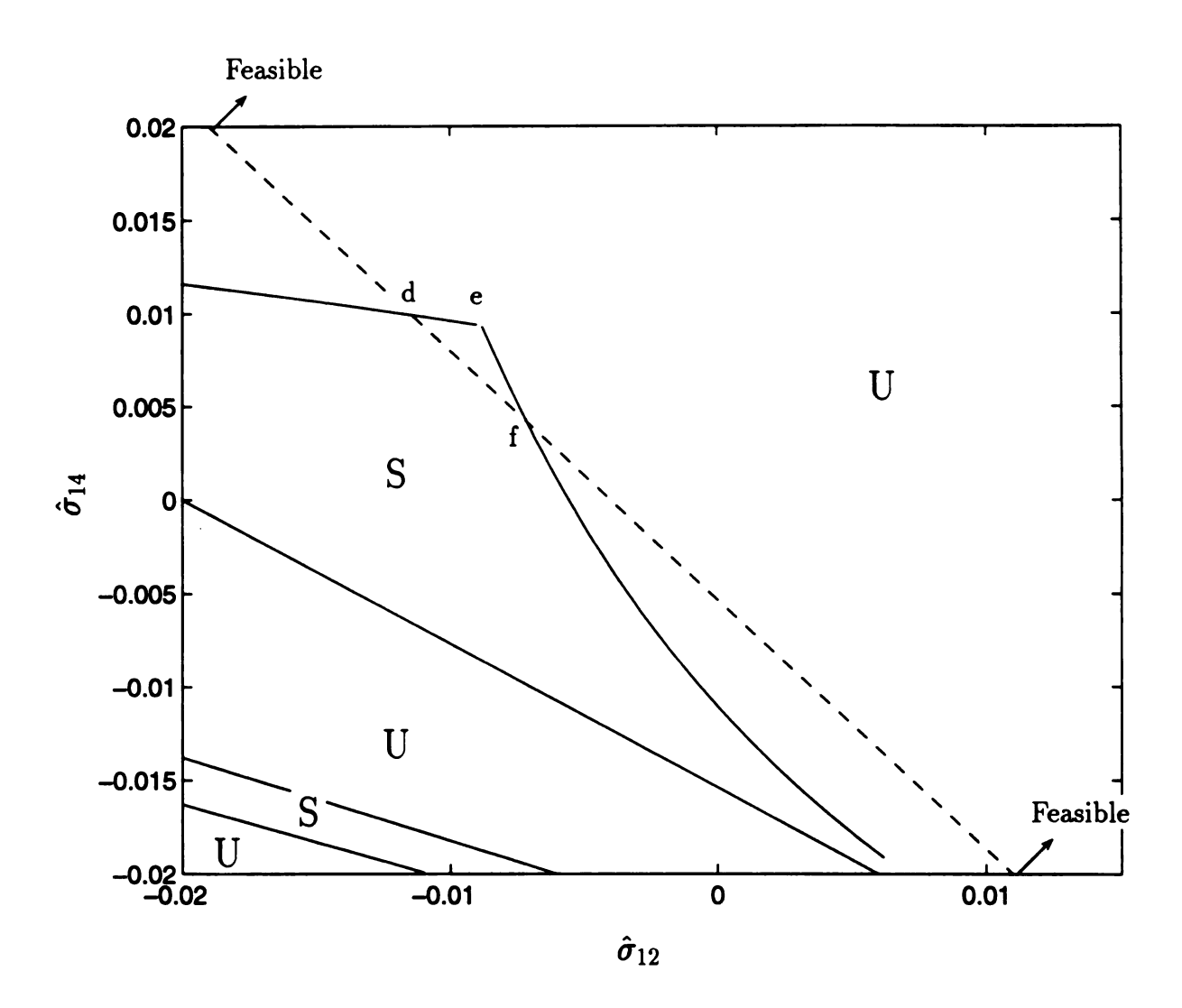


Figure 6.5: The stability and feasibility boundaries of the solutions with isotropy subgroup  $\mathbf{S_1} \times \mathbf{S_1} \times \mathbf{S_2}$  for  $\hat{\Gamma}_{\theta} = 0.035$ ,  $\hat{\mu}_a = 0.005$ , n = 2 and  $\nu = 0.1662$ .

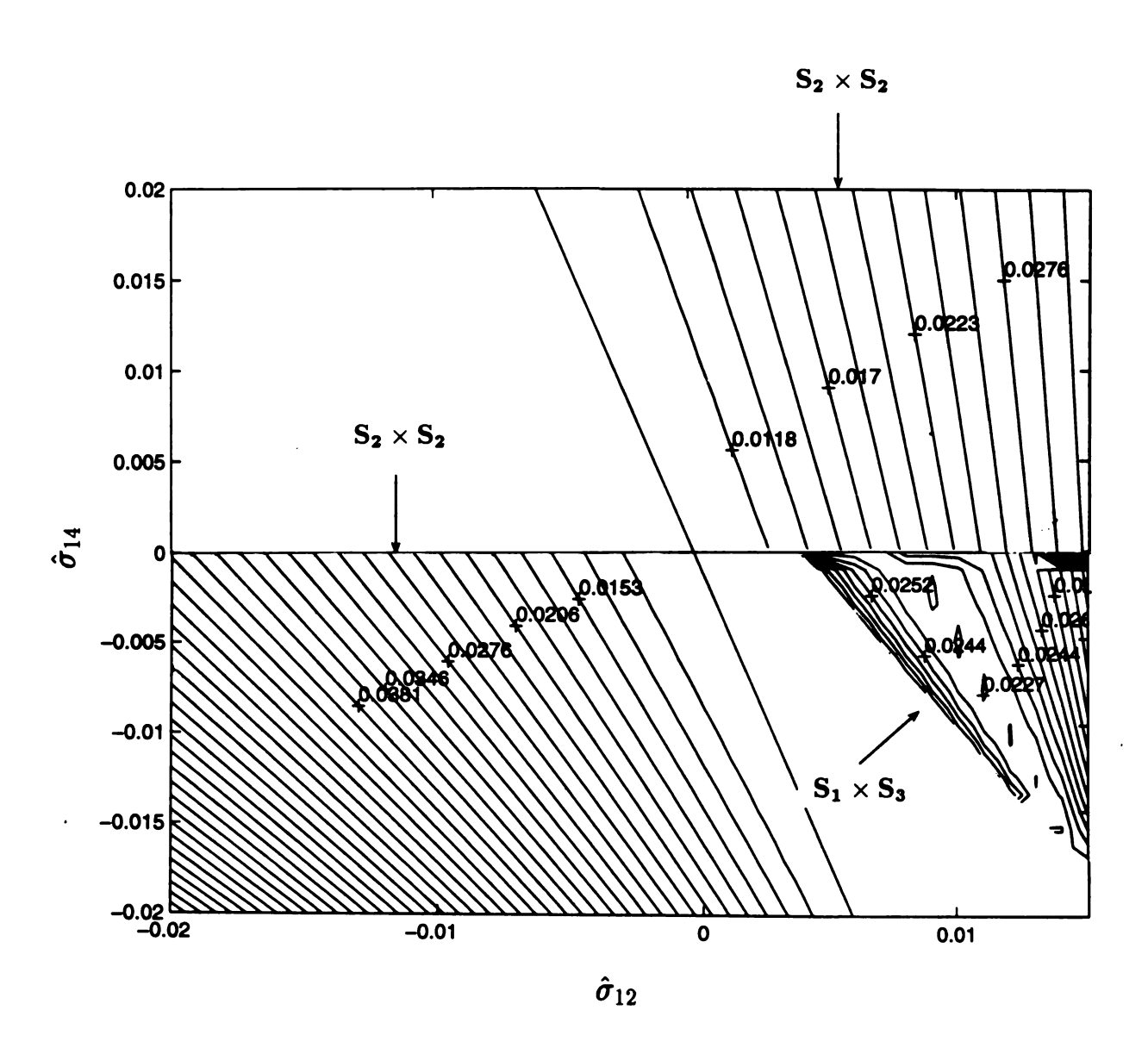


Figure 6.6: The contours of the rotor acclerations for  $\hat{\Gamma}_{\theta}=0.035,$   $\hat{\mu}_{a}=0.005,$  n=2 and  $\nu=0.1662.$ 

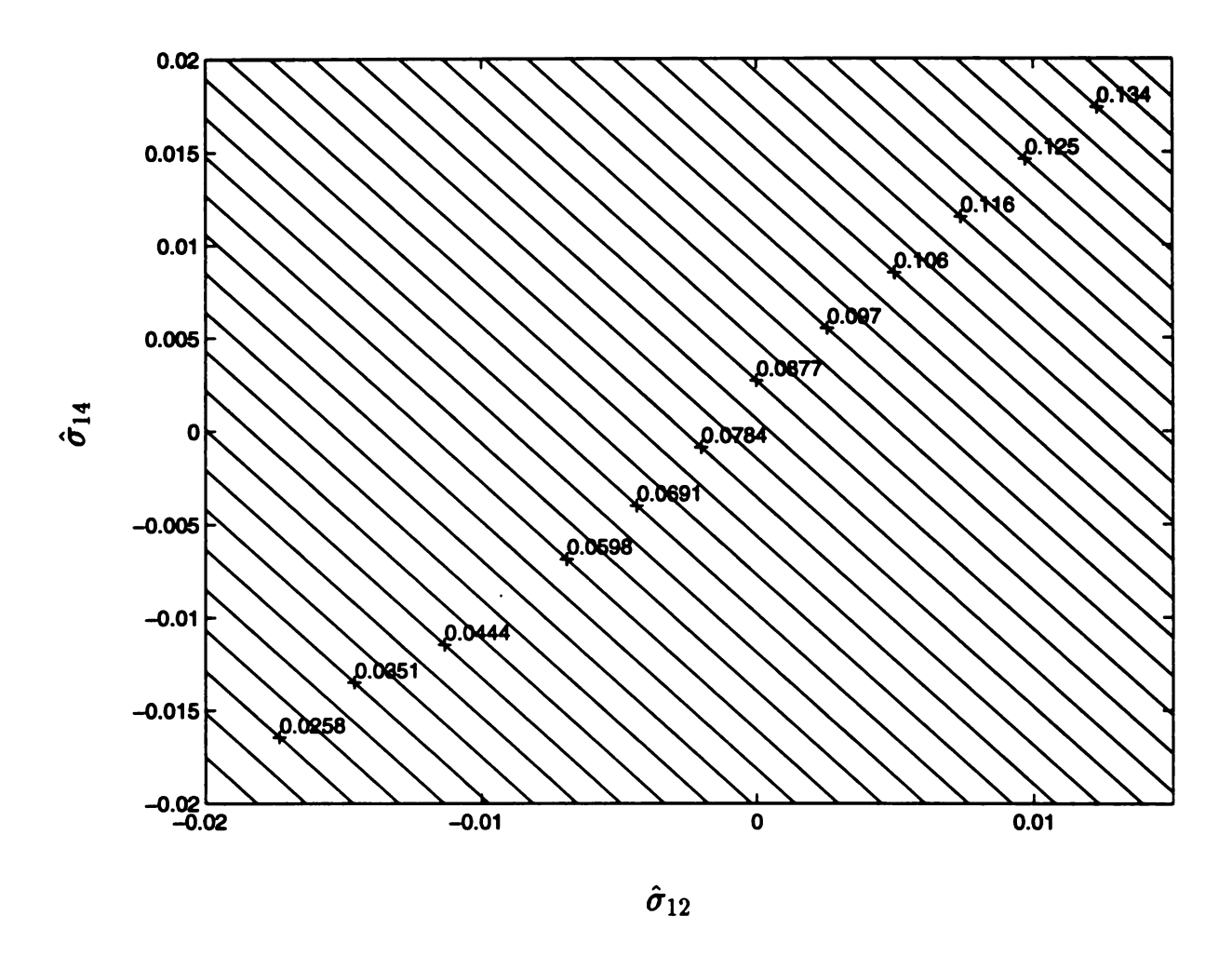


Figure 6.7: The feasible disturbing torque range of the  $S_2 \times S_2$  solution branch for  $\hat{\mu}_a = 0.005$ , n = 2 and  $\nu = 0.1662$ .

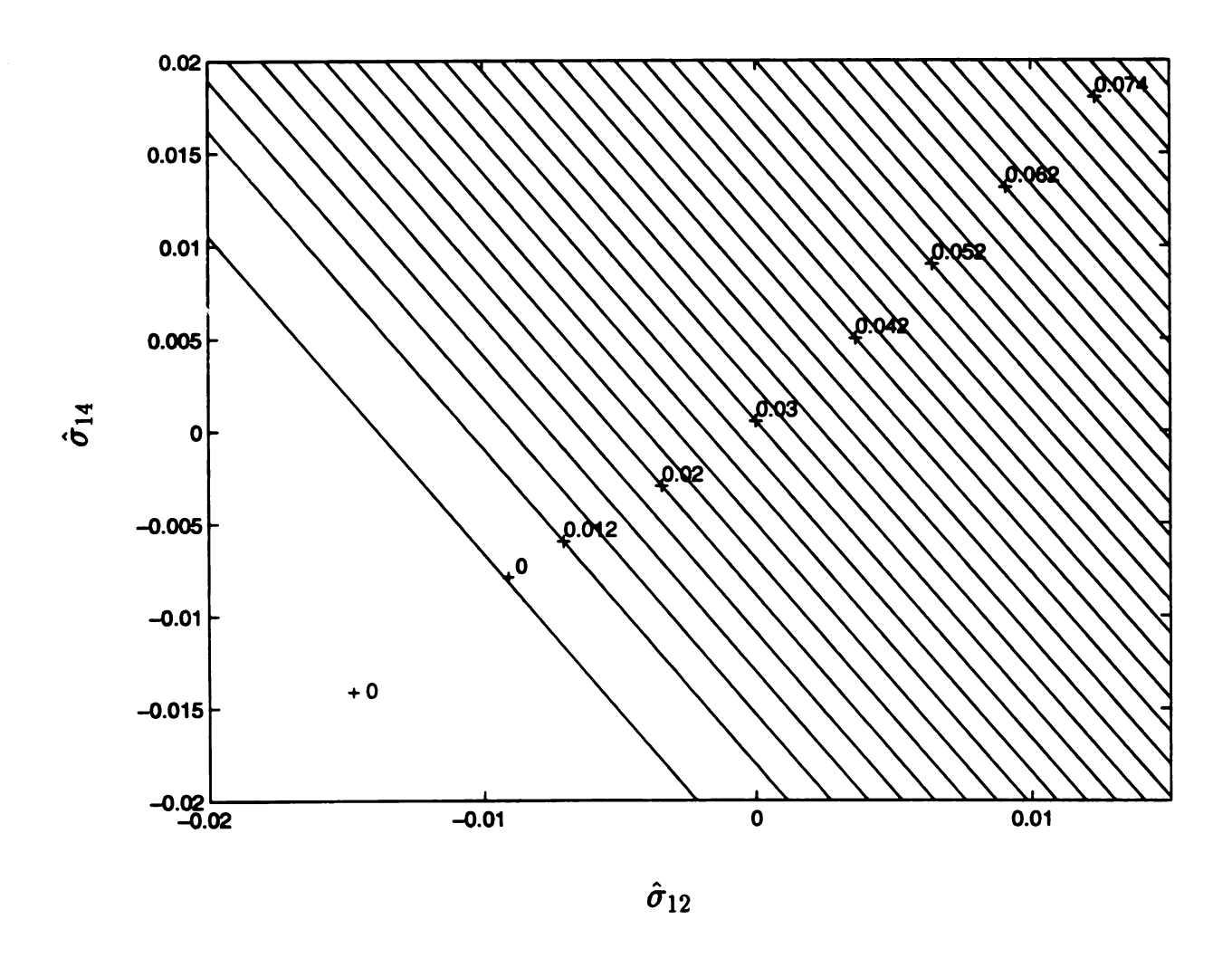


Figure 6.8: The feasible disturbing torque range of the  $S_1 \times S_3$  solution branch for  $\hat{\mu}_a = 0.005, n = 2$  and  $\nu = 0.1662$ .

#### 6.4.2 Arbitrary Pairs of Absorbers

The similar analysis can be conducted for a system with an arbitrary number of pairs of absorbers. The following conclusions are drawn from considerations of results obtained from analysis and simulations of systems with one, two and three pairs of absorbers (the later results are not presented here).

- As the number of absorbers increases, the number of existing solution branches increases; e.g., there exist five distinct mode shapes of solution branches for N=6. This fact complicates the analysis. However, only the solutions with isotropy subgroups  $S_{N/2} \times S_{N/2}$  and  $S_1 \times S_{N-1}$  survive as stable and feasible solutions without vulnerability of violating the cusp condition.
- The dependence of the absorber performance, in terms of the two measures, on the imperfection parameters ô<sub>12</sub> and ô<sub>14</sub> is generically similar to that for N = 4. Positive, small ô<sub>12</sub> and ô<sub>14</sub>, leading to a stable S<sub>N/2</sub>×S<sub>N/2</sub> response, are suggested to render smaller rotor accelerations and keep the absorber motions within the cusp levels.

#### 6.5 Remarks and Design Guidelines

The results given above are based on scaling assumption (6.10), which says that the differences in the paths are even smaller than the general levels of imperfections and mistunings. Based on simulations, similar to the results obtained for the case N=2 in the last chapter, the existence of small nonzero  $\hat{\sigma}_{ij}$ ,  $2 \leq i \leq N$ , slightly decreases the applicable torque range and increases the rotor acceleration. Furthermore, odd  $(\hat{\sigma}_{ij}, j = 1, 3, ....)$  and higher  $(\hat{\sigma}_{ij}, j \geq 4)$  order imperfections have no distinguishable effects on the absorber performance.

In summary, the above results indicate that the following general guidelines be followed when designing the paths for a multi-pair subharmonic absorber system:

- The absorber paths should be kept as identical as possible.
- The imperfection parameters  $\hat{\sigma}_{12}$  and  $\hat{\sigma}_{14}$  should be selected to be small and positive.
- One can refer to the predicted dynamics and performance evaluations (for example, represented by Figure 6.3 to Figure 6.8, for N=4) in order to choose values of  $\hat{\sigma}_{12}$  and  $\hat{\sigma}_{14}$  for a particular specification in terms of vibration level or torque range.

#### CHAPTER 7

#### CONCLUSIONS AND FUTURE WORK

This study focused primarily on investigating the nonlinear dynamics of a rotating system with multiple centrifugal pendulum vibration absorbers (CPVA's). It is motivated by the fact that in practical implementations the total absorber inertianeeds to be divided into several absorber masses that are stationed about and/or along the axis of rotation, due to spatial and balancing considerations. If all the absorbers move in exact unison, the absorber designs suggested by researchers in the past sustain.

However, in chapter 3, through a proposed methodology including proper transformations and the method of averaging, it was shown that for certain absorber designs the unison motion of N identical absorbers may become unstable at a moderate level of the disturbing torque. The corresponding stability criterion was derived. it was found that the critical disturbing torque level is proportional to the square root of the absorber damping when viscous damping is assumed.

In chapter 4, the post-bifurcation performance of the absorbers was evaluated by solving for the resultant system response via symmetric bifurcation theory. With the ability to compute two performance measures, the rotor acceleration and the applicable range of the disturbing torque, the absorber absorber performance was re-assessed. It was found that the distribution of the absorber inertia results in a drastic decrease of the disturbing torque range and a slight decrease of the rotor acceleration.

Utilizing the same methodology, in chapter 5, the next effort was given to an investigation of the effects of path imperfections and mistuning on the dynamics

of a system with a pair of subharmonic absorbers. Based on the analytical results obtained, it was found that the effects of path mistuning and symmetric imperfections dominate non-symmetric imperfections, due to resonance effects. It was also found that differences between the two paths of the absorbers have a generally deleterious effect on system performance. Furthermore, by neglecting higher-order dynamics, the average mistunings and imperfections at 2nd and 4th order can be used to design systems that trade off between the operating range of the system and the level torsional vibrations.

In chapter 6, the study in the previous chapter was extended to the case with multiple pairs of subharmonic absorbers. As found in the case with a single pair of absorbers, the average mistunings and imperfections dominate the absorber performance due to resonances. It was also found that the response in which the absorbers move in two unison groups, half in each and exactly out-of-phase, is the ideal response of the system in terms of absorber performance. Specific design guidelines for absorber paths were distilled based on some case studies and simulations.

The analytical work presented in this dissertation is part of a larger framework for absorber dynamics analysis. Listed below are the additional specific problems to be investigated in the future, which include analytical and experimental studies.

#### • Circular Paths

The intentionally-mistuned circular paths are easily manufactured and widely used in industry. A recently completed perturbation analysis and simulations [55] have shown that for the single-absorber and damped system, a rotor fitted with absorbers riding on "mistuned" circular paths can exhibit excellent performance in terms of vibration reduction in the large torque range, even though perfectly tuned tautochronic absorbers are more effective in the low and moderate torque operating range. A systematic analysis on the damped and multi-absorber system is needed for further generalization of the aforemen-

tioned results.

#### • Multi-Harmonic Torque Inputs

In most applications, the applied torque on the rotor is not a pure harmonic. For IC engines, the torque acting on the crankshaft is generated by the gas pressure in the cylinders and through the inertial affects of pistons and other moving components as they transmit torque through crank throws and connecting rods. This torque is periodic in the rotating angle of the crankshaft, and enters the system equations as a complicated combination of external and parametric excitation which is dependent on the velocity and the acceleration of the crankshaft. However, it can be approximated well by its first several harmonics. To reflect this fact an analysis for systems under general types of multi-harmonic excitation is needed.

#### • Nonstationary Conditions

There are no reports in the literature dealing with the potential problems associated with transitions in rotational speed; all analyses have been carried out for the case in which the average rotor speed remains fixed. The results are applicable to the aircraft and helicopter applications, but for other applications, e.g., automotive engines, speeds vary in many different ways. It is of interest to consider the effects of such nonstationary operating conditions. Relevant analytical work should be possible since the time scale for the speed changes is slow compared to that of rotation. Herein, asymptotic methods for nonstationary problems may be applied [37].

#### Flexible Shafts

In all aforementioned analyses, the rotor is assumed to be perfectly rigid. However, a system with large but finite rotational flexibility may exhibit different dynamics, especially when the absorbers and the applied torques are distributed along the axis of the rotor. This design strategy is actually used in powertrains to maintain balance and distribute stress along the crankshaft. To investigate the related dynamics, the natural oscillating frequencies of the rotor would be first assumed much larger than that of each absorber subsystem; i.e., the crankshaft is much more "stiff" than each absorber. The equations of motion can then be re-arranged into a singular perturbation form in which the global dynamics is decomposed into fast and slow components, captured by invariant manifolds in the phase space subsystem [19, 8]. Our task is to determine the parameter ranges for which the long-time behavior of the system can be simply described by the slow manifold, in which case the crankshaft torsional dynamics are negligible when compared to the "soft" dynamics of each absorber system. However, it is expected that the effects of finite flexibility will have a similar role to that of imperfections, thereby leading to the realistic possibility of localization of absorber response.

#### • Experiments

In all aforementioned theoretical developments of CPVA systems, the system dynamics is idealized in several aspects in order to obtain analytical estimates of system behavior. For example, the damping is taken to be small and of viscous type and the dynamic effects of rollers are ignored in modeling, to name just two of several. An experimental device needs to be built in the laboratory to verify the validity of the designs offered by the analytical models, and also to provide a measuring stick for the discrepancies between desired/predicted absorber performance and reality. Borowski et al. [3] conducted an experimental study in which it was demonstrated that attaching a CPVA system to an automotive engine crankshaft can actually decrease noise and vibration levels inside a car, but their conclusions were based on qualitative measures from the passengers' feelings. To evaluate the absorber performance on more solid ground, we need

to acquire quantitative measures of vibration levels by building an experimental model in the laboratory and carrying out systematic, controlled experiments. The challenging parts of the experimental buildup would be: (1) precision control of the manufacture of the absorber paths; (2) dynamical measurement of absorber motions; and (3) measurement and quantification of dissipation mechanisms.

### **APPENDICES**

#### APPENDIX A

THE EXPRESSIONS FOR  $\frac{\partial H_1}{\partial \varphi_i}\Big|_{S.S.}$ ,  $\frac{\partial H_2}{\partial r_i}\Big|_{S.S.}$ ,  $\frac{\partial H_1}{\partial \varphi_j}\Big|_{S.S.}$  and  $\frac{\partial H_2}{\partial r_j}\Big|_{S.S.}$ 

The terms  $\frac{\partial H_1}{\partial \varphi_i}\Big|_{s,s}$ ,  $\frac{\partial H_2}{\partial r_i}\Big|_{s,s}$ ,  $\frac{\partial H_1}{\partial \varphi_j}\Big|_{s,s}$  and  $\frac{\partial H_2}{\partial r_j}\Big|_{s,s}$  in (3.16) are given by

$$\frac{\partial H_1}{\partial \varphi_i}\Big|_{s.s.} = \frac{1}{8} + \frac{1}{(n^2 + n^4)^2 r^4} \left[ (1 - (n^2 + n^4)r^2)^{\frac{3}{2}} - \frac{1}{8} (3(n^2 + n^4)^2 r^4 - 12(n^2 + n^4)r^2 + 8) \right] 
\frac{\partial H_1}{\partial \varphi_j}\Big|_{s.s.} = -\frac{\partial H_1}{\partial \varphi_i}\Big|_{s.s.} 
\frac{\partial H_2}{\partial r_i}\Big|_{s.s.} = \frac{1}{8(n^2 + n^4)^2 r^5} \left[ (n^2 + n^4)^2 r^4 + 4(n^2 + n^4)r^2 - 8 + 8\sqrt{1 - (n^2 + n^4)r^2} \right] 
\frac{\partial H_2}{\partial r_j}\Big|_{s.s.} = -\frac{\partial H_2}{\partial r_i}\Big|_{s.s.}$$

The above results were obtained using contour integrals and the residue theorem.

#### APPENDIX B

#### ON THE EIGENVALUES OF C

In section 3.3, we claim that if  $C_{2N\times 2N}$  is a block matrix of the form

$$C_{2N\times 2N} = \begin{bmatrix} A_{2\times 2} & B_{2\times 2} & . & B_{2\times 2} \\ B_{2\times 2} & A_{2\times 2} & . & B_{2\times 2} \\ . & . & . & B_{2\times 2} \\ B_{2\times 2} & B_{2\times 2} & B_{2\times 2} & A_{2\times 2} \end{bmatrix},$$

then an eigenvalue of [A-B] is an (N-1) times repeated eigenvalue of C. Furthermore, an eigenvalue of [A+(N-1)B] is an eigenvalue of C. Since the proofs for different N's are similar, we provide only the proof for N=4 here.

Let  $\lambda_1$  be an eigenvalue of [A-B] and the associated eigenvector be u, and thus,

$$[A - B]u = \lambda_1 u. \tag{B.1}$$

We further define

$$v_1 \equiv \left[egin{array}{c} u \ -u \ 0 \ 0 \ 0 \end{array}
ight] v_2 \equiv \left[egin{array}{c} u \ 0 \ -u \ 0 \end{array}
ight] v_3 \equiv \left[egin{array}{c} u \ 0 \ 0 \ -u \end{array}
ight].$$

Based on (B.1), one can verify that

$$Cv_1 = \lambda_1 v_1$$
,  $Cv_2 = \lambda_1 v_2$ , and  $Cv_3 = \lambda_1 v_3$ .

Since  $v_1$ ,  $v_2$  and  $v_3$  are independent, an eigenvalue of [A-B],  $\lambda_1$ , is a 3 times repeated eigenvalue for C.

Let  $\lambda_2$  be an eigenvalue of [A + (N-1)B] and the associated eigenvector be w, and thus,

$$[A+3B]w = \lambda_2 w. (B.2)$$

We further define

$$v_{4} \equiv \left[egin{array}{c} w \ w \ w \ w \end{array}
ight].$$

Similarly, one can verify that

$$Cv_4 = \lambda_2 v_4$$

based on (B.2). Thus, an eigenvalue of [A + 3B] is an eigenvalue of C. Note that  $v_1, v_2, v_3$  and  $v_4$  are independent regardless of the choices of the eigenvectors u and w. Furthermore, we know that [A - B] and [A + 3B] have two sets of independent eigenvectors  $(u_1, u_2)$  and  $(w_1, w_2)$ , respectively, and each pair of eigenvectors spans  $R^2$ . Hence, the following eight eigenvectors spans  $R^3$ :

$$\left[egin{array}{c} u_1 \ -u_1 \ 0 \ 0 \ \end{array}
ight] \left[egin{array}{c} u_2 \ -u_2 \ 0 \ \end{array}
ight] \left[egin{array}{c} u_1 \ 0 \ -u_1 \ \end{array}
ight] \left[egin{array}{c} u_2 \ 0 \ \end{array}
ight] \left[egin{array}{c} u_1 \ 0 \ \end{array}
ight] \left[egin{array}{c} u_2 \ 0 \ \end{array}
ight] \left[egin{array}{c} w_1 \ w_1 \ \end{array}
ight] \left[egin{array}{c} w_2 \ w_2 \ \end{array}
ight].$$

We can conclude that two eigenvalues of C are the eigenvalues of [A+3B] and the other six eigenvalues of C are the thrice-repeated eigenvalues of [A-B]. The proof is similar for an arbitrary N.

#### **APPENDIX C**

## ON THE EIGENVALUES OF [A + (N-1)B]

In section 3.3, we claim that all the real parts of the eigenvalues of [A+(N-1)B] are negative. To show this is equivalent to prove that its trace is negative and its determinant is positive. From (3.16), they can be determined in series form as follows

$$Trace[A + (N-1)B] = -\tilde{\mu}_a,$$

$$Det[A + (N-1)B] = \frac{n^2 + \tilde{\mu}_a^2}{4} + \left(\frac{n^4}{4} - \frac{n^6}{4}\right)r^2 + \left[15n^2 + 10n^4 + 7n^6 - \tilde{\mu}_a^2(1+n^2)^2\right]\frac{n^4r^4}{64} + \left[(1+n^2)(40n^2 + 10n^4 - 6n^6 - 3\tilde{\mu}_a^2(1+n^2)^2)\right]\frac{n^6r^6}{256} + \mathcal{O}(r^7).$$

$$(C.1)$$

Obviously the trace is negative. (Since  $B_{11} = B_{22} = 0$ , this trace is the same as the trace of [A - B]. See Appendix D for the proof of (C.1).) The general proof that Det[A + (N-1)B] is positive appears to be quite difficult, so we satisfy ourselves here by proving that the sum of the first two terms in the series is positive. Since the function  $g_i(s_i)$  in (3.3) is required to be real, r must satisfy  $r \leq \frac{1}{n\sqrt{n^2+1}}$ . Under this condition, we can derive that the sum of the first two terms in Det[A + (N-1)B] is positive if

$$\frac{1}{n^2 + n^4} < \frac{n^2 + \tilde{\mu}_a^2}{n^6 - n^4}$$

$$140$$

This inequality can be proved by the fact

$$\frac{n^6 - n^4}{n^2 + n^4} - n^2 = \frac{-2n^4}{n^2 + n^4} < 0 < \tilde{\mu}_a^2, \quad \text{for } n = 1, 2, 3, \dots$$

Thus, for sufficiently small r, it follows that Det[A + (N-1)B] is positive.

#### APPENDIX D

### PROOF OF EQUATION (3.17)

In section 3.3, we claim that

$$Trace[A-B] = -\tilde{\mu}_a.$$

To prove this, we first show that

$$F_{2}(r) - F_{1}(r) = \frac{1}{2\pi} \int_{0}^{2\pi} \cos 2x [1 - (n^{2} + n^{4})r^{2} \cos^{2} x]^{\frac{1}{2}} dx$$

$$= \frac{1}{4\pi} \int_{0}^{2\pi} [1 - (n^{2} + n^{4})r^{2} \cos^{2} x]^{\frac{1}{2}} d(\sin 2x)$$

$$= \frac{-(n^{2} + n^{4})}{2\pi} \int_{0}^{2\pi} [r \cos(x) \sin(x)]^{2} [1 - (n^{2} + n^{4})r^{2} \cos^{2} x]^{\frac{-1}{2}} dx$$

$$= r \frac{\partial F_{1}}{\partial r}.$$

Note that the third step is completed using integration by parts. Incorporating the above result into the expressions for  $A_{11}$  and  $A_{22}$  in Jacobian (3.16), we can show that

$$Trace[A - B] = A_{11} + A_{22} = -\tilde{\mu}_a.$$

#### APPENDIX E

# **JUSTIFICATION OF** $\tilde{\bar{\psi}}_i \simeq \tilde{\bar{\psi}}_j, \ \forall \ 2 \leq i, j \leq N$

In order to justify the assumption  $\tilde{\psi}_i \simeq \tilde{\psi}_j$ ,  $\forall \, 2 \leq i, j \leq N$ , in the post-bifurcation stage (cf. equations (4.8)), the transformation with  $\eta_1$  capturing the dynamics in  $\mathbf{V}$  and the remaining  $\eta_i$  ( $2 \leq i \leq N$ ) capturing the dynamics in  $\mathbf{W}$ , where all  $\eta_i$ 's are orthogonal to each other, is employed in place of transformation (4.1). Then, by also introducing the angular transformation

$$\eta_{i} = \varrho_{i}\cos(\tau_{i} - n\theta) \quad \text{and} \quad \eta_{i}^{'} = n\varrho_{i}\sin(\tau_{i} - n\theta), \quad 2 \leq i \leq N,$$
(E.1)

and proceeding along the usual lines for the application of averaging, one arrives at the following steady-state conditions, in place of equations (4.8),

$$0 = \frac{-\tilde{\mu}_a \tilde{\tilde{\varrho}}_i}{2} + \frac{\tilde{\Gamma}_\theta^2 \tilde{\tilde{\varrho}}_i}{4n} \sin(2\tilde{\tilde{\tau}}_i), \qquad (E.2a)$$

$$0 = \frac{\tilde{\Gamma}_{\theta}^2 \tilde{\bar{\varrho}}_i}{4n} \cos(2\tilde{\bar{\tau}}_i) - \frac{(N-1)n^3}{4} \tilde{\bar{\varrho}}_i \left(\sum_{j=2}^N \tilde{\bar{\varrho}}_j^2\right). \tag{E.2b}$$

where  $\tilde{\bar{\varrho}}$  and  $\tilde{\bar{\tau}}$  are the approximate (averaged and truncated) versions of  $\varrho$  and  $\tau$ . The above equations give

$$\tilde{\tilde{\tau}}_i = \tilde{\tilde{\tau}}_j, \pmod{\pi} \ \forall i, j \in \mathcal{N}.$$
 (E.3)

By the definitions of the  $\xi_i$ 's and the  $\eta_i$ 's, each  $\xi_i$  with  $i \in \mathcal{N}$  is a linear combination of the  $\eta_i$ 's with  $i \in \mathcal{N}$ . Hence,  $\tilde{\bar{\psi}}_i = \tilde{\bar{\psi}}_j$ ,  $(\text{mod } \pi) \ \forall \ i, j \in \mathcal{N}$ . Now, choose an arbitrary  $i_0 \in \mathcal{N}$ . For all  $j_0 \in \mathcal{N}$  with  $\tilde{\bar{\psi}}_{i_0} = \tilde{\bar{\psi}}_{j_0} + \pi \pmod{2\pi}$ , replace  $(\tilde{\bar{\rho}}_{j_0}, \tilde{\bar{\psi}}_{j_0})$ 

by  $(-\tilde{\bar{\rho}}_{i_0},\tilde{\bar{\psi}}_{i_0})$  to equivalently represent the signal  $s_{j_0}$ , and then proceed with the analysis in section 4. One finds that the results are the same as those obtained if  $\tilde{\bar{\psi}}_i = \tilde{\bar{\psi}}_j \ \forall \ i,j \in \mathcal{N}$  is assumed.

#### APPENDIX F

**PROOF OF** 
$$Trace[A + (N-2)B] < 0$$
 **AND**  $Det[A + (N-2)B] > 0$  **AS**  $\hat{\bar{\rho}} \rightarrow 0^+$ 

In section 4.4.3, it is claimed that on the  $S_1 \times S_{N-1}$  branch with  $\hat{\psi} \simeq \frac{-3\pi}{4}$ , Trace[A+(N-2)B]<0 and Det[A+(N-2)B]>0 as  $\hat{\bar{\rho}}\to 0^+$  near the bifurcation point. Through a nontrivial computation it can be shown that

$$Trace[A + (N - 2)B] = -\tilde{\mu}_a < 0,$$

$$Det[A + (N - 2)B] = \frac{1}{256} \left\{ 4n^6(N - 1)^2 N^2 \hat{\bar{\rho}}^4 + 7\tilde{\mu}_a^2(N - 2)^2 (n^2 + n^4)^2 \hat{\bar{\rho}}^2 \hat{\bar{\rho}}_1^2 + 16(N - 2)\tilde{\mu}_a^2(n^2 + n^4)\hat{\bar{\rho}}\hat{\bar{\rho}}_1 \cos(\hat{\bar{\psi}} - \hat{\bar{\psi}}_1) - 8(N - 2)^2 \tilde{\mu}_a^2(n^2 + n^4)^2 \hat{\bar{\rho}}^2 \hat{\bar{\rho}}_1^2 \cos(2\hat{\bar{\psi}} - 2\hat{\bar{\psi}}_1) - 16(N - 2)(N - 1)N\tilde{\mu}_a n^3(n^2 + n^4)\hat{\bar{\rho}}^3 \hat{\bar{\rho}}_1 \sin(\hat{\bar{\psi}} - \hat{\bar{\psi}}_1) \right\}.$$
(F.1)

On the  $S_1 \times S_{N-1}$  solution branch with  $\hat{\bar{\psi}} \simeq \frac{-3\pi}{4}$ ,

$$\cos(\hat{\bar{\psi}} - \hat{\bar{\psi}}_1) \simeq \frac{1}{\sqrt{2}}, \quad \cos(2\hat{\bar{\psi}} - 2\hat{\bar{\psi}}_1) \simeq 0, \quad \text{and} \quad \sin(\hat{\bar{\psi}} - \hat{\bar{\psi}}_1) \simeq \frac{-1}{\sqrt{2}}. \quad (F.2)$$

Thus, Det[A+(N-2)B]>0 on this branch as  $\hat{\bar{\rho}}\to 0^+$  near the bifurcation point.

#### APPENDIX G

# THE LOW-ORDER APPROXIMATION OF $yy'(\theta)$

To obtain the expressions for  $yy'(\theta)$  in equation (4.22), simplification is carried out in two steps. First, it can be shown that

$$n^2 \xi_1 + \tilde{\Gamma}_{\theta} \sin(n\theta) \simeq 0 \tag{G.1}$$

by incorporating the approximate steady-state solutions for  $\rho_1$  and  $\psi_1$  in equations (4.7). Second, the remaining term is reduced based on the corresponding truncated steady-state equations (4.8). It can be shown that before the bifurcation the absorber motions undergo unison motion, which yields

$$\frac{2n^2}{N} \sum_{j=1}^{N} s_j s_j' = 2n^2 \xi_1 \xi_1' 
= n^3 \tilde{\rho}_1^2 \sin(2\tilde{\psi}_1 - 2n\theta).$$
(G.2)

After the bifurcation, using the transformations given in equations (4.2) and (4.4) yields

$$\frac{2n^{2}}{N} \sum_{j=1}^{N} s_{j} s_{j}^{'} = n^{3} \left[ \tilde{\bar{\rho}}_{1}^{2} \sin(2\tilde{\bar{\psi}}_{1} - 2n\theta) - (N-1) \sum_{j \neq 1} \tilde{\bar{\rho}}_{j}^{2} \sin(2\tilde{\bar{\psi}}_{j} - 2n\theta) + \sum_{j,k \neq 1} \sum_{k} 2\tilde{\bar{\rho}}_{j} \tilde{\bar{\rho}}_{k} \sin(\tilde{\bar{\psi}}_{j} + \tilde{\bar{\psi}}_{k} - 2n\theta) \right].$$
(G.3)

Utilizing some trigonometric identities and the approximate solutions given in equations (4.7), one can show

R.H.S of (G.3) = 
$$\cos(2\tilde{\psi}_i - 2n\theta) \{n^3 \tilde{\rho}_1^2 \sin(2\tilde{\psi}_i)\}$$

$$\begin{split} &+n^{3} \sum_{j \neq 1, i} \{ 2\tilde{\bar{\rho}}_{i} \tilde{\bar{\rho}}_{j} \sin(\tilde{\bar{\psi}}_{i} - \tilde{\bar{\psi}}_{j}) - (N-1)\tilde{\bar{\rho}}_{j}^{2} \sin[2(\tilde{\bar{\psi}}_{i} - \tilde{\bar{\psi}}_{j})] \} \\ &+n^{3} \sum_{j, k \neq 1, i} \sum_{k} 2\tilde{\bar{\rho}}_{j} \tilde{\bar{\rho}}_{k} \sin(2\tilde{\bar{\psi}}_{i} - \tilde{\bar{\psi}}_{j} - \tilde{\bar{\psi}}_{k}) \} \\ &+ \sin(2\tilde{\bar{\psi}}_{i} - 2n\theta) \{ n^{3} \tilde{\bar{\rho}}_{1}^{2} \cos(2\tilde{\bar{\psi}}_{i}) + (N-1)n^{3} \tilde{\bar{\rho}}_{i}^{3} \\ &+ n^{3} \sum_{j \neq 1, i} \{ 2\tilde{\bar{\rho}}_{i} \tilde{\bar{\rho}}_{j} \cos(\tilde{\bar{\psi}}_{i} - \tilde{\bar{\psi}}_{j}) - (N-1)\tilde{\bar{\rho}}_{j}^{2} \cos[2(\tilde{\bar{\psi}}_{i} - \tilde{\bar{\psi}}_{j})] \} \\ &+ n^{3} \sum_{j, k \neq 1, i} \sum_{k} 2\tilde{\bar{\rho}}_{j} \tilde{\bar{\rho}}_{k} \cos(2\tilde{\bar{\psi}}_{i} - \tilde{\bar{\psi}}_{j} - \tilde{\bar{\psi}}_{k}) \}, \qquad 2 \leq i \leq N. \end{split}$$

$$(G.4)$$

Incorporating the truncated averaged equations in equation (3.12) yields

R.H.S of (G.4) = 
$$2\tilde{\mu}_a \cos(2\tilde{\psi}_i - 2n\theta)$$
,  $2 \le i \le N$ . (G.5)

Based on the results in Appendix B, one finds

$$2\tilde{\mu}_a \cos(2\tilde{\psi}_i - 2n\theta) = 2\tilde{\mu}_a \cos(2\tilde{\psi} - 2n\theta), \qquad 2 \le i \le N,$$

after the bifurcation.

# Here are less than the party of the party of

#### APPENDIX H

# AVERAGED EQUATIONS IN CARTESIAN COORDINATES

The truncated, averaged equations expressed in Cartesian coordinates are given by

$$\begin{split} \frac{dA_{\xi}}{d\hat{\theta}} &= \frac{-1}{2}\tilde{\mu}_{a}A_{\xi} + \left(\frac{\tilde{\delta}_{\xi2}}{n} + \frac{n}{4}\right)B_{\xi} + \frac{\tilde{\delta}_{\eta2}}{n}B_{\eta} + \frac{1}{4}\tilde{\Gamma}_{\theta}B_{\xi} \\ &- c_{n2}B_{\xi}(A_{\xi}^{2} + B_{\xi}^{2}) + c_{n5}A_{\xi}A_{\eta}B_{\eta} - c_{n6}B_{\xi}A_{\eta}^{2} + c_{n7}B_{\xi}B_{\eta}^{2} \\ &+ \frac{3\tilde{\delta}_{\eta4}}{2n}\left(A_{\eta}^{2}B_{\eta} + A_{\xi}^{2}B_{\eta} + 3B_{\eta}B_{\xi}^{2} + B_{\eta}^{3} + 2A_{\eta}A_{\xi}B_{\xi}\right), \end{split} \tag{H.1a} \\ \frac{dB_{\xi}}{d\hat{\theta}} &= \frac{-1}{2}\tilde{\mu}_{a}B_{\xi} - \left(\frac{\tilde{\delta}_{\xi2}}{n} + \frac{n}{4}\right)A_{\xi} - \frac{\tilde{\delta}_{\eta2}}{n}A_{\eta} + \frac{1}{4}\tilde{\Gamma}_{\theta}A_{\xi} \\ &+ c_{n2}A_{\xi}(A_{\xi}^{2} + B_{\xi}^{2}) - c_{n5}B_{\xi}A_{\eta}B_{\eta} + c_{n6}A_{\xi}B_{\eta}^{2} - c_{n7}A_{\xi}A_{\eta}^{2}, \\ &- \frac{3\tilde{\delta}_{\eta4}}{2n}\left(B_{\eta}^{2}A_{\eta} + B_{\xi}^{2}A_{\eta} + 3A_{\eta}A_{\xi}^{2} + A_{\eta}^{3} + 2B_{\eta}A_{\xi}B_{\xi}\right), \end{split} \tag{H.1b} \\ \frac{dA_{\eta}}{d\hat{\theta}} &= \frac{-1}{2}\tilde{\mu}_{a}A_{\eta} + \frac{\tilde{\delta}_{\xi2}}{n}B_{\eta} + \frac{\tilde{\delta}_{\eta2}}{n}B_{\xi} + \frac{1}{4}\tilde{\Gamma}_{\theta}B_{\eta} \\ &+ c_{n4}B_{\eta}(A_{\eta}^{2} + B_{\eta}^{2}) + c_{n5}A_{\eta}A_{\xi}B_{\xi} - c_{n6}B_{\eta}A_{\xi}^{2} + c_{n7}B_{\eta}B_{\xi}^{2}, \\ &+ \frac{3\tilde{\delta}_{\eta4}}{2n}\left(A_{\xi}^{2}B_{\xi} + A_{\eta}^{2}B_{\xi} + 3B_{\xi}B_{\eta}^{2} + B_{\xi}^{3} + 2A_{\xi}B_{\eta}A_{\eta}\right) \end{aligned} \tag{H.1c} \\ \frac{dB_{\eta}}{d\hat{\theta}} &= \frac{-1}{2}\tilde{\mu}_{a}B_{\eta} - \frac{\tilde{\delta}_{\eta2}}{n}A_{\xi} - \frac{\tilde{\delta}_{\xi2}}{n}A_{\eta} + \frac{1}{4}\tilde{\Gamma}_{\theta}A_{\eta} \\ &- c_{n4}A_{\eta}(A_{\eta}^{2} + B_{\eta}^{2}) - c_{n5}A_{\xi}B_{\xi}B_{\eta} + c_{n6}A_{\eta}B_{\xi}^{2} - c_{n7}A_{\eta}A_{\xi}^{2} \\ &- \frac{3\tilde{\delta}_{\eta4}}{2n}\left(B_{\xi}^{2}A_{\xi} + B_{\eta}^{2}A_{\xi} + 3A_{\xi}A_{\eta}^{2} + A_{\xi}^{3} + 2B_{\xi}A_{\eta}B_{\eta}\right). \end{aligned} \tag{H.1d}$$

where

$$c_{n5} = \frac{4n^3 - n^5}{128} + \frac{3\tilde{\delta}_{\xi 4}}{n}, \quad c_{n6} = \frac{12n^3 + n^5}{256} - \frac{3\tilde{\delta}_{\xi 4}}{2n} \quad \text{and} \quad c_{n7} = \frac{-4n^3 - 3n^5}{256} + \frac{3\tilde{\delta}_{\xi 4}}{2n}.$$

Applying assumption (5.19), the above equations become

$$\begin{split} \frac{dA_{\xi}}{d\hat{\theta}} &= \frac{-1}{2}\tilde{\mu}_{a}A_{\xi} + \left(\frac{\tilde{\delta}_{\xi2}}{n} + \frac{n}{4}\right)B_{\xi} + \frac{1}{4}\tilde{\Gamma}_{\theta}B_{\xi} - c_{n2}B_{\xi}(A_{\xi}^{2} + B_{\xi}^{2}) \\ &+ c_{n5}A_{\xi}A_{\eta}B_{\eta} - c_{n6}B_{\xi}A_{\eta}^{2} + c_{n7}B_{\xi}B_{\eta}^{2}, \end{split} \tag{H.2a} \\ \frac{dB_{\xi}}{d\hat{\theta}} &= \frac{-1}{2}\tilde{\mu}_{a}B_{\xi} - \left(\frac{\tilde{\delta}_{\xi2}}{n} + \frac{n}{4}\right)A_{\xi} + \frac{1}{4}\tilde{\Gamma}_{\theta}A_{\xi} + c_{n2}A_{\xi}(A_{\xi}^{2} + B_{\xi}^{2}) \\ &- c_{n5}B_{\xi}A_{\eta}B_{\eta} + c_{n6}A_{\xi}B_{\eta}^{2} - c_{n7}A_{\xi}A_{\eta}^{2}, \end{split} \tag{H.2b} \\ \frac{dA_{\eta}}{d\hat{\theta}} &= \frac{-1}{2}\tilde{\mu}_{a}A_{\eta} + \frac{\tilde{\delta}_{\xi2}}{n}B_{\eta} + \frac{1}{4}\tilde{\Gamma}_{\theta}B_{\eta} + c_{n4}B_{\eta}(A_{\eta}^{2} + B_{\eta}^{2}) \\ &+ c_{n5}A_{\eta}A_{\xi}B_{\xi} - c_{n6}B_{\eta}A_{\xi}^{2} + c_{n7}B_{\eta}B_{\xi}^{2}, \end{split} \tag{H.2c} \\ \frac{dB_{\eta}}{d\hat{\theta}} &= \frac{-1}{2}\tilde{\mu}_{a}B_{\eta} - \frac{\tilde{\delta}_{\xi2}}{n}A_{\eta} + \frac{1}{4}\tilde{\Gamma}_{\theta}A_{\eta} - c_{n4}A_{\eta}(A_{\eta}^{2} + B_{\eta}^{2}) \\ &- c_{n5}A_{\xi}B_{\xi}B_{\eta} + c_{n6}A_{\eta}B_{\xi}^{2} - c_{n7}A_{\eta}A_{\xi}^{2}. \end{aligned} \tag{H.2d}$$

#### APPENDIX I

#### STABILITY OF SOLUTIONS ON SM1<sup>+</sup>

Incorporating the SM1<sup>+</sup> solutions given by equation (5.25) into the sub-block matrix B in the corresponding Jacobian, one can obtain the determinant of B,  $D_{B1+}$ . It is given by

$$\begin{split} D_{B1+} &= -\frac{\tilde{\Gamma}_{\theta}^{2}}{16} + \frac{\tilde{\mu}_{a}^{2}}{4} + \frac{\tilde{\delta}_{\xi^{2}}^{2}}{n^{2}} \\ &- \left(\frac{c_{n6} + c_{n7}}{16c_{n2}}\right) \left(\tilde{\Gamma}_{\theta}^{2} - 4\tilde{\mu}_{a}^{2}\right)^{\frac{1}{2}} \left[ \left(\tilde{\Gamma}_{\theta}^{2} - 4\tilde{\mu}_{a}^{2}\right)^{\frac{1}{2}} + \frac{4\tilde{\delta}_{\xi^{2}}}{n} + n \right] \\ &+ \left(\frac{c_{n6}^{2} - 6c_{n6}c_{n7} + c_{n7}^{2} - c_{n5}^{2}}{128c_{n2}^{2}} \right) \left[ \left(\tilde{\Gamma}_{\theta}^{2} - 4\tilde{\mu}_{a}^{2}\right)^{\frac{1}{2}} + \frac{4\tilde{\delta}_{\xi^{2}}}{n} + n \right]^{2} \\ &+ \left(\frac{c_{n5}^{2} - c_{n6}^{2} - 2c_{n6}c_{n7} - c_{n7}^{2}}{128c_{n2}^{2}} \right) \left(1 - \frac{8\tilde{\mu}_{a}}{\tilde{\Gamma}_{\theta}^{2}}\right) \left[ \left(\tilde{\Gamma}_{\theta}^{2} - 4\tilde{\mu}_{a}^{2}\right)^{\frac{1}{2}} + \frac{4\tilde{\delta}_{\xi^{2}}}{n} + n \right]^{2} \\ &- \left[ \frac{(c_{n6} - c_{n7})\tilde{\delta}_{\xi^{2}}}{4c_{n2}n} \right] \left[ \left(\tilde{\Gamma}_{\theta}^{2} - 4\tilde{\mu}_{a}^{2}\right)^{\frac{1}{2}} + \frac{4\tilde{\delta}_{\xi^{2}}}{n} + n \right]. \end{split}$$

#### APPENDIX J

#### STABILITY OF SOLUTIONS ON SM2+

Incorporating the SM2<sup>+</sup> solutions given by equation (5.26) into the sub-block matrix A in the corresponding Jacobian, one can obtain the determinant of A,  $D_{A2+}$ . It is given by

$$\begin{split} D_{A2+} &= \frac{\tilde{\delta}_{\xi 2}}{2} - \frac{\tilde{\Gamma}_{\theta}^{2}}{16} + \frac{\tilde{\mu}_{a}^{2}}{4} + \frac{\tilde{\delta}_{\xi 2}^{2}}{n^{2}} + \frac{n^{2}}{16} \\ &+ \left(\frac{c_{n6} + c_{n7}}{16c_{n4}}\right) \left(\tilde{\Gamma}_{\theta}^{2} - 4\tilde{\mu}_{a}^{2}\right)^{\frac{1}{2}} \left[ \left(\tilde{\Gamma}_{\theta}^{2} - 4\tilde{\mu}_{a}^{2}\right)^{\frac{1}{2}} - \frac{4\tilde{\delta}_{\xi 2}}{n} \right] \\ &+ \left(\frac{c_{n6}^{2} - 6c_{n6}c_{n7} + c_{n7}^{2} - c_{n5}^{2}}{128c_{n4}^{2}} \right) \left[ \left(\tilde{\Gamma}_{\theta}^{2} - 4\tilde{\mu}_{a}^{2}\right)^{\frac{1}{2}} - \frac{4\tilde{\delta}_{\xi 2}}{n} \right]^{2} \\ &+ \left(\frac{c_{n5}^{2} - c_{n6}^{2} - 2c_{n6}c_{n7} - c_{n7}^{2}}{128c_{n4}^{2}} \right) \left(1 - \frac{8\tilde{\mu}_{a}}{\tilde{\Gamma}_{\theta}^{2}}\right) \left[ \left(\tilde{\Gamma}_{\theta}^{2} - 4\tilde{\mu}_{a}^{2}\right)^{\frac{1}{2}} - \frac{4\tilde{\delta}_{\xi 2}}{n} \right]^{2} \\ &- \left(\frac{c_{n6} - c_{n7}}{4c_{n4}}\right) \left(\frac{\tilde{\delta}_{\xi 2}}{n} + \frac{n}{4}\right) \left[ \left(\tilde{\Gamma}_{\theta}^{2} - 4\tilde{\mu}_{a}^{2}\right)^{\frac{1}{2}} - \frac{4\tilde{\delta}_{\xi 2}}{n} \right] \end{split}$$

#### APPENDIX K

# THE NUMERICAL ALGORITHM FOR COUPLED-MODE SOLUTIONS

The coupled-mode solutions are numerically computed by carrying out the following steps.

- 1. Compute the possible sets of solutions for  $\bar{r}_{\xi}$  and  $\bar{r}_{\eta}$  using the polynomial (5.37).
- 2. For each set of solutions for  $\bar{r}_{\xi}$  and  $\bar{r}_{\eta}$ , calculate the corresponding applied torque amplitude by combining equations (5.34a) and (5.34c), which gives

$$2\tilde{\mu}_a(\bar{r}_{\xi}^2 + \bar{r}_{\xi}^2) + \tilde{\Gamma}_{\theta}\left(\bar{r}_{\eta}^2 \sin 2\bar{\varphi}_{\eta} + \bar{r}_{\xi}^2 \sin 2\bar{\varphi}_{\xi}\right) = 0. \tag{K.1}$$

The dependence of equation (K.1) on  $\bar{\varphi}_{\eta}$  and  $\bar{\varphi}_{\eta}$  is then eliminated by using equations (5.36a) and (5.36b). This results in a nonlinear algebraic equation which can be used to solve for  $\tilde{\Gamma}_{\theta}$  for given values of  $\bar{r}_{\xi}$  and  $\bar{r}_{\eta}$ . Thus, one can find the values of  $\bar{r}_{\xi}$  and  $\bar{r}_{\eta}$  for a given  $\tilde{\Gamma}_{\theta}$  in a reverse manner. Using equations (5.36a) and (5.36b) again, one can determine the corresponding phases  $\bar{\varphi}_{\xi}$  and  $\bar{\varphi}_{\eta}$ .

**BIBLIOGRAPHY** 

#### **BIBLIOGRAPHY**

- [1] S. T. Ariaratnam and N. Sri Namachchivaya. Periodically perturbed nonlinear gyroscopic systems. *Journal of Structral Mechanics*, 114(2):153-175, 1986.
- [2] A. K. Bajaj, P. Davies, and Chang S. I. On internal resonances in mechanical systems. In *Nonlinear Dynamics and Stochastic Mechanics*, pages 69-94. Kliemann, W. and Sri Namachchivaya, N., editors, CRC press, 1995.
- [3] V. J. Borowski, H. H. Denman, D. L. Cronin, S. W. Shaw, J. P. Hanisko, L. T. Brooks, D. A. Milulec, W. B. Crum, and M. P. Anderson. Reducing vibration of reciprocating engines with crankshaft pendulum vibration absorbers. 1991. SAE Technical Paper Series 911876.
- [4] B. A. C. Bulter. Rotating pendulum absorbers using one or more shell balls as pendulum masses, rolling on elliptic and parabolidal tracks. *British Patent No.* 520,787, 1938.
- [5] B. C. Carter. British Patent No. 337,446, 1929.
- [6] C-P. Chao, C-T. Lee, and S. W. Shaw. Non-unison dynamics of multiple centrifugal pendunlum vibration absorbers. *Journal of Sound and Vibration*, 1997, to appear.
- [7] C-P. Chao, S. W. Shaw, and C-T. Lee. Stability of the unison response for a rotating system with multiple centrifugal pendunlum vibration absorbers. *ASME Journal of Applied Mechanics*, 64:149-156, 1997.
- [8] S. L. Chen and S. W. Shaw. A fast-manifold approach to melnikov functions for slowly-varying oscillators. *International Journal of Bifurcation and Chaos*, 6:1575-1578, 1996.
- [9] R. Chilton and Reed Propeller Company. Rotating pendulum absorbers with bifilar suspension using crankweb counterweights as pendulum masses. *British Patent No.* 460,088, 1935.
- [10] G. Cicogna. Symmetry breakdown from bifurcations. Lettere al Nuovo Cimento, 31:600-602, 1981.
- [11] D. L. Cronin. Shake reduction in an automobile engine by means of crankshaft-mounted pendulums. *Mechanism and Machine Theory*, 27(5):517-533, 1992.
- [12] F. R. E. Crossley. The free oscillation of the centrifugal pendulum with wide angles. ASME Journal of Applied Mechanics, 19:315-319, September 1952.

- [13] F. R. E. Crossley. The forced oscillation of the centrifugal pendulum with wide angles. ASME Journal of Applied Mechanics, 20:41-47, March 1953.
- [14] J. P. Den Hartog. Tuned pendulums as torsional vibration eliminators. In Stephen Timoshenko 60th Anniversary Volume, pages 17-26, New York, 1938. The Macmillan Company.
- [15] H. H. Denman. Remarks on brachistochrone-tautochrone problems. American Journal of Physics, 53:781-782, 1985.
- [16] H. H. Denman. Tautochronic bifilar pendulum torsion absorbers for reciprocating engines. *Journal of Sound and Vibration*, 159:251-277, 1992.
- [17] E. Doedel. Auto: software for continuation and bifurcation problemms in ordinary dofferential equations. Department of Applied Mathematics, California Institute of Technology, Pasadena, CA, 1985.
- [18] David S. Dummit and Richard M. Foote. Abstract Algebra. Prentice Hall, Englewood Cliffs, NJ, 1991.
- [19] I. T. Georgiou, A. K. Bajaj, and M. Corless. Invariant manifold and chaotic vibrations in singuarly perturbed nonlinear oscillators. *International Journal of Engineering Science*, submitted.
- [20] M. Golubitsky, I. Stewart, and D. G. Schaeffer. Singularities and Groups in Bifurcation Theory. Volume II, Springer-Verlag, New York, 1988.
- [21] M. H. Hamouda and G. A. Pierce. Helicopter vibration suppression using simple pendulum absorbers on the rotor blade. *Journal of American Helicopter Society*, 29(3):19-29, July 1984.
- [22] G. S. Happawana, A. K. Bajaj, and O. D. I. Nwokah. A singular perturbation analysis of eigenvalue veering and modal sensitivity in perturbed linear periodic systems. *Journal of Sound and Vibration*, 160(2):225-242, 1993.
- [23] R. J. Harker. Theory of centrifugal tuned vibration absorber. *Journal of Aeronautical Science*, 11(246):197-204, 1944.
- [24] T. J. Healey and J. A. Treacy. Exact block diagonalization of large eigenvalue problems for structures with symmetry. *International Journal for Numerical Methods in Engineering*, 31:265-285, 1991. Pitman, Boston.
- [25] C. H. Hodges. Confinement of vibration by structural irregularity. *Journal of Sound and Vibration*, 82(3):411-424, 1982.
- [26] B. Kelley, Lynn R. R., and Wagner F. J. Device to alter dynamic characteristics of rotor systems. United States Patent 3035643, 1959. owned by Bell Aerospace Corporation.

- [27] W. Ker Wilson. Practical Solution of Torsional Vibration Problems, chapter XXX. Volume IV, Chapman and Hall Ltd, London, 3rd edition, 1968.
- [28] C-T. Lee and S. W. Shaw. A comparative study of nonlinear centrifugal pendulum vibration absorbers. In *Nonlinear and Stochastic Dynamics*, *ASME WAM*, volume AMD-Vol. 192/DE-Vol. 78, pages 91–98, 1994.
- [29] C-T. Lee and S. W. Shaw. Nonlinear dynamic response of paired centrifugal pendunlum vibration absorbers. *Journal of Sound and Vibration*, 203(5):731–743, 1997.
- [30] C-T. Lee, S. W. Shaw, and V. T. Coppola. A subharmonic vibration absorber for rotating machinary. ASME Journal of Vibration and Acoustics, 1997, to appear.
- [31] T. C. Lim. Dynamics of systems with rotating pendulums as vibration absorbers. Master's thesis, Department of Mechanical Engineering, University of Missouri-Rolla, 1986.
- [32] J. F. Madden. Constant frequency bifilar vibration absorber. United States Patent No. 4218187, 1980.
- [33] E. Meissner. Equalising the speed of rotating shafts by means of oscillating systems. In *Proceeding of 3rd international congress for applied mechanics*, page 199, 1930.
- [34] C. A. Meyer and H. B. Saldin. Modal tests of two types of vibration absorbers. Journal of Applied Mechanics, 9:A59-A64, 1942.
- [35] W. Miao and T. Mouzakis. Bifilar analysis study Volume I. NASA Report 159227, August 1980.
- [36] W. Miao and T. Mouzakis. Nonlinear characteristics of the rotor bifilar absorber. 37th American Helicopter Society Forum, 1981.
- [37] Y. A. Mitropolsky. Problems in the Aymptotic Theory of Nonstationary Vibrations. Daniel Davey, New York, 1965.
- [38] A. Moore. The control of torsional vibration in radial aircraft engines by means of tuned pendulums. *Journal of Aeronautical Science*, 9:229, 1942.
- [39] J. A. Murdock. *Perturbations: Theory and Methods*. John Wiley & Sons, New York, 1991.
- [40] V.R. Murthy and C.E. Hammond. Vibration analysis of rotor blades with pendulum absorbers. *Journal of Aircraft*, 18:23-29, 1981.
- [41] D. E. Newland. Nonlinear aspects of the performance of centrifugal pendunlum vibration absorbers. ASME Journal of Engineering for Industry, 86:257-263, 1964.

- [42] O'Connor. The viscous torsional vibration damper. Society of Automotive Engineering Quarterly Transactions, 1:87, 1947.
- [43] W. F. Paul and K. C. Mard. Vibration damped helicopter rotors. United States Patent 3540809, 1970. owned by United Aircraft Corporation.
- [44] Pierce. Rubber mounted dampers, examples of application. Transactions of Society of Automotive Engineering, 53:480, 1945.
- [45] C. Pierre and E. H. Dowell. Localization of vibrations by structure irregularity. Journal of Sound and Vibration, 114(3):549-564, 1987.
- [46] R. Plunkett. Vibration damping. Applied Mechanics Review, 6(7):313-315, 1953.
- [47] F. P. Porter. Centrifugal pendulum dynamic damper. In S.A.E. War Engineering Board Publication, page 269, 1945. Evaluation of Effects of Torsional Vibration.
- [48] R. E. Reed. The use of the centrifugal pendulum absorber for the reduction of linear vibration. *Journal of Applied Mechanics*, 16:19-194, 1949.
- [49] E. M. M. B. Salomon. British Patent No. 401,962, 1932.
- [50] R. R. Sarazin. Rotating pendulum absorbers with bifilar suspension. British Patent No. 379,165, 1930.
- [51] R. R. R. Sarazin. British Patent No. 444,222, 1935.
- [52] M. Sharif-Bakhtiar. Finite Amplitude Effects on the Dynamic Performance of the Centrifugal Pendulum Vibration Absorber. PhD thesis, Michigan State University, 1989.
- [53] M. Sharif-Bakhtiar and S. W. Shaw. The dynamic response of a centrifugal pendenlum vibration absorber with motion-limiting stops. *Journal of Sound and Vibration*, 126(2):221-235, 1988.
- [54] M. Sharif-Bakhtiar and S. W. Shaw. Effects of nonlinearities and damping on the dynamic response of a centrifugal pendulum absorber. ASME Journal of Vibration and Acoustics, 114:305-311, 1992.
- [55] S. W. Shaw, V. K. Garg, and C-P. Chao. Attenuation of engine torsional vibrations using tuned pendulum absorbers. volume 2, pages 713-722. The Society of Automotive Engineers, 1997. SAE Noise and Vibration Conference and Exposition.
- [56] S. W. Shaw and C-T. Lee. On the nonlinear dynamics of centrifugal pendulum vibration absorbers. In Smart Structures, Nonlinear Vibration, and Control, pages 247-309. Guran A. and Inman D. J., editors, Prentice Hall Inc., New Jersey, 1995.

- [57] S. W. Shaw and Wiggins S. Chaotic motions of a torsional vibration absorber. Journal of Applied Mechanics, 55:952-958, 1988.
- [58] A. Stieglitz. Influence of pendular masses on torsional vibration. Yearbook of Aeronautical Research, 2:164, 1938.
- [59] J. Stoer and R. Bulirsch. Introduction to Numerical Analysis. Springer-Verlag, New York, 2nd edition, 1976.
- [60] C. F. Taylor. The Internal-Combustion Engine in Theory and Practice, volume 2, chapter 8. The M. I. T. Press, Cambridge, Massachusetts, revised edition, 1985.
- [61] E. S. Taylor. Eliminating crankshaft torsional vibration in radial aircraft engines. SAE Journal, 38:81-89, March 1936.
- [62] A. F. Vakakis and T. K. Centikaya. Mode localization in a class of multidegree-of-freedom systems with cyclic symmetry. SIAM Journal on Applied Mathematics, 53:265-282, 1993.
- [63] A. Vanderbauwhede. Local bifurcation and symmetry. Research Notes in Mathematics, 75, 1982.
- [64] M. A. Wachs. The main rotor bifilar absorber and its effect on helicopter reliability/maintainability. 1973. SAE Technical Paper Series 730894.
- [65] Y. Wang, S. W. Shaw, and C-P. Chao. Design of pendulum absobrers for transverse vibration attenutation of rotating beams. 16th ASME Biennial Conference on Mechanical Vibration and Noise, Sep 9-13, 1997.
- [66] G. White. Allied Aircraft Piston Engines of World War II. SAE Inc., Warrendale, PA, 1995.
- [67] X. L. Yang and P. R. Sethna. Local and global bifurcations in parametrically excited vibrations of nearly square plates. *International Journal of Non-Linear Mechanics*, 26(2):199-220, 1991.
- [68] M. I. Young. Optimal design and control of centrifugally tuned dynamic vibration absorbers. In H. E. Leipholz, editor, Structural Control Proceedings of the Second International Symposium on Structural Control held in University of Waterloo, Ontario, Canada, July 15-17, 1985, pages 768-776. Martinus Nijhoff Publishers, Dordrecht, Netherlands, 1987.
- [69] R. W. Zdanowich and T. S. Wilson. The elements of pendulum dampers. Proceedings of Institute of Mechanical Ensineers, 143:182, 1940.

•			•
· !			
•			
1			
l			
•			
1			
,			
r			
•			
• *			
•			

MICHIGAN STATE UNIV. LIBRARIES
31293015703147